NASA CR-66952
1715

15

CLASSIFICATION CHANGE

TO = UNCLASSIFIED ~~CONFIDENTIAL~~

By authority of T.D. No. 75-159

Changed by [illegible] Date 12/10/74

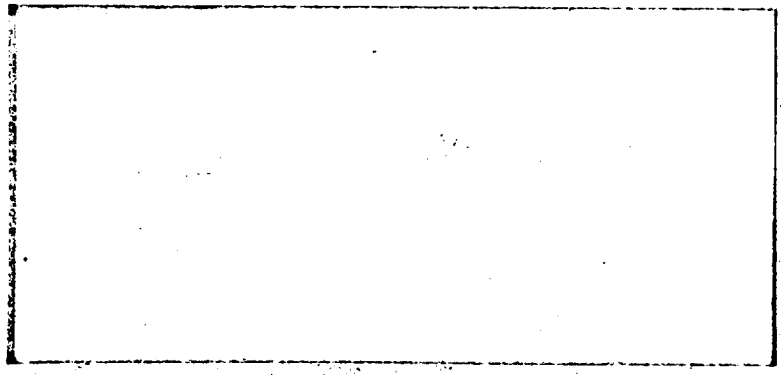

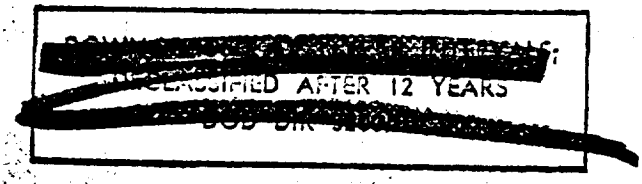

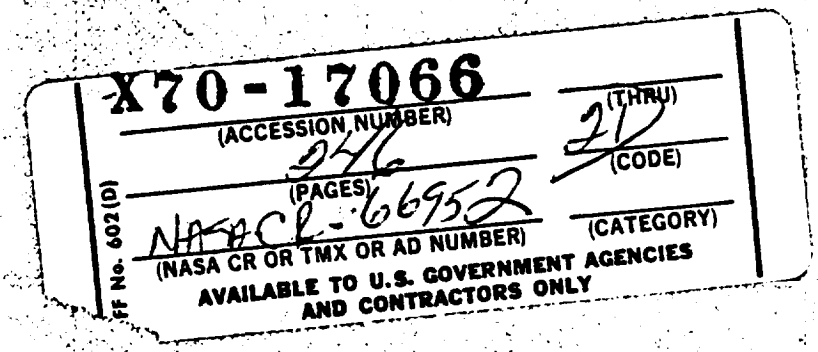

GARRETT

AIRESEARCH MANUFACTURING COMPANY
A DIVISION OF THE GARRETT CORPORATION
9851-9951 SEPULVEDA BLVD. • LOS ANGELES, CALIFORNIA 90009
TELEPHONE: SPRING 6-1010, ORCHARD 0-0131 • CABLE: GARRETTAIR LOS ANGELES

(NASA-CR-66952) HYPERSONIC RESEARCH ENGINE PROJECT. PHASE 2: CHEMICAL KINETICS STUDY FOR A SUPERSONIC COMBUSTOR MODEL, DATA ITEM NO. 54.10 (AiResearch Mfg. Co., Los Angeles, Calif.) 246 p

N75-78201

Unclas
00/98 42368

AIRESEARCH MANUFACTURING COMPANY
Los Angeles, California

HYPERSONIC RESEARCH ENGINE PROJECT-PHASE II CHEMICAL KINETICS STUDY FOR A SUPERSONIC COMBUSTOR MODEL(U)

DATA ITEM NO. 54.10
NASA CONTRACT NO. NAS1-6666

Document No. AP-70-6319

Number of pages 243

Original date 20 May 1970

Prepared by Engineering Staff

Edited by W. Platte

Approved by Henry J. Lopez
HRE Program Manager

Revision	Date	Pages Affected (Revised, Added, Eliminated)

FOREWORD

The analytical report contained herein is submitted to the NASA Langley Research Center by the AiResearch Manufacturing Company of Los Angeles, California, in accordance with the guidelines of Paragraph 5.7.3.2.1, NASA Statement of Work L-4947-B (Revised).

This report describes the chemical kinetic study for the Supersonic Combustor Model which was performed by AiResearch in support of the combustor program phase of the Hypersonic Research Engine Project.

CONTENTS

ILLUSTRATIONS

ILLUSTRATIONS (Continued)

ILLUSTRATIONS (Continued)

ILLUSTRATIONS (Continued)

ILLUSTRATIONS (Continued)

TABLES

1. SUMMARY

The problems of supersonic combustion in a diverging duct were examined analytically, and the results of this study were compared with test results from the HRE two-dimensional combustor rig. The effects of temperature, pressure, duct divergence, amount of vitiation and initial concentration of radicals on the chemical kinetics of the hydrogen-air system were investigated. It was found that supersonic combustion of hydrogen-air in a diverging duct at low mixed temperatures (around 2000°R) is very sensitive to chemical kinetics effects. The ignition delay time decreased with increasing pressure but this effect was reversed in the pressure range of 1 to 15 atm depending on the initial temperature. The ignition process was enchanced by the presence of free radicals, but the relative effects diminished rapidly as the initial concentration was increased.

A detailed chemical-kinetic simulation of the HRE two-dimensional combustor test results indicated that low chemical efficiencies in the second stage were not caused by chemical-kinetics but were due to inadequate mixing. This conclusion was further strengthed by tests reported by General Electric (Reference 1-1) in which low chemical efficiencies were observed when fuel was injected into a constant-area duct followed by a divergence section, with an inlet static temperature as high as 2500°R.

It is postulated that intimate mixing requires turbulence with small but high energy level eddies. The various injector geometries used in the two-dimensional combustor tests probably did not cause sufficient turbulence in the mainstream, evidenced by lack of sufficient flow separation. The low level of turbulence could be due to the favorable pressure gradient in the diverging duct and to the relatively high temperatures upstream of the second stage injectors. Further exploration in this area is urgently needed.

The analytical simulation of the AIM engine indicated that the chemical-kinetics effects will not adversely affect the second-stage combustion process in the flight Mach number range of 6 to 8.

The results from the two-dimensional combustor tests lead to the prediction of low second-stage combustor efficiencies in the AIM engine unless methods for enhancing the mixing process can be devised. Turbulence could be generated by a metallic coating on the combustor walls. This coating can be applied with varying degrees of surface roughness to produce different levels of turbulence.

Currently, five additional igniter stations are being installed in the AIM combustor. The igniter jets are directed upstream to produce additional sources of turbulence as well as ignition energy.

2. INTRODUCTION

The problems of supersonic combustion in a diverging duct were evident in the HRE two-dimensional combustor component test program. In these tests low chemical efficiencies, in the order of 50 to 60 percent, were encountered regardless of injector geometry, equivalence ratios, and inlet total temperature. Various injector geometries and equivalence ratios aimed at improving the mixing, and high inlet total temperatures (3800°R) which should enhance the chemical reactions were tried. However, all attempts failed to improve the combustor performance. A subsequent survey of the literature indicated that low chemical efficiencies were also obtained by a number of investigators (Reference 1-1, 1-2, and 2-1) whenever a diverging duct was used. Cookson (Reference 2-1) found that a hydrogen diffusion flame could not be maintained in a simple conical combustor of 0.75 deg divergence and 30 in. long. Combustion was observed to occur after the Mach disc which was formed at the combustor exit. Cookson's experiments strongly suggest that chemical kinetics have a significant affect on the problem. Therefore, an investigation was initiated to study the various effects of chemical kinetics using existing computer programs in order to obtain a better understanding of the problem.

The investigation was divided into four phases. First, a parametric study was conducted to obtain the basic understanding of the chemical kinetics from the effects of various independent variables such as temperature, pressure, divergence, degree of vitiation, and initial concentration of radicals; second, the mechanism of ignition delay was examined in a simplified analytical form in order to obtain the essential correlation parameters which otherwise could not be obtained from computer programs; and third, a comparison was made between the computer program results and Cookson's experiments in order to substantiate the validity of the kinetics programs. Fully-mixed and partially-mixed models were simulated in a shear-layer combustion program (Reference 2-2) to try and analyze and compare with the results from the two-dimensional combustor test program. Finally, a chemical kinetic analysis of the AIM engine was performed. A brief examination of chemical kinetics using a two-dimensional kinetics program was also made.

3. PARAMETRIC STUDIES

An investigation of the chemical kinetics of a premixed hydrogen-air system was conducted. The investigation was directed toward clarifying the effects of static temperature, static pressure, flow velocity, equivalence ratio, vitiation, initial radical concentration, and combustor divergence on the chemical kinetics. These effects were determined through use of a one-dimensional chemical kinetics computer program (Reference 3-1).

3.1 THE DETAILED HYDROGEN-AIR CHEMICAL KINETIC MODEL

The reaction mechanism of the hydrogen-air reaction assumed to be comprised of the 11 reactions is shown in Table 3.1-1.

TABLE 3.1-1

HYDROGEN-AIR REACTIONS

(4)	$H_2 + M = H + H + M$	
(9)	$O_2 + M = O + O + M$	(chain-initiating steps)
(11)	$H_2 + O_2 = OH + OH$	
(1)	$H_2 + OH = H_2O + H$	(chain-carrying steps)
(8)	$O + H + M = OH + M$	
(2)	$H + O_2 = OH + O$	
(3)	$O + H_2 = OH + H$	(chain-branching steps)
(7)	$H_2O + O = OH + OH$	
(6)	$HO_2 + H_2 = H_2O_2 + H$	
(5)	$H + O_2 + M = HO_2 + M$	(chain-breaking steps)
(10)	$H + OH + M = H_2O + M$	

The symbol M represents a "third body", i.e., any chemical species. The third body acts as an energy source or sink in chemical reactions. Steps 2, 3, and 7 are branching reactions since two chain carriers appear in the products while only one enters into the reaction. Steps 5 and 10 serve to break the hydrogen-oxygen chain by removing (H) and (OH) from the mixture. Thus, chain-branching reactions are responsible for the production of progressively larger concentrations of chain carriers. Unless the chain-branching reactions are balanced by chain-breaking reactions, the reaction rate will increase until it becomes sufficiently rapid to be classified as an explosion.

The reaction rate constants are expressed in the standard Arrhenius form given by

$$K_f = DT^E \exp. \frac{F}{T}$$

$$K_b = \frac{K_f}{K_{EQ}}$$

$$K_{EQ} = DCT^{EC} \exp. (FC/T)$$

where D, E, F, DC, EC and FC are the constants and are presented in Table 3.1-2. The constant, D, for reaction (5) was multiplied by the weighted third body efficiency factor, b_w.

3.2 RESULTS AND DISCUSSION

3.2.1 Effect of Static Temperature

Chemical kinetic calculations were made as a function of initial static temperature for clean air as defined in Table 3.2-1. In all of these calculations, the initial static pressure (P = 1 atm), equivalence ratio (ϕ = 0.5), initial flow velocity (V = 4500 ft/sec) and combustor flow area were held constant.

The results of these studies are presented in Figures 3.2-1 through 3.2-7. In Figure 3.2-1, there appears a significant time delay before any appreciable temperature rise is observed. This period is referred to as the ignition delay period. During this period, little change occurs in hydrogen molecular species but large changes in H_2O, O, H, and OH concentrations occur as shown in Figures 3.2-4, 3.2-5, and 3.2-6. The two body reactions are relatively fast and lead to an overproduction of radicals. At the end of ignition delay period, the third body reactions begin to play a dominant role leading to recombination and depletion of radicals with the accompanying energy release. The time for the process to proceed from the end of ignition delay to an equilibrium state is referred to as the reaction time. Due to an inherent difficulty of the computer program in reaching the equilibrium state, the computations were limited to 3 min of computer time; therefore, the final equilibrium state was not reached in most cases.

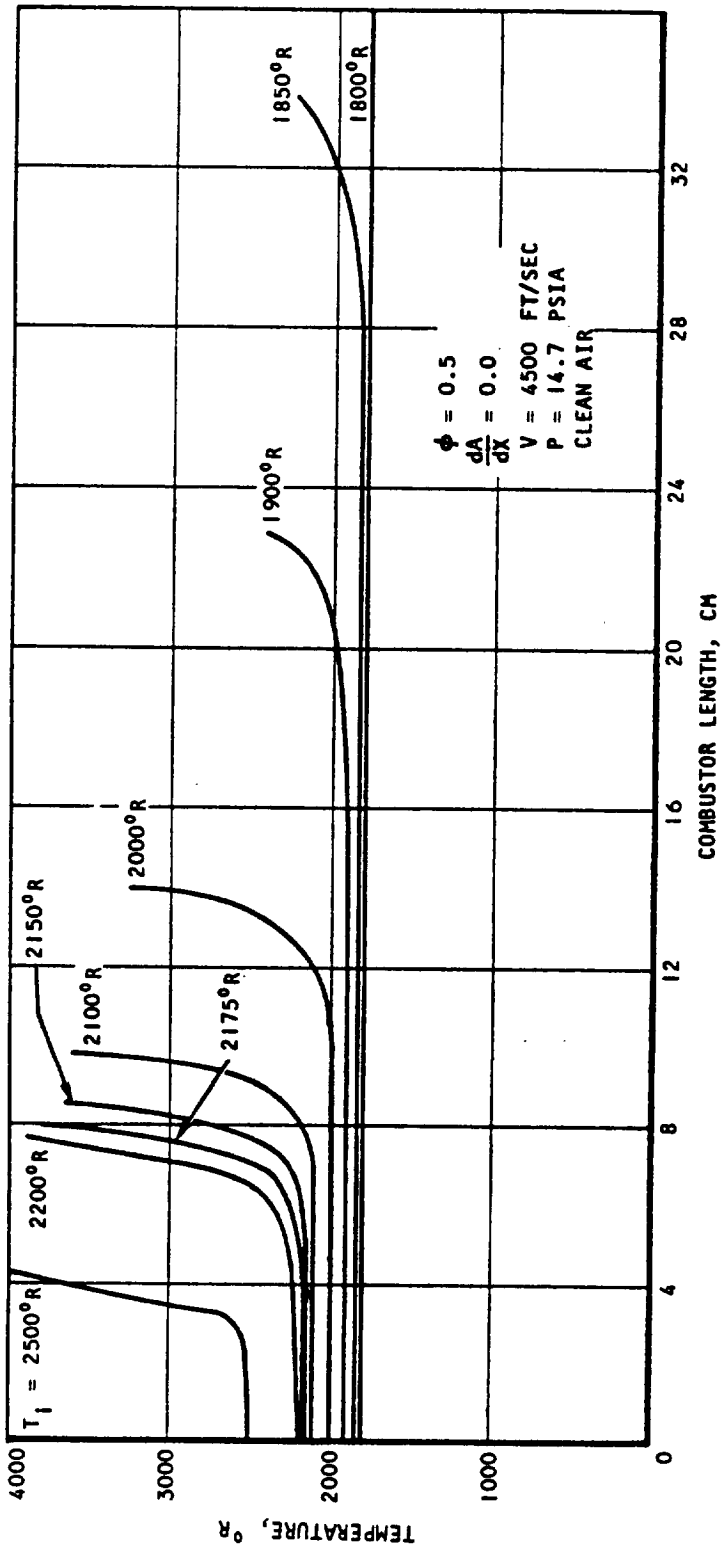

S-53922

Figure 3.2-1. Effect of Initial Static Temperature on Combustor Length

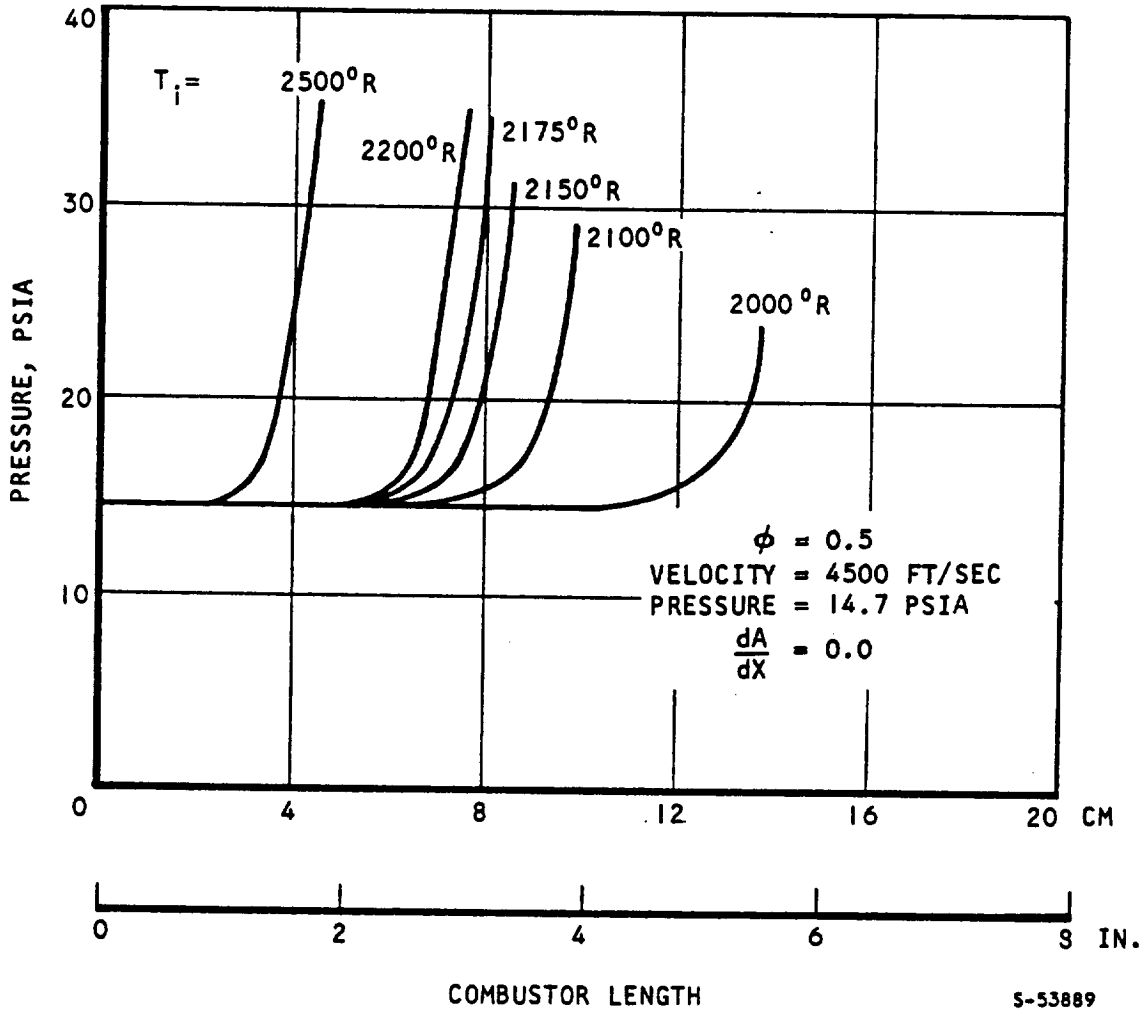

Figure 3.2-2. Effect of Initial Static Temperature on Static Pressure

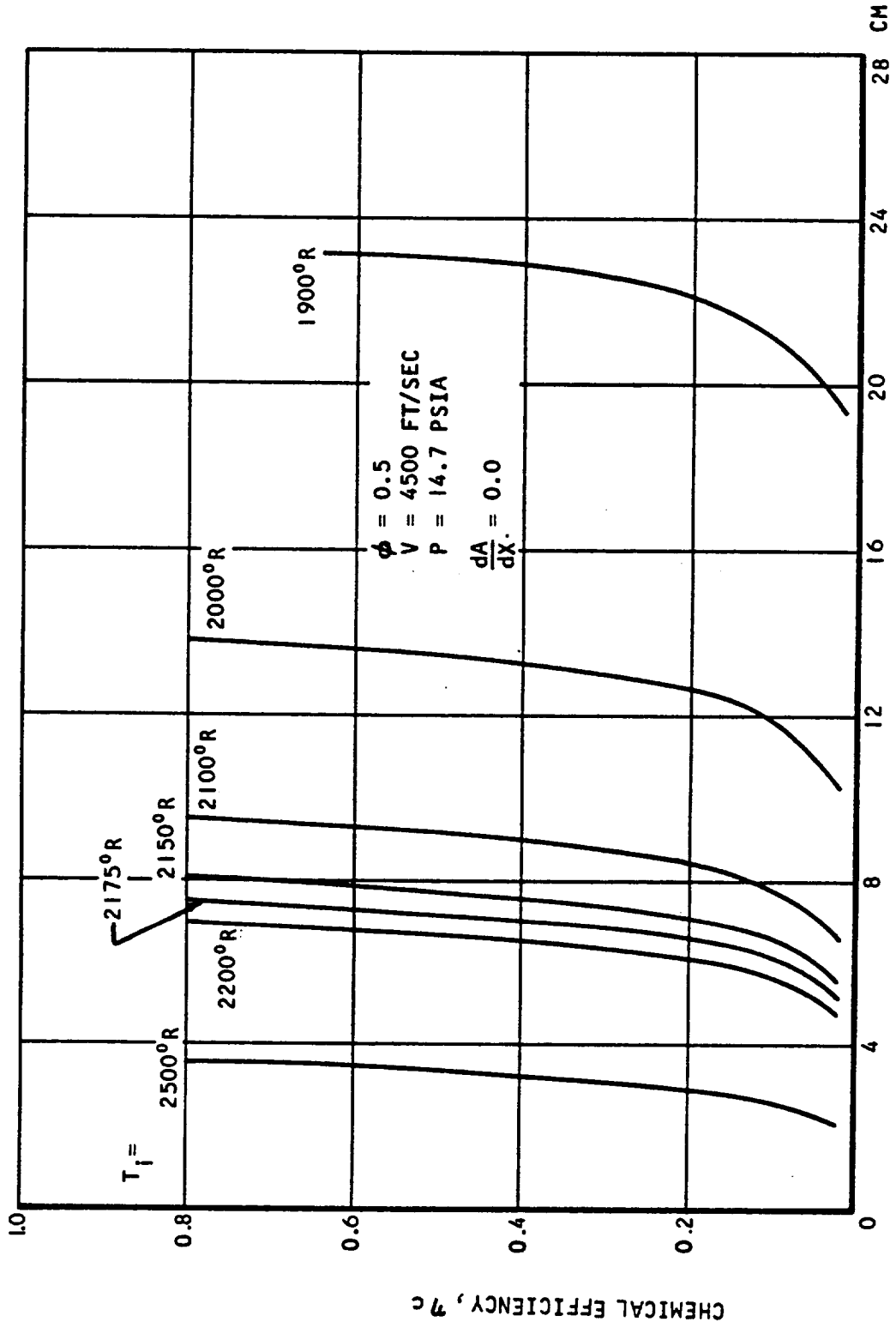

Figure 3.2.3. Effect of Initial Static Temperature on Chemical Efficiency

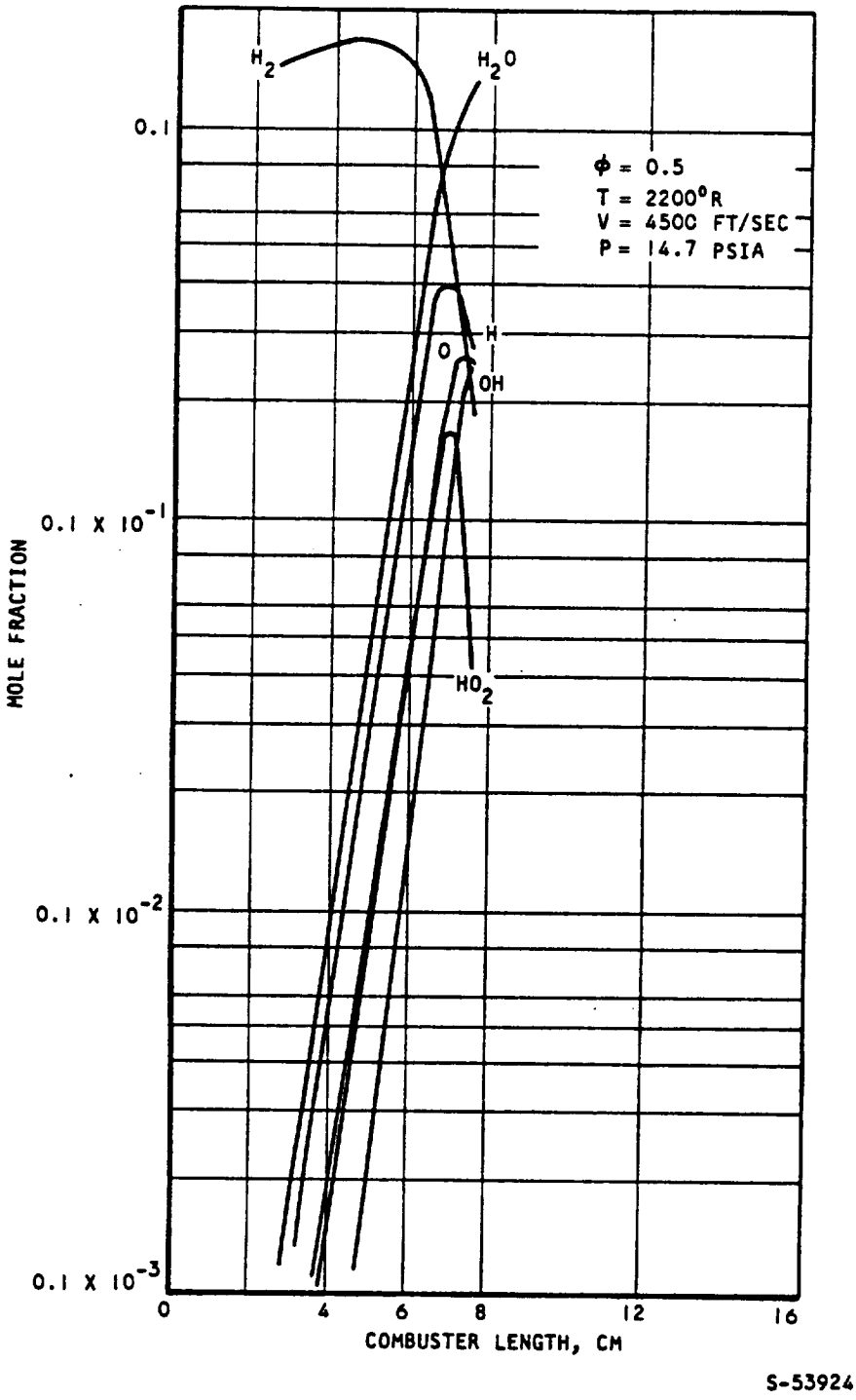

Figure 3.2-4. Species Concentration as a Function of Combustor Length for an Initial Static Temperature of 2200°R

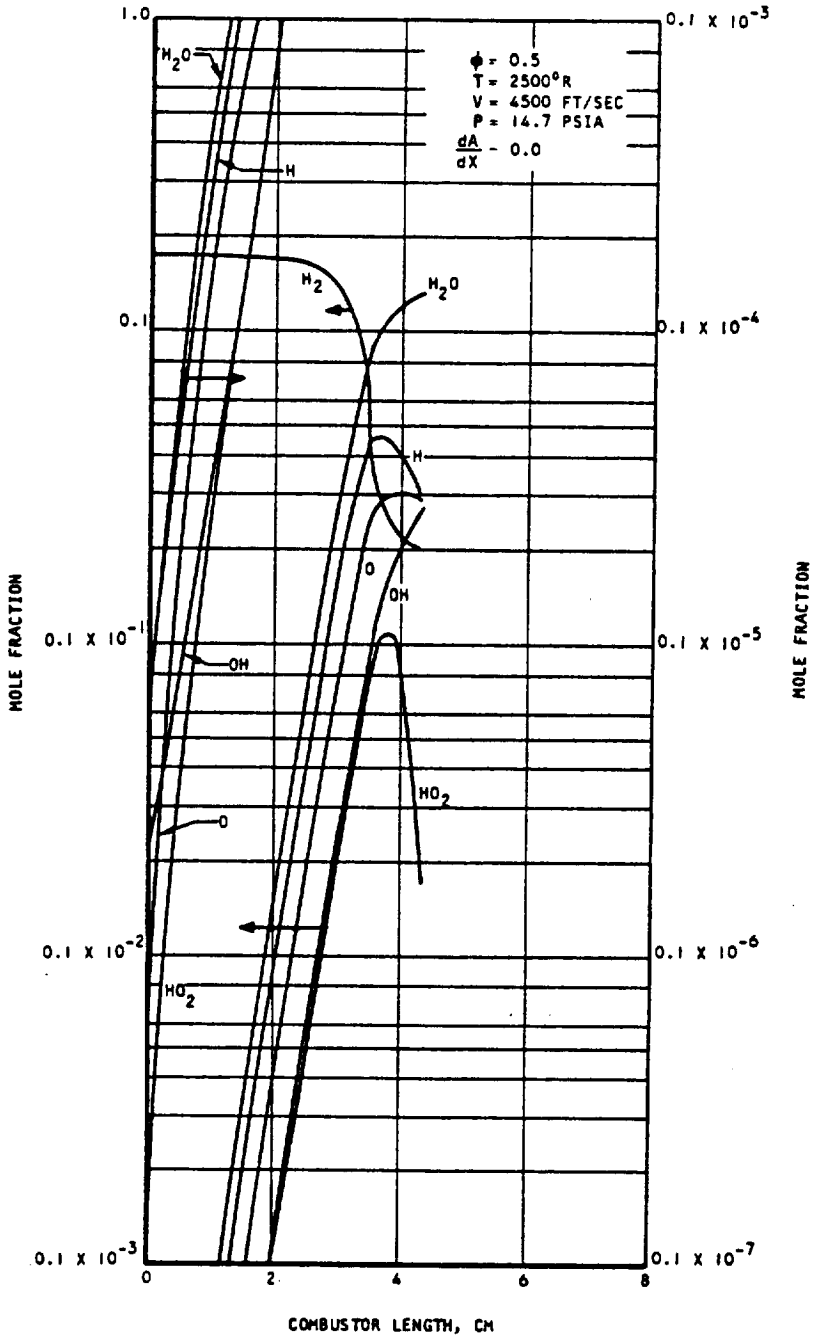

S-53951

Figure 3.2-5. Species Concentration as a Function of Combustor Length for an Initial Static Temperature

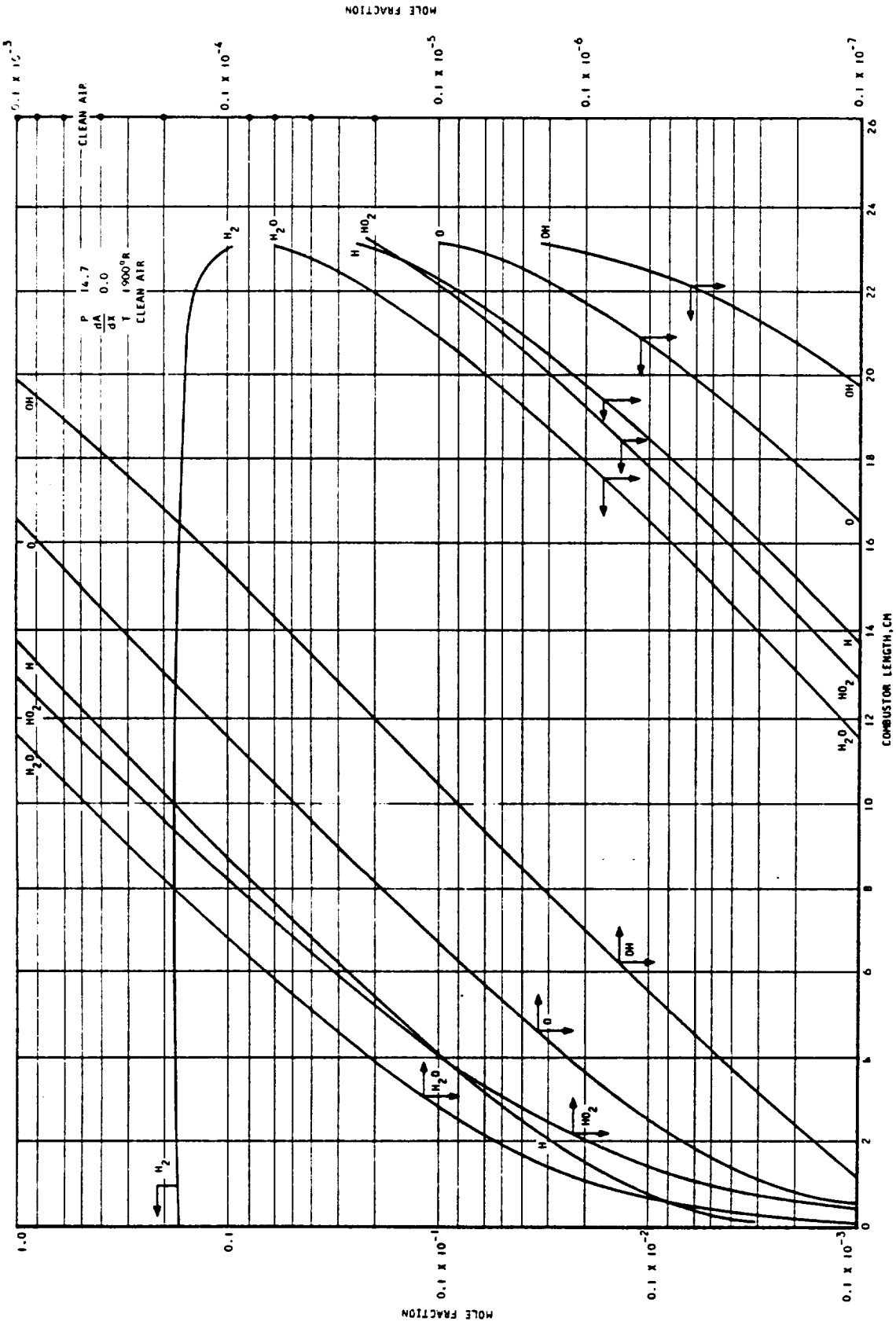

Figure 3.2-6. Species Concentration as a Function of Combustor Length for a Static Temperature of 1900°R

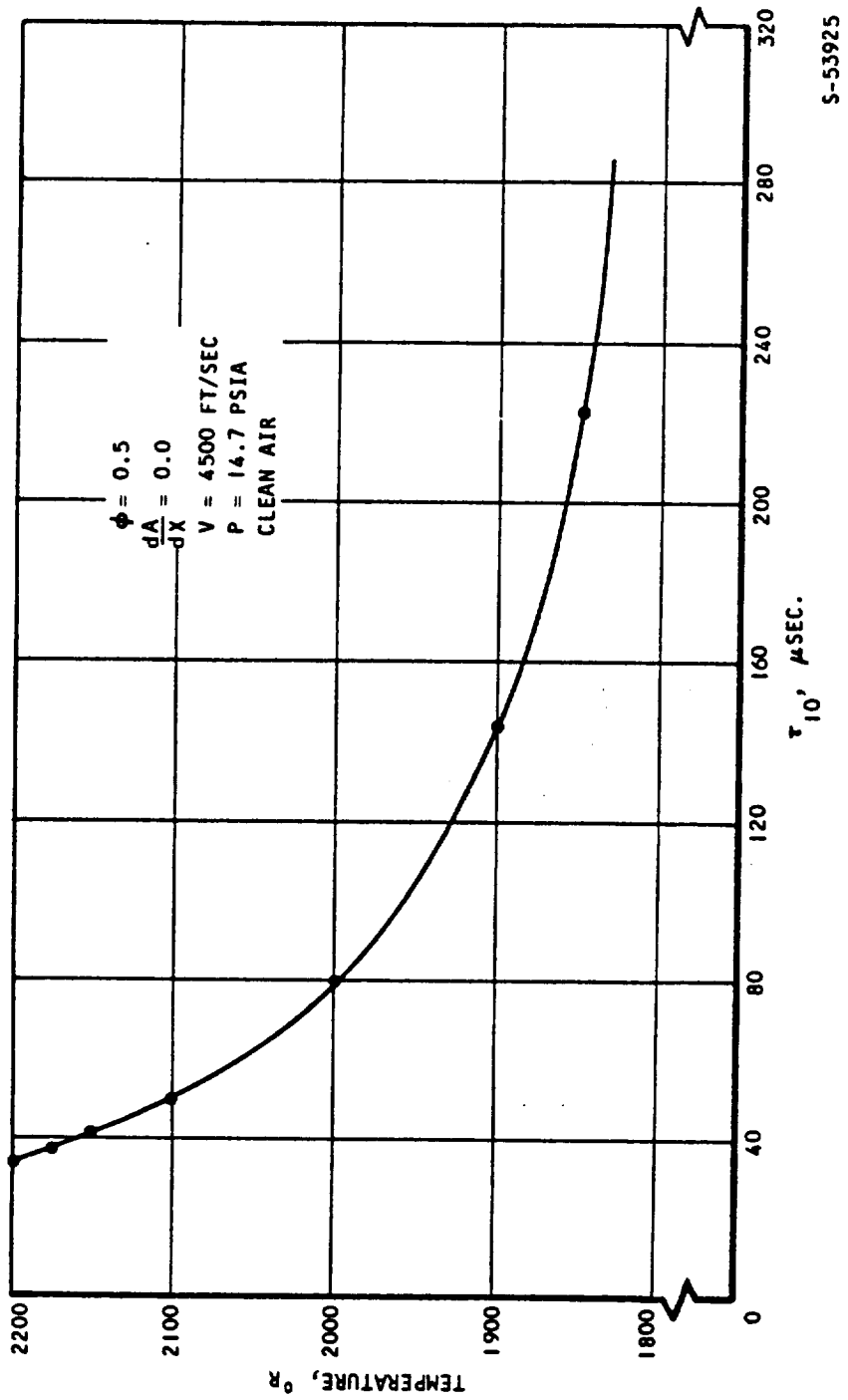

Figure 3.2-7. Effect of Initial Static Temperature on Total Ignition Delay

TABLE 3.1-2 (REFERENCE 3-5)

REACTION-RATE CONSTANTS

	D	E	F	DC	EC	FC
1	.23000+14	.00000	-.26200+04	.21592-01	.28430-00	..79233+04
2	.10000+15	.00000	-.80500+04	.40779+03	-.41038-00	-.86628+04
3	.12000+14	.00000	-.46300+04	.18825+01	.21810-01	-.91546+03
4	.10000+22	-.15000+01	-.51900+05	.26160+01	.63998-02	-.52421+05
5	.86000+15*	.00000	.64400+03	.69905-01	.28001-00	.23858+05
6	.54000+12	.00000	-.12090+05	.66604-00	-.46383-01	-.76370+04
7	.29000+15	.00000	-.94000+04	.87164+02	-.26247-00	-.88387+04
8	.40000+19	-.10000+01	.00000	.51895-00	.15772-01	.51506+05
9	.11370+26	-.25000+01	-.59400+05	.78438+03	-.42620-00	-.60168+05
10	.75000+20	-.10000+01	.00000	.59569-02	.27819-00	.60344+05
11	.25000+13	.0000	-.19630+05	.76439+03	-.38806-00	-.95775+04

$$b_w = 5.0\ X_{H_2} + 1.75\ X_{O_2} + 2.5\ X_{N_2} + 1.00\ X_{AR} + 30.0\ X_{H_2O}$$

*2.2 + 15 used in calculations reported in Section 6.

There are a number of quantitative definitions of the ignition delay time which can be found in the literature:

(a) The time required for the concentration of OH radical to reach 10^{-6} mole/liter (Reference 3-2)

(b) The time at which a point of inflection of atomic hydrogen is observed (Reference 3-3)

(c) The location of the intersection of the slopes of the initial and maximum temperature rise (Reference 3-4)

(d) The time at which a point of inflection of OH radicals is observed

(e) The point of 0.1 percent density decrease

(f) The time it takes for the temperature to increase 5 percent of the total temperature rise (Reference 3-5)

All these assumptions in defining the ignition delay period are reasonable and lead to the same conclusion (Reference 3-6). For convenience, definition (a) is used in this report. The summarized results are shown in Figure 3.2-7. As expected, the ignition delay increases with decreasing temperature and does not ignite at all when temperature decreases to 1800°R. The resultant pressure and chemical efficiency variations are presented in Figures 3.2-2 and 3.2-3. The chemical efficiency is an approximation based on the percentage of reacted hydrogen molecules by weight. For complete combustion, the percentage of unreacted hydrogen molecules increases with combustion temperature. Therefore, the approximation of chemical efficiency will be pessimistic, especially at high combustion temperatures. The approximation was used as a calculation convenience and is permissible because only qualitative results are being sought.

TABLE 3.2-1

MASS FRACTIONS OF REACTING FLOW
(EQUIVALENCE RATIO = 0.5)

	Clean Air	5.05 Percent Vitiation Static Temperature		49.25 Percent Vitiation Static Temperature	
		2000°R	2300°R	2000°R	2300°R
H	1.000-09	1.000000-09	1.0000-09	1.000000-09	1.00000-09
O	1.0000-09	1.000000-09	0.296-07	1.000000-09	0.346-07
N_2	0.7569-00	0.71959-00	0.71981-00	0.38336-00	0.38348-00
H_2	0.1440-01	0.14634-01	0.14634-01	0.17194-01	0.17194-01
O_2	0.2287-00	0.23228-00	0.23206-00	0.27292-00	0.27279-00
OH	1.0000-09	0.345-06	0.3438-05	0.116-05	0.116-04
H_2O	1.0000-09	0.33491-01	0.33491-01	0.32653-00	0.32653-00
HO_2	1.0000-09	1.000000-09	1.0000-09	1.000000-09	0.330-07
H_2O_2	1.0000-09	1.000000-09	1.0000-09	1.000000-09	1.0000-09

3.2.2 Effect of Pressure

Chemical kinetics calculations were made for a hydrogen-air mixture at a temperature of 1900°R for several initial pressures in a constant area duct. The ignition delay times obtained from these calculations are presented in Figure 3.2-8. At low pressures, the collision rate of molecules is small due to the low density of the mixture, therefore, the chain-branching reactions are slow which results in long ignition delays. As the pressure is increased, more and more molecules collide per second and chain-branching reactions become faster and faster resulting in shorter ignition delays. However, when the pressure is further increased, the ignition delay time reaches a minimum point beyond which it increases with increasing pressure. This phenomenon is caused by the following chain-breaking reaction:

$$H + O_2 + M = HO_2 + M$$

where M represents any kind of molecules, such as H_2, O_2, H_2O, N_2, etc. Ordinarily HO_2 is a very unstable combination of hydrogen and oxygen because more energy is released upon its formation than is required to bring about its decomposition. However, if another molecule is present to absorb the excess energy released from the formation of HO_2, the latter may exit as an intermediate product in the chain reaction. The "third body", M, acts as an energy acceptor and stabilizer to this reaction. This reaction serves to break the hydrogen-oxygen chain reaction by removing the free hydrogen atom from the mixture. As the pressure increases, the concentration of "third body" increases and the effect of chain-breaking becomes greater than the effect of chain-branching; therefore, it increases the ignition delay time.

Figures 3.2-9, 3.2-10, and 3.2-11 show the temperature, pressure, and chemical efficiency distribution along a constant area combustor with various inlet static pressures. The concentration of species is given in Figure 3.2-12 at an inlet pressure of 25 psia.

The effect of pressure on ignition delay for an initial temperature of 2200°R is presented in Figure 3.2-13. The ignition delay time decreases with increasing pressure and no minimum point was observed up to a pressure of 65 psia. The reaction is slowed down slightly in the range of pressures from 65 to 100 psia. Figures 3.2-14, 3.2-15, and 3.2-16 show the temperature, pressure and chemical efficiency distributions, respectively, along the duct with initial inlet temperatures of 2200°R.

Calculations were also made for other inlet temperatures which are shown in Figure 3.2-17. As the static temperature is increased from 1900°R to 2200°R, the pressure at which the minimum delay time occurs moves progressively to higher values and the curves become flatter. Thus, at the higher initial temperature of 2200°R, ignition delay was not affected as much by static pressure as at an initial temperature of 1900°R.

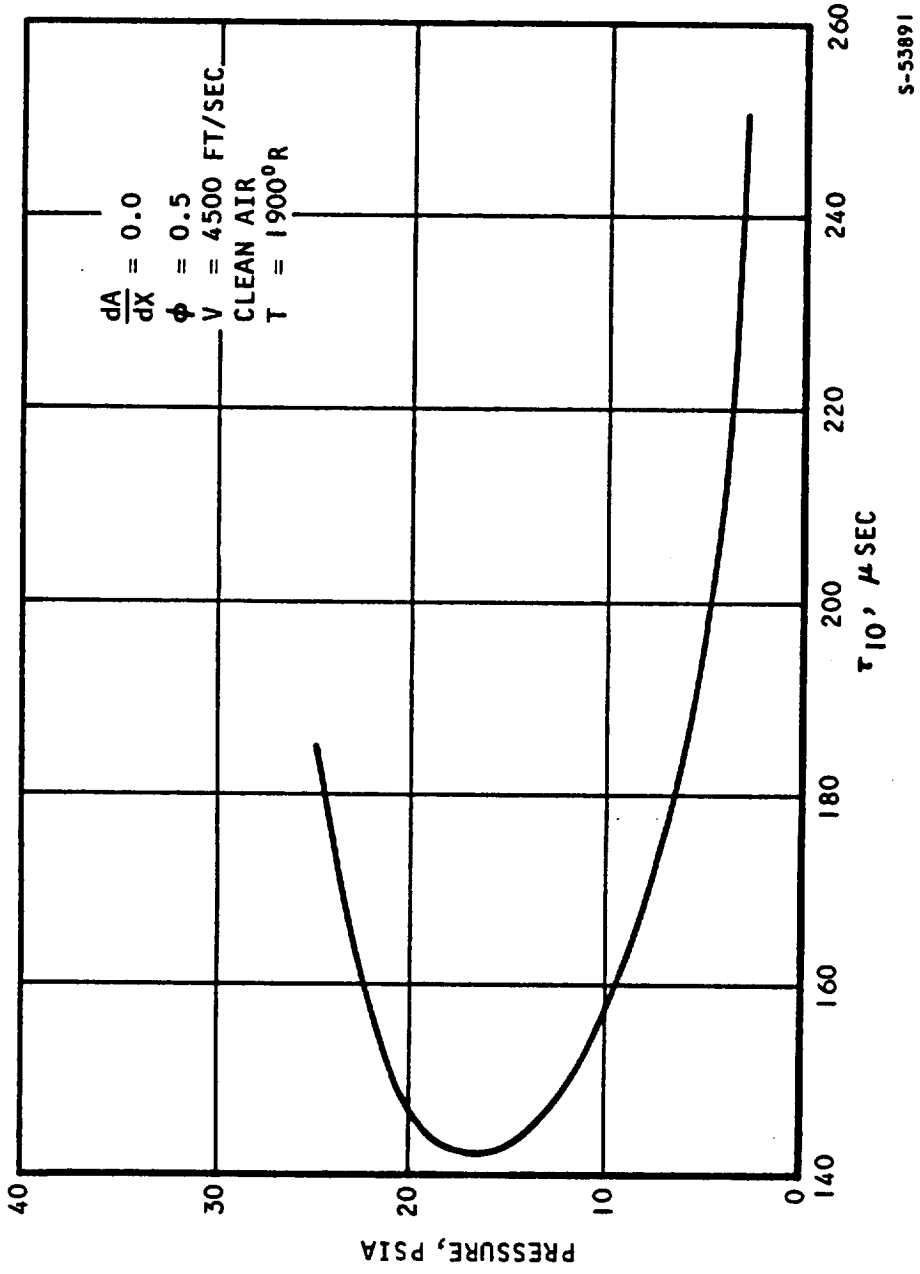

Figure 3.2-8. Effect of Initial Static Pressure on Total Ignition Delay

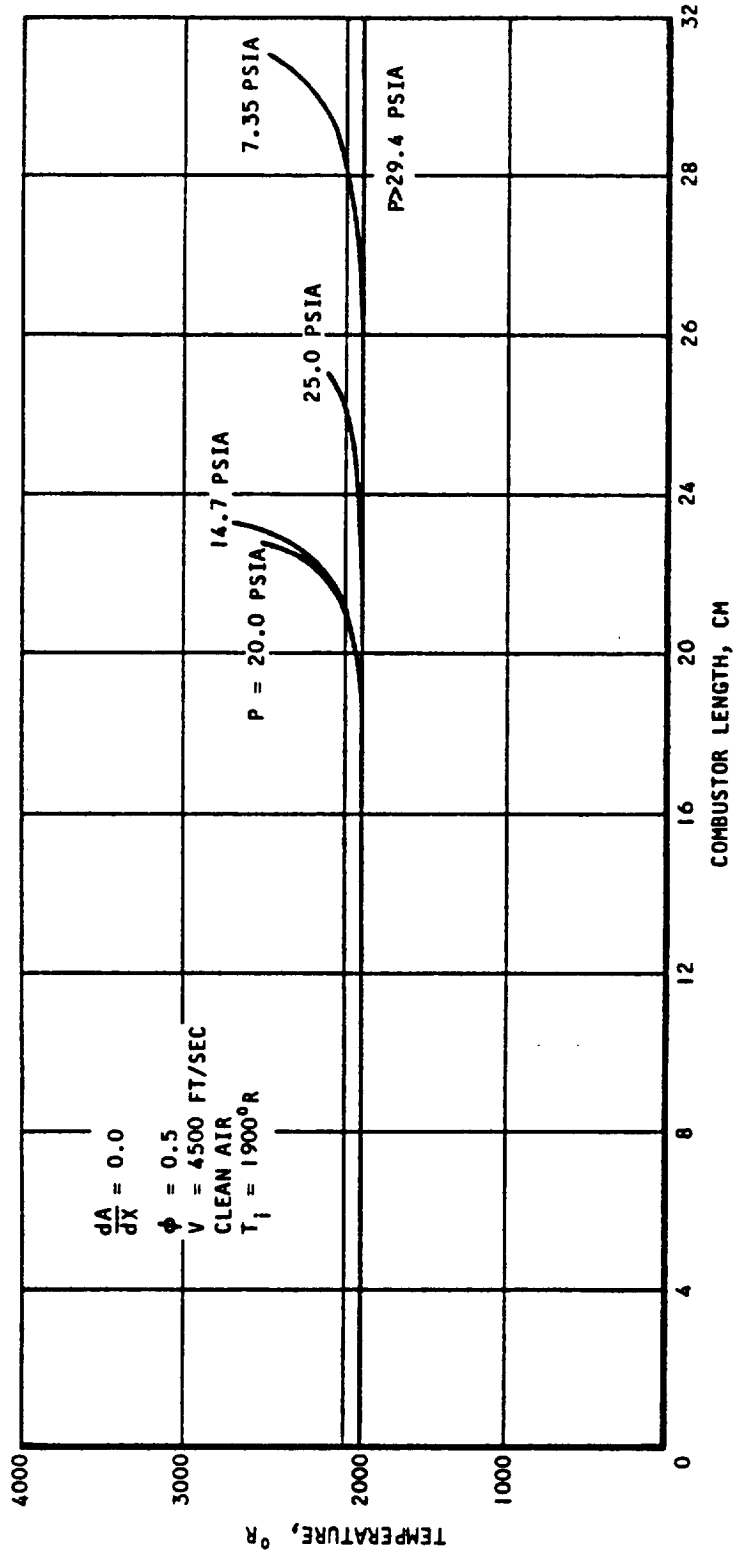

S-53926

Figure 3.2-9. Effect of Initial Static Pressure on Combustor Length and Temperature

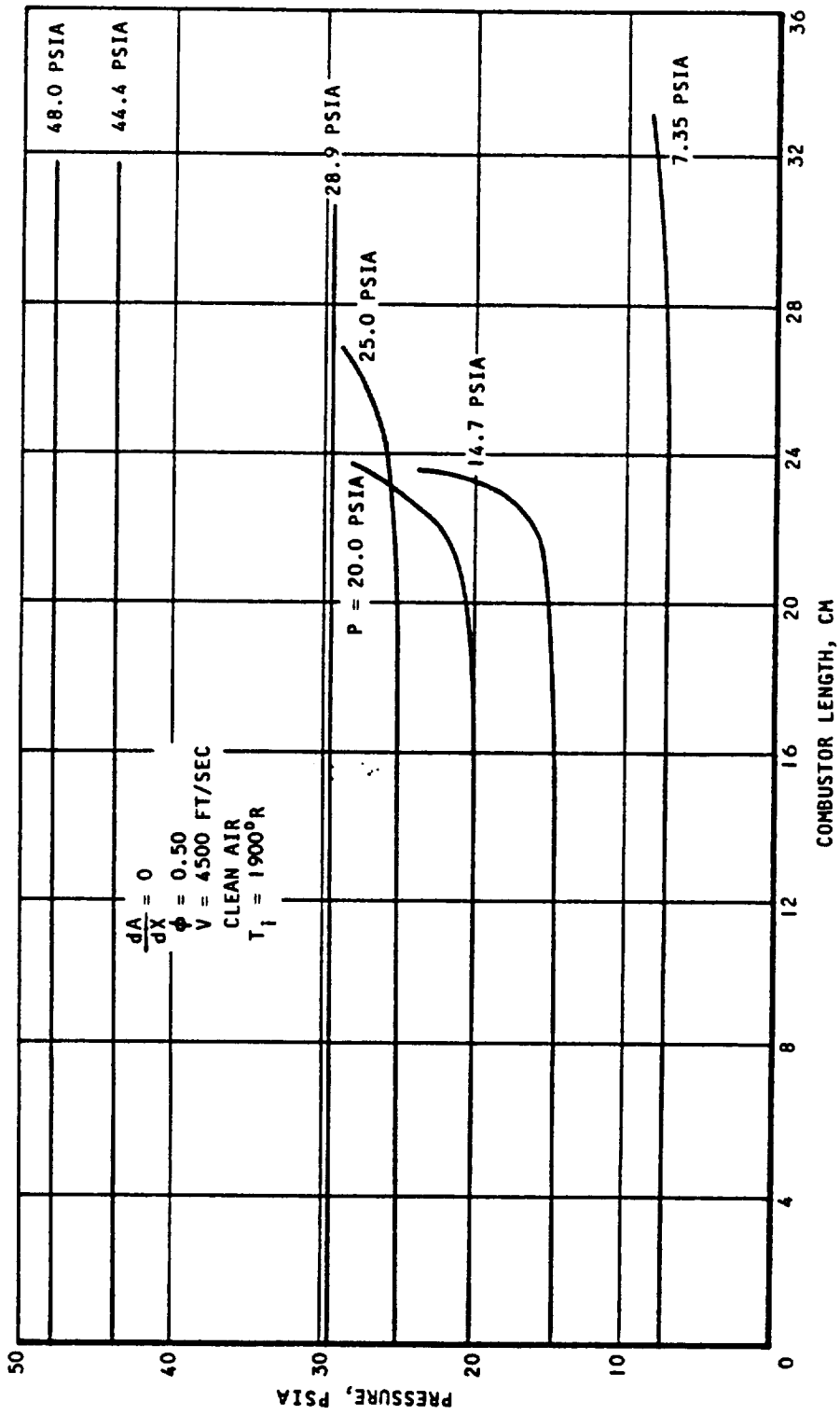

Figure 3.2-10. Effect of Initial Static Pressure on Pressure as a Function of Combustor Length

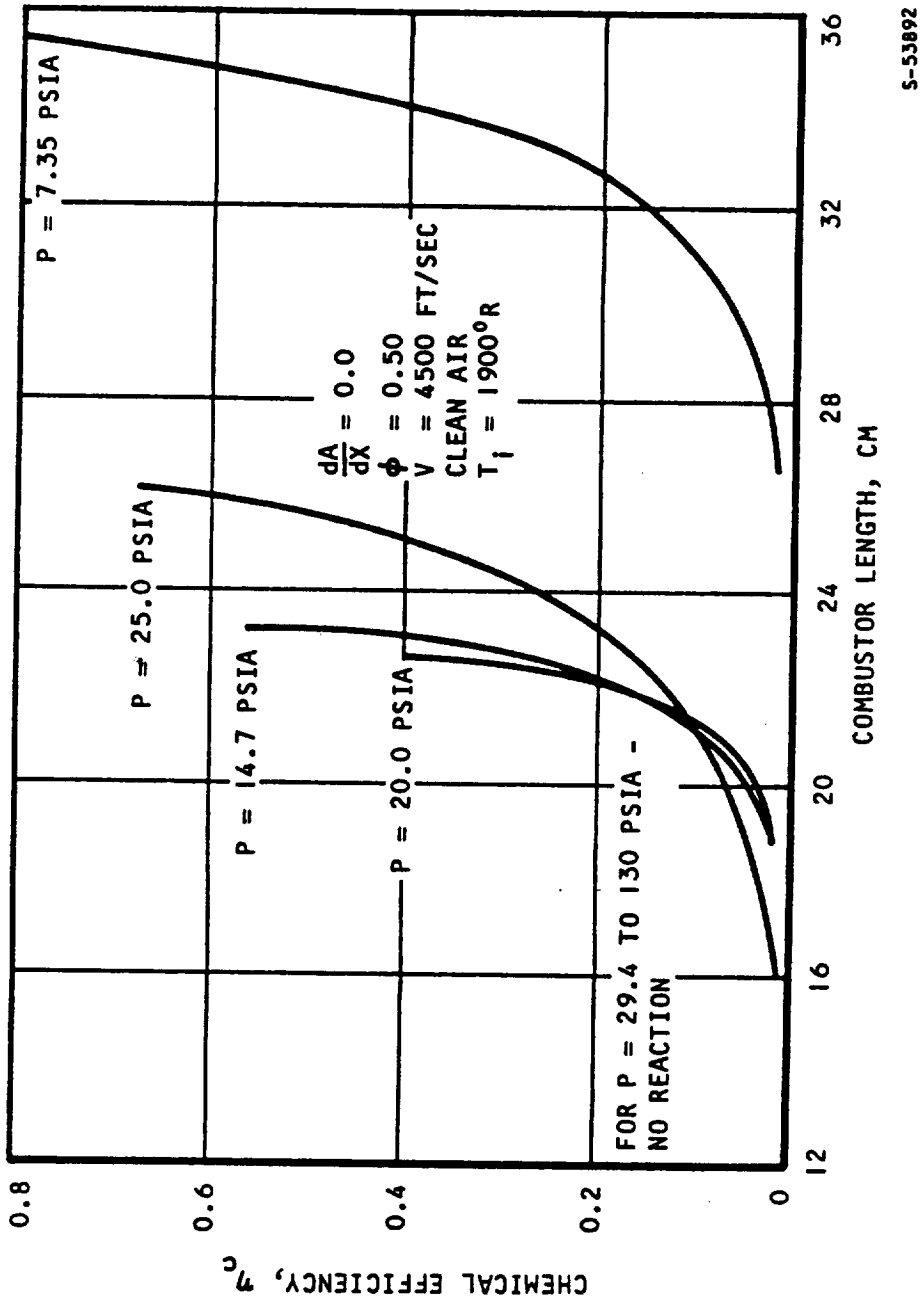

Figure 3.2-11. Effect of Initial Static Pressure on Chemical Efficiency as a Function of Combustor Length

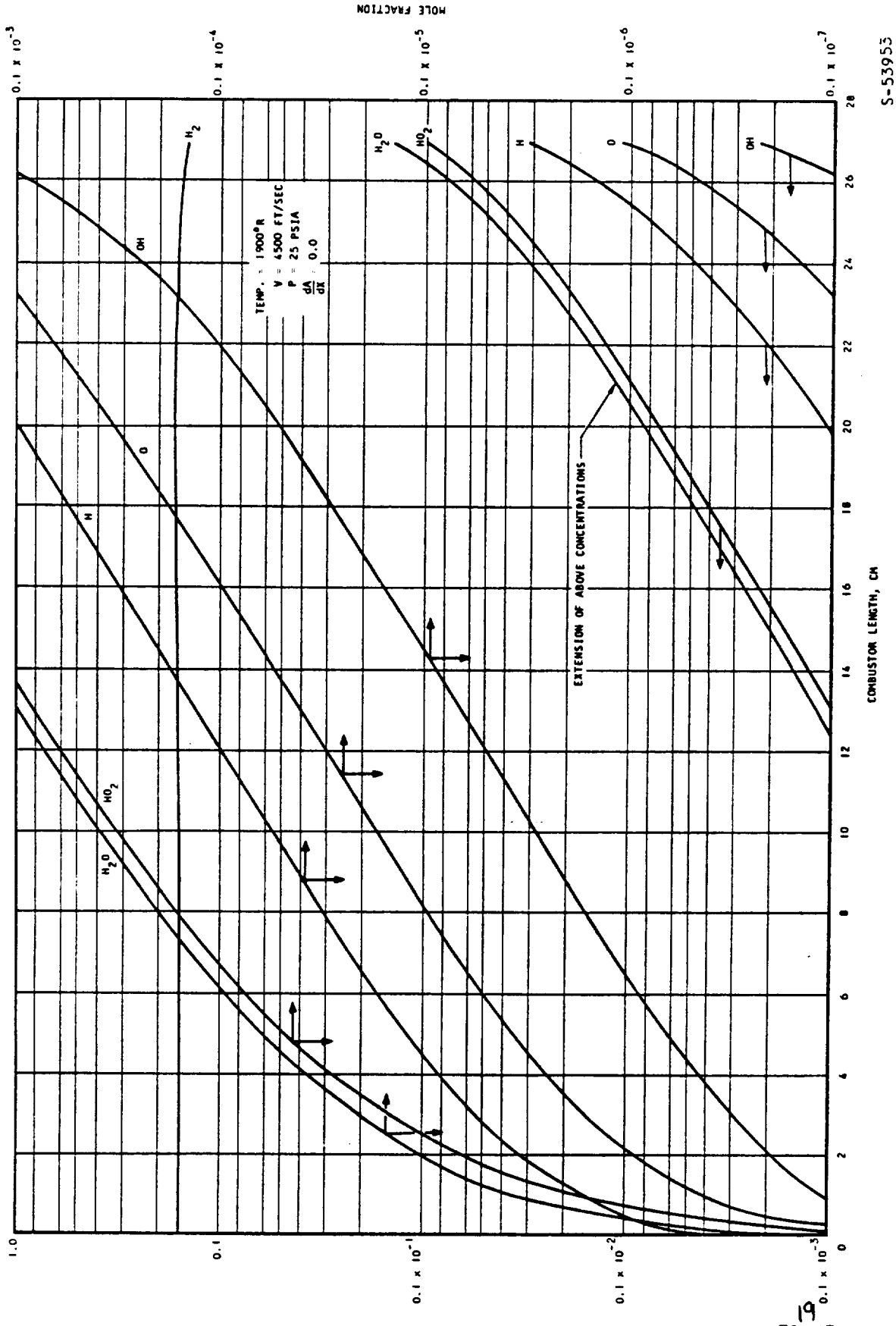

Figure 3.2-12. Species Concentration as a Function of Combustor Length

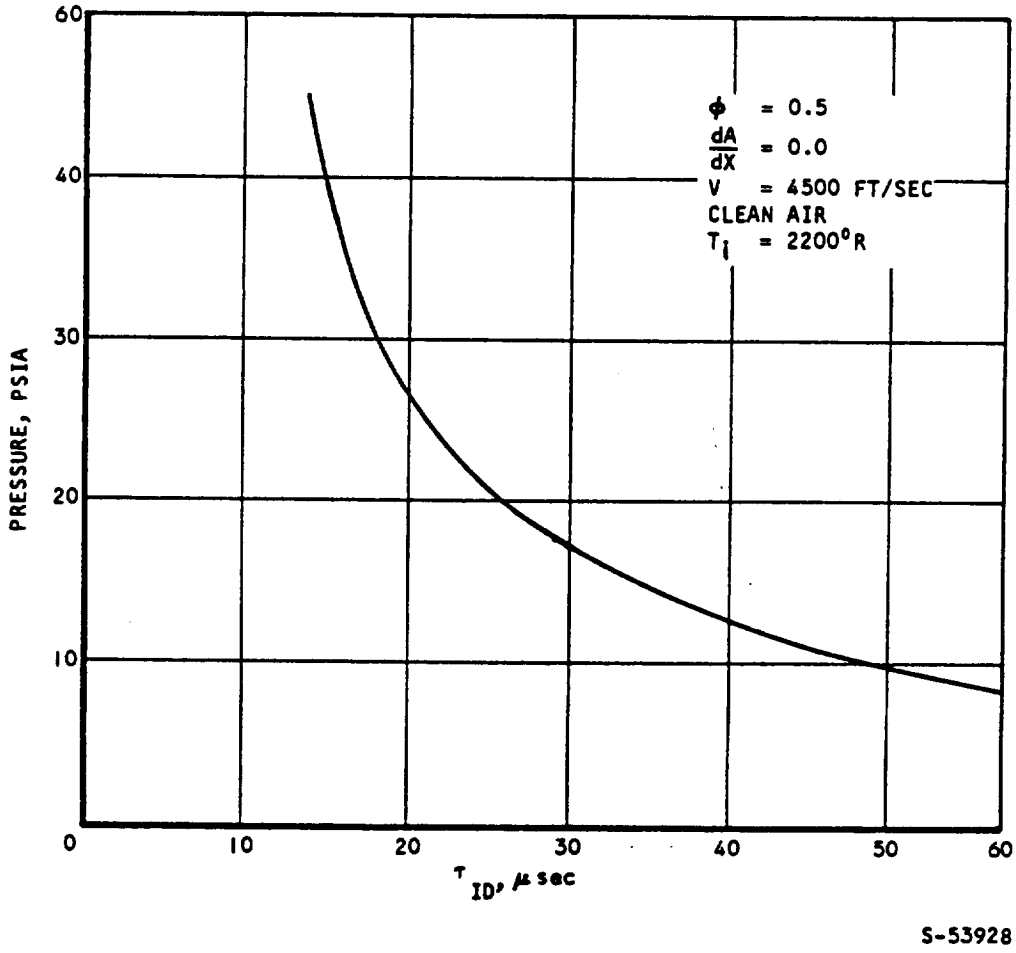

Figure 3.2-13. Effect of Initial Static Pressure on Ignition Delay

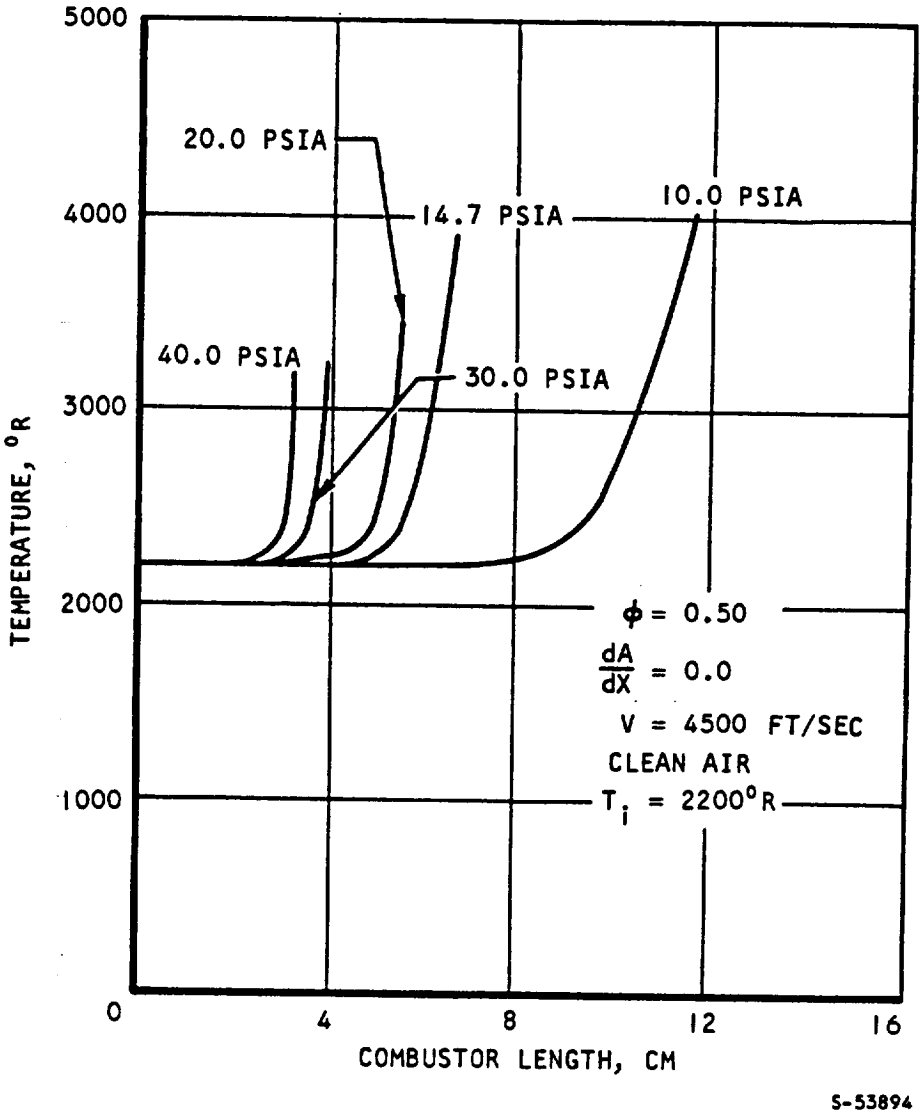

Figure 3.2-14. Effect of Initial Static Pressure on Temperature as a Function of Combustor Length

significant. Therefore, at low initial static temperatures, vitiation caused higher ignition delays. At initial static temperatures above 2200°R the difference in ignition delay time for vitiated and clean air were less than 20 μsec and therefore can be considered negligible.

3.2.5 Effect of Initial Radicals (Carriers)

In order to see the effect of initial radicals or carriers on the chemical reaction as a function of initial static temperature, chemical kinetic studies were made for two vitiated mixtures with initially non-equilibrium free-radical concentrations (see Table 3.2-2). Results are shown in Figures 3.2-23 through 3.2-28 as plots of temperature, chemical efficiency, and pressure versus combustor length with different initial temperatures for 10 percent and 2 percent of initial carriers. The percent of carriers indicates the amount of hydrogen consumed in a constant area duct if the initial temperatures were 2200°R. As expected, the presence of initial carriers accelerated the chemical reaction by the chain-branching reactions of Table 3.1-1, steps 2, 3, and 7. Initial carriers had the effect of transposing the region of long ignition delay to lower temperatures. The autoignition temperatures (those temperatures below which chemical reaction ceased to occur) were lowered to 1600°R and 1400°R for the vitiated mixtures of 2-percent and 10-percent reacted-chain carriers respectively, as compared to 1800°R for clean air. Ignition delay could not be determined by the previously used criterion of OH concentration because of the presence of initial carriers. Results based on the chemical efficiencies of 80 percent and 40 percent for both vitiated mixtures and clean air are shown in Figure 3.2-29. For a given combustor length, Figure 3.2-29 gives the required initial static temperature to produce a given chemical efficiency.

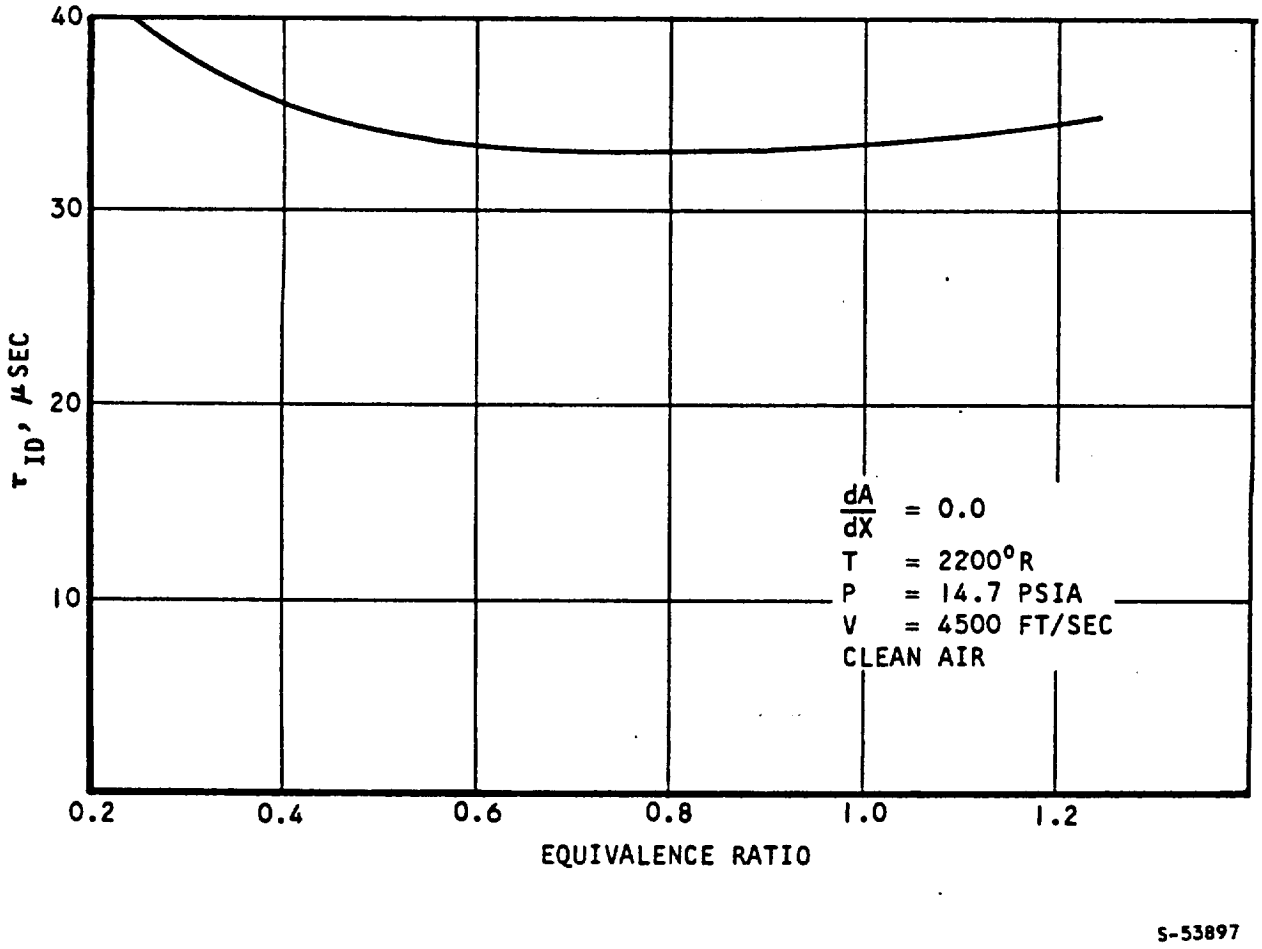

Figure 3.2-18. Effect of Equivalence Ratio on Ignition Delay

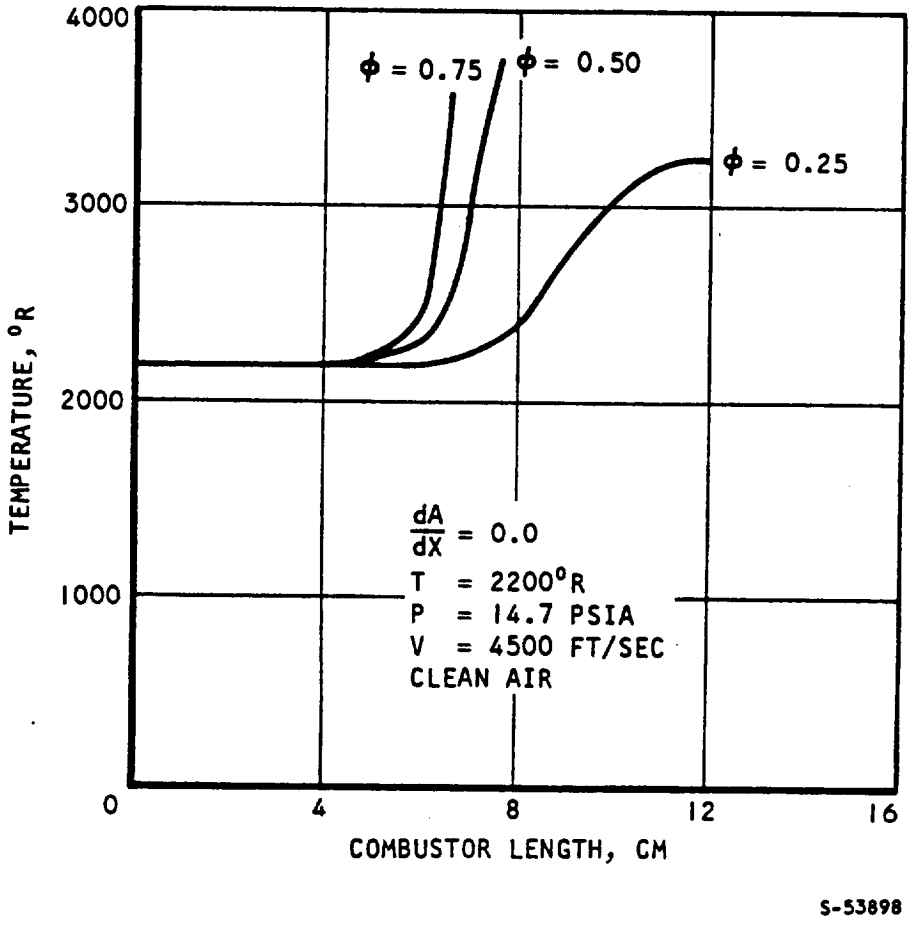

Figure 3.2-19. Effect of Equivalence Ratio on Static Temperature as a Function of Combustor Length

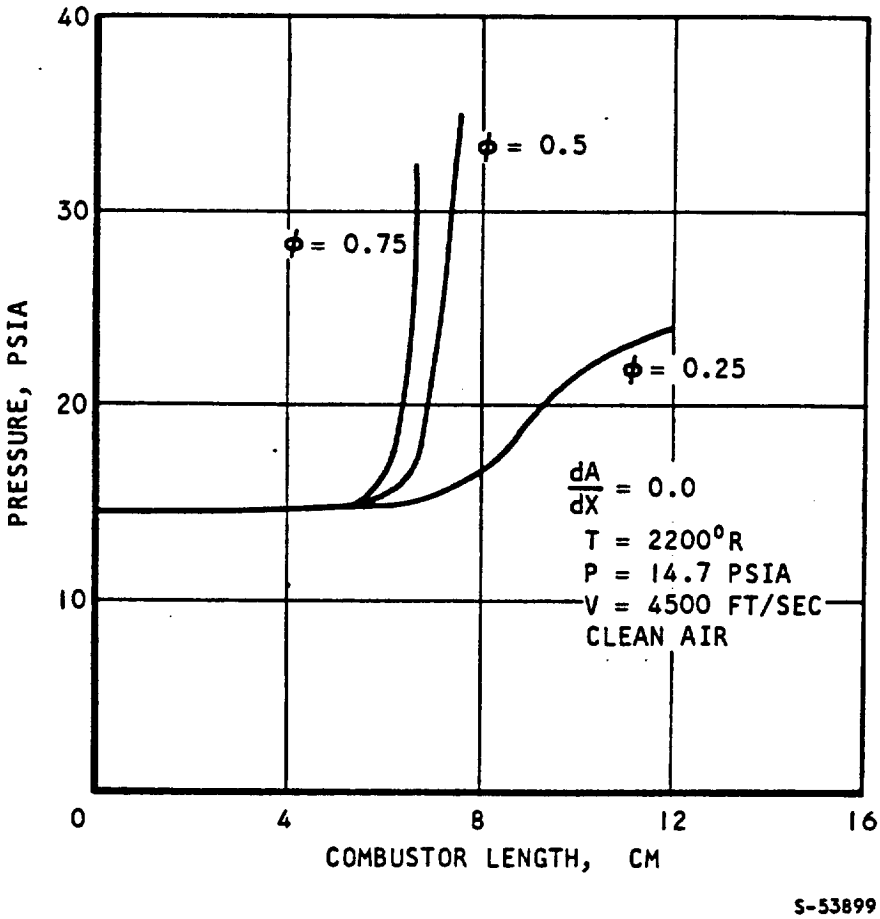

Figure 3.2-20. Effect of Equivalence Ratio on Static Pressure as a Function of Combustor Length

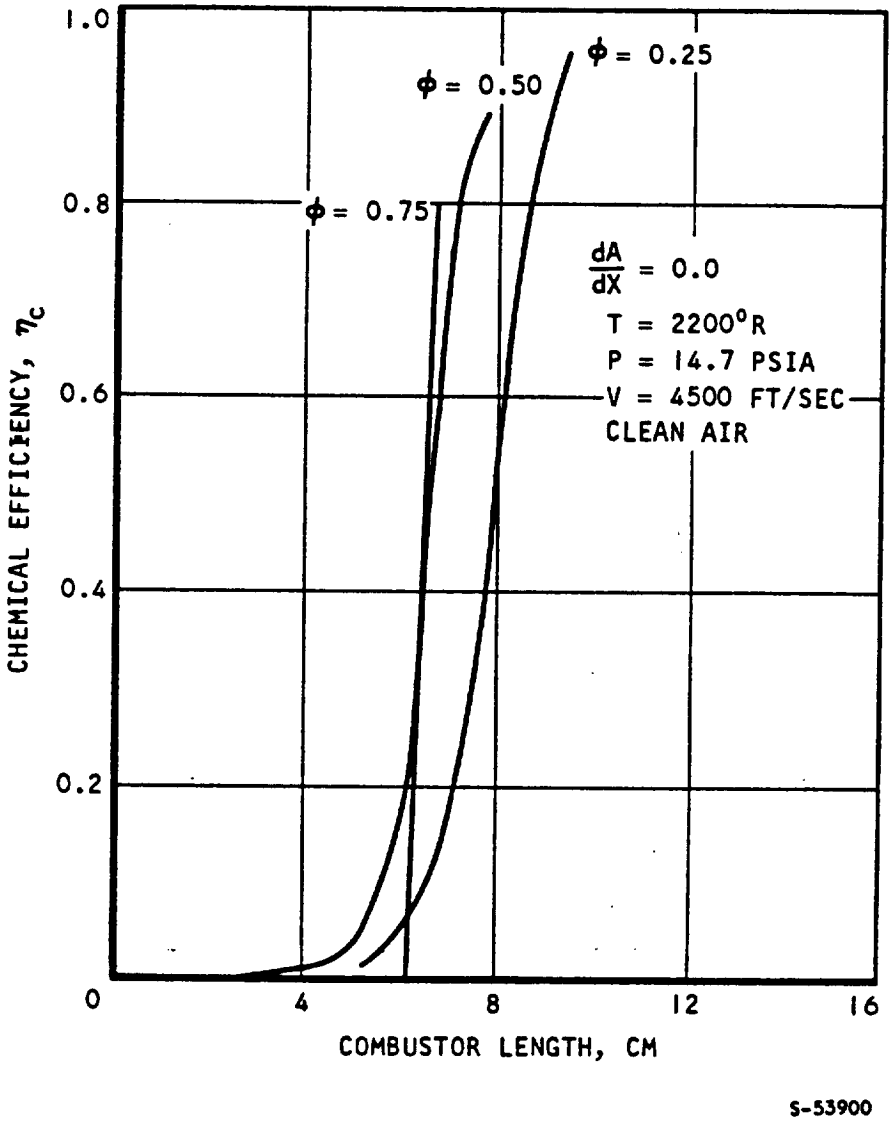

Figure 3.2-21. Effect of Equivalence Ratio on Chemical Efficiency as a Function of Combustor Length

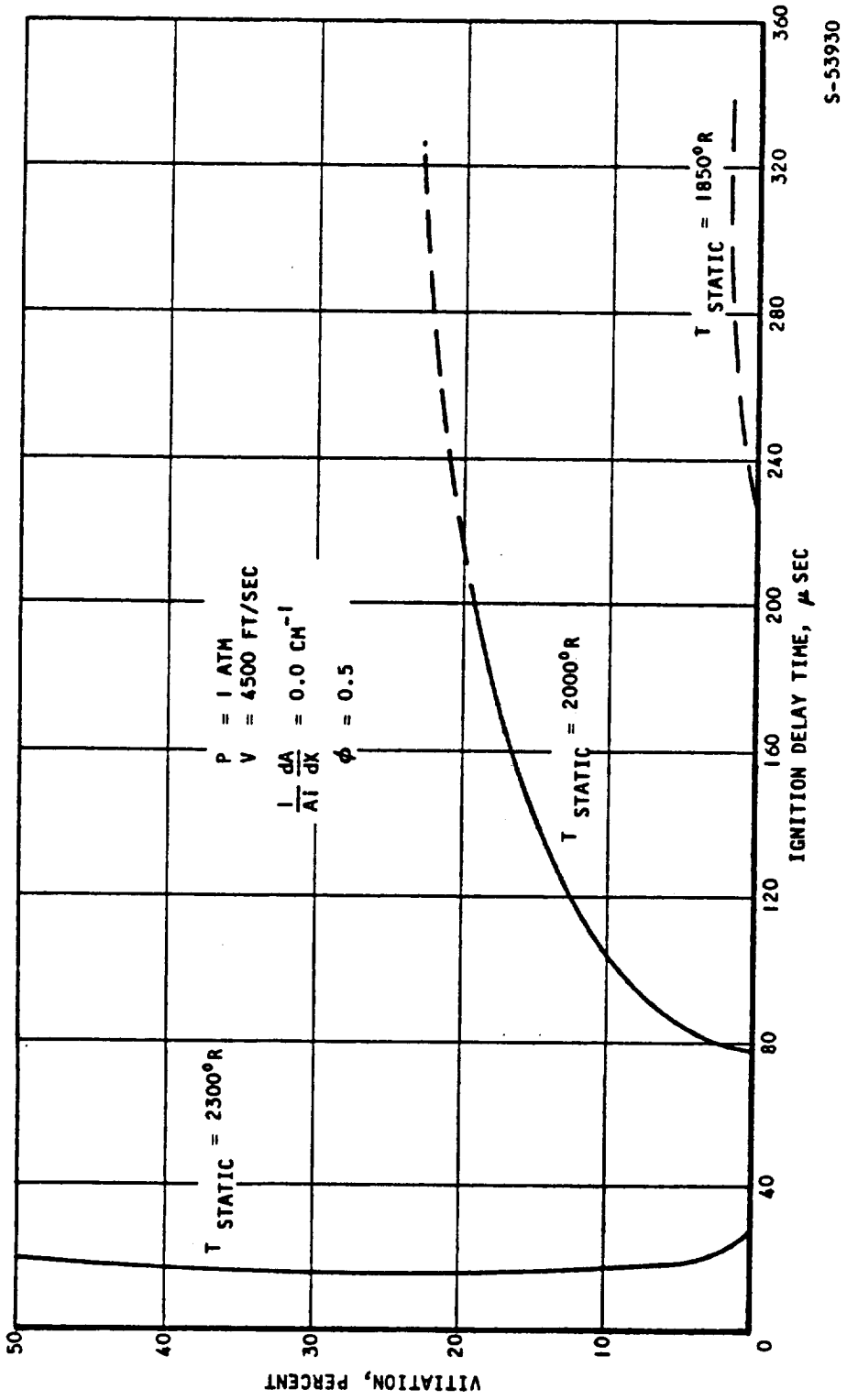

Figure 3.2-22. Effect of Vitiation on Ignition Delay Time

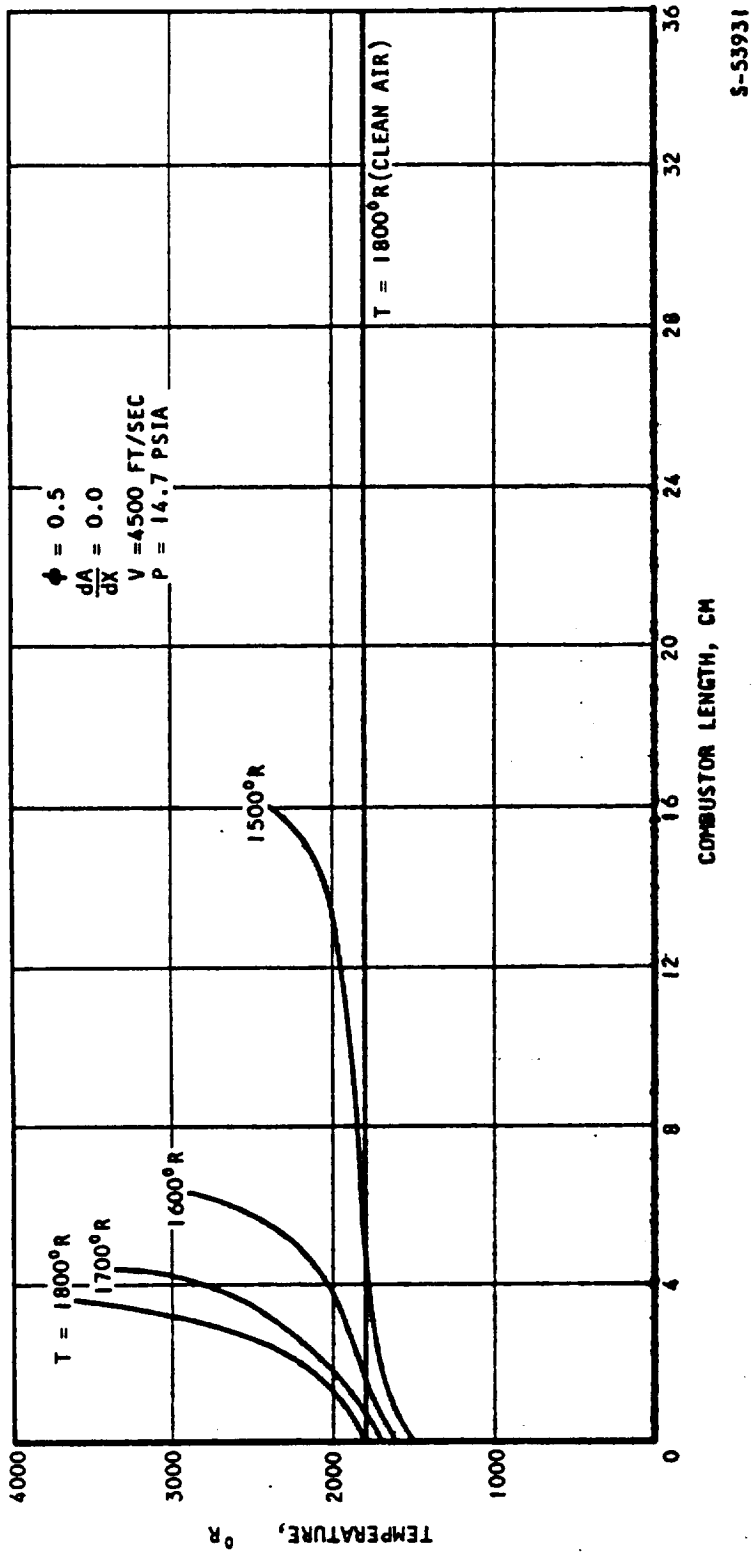

Figure 3.2-23. Effect of 10-Percent Carriers on Static Temperature as a Function of Combustor Length for Several Initial Static Temperatures

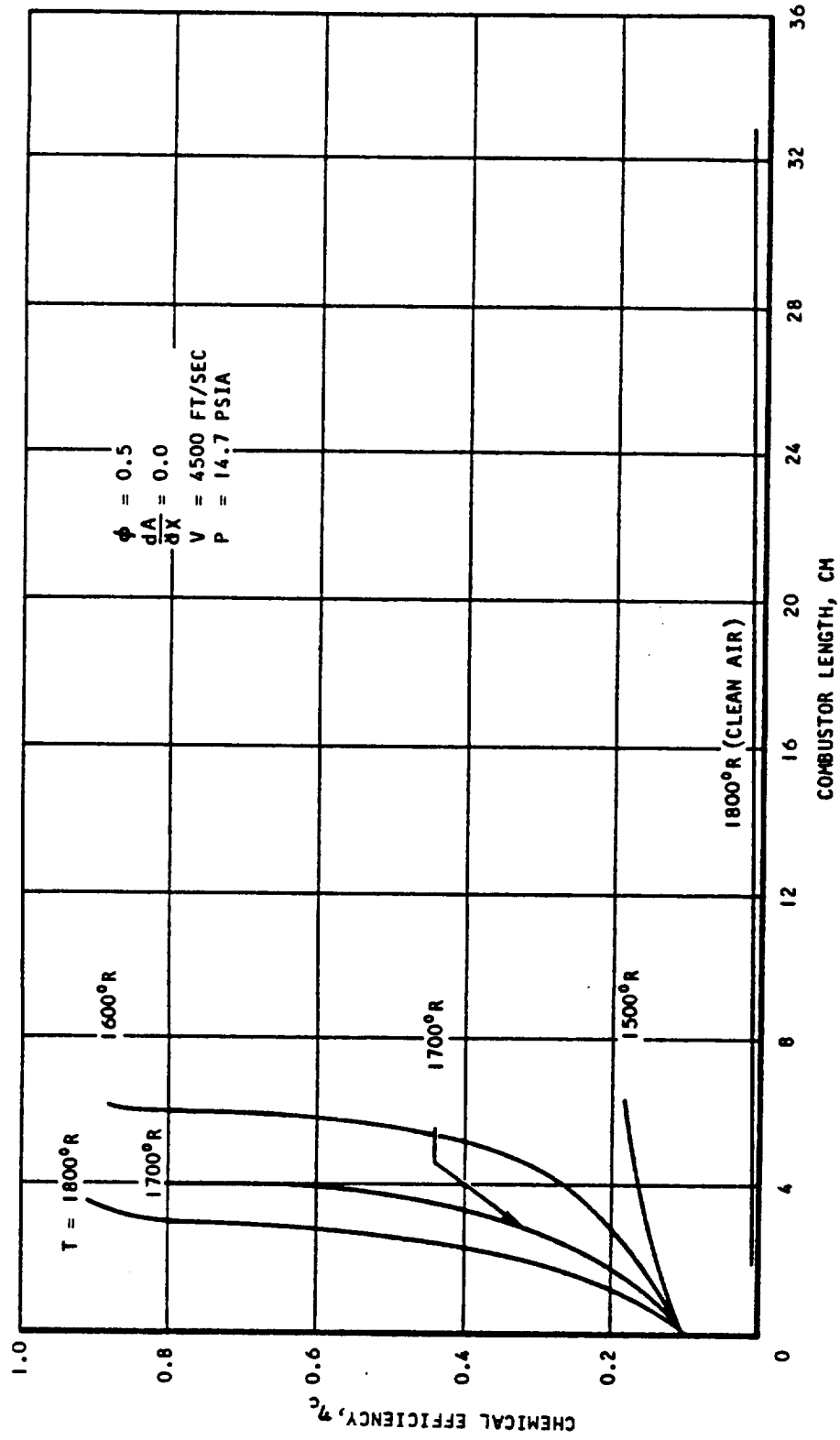

Figure 3.2-24. Effect of 10-Percent Carriers on Chemical Efficiency as a Function of Combustor Length for Several Initial Static Temperatures

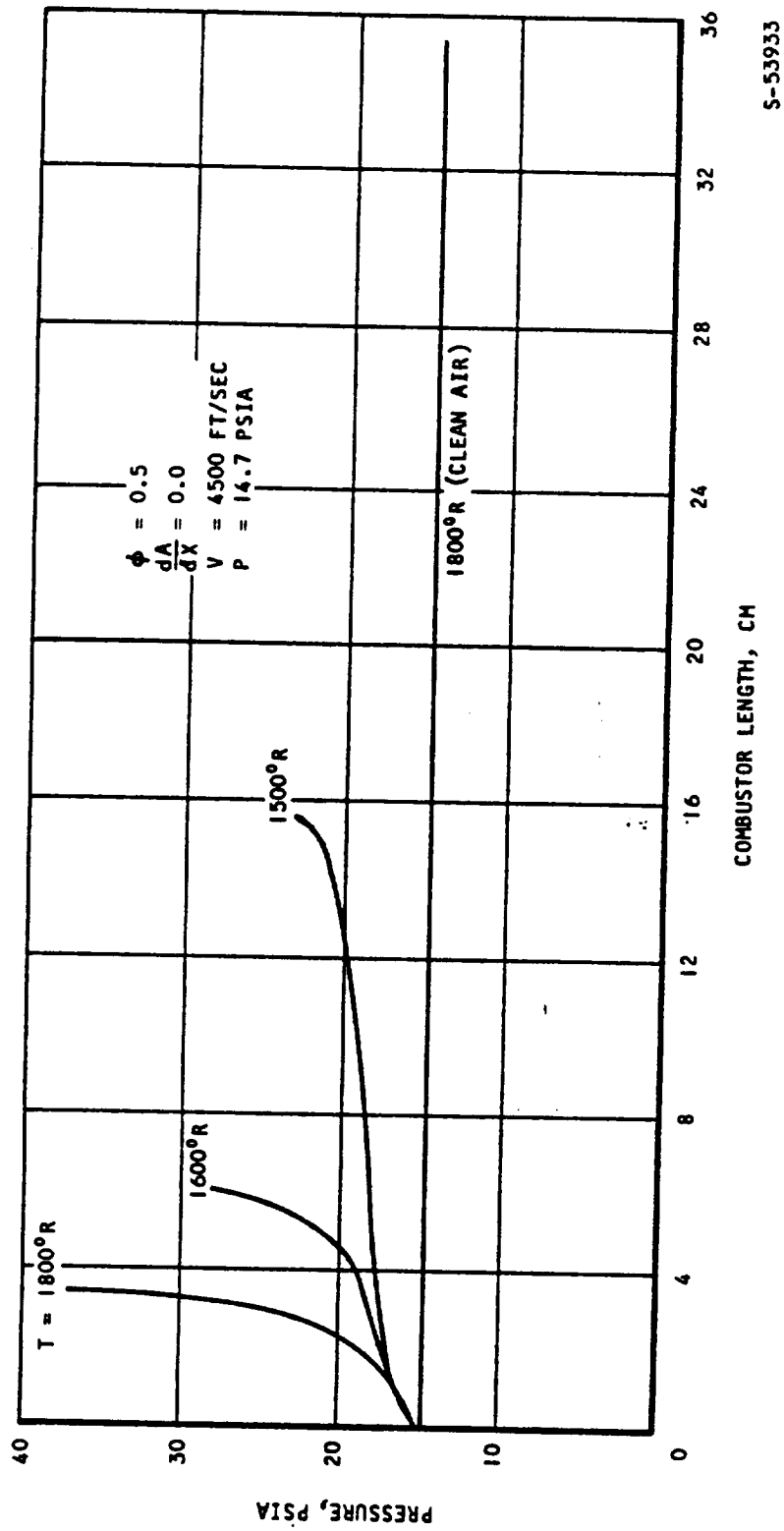

Figure 3.2-25. Effect of 10-Percent Carriers on Static Pressure as a Function of Combustor Length for Several Initial Static Temperatures

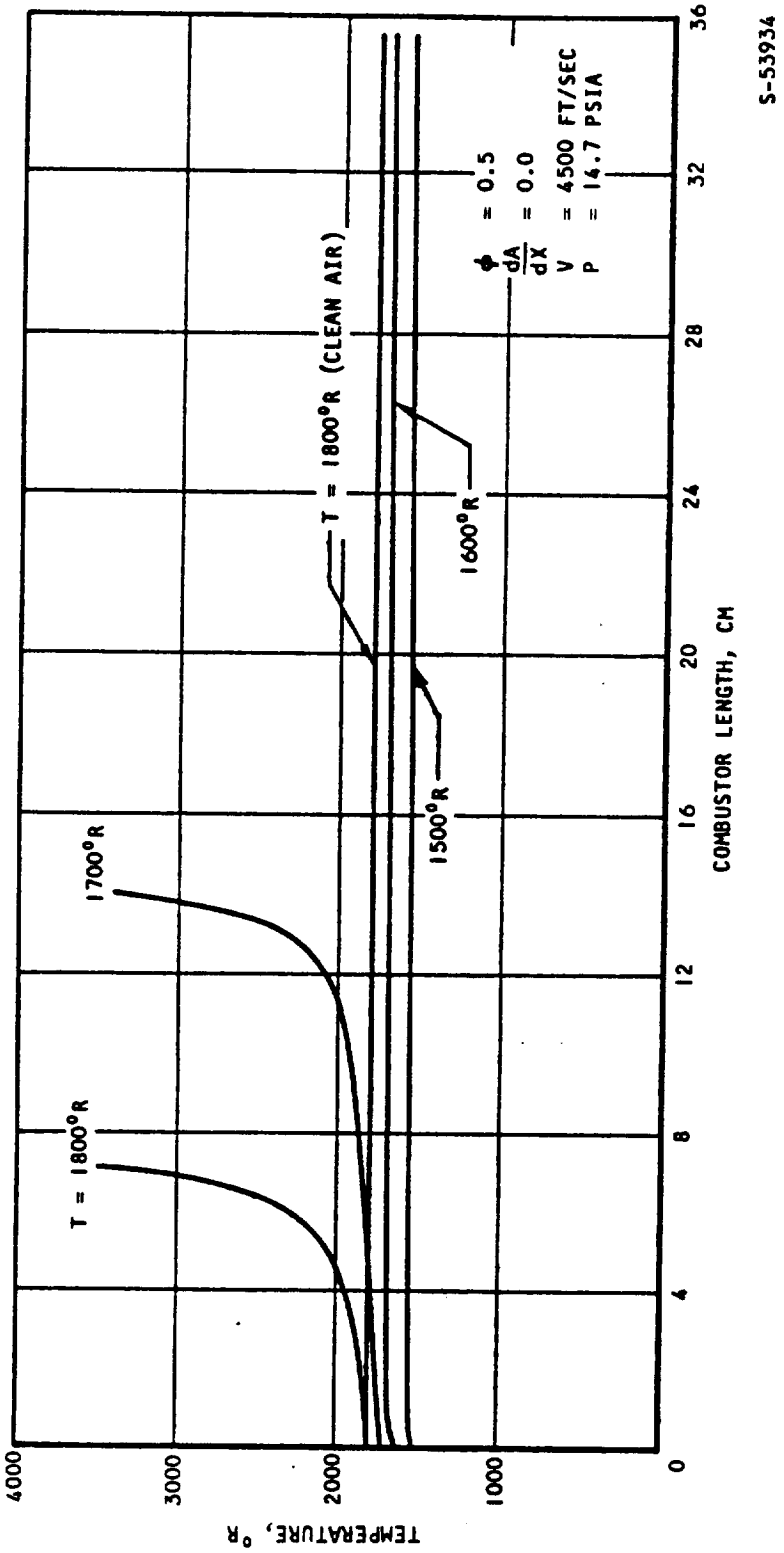

Figure 3.2-26. Effect of 2-Percent Carriers on Static Temperature as a Function of Combustor Length for Several Initial Static Temperatures

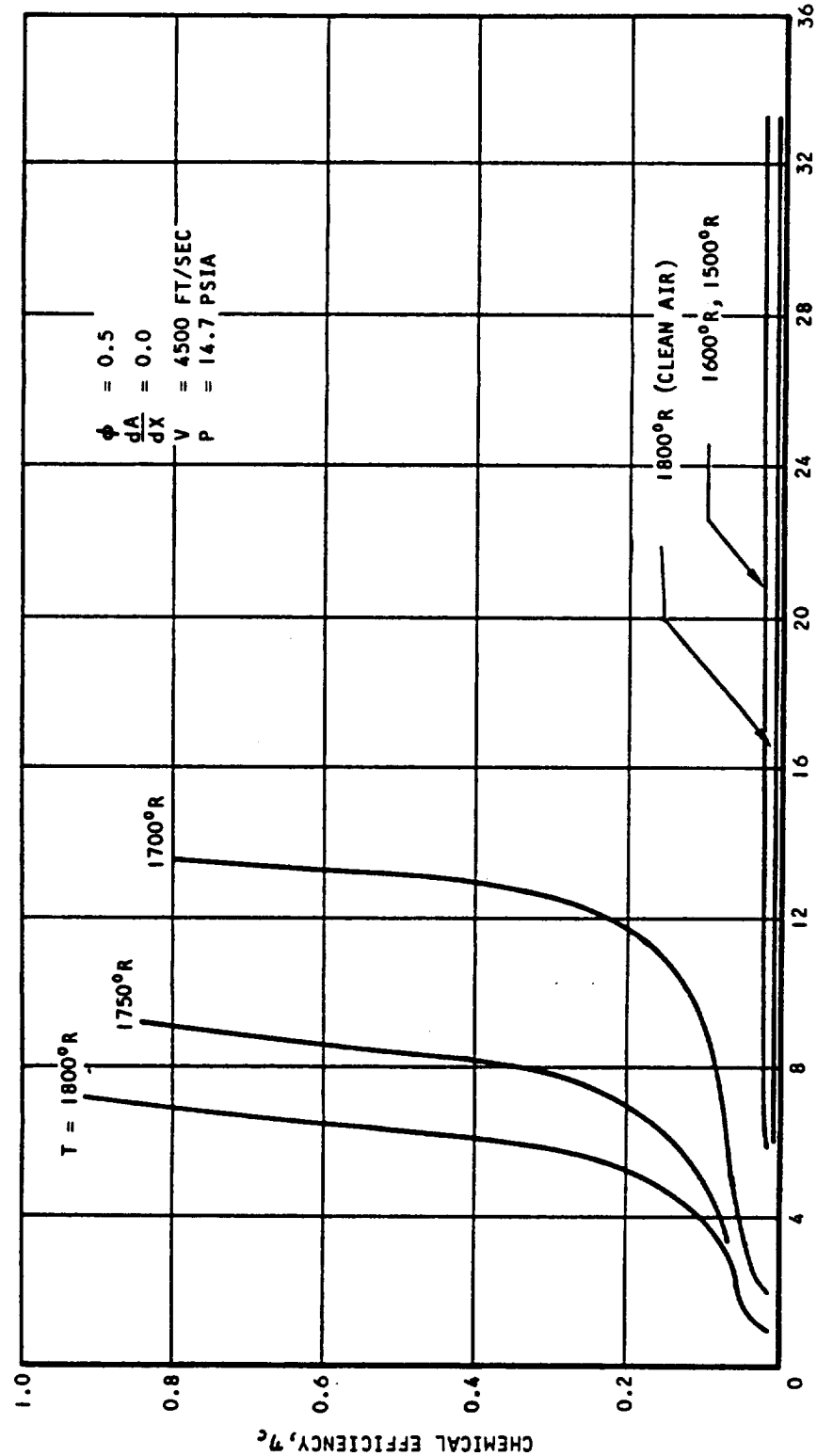

Figure 3.2-27. Effect of 2-Percent Carriers on Chemical Efficiency as a Function of Combustor Length for Several Initial Static Temperatures

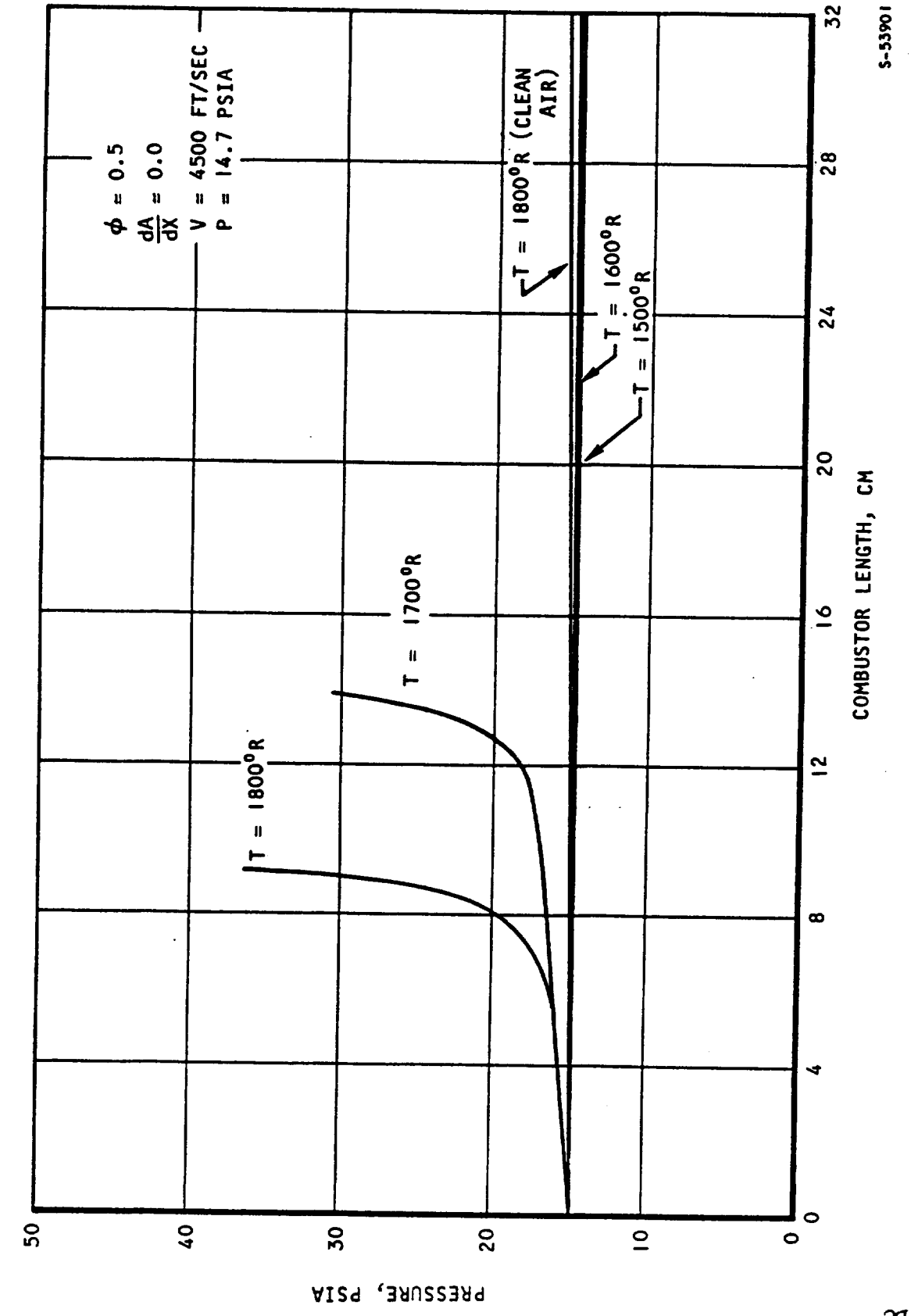

Figure 3.2-28. Effect of 2-Percent Carriers on Static Pressure as a Function of Combustor Length for Several Initial Static Temperatures

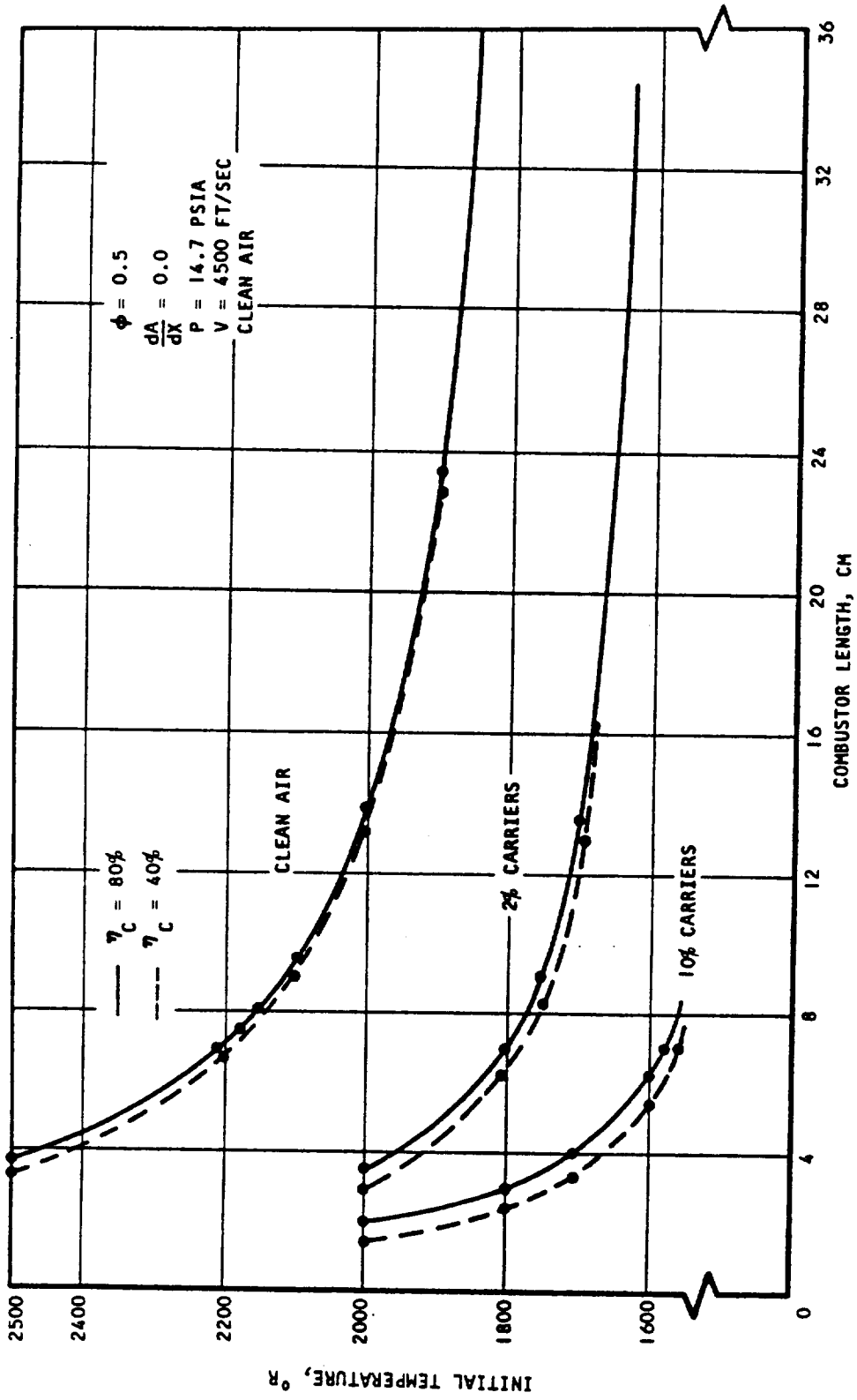

Figure 3.2-29. Effect of Percentage of Carriers on Initial Static Temperatures as a Function of Required Combustor Length and Chemical Efficiency

TABLE 3.2-2

MASS FRACTIONS OF REACTING FLOW WITH INITIAL CARRIERS
(EquivalerceRatio = 0.5)

	2 Percent Carriers*	10 Percent Carriers*
H	0.63844118-04	0.30009153-03
O	0.34673790-03	0.16987557-02
N_2	0.75690000-00	0.75690000-00
H_2	0.14104986-01	0.12964130-01
O_2	0.22605520-00	0.21569300-00
OH	0.88783859-04	0.44593853-03
H_2O	0.18617049-02	0.9132536-02
HO_2	0.58185451-03	0.28683717-02
H_2O_2	0.12234745-06	0.64002613-06

*Percent carriers indicates the amount of hydrogen consumed in a constant-area duct if the initial temperatures were 2200°R.

3.2.6 Effect of the Divergence

The effect of divergence was calculated for clean air as a function of initial static temperature. The results for an initial temperature of 2500°R are presented in Figures 3.2-30, 3.2-31, and 3.2-32 for different values of $\frac{1}{Ai}\frac{dA}{dx}$ (change of area ratio per unit length).

Examination of Figure 3.2-30 indicated that ignition delay increased with with increasing divergence $\left(\frac{1}{Ai}\frac{dA}{dx}\right)$ and that the reaction proceeded very slowly at values of divergence greater than approximately 1/10 cm^{-1}. The increased ignition delay with divergence was due to the relative production rates in the chain-branching and chain-breaking reactions. At low values of divergence, the production rates in the chain-branching reactions were sufficient to offset the production rates in the chain-breaking reactions. At large values of divergence, the decreasing values of pressure and temperature effectively quenched the chain-branching reactions and the production of chain carriers was not sufficient to initiate the highly exothermic recombination reactions. For example, to achieve a chemical efficiency of 80 percent within a combustor length of 4 cm, the required initial static temperature would be 1670°R, 1910°R and 2410°R for 10-percent, 2-percent and 0-percent carriers, respectively.

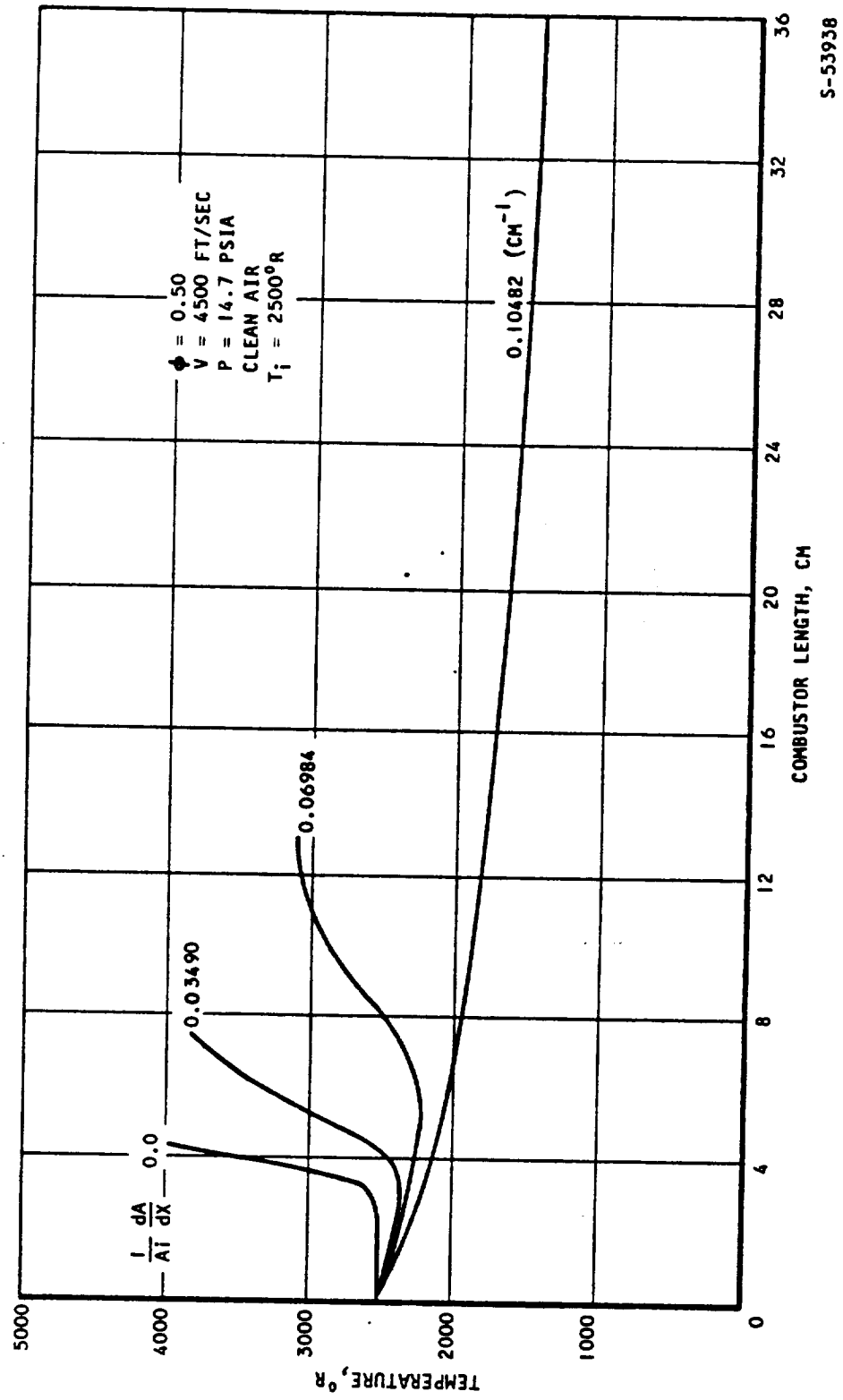

Figure 3.2-30. Effect of Divergence on Static Temperature as a Function of Combustor Length

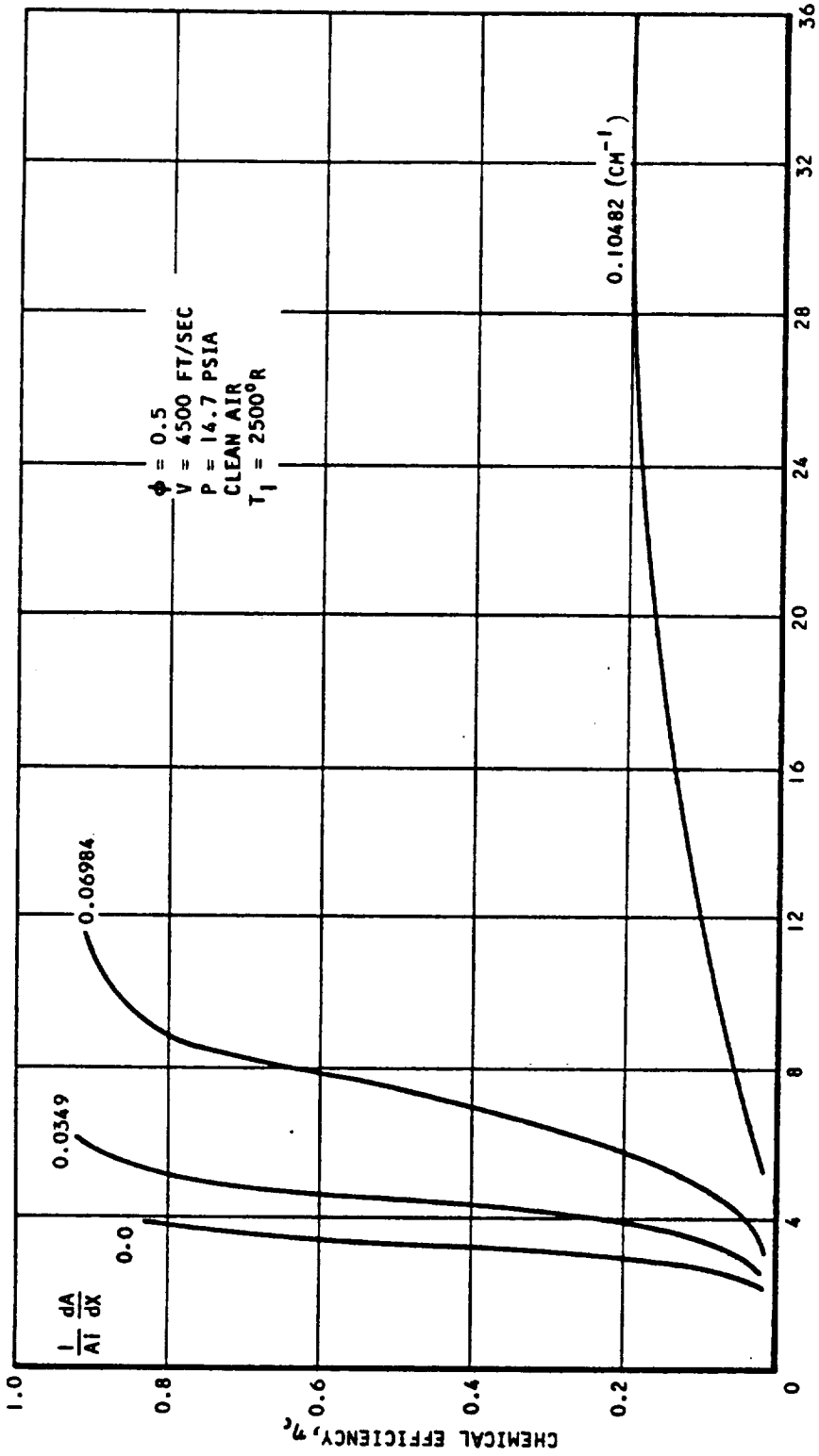

Figure 3.2-31. Effect of Divergence on Chemical Efficiency as a Function of Combustor Length

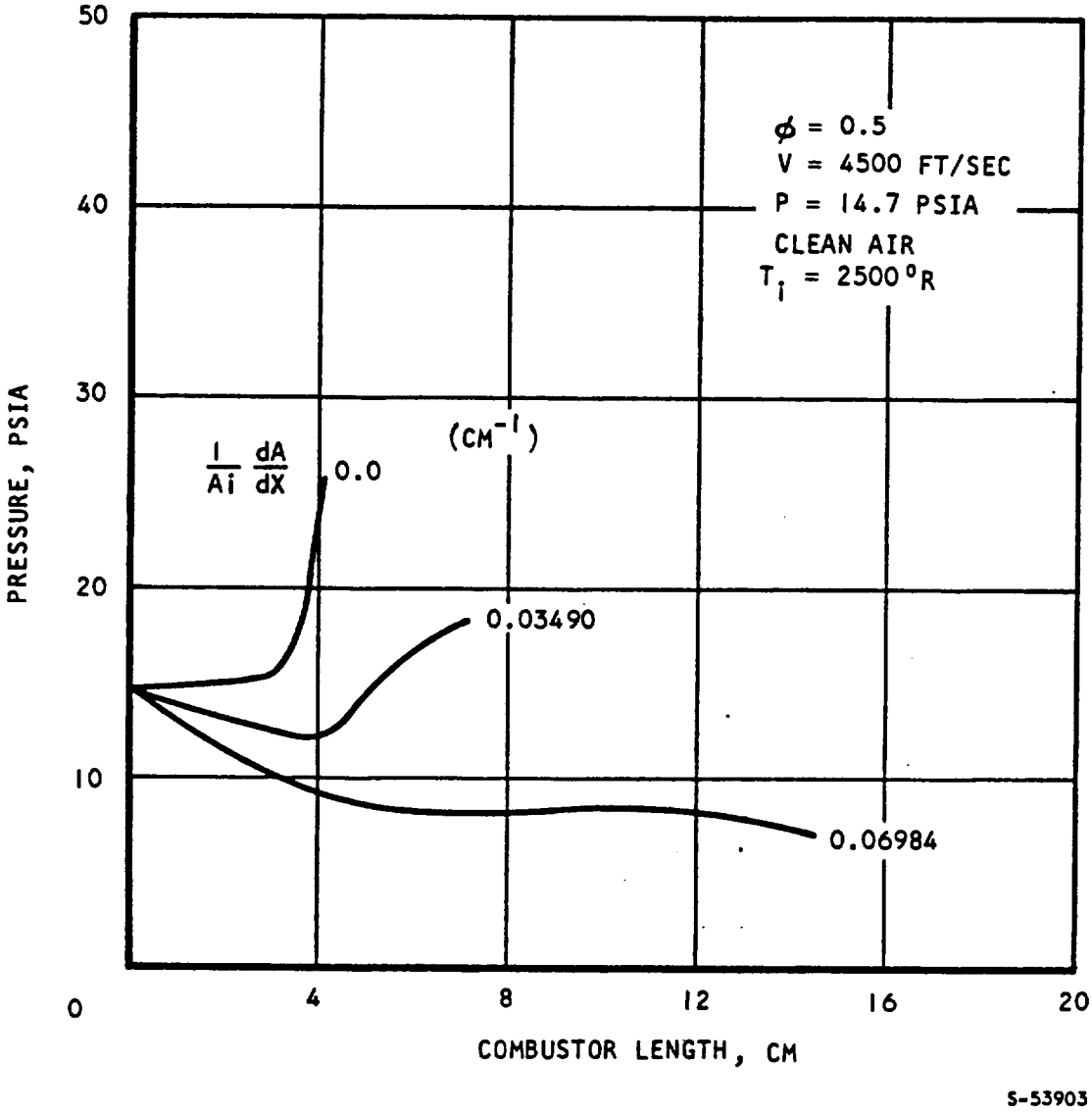

Figure 3.2-32. Effect of Divergence on Static Pressure as a Function of Combustor Length

Calculations were also made for clean air at an initial static temperature of 2200°R. The results presented in Figures 3.2-33, 3.2-34, and 3.2-35 indicated a trend similar to the higher initial static temperature case with the reaction essentially quenched for values of divergences greater than about $6/100\ cm^{-1}$.

Examination of Figure 3.2-33 indicated that ignition would occur in a diverging duct when concentration of OH had reached 10^{-6} moles/liter before the temperature had decreased below about 1950°R.

In Figure 3.2-36, the ignition delays plotted versus $\frac{1}{A}\frac{dA}{dx}$ for initial static temperatures of 2200°R, 2350°R, and 2500°R indicated that the effect of divergence on ignition delay decreased with increasing initial static temperature. The effect of increasing divergence was to increase the length required for combustion. This increased length was due to (1) the temperature and pressure effects on ignition delay, and (2) increased flow velocity.

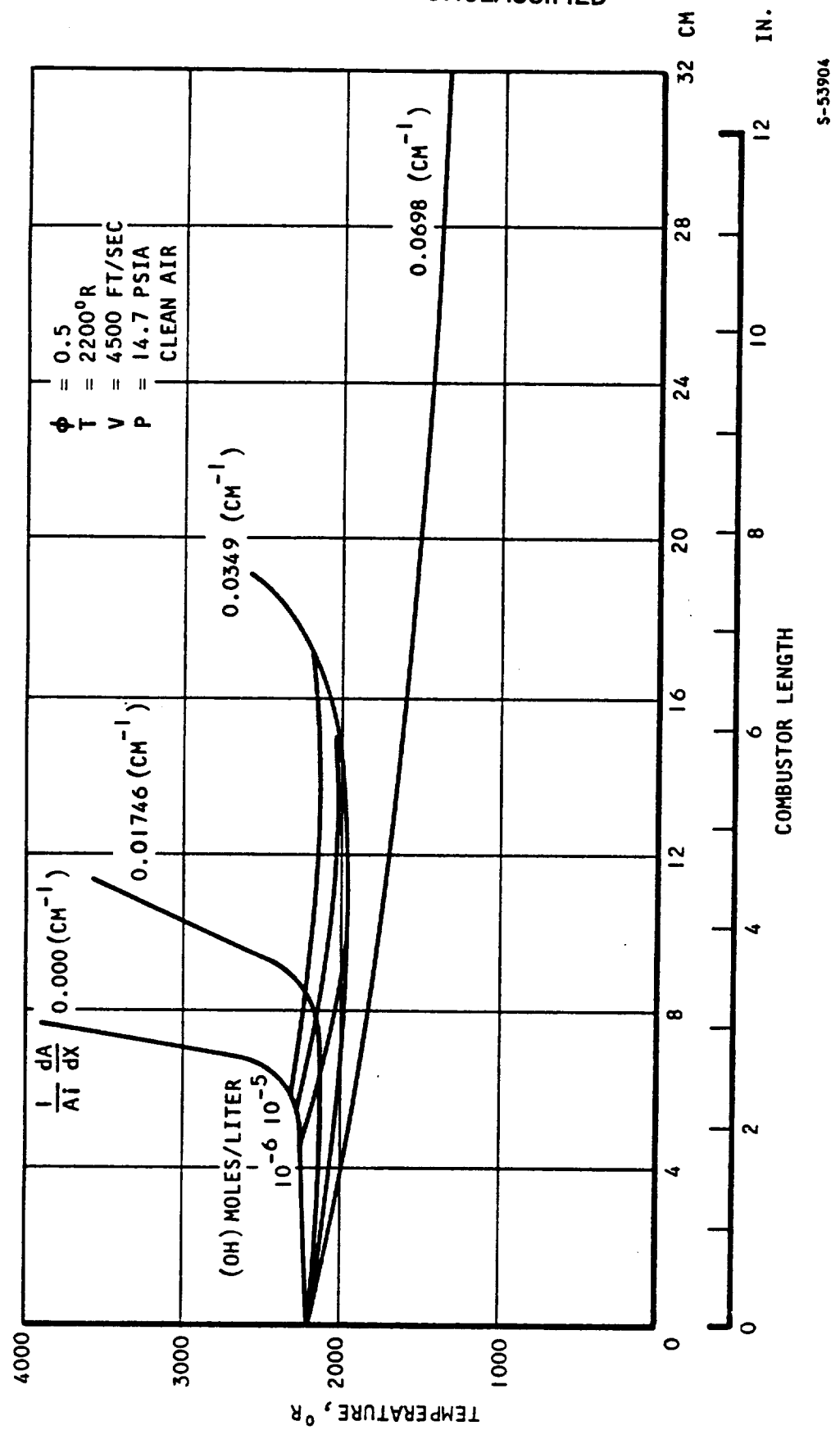

Figure 3.2-33. Effect of Divergence on Static Temperature as a Function of Combustor Length

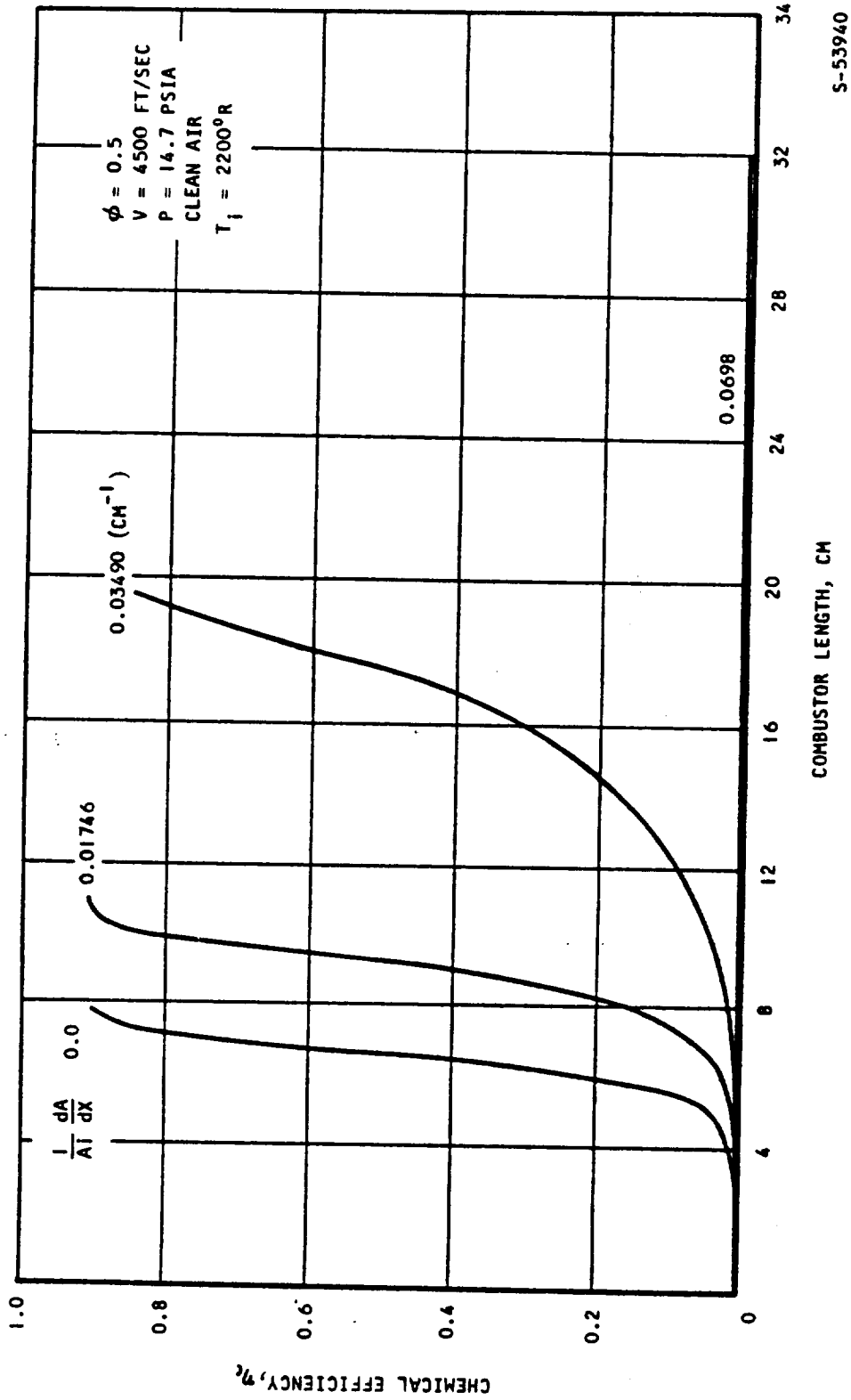

Figure 3.2-34. Effect of Divergence on Chemical Efficiency as a Function of Combustor Length

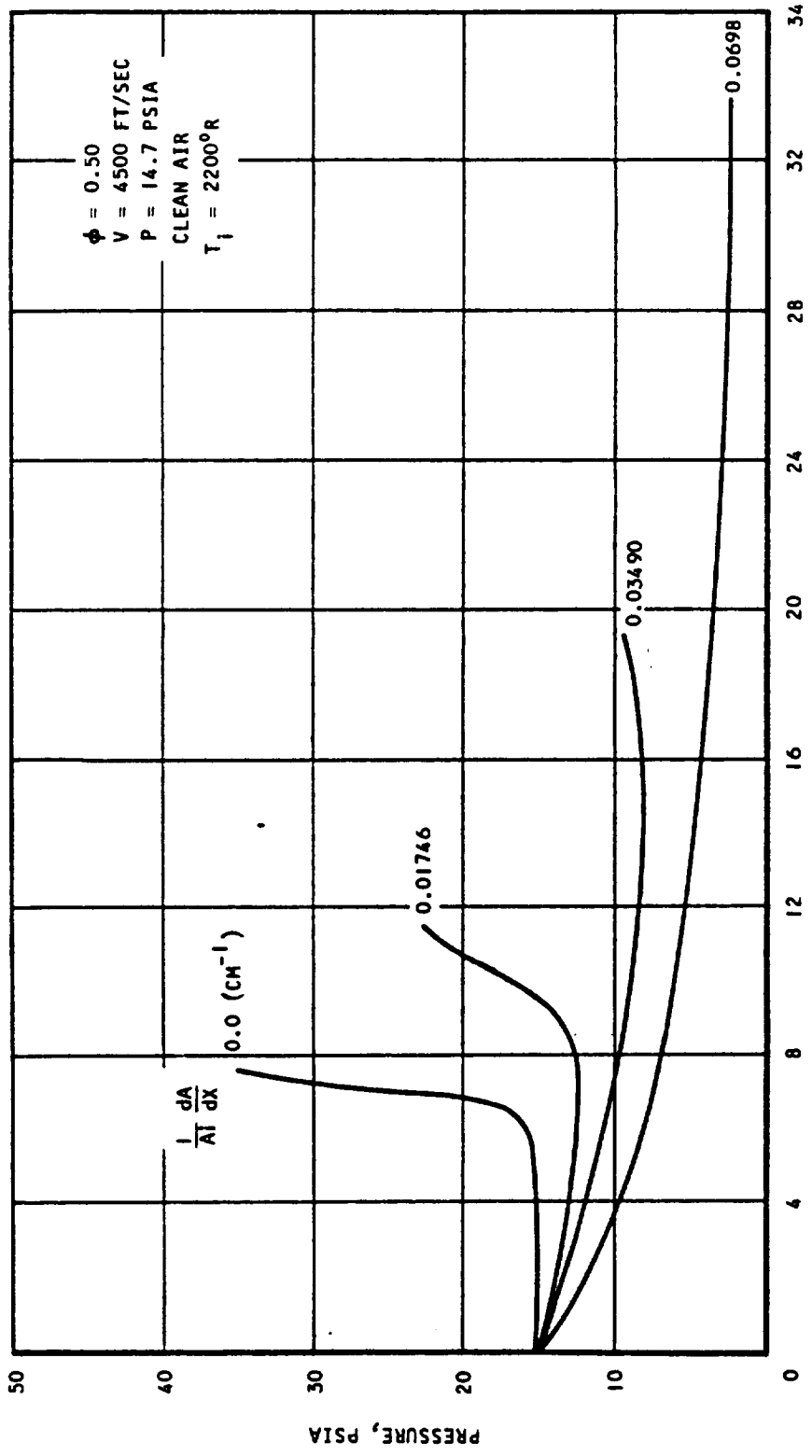

Figure 3.2-35. Effect of Divergence on Static Pressure as a Function of Combustor Length

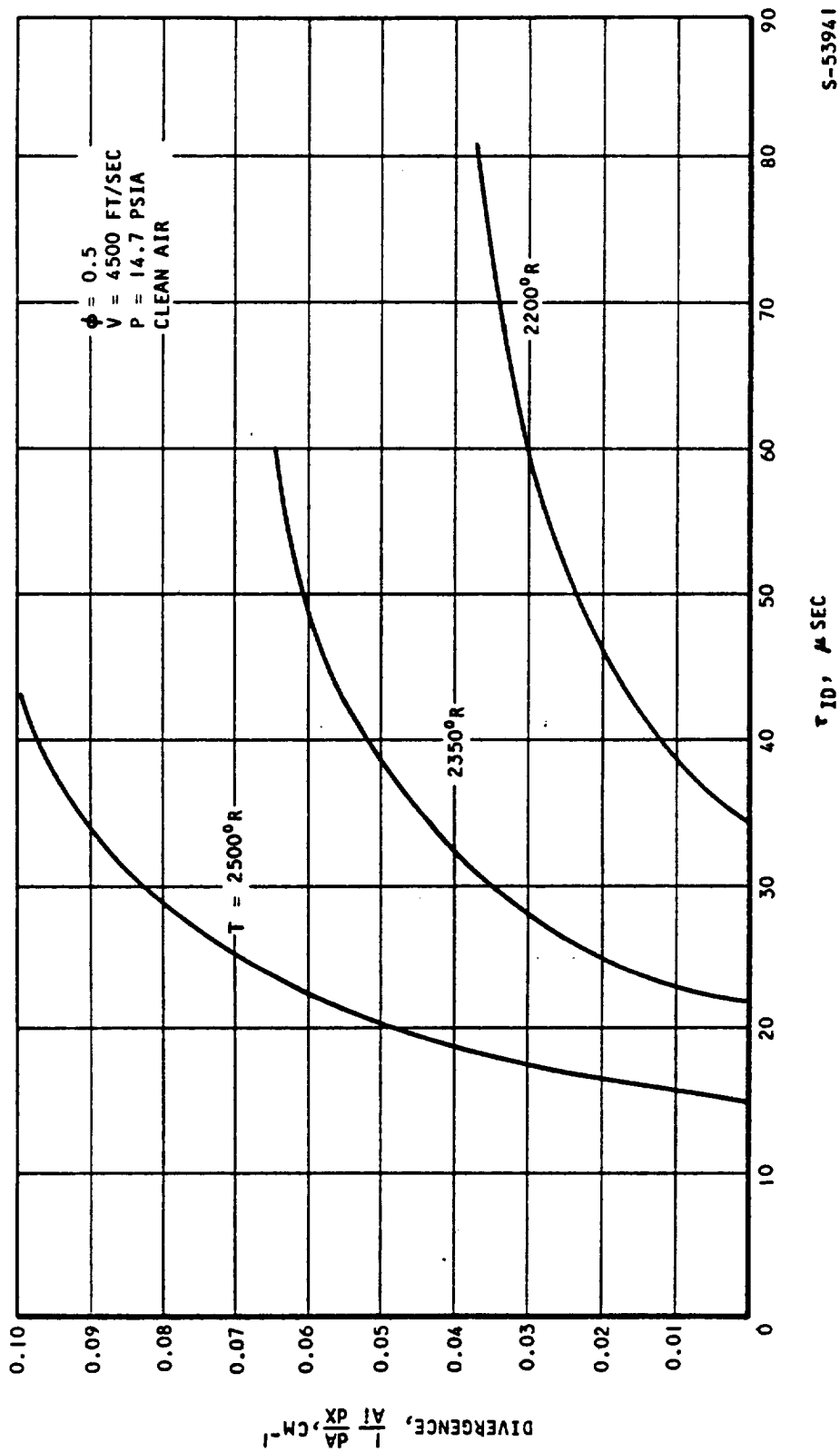

Figure 3.2-36. Effect of Divergence on Ignition Delay as a Function of Initial Static Temperature

4. CHEMICAL KINETICS DURING THE IGNITION DELAY PERIOD

Although more than a dozen chemical reactions are involved in a hydrogen-air combustion process, not all reactions are significant at all times. In the isothermal induction period the major change is in the buildup of the atomic species (H) and (O) and the (OH) radicals. The significant reactions are either mildly exothermic or endothermic, and the system is essentially at a constant temperature. The production rates in reactions which involve large activation energies are insignificant during this isothermal induction period. The length of this period is affected both by the initial temperature and by the pressure. For the HRE application, the ignition delay must be considerably less than one millisecond. Significant production rates occur in the following reactions during the induction period:

$$H + O_2 \xrightarrow{k_1} OH + O \qquad k_1 = 5.64 \times 10^{10}\, e^{-\frac{15.1}{RT}} \qquad \text{(Ref 3-4)} \qquad (4\text{-}1)$$

$$H + O_2 + M \xrightarrow{k_2} HO_2 + M \qquad k_2 = 8.6 \times 10^{8}\, e^{+\frac{1.28}{RT}} \qquad \text{(Ref 3-5)} \qquad (4\text{-}2)$$

$$O + H_2 \xrightarrow{k_3} OH + H \qquad k_3 = 1.2 \times 10^{10}\, e^{-\frac{9.2}{RT}} \qquad \text{(Ref 3-4)} \qquad (4\text{-}3)$$

$$H_2 + OH \xrightarrow{k_4} H_2O + H \qquad k_4 = 4.2 \times 10^{9}\sqrt{T}\, e^{-\frac{10}{RT}} \qquad \text{(Ref 3-4)} \qquad (4\text{-}4)$$

Where the reactance concentration is in units of mole/liter, R is in kilo-cal/mole ^{0}K, T is in ^{0}K, and the unit for time is seconds.

From the above equations the net production rates of (OH), (H) and (O) can be readily written:

$$\frac{d[OH]}{dt} = k_1[H][O_2] + k_3[H_2][O] - k_4[H_2][OH] \qquad (4\text{-}5)$$

$$\frac{d[H]}{dt} = -k_1[H][O_2] - k_2[H][O_2][M] + k_3[H_2][O] + k_4[H_2][OH] \qquad (4\text{-}6)$$

$$\frac{d[O]}{dt} = k_1[H][O_2] - k_3[O][H_2] \qquad (4\text{-}7)$$

Observing the numerical solutions for more complete reactions in Section 3, the relationship

$$\frac{[O]}{[H]}$$

remained relatively constant for a given initial condition. Also during the ignition delay period, the molecular concentrations did not change materially, and the ratio of $\frac{[H_2]}{[O_2]}$ defined as 2ϕ could be considered constant. Therefore, in order to simplify the solution the following quantity denoted by symbol B, will be treated as a constant.

$$B = \frac{k_3 [H_2][O]}{k_1 [O_2][H]}$$

Substituting these two definitions into Equations (4-5), (4-6), and (4-7) results in the following equations.

$$\frac{d[OH]}{dt} = a_1 [H] - a_2 [OH] \tag{4-8}$$

$$\frac{d[H]}{dt} = a_2 [OH] - a_4 [H] \tag{4-9}$$

$$\frac{d[O]}{dt} = a_3 [H] \tag{4-10}$$

where:
$$\begin{aligned} a_1 &\equiv [O_2]\, k_1 (1 + B) \\ a_2 &\equiv [O_2]\, k_4\, 2\phi \\ a_3 &\equiv [O_2]\, k_1 (1 - B) \\ a_4 &\equiv [O_2]\{k_1 (1 - B) + k_2 [M]\} \end{aligned} \tag{4-11}$$

Equations (4-8) and (4-9) are coupled and are independent of the atomic oxygen concentration. The solution of Equation (4-8) and (4-9) is

$$[OH] = b_1 e^{m_1 t} + b_2 e^{m_2 t} \tag{4-12}$$

$$[H] = \frac{a_2 b_1}{a_4 + m_1} e^{m_1 t} + \frac{a_2 b_2}{a_4 + m_2} e^{m_2 t} + b_3 e^{-a_4 t} \tag{4-13}$$

where b_1, b_2 and b_3 are constants to be evaluated, and m_1 and m_2 are

$$m_1 = \frac{-(a_2 + a_4) + \sqrt{(a_2 + a_4)^2 + 4a_2 (a_1 - a_4)}}{2} \qquad (4\text{-}14)$$

$$m_2 = \frac{-(a_2 + a_4) - \sqrt{(a_2 + a_4)^2 + 4a_2 (a_1 - a_4)}}{2} \qquad (4\text{-}15)$$

The term involving m_2 has a large negative value and dissipates rapidly, and only m_1 is of significance. For the range of temperatures and pressures important to HRE operation, ($900^0K < T < 1400^0K$ and pressure $\simeq$ 1 ATm) the values for a_1, a_2 and a_4 are:

		$\phi = 0.5$	$\phi = 1.0$
$T = 900^0K$	a_1	$= 2.35 \times 10^4 (1 + B)$	Same as for $\phi = 0.5$
	a_2	$= 7.4 \times 10^5$	1.48×10^6
	a_4	$= 2.3 \times 10^4 (1 - B) + 3.5 \times 10^4$	Same as for $\phi = 0.5$
$T = 1400^0K$	a_1	$= 4.8 \times 10^5 (1 + B)$	Same as for $\phi = 0.5$
	a_2	$= 8.6 \times 10^6$	1.7×10^7
	a_4	$= 4.8 \times 10^5 (1 - B) + 2.7 \times 10^4$	Same as for $\phi = 0.5$

For temperature exceeding 1400^0K the ignition delay time will be in microseconds.

The value of B for the stated critical conditions is approximately 0.8. From the above table, a_2 is an order of magnitude larger than a_1 or a_4.

The exponent m_1 is then approximated

$$\begin{aligned} m_1 &\simeq \frac{a_2 (a_1 - a_4)}{a_2 + a_4} \\ &\simeq a_1 - a_4 \\ &= [O_2]\{k_1 (1 + B) - k_1 (1 - B) + k_2 [M]\} \\ &= [O_2]\{2 k_1 B - k_2 [M]\} \end{aligned} \qquad (4\text{-}16)$$

The [OH] concentration is then given by

$$[OH] = [OH]_i \, e^{[O_2]\{2k_1 B - k_2[M]\}\tau} \tag{4-17}$$

Using the definition of ignition delay as the time for the [OH] radical to achieve a concentration of 10^{-6} mole/liter, then

$$\frac{10^{-6}}{[OH]_i} = e^{[O_2]\{2kB_1 - k_2[M]\}\tau} \tag{4-18}$$

or

$$\tau = \frac{\ln \frac{10^{-6}}{[OH]_i}}{[O_2]_i \{2k_1 B - k_2 [M]_i\}}$$

Equation (4-18) was plotted in Figure 4.1-1 for pressures of 1/2, 1, and 2 atmospheres for the temperature range between 900°K and 1400°K.

Also shown in Figure 4.1-1 were the shock tube experimental results taken from Ref 4-1. The definition of ignition delay used in Ref 4-1 was based on the sharp rise in temperature observed by the infra red optical system. If this sharp temperature rise occurs near an [OH] concentration of 10^{-6} moles/liter, then the agreement between theory and experiment is reasonable.

The oxygen concentration and the molar concentration [M] of the mixture can be replaced by pressure in Equation (4-18).

$$\tau = \frac{1}{a_5 P - a_6 P^2} \tag{4-19}$$

where: $a_5 = \dfrac{0.0037 B k_1}{T \ln \frac{10^{-6}}{[OH]_i}} \quad \dfrac{cm^2}{sec\ gm}$

$$a_6 = \frac{1.7 \times 10^{-5} k_2}{T^2 \ln \frac{10^{-6}}{[OH]_i}} \quad \frac{cm^2}{sec\ gm}$$

P in units of gm/cm^2

T in °k

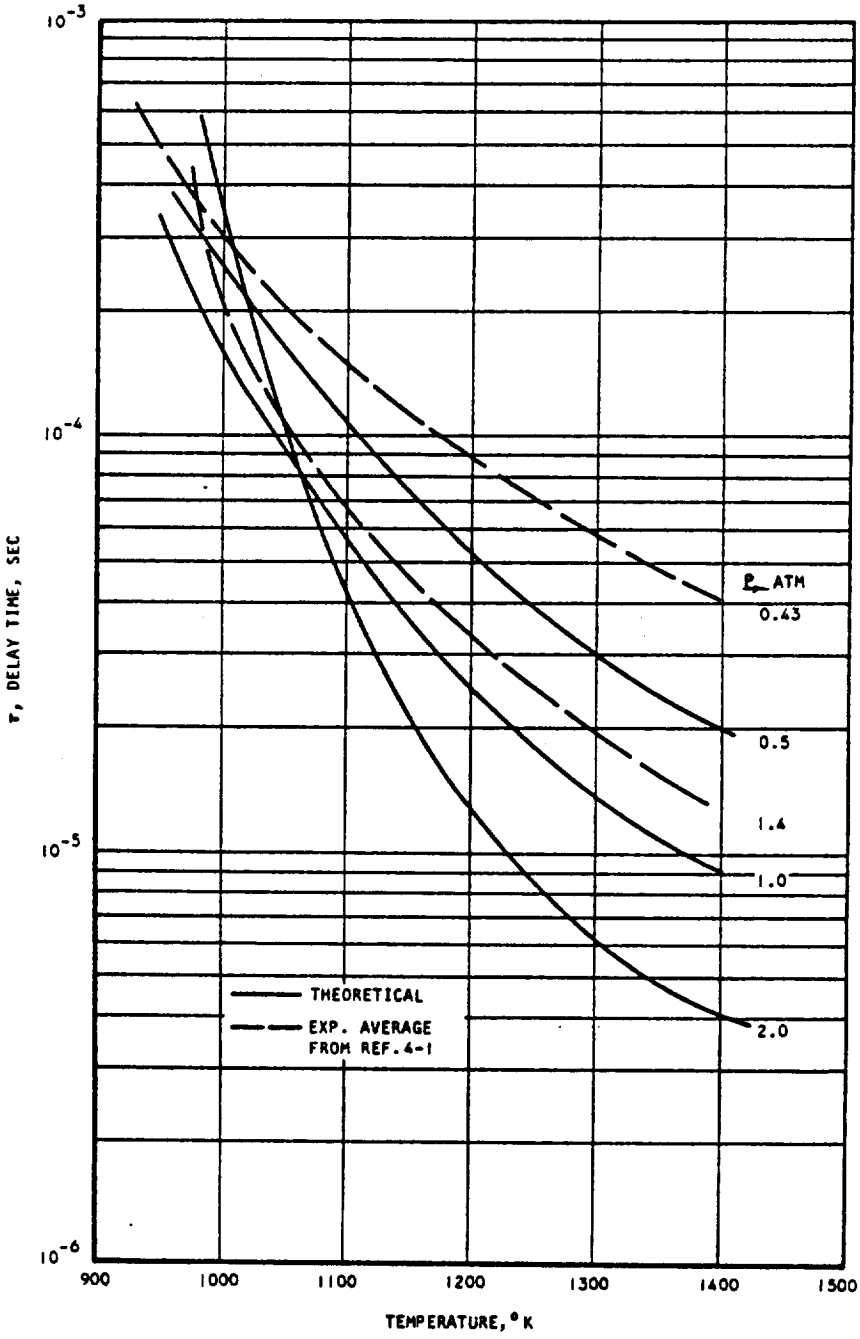

S-53947

Figure 4.1-1. Comparison of Theoretical and Experimental Ignition Delay Times

Equation (4-19) has a minimum when the pressure is varied.

$$\frac{d\tau}{dp} = -\frac{a_5 - 2a_6 p}{[a_5 p - a_6 p^2]^2} = 0$$

or

$$p = \frac{a_5}{2a_6} = \frac{109\ Bk_1}{k_2}\ T$$

$$= 7100\ BTe^{-16.38/RT}$$

For B = 0.8 the minimum delay time occurs at the following pressures. The solutions from numerical integration are also listed for comparison.

T, °K	Simplified Solution P, atm	Numerical Solution P, atm
1000	1.45	1
1140	4.4	2.7

The disagreement between these two methods may be attributed to the ignorance of the third body effects of water vapor in the simplified solution.

The ignition delay is also affected by the initial [OH] concentration. The influence of this factor can be deduced from equation (4-18) as follows:

$$\tau \propto \left(\log 10^{-6} - \log [OH]_i\right)$$

Increasing the initial [OH] concentration will reduce the ignition time. A typical initial [OH] concentration is 10^{-10} mole/liter at 1000°K. A tenfold increase of this value produces a 25 percent reduction of the delay time while a 100-fold increase results in a 50-percent reduction as calculated below:

$$\frac{\tau_{10\ fold\ [OH]}}{\tau_{[OH]_i = 10^{-10}}} = \frac{-6 - (-9)}{-6 - (-10)} = \frac{3}{4}$$

$$\frac{\tau_{100\ fold\ [OH]}}{\tau_{[OH]_i = 10^{-10}}} = \frac{-6 - (-8)}{-6 - (-10)} = \frac{1}{2}$$

The increasing ignition delay in the second explosion limit is clearly illustrated by Figure 4.1-1. For an initial temperature of 1000°K or less, the ignition delay time increases with pressure. This phenomena has been known for some time and is due to the formation of the $[HO_2]$ radial by reaction 2 which is $(H + O_2 + M \rightarrow HO_2 + M)$. This reaction removes the atomic hydrogen without the benefit of producing a new active species. Since it is a three-body-collision process, its rate is proportional to the second power of the pressure as compared with the two-body-collision process which is proportional to the first power of the pressure. The ignition delay time will increase with increasing pressure when the rate of reaction 2 increases faster than reaction 3.

The initial rate of [OH] production is primarily given by the molecular collision denoted by the reaction

$$H_2 + O_2 \xrightarrow{k_5} 2OH$$

At time zero, it is assumed that the production rate of [OH] in the above reaction balance the [OH] consumption rate of reaction 4.

$$\left(\frac{d[OH]}{dt}\right)_{t=0} = 2k_5[H_2][O_2] - k_4[H_2][OH] = 0$$

$$[OH]_i = \frac{2k_5}{k_4}[O_2] \qquad (4\text{-}20)$$

The calculated data presented in Figure 4.1-1 were computed based on the initial [OH] concentration given by Equation (4-20).

5. TWO-DIMENSIONAL EFFECTS IN A DIVERGING COMBUSTOR

A few exploratory calculations were made in order to investigate two-dimensional effects in supersonic combustion of a premixed gas in a diverging combustor. Since this effort was very limited in scope, only a brief qualitative discussion will be given here.

Numerical solutions were obtained using the method of characteristics with finite chemical kinetics in an axisymmetric combustor. The computer program described in Reference 5-1 and 5-2 was used to obtain these solutions.

The hot portion of a boundary layer can give beneficial effects in the initiation of combustion (assuming that there is fuel in the boundary layer). Ignition and combustion in the boundary layer can produce an expansion of the boundary stream tube. Compression waves are induced in the main flow where the stream tube begins to expand. Farther downstream, when combustion is nearly complete in the boundary layer, expansion waves appear in the main flow. This situation is depicted schematically in Figure 5.0-1. At the duct centerline the pressure waves appear downstream of the start of the compression surfaces. For typical AIM Mach numbers this distance is of the order of the duct height.

Compression heating of the mainstream, caused by combustion in the boundary layer stream tube, was predicted in Reference 5-3 using a quasi-two-dimensional model which assumed a uniform pressure across the combustor's height. The "overshoot" (See Figure 5.0-1) predicted by the truly two-dimensional solution has an effect on combustion which is usually benefical and which is not predicted by the quasi-two-dimensional approach.

However, the beneficial effect of a high initial temperature in the boundary layer can be offset. When a diverging portion of the combustor is reached, the boundary layer stream tube is the first to be turned (expanded). This can result in quenching of combustion in the boundary layer.

Also, choking can occur in a single stream tube, possibly leading to a disturbance which propagates upstream in the combustor and causes an adjustment in the air flow. Such a disturbance cannot be predicted using the existing steady-state model. However, this phenomenon could conceivably occur in a real combustor and be a factor in boundary-layer separation.

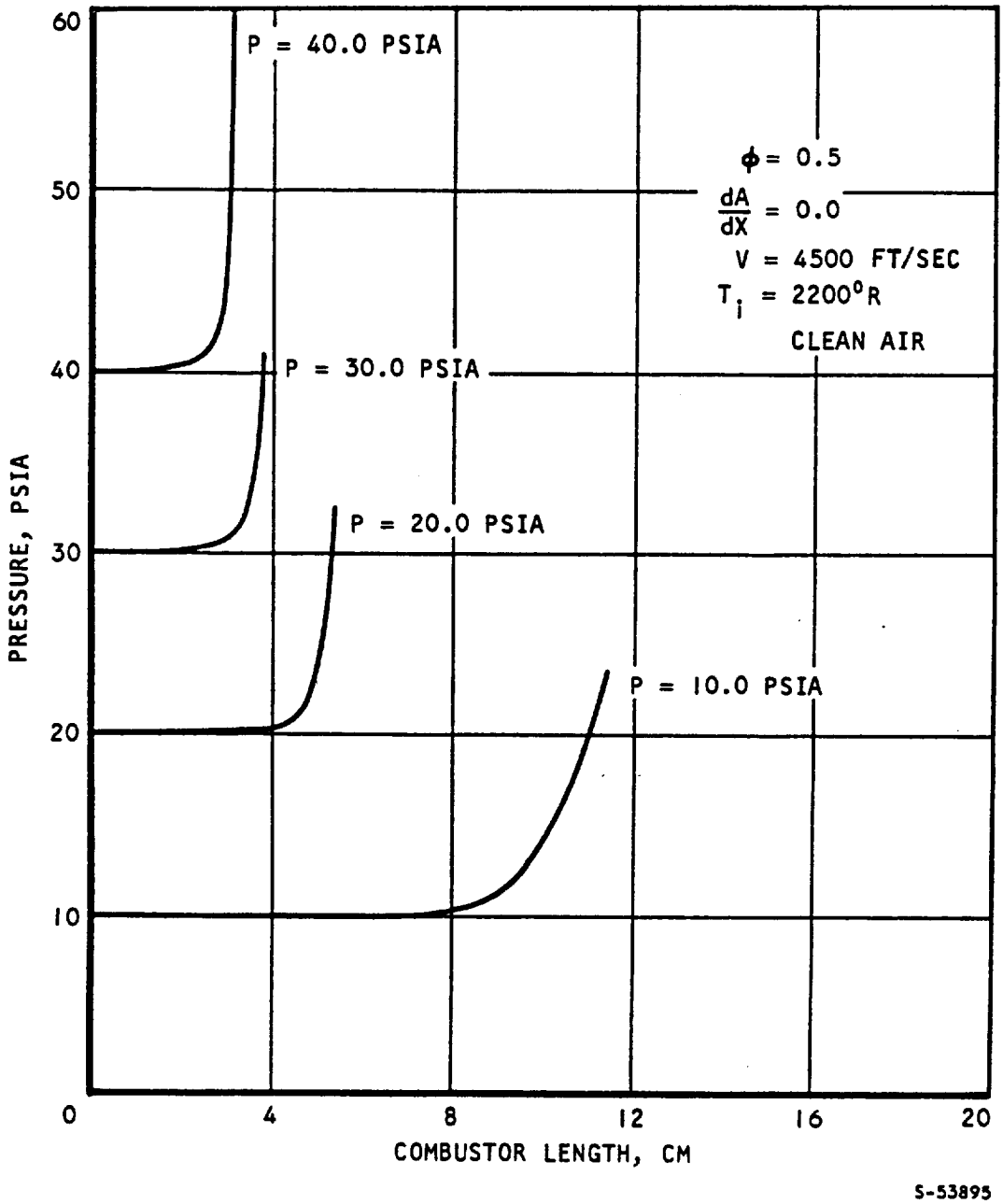

Figure 3.2-15. Effect of Initial Static Pressure on Pressure as a Function of Combustor Length

$\phi = 0.50$

$\frac{dA}{dX} = 0.0$

$V = 4500$ FT/SEC

CLEAN AIR

$T_i = 2200^{\circ}R$

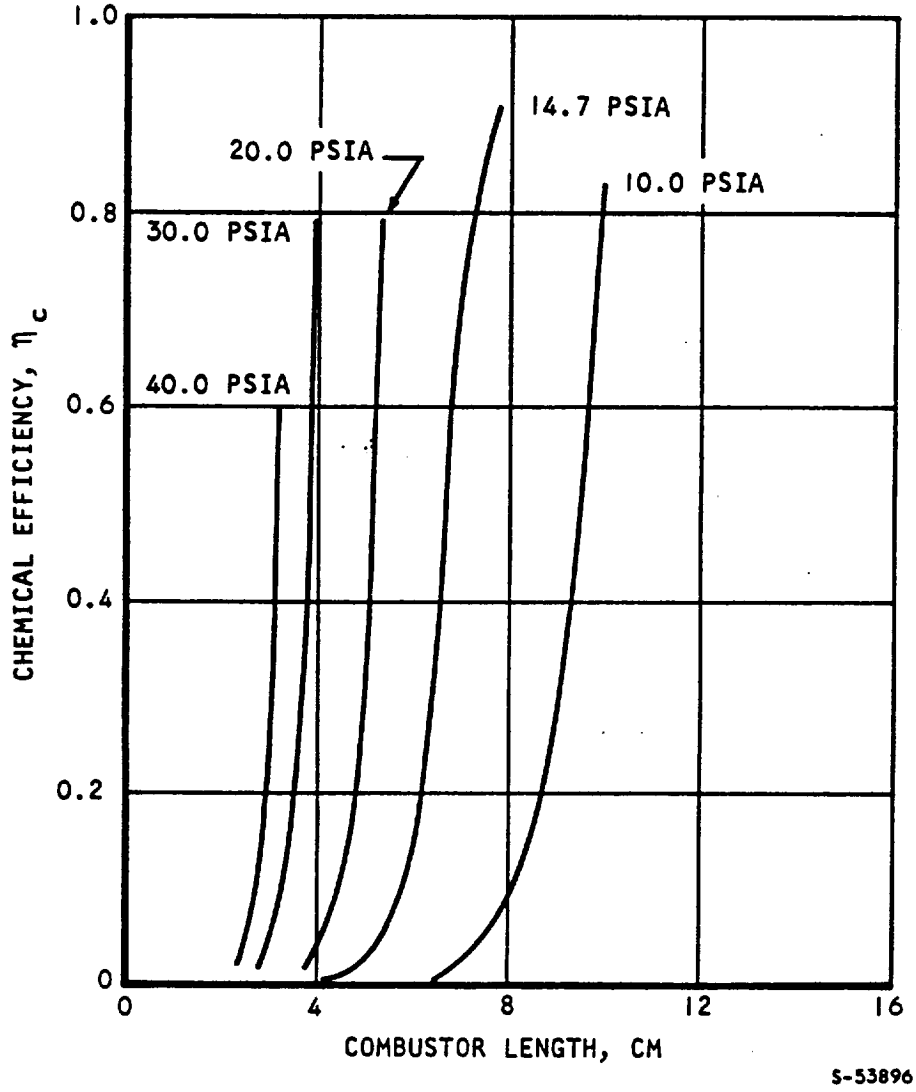

Figure 3.2-16. Effect of Initial Static Pressure on Chemical Efficiency as a Function of Combustor Length

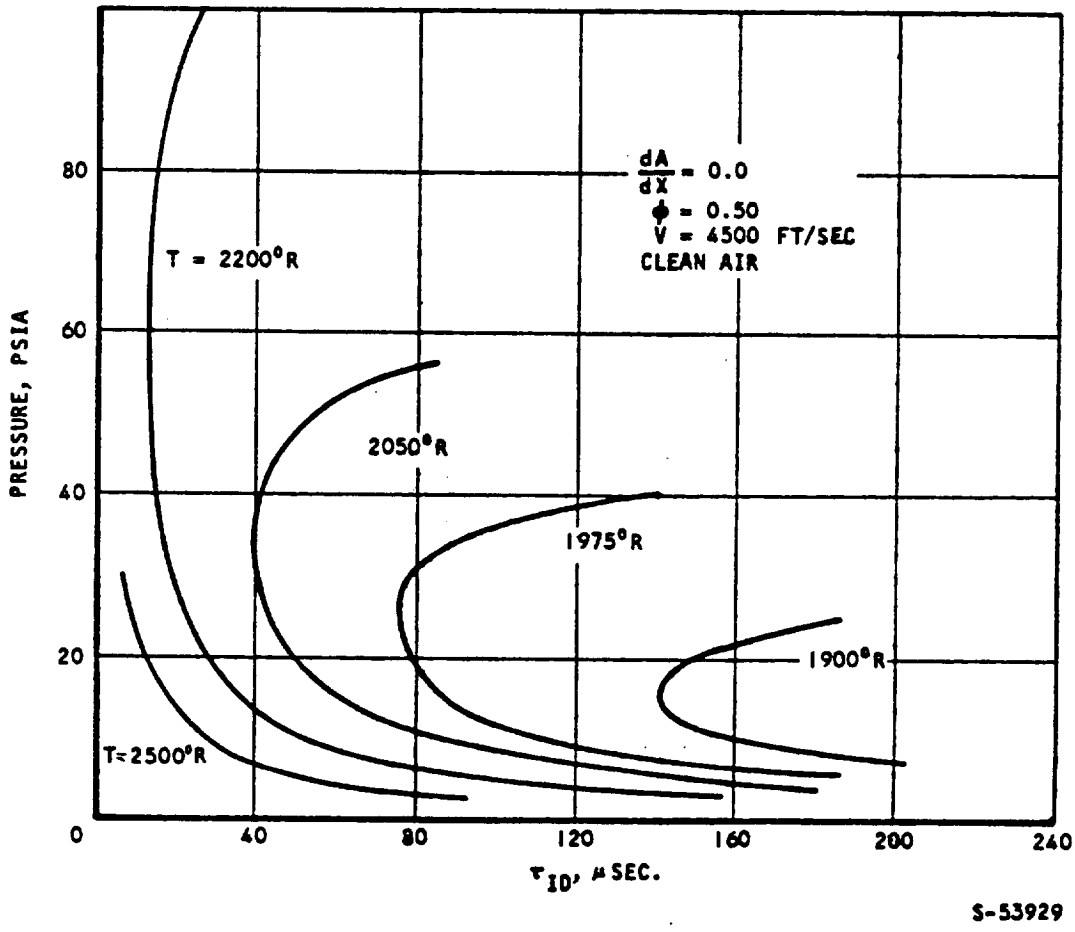

Figure 3.2-17. Effect of Initial Static Pressure and Temperature on Ignition Delay

3.2.3 Effect of Equivalence Ratio

Chemical kinetics were calculated as a function of equivalence ratio with clean air. Results presented in Figures 3.2-18 through 3.2-21 indicated that ignition delays are essentially constant for the range of equivalence ratios investigated.

3.2.4 Vitiation Effects

Precombustion of hydrogen with oxygen replenishment as a means of perheated air is denoted by the term "vitiated air." The effect of this vitiated air on the ignition delay time of the H_2 -air reaction was investigated.

Clean air at several initial total temperatures was precombusted at a pressure of 20 atm with varying amounts of hydrogen at room temperature. The combustion products were then expanded to a pressure of 1 atm in order to obtain their equilibrium compositions. Note that in the precombustion, oxygen was added to preserve the same O_2 mole fraction as in clean air. The percent of vitiation or percent of fuel by weight (fuel considered as H_2 and O_2 with the weight of O_2 12.2 times that of H_2) was varied from 0 to 50 percent (see Table 3-2-1).

Chemical kinetic calculations were then made starting with the vitiated equilibrium species concentrations at 1 atm pressure. Hydrogen at an equivalence ratio of 0.5 was allowed to react at constant area with the vitiated air. The initial conditions consisted of a static pressure of 1 atm and a velocity of 4500 ft/sec at several initial static temperatures from 1850°R to 2300°R. The results of these calculations are presented in Figure 3.2-22. Ignition delays were determined from the time required for the OH concentration to reach 10^{-6} moles/liter. The dotted lines are the estimated values.

Examination of Figure 3.2-22 indicated that the degree of vitiation had a strong effect on ignition delay time at 1850°R and 2000°R, but a negligible effect at 2300°R. Even small amounts of vitiation at 1850°R caused the ignition delay time to increase very rapidly and for all practical purposes caused chemical reactions to cease. Chemical reactions also ceased at 2000°R initial temperature near 25 percent vitiation.

As the amount of vitiation increased, so did the amount of water vapor and OH. The initial concentrations were shown in Table 3.2-1. The water vapor acts as a very efficient third body (third bodies act as energy sources or sinks in chemical reactions) as shown in the reaction:

$$H + O_2 + M = HO_2 + M$$

This reaction removed H from the mixture causing a quenching of the chain-branching reaction. At low temperature, the chain-breaking reaction $H + O_2 + M = HO_2 + M$ predominated. At the higher temperatures, the thermal dissociation of H_2O and chain-branching $HO_2 + H_2 = H_2O_2 + H$ then became

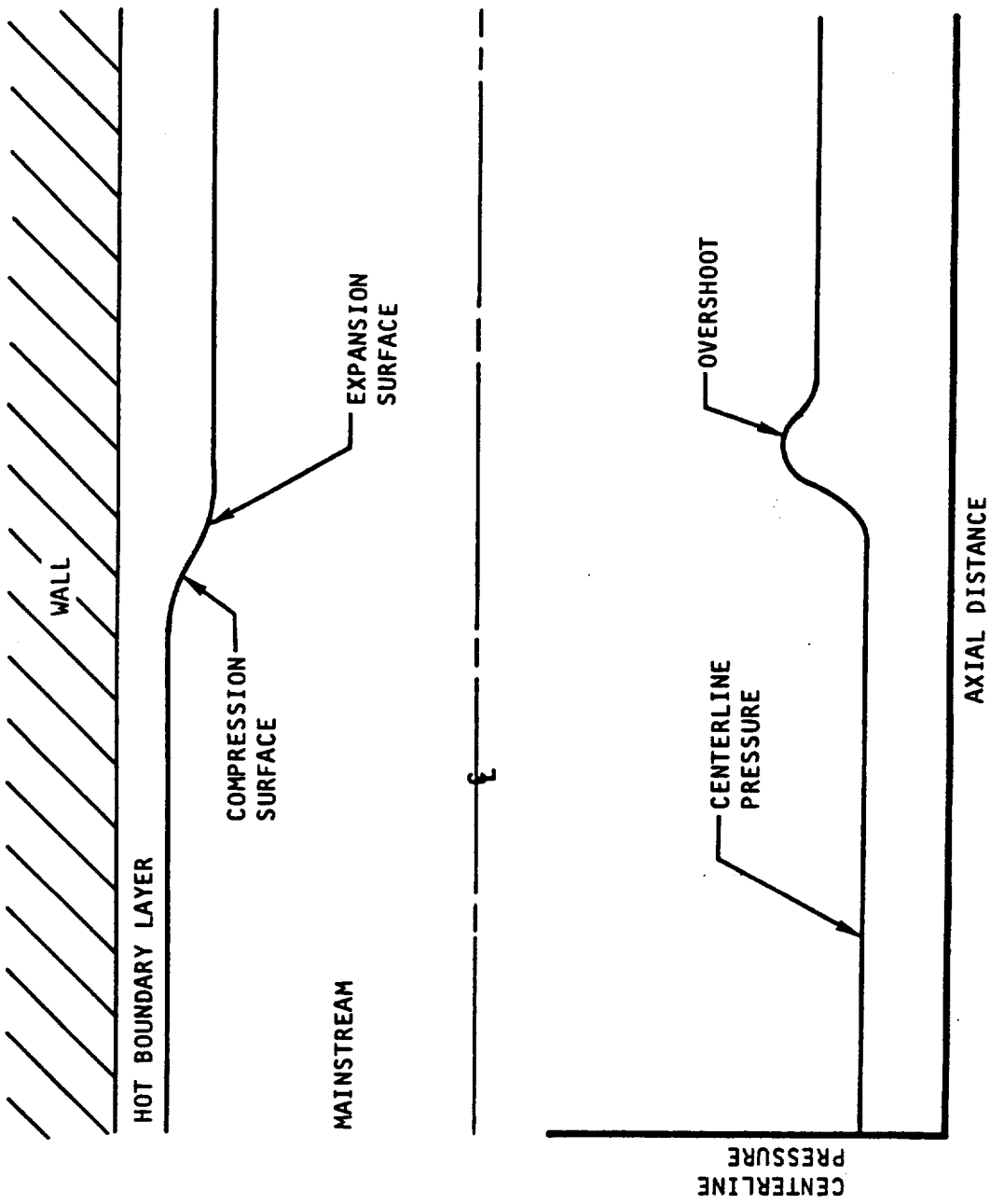

Figure 5.0-1. Mainstream Compression by Burning in the Boundary Layer

6. COMPARISON WITH TEST DATA

Considerable attention has been given to the theoretical chemical kinetics of premixed hydrogen-air supersonic combustors. However, little of this work has been done for diverging combustors of specified geometry. In this type of combustor, conditions can occur in which the expansion waves cause the temperature and pressure to decrease from their entrance values with combustor length. By contrast, if constant pressure, constant area, or constant Mach number is assumed, the temperature never decreases appreciably (unless large wall heat losses are considered).

Because the rates of the elementary chemical reactions in the hydrogen-air combustion system are strongly dependent on concentrations and temperature, it seems plausible that under some conditions divergence of a supersonic combustor could lead to significant adverse effects on the chemical kinetics even though the initial temperature is above the autoignition temperature.

Experimental results reported by Cookson, Flanagan, and Penney (Reference 2-1) provide an example of conditions under which a small change in divergence angle had a dramatic effect on combustion.

Cookson et al. report that for a combustor inlet air total temperature of approximately 1900°K and at Mach 1.98, a flame was initiated in a combustor which consisted of a 5-in.-long constant-area section followed by a 25-in.-long conical section diverging at a 1-deg angle; however, with the same inlet conditions no combustion took place within a completely divergent duct, even with a divergence angle as small as 0.75 deg.

Axial injection was used in Cookson's experiments. This eliminates complicating effects associated with cross-stream injection and makes the experiments more amenable to one-dimensional analysis.

In an attempt to explain Cookson's results, chemical kinetic calculations were made using two different computer programs, each using a different set of chemical kinetic rate constants. The first program used (Zupniks) is described in Reference 3-1.; the second (Frey's) in Reference 2-2. The chemical reactions and rate constants used in the two programs are listed in Tables 6.0-1 and 3.1-2. For initial calculations the higher frequency factor listed in Table 3.1-2 was used for reaction 5.

Because the analytical models used were one-dimensional, there was some question as to what initial conditions were appropriate. In the Cookson experimental work the fuel and air started out unmixed at the combustor entrance. For the chemical kinetic calculations, premixing was assumed. All initial parameters were kept constant except the initial temperature, the

TABLE 6.0-1

REACTIONS USED IN THE SHEAR LAYER COMBUSTION PROGRAM

Reaction	A	N	B	Reference
$H_2 + M = H + H + M$	7.5×10^{18}	1.0	0.0	6-5
$O_2 + M = O + O + M$	1.9×10^{16}	0.5	0.0	6-5
$H_2 + O_2 = OH + OH$	1.4×10^{13}	0.015	49.2644	6-5
$H_2O + H = OH + H_2$	6.0×10^{11}	-0.5	5.0	6-5
$OH + M = O + H + M$	2.0×10^{18}	1.0	0.0	6-5
$O_2 + H = OH + O$	3.2×10^{11}	-0.47	0.1	6-5
$H_2 + O = OH + H$	1.4×10^{12}	0.0	5.19	6-5
$H_2O + O = OH + OH$	1.0666×10^{13}	0.0134	0.96671	6-5
$H_2O_2 + H = H_2 + HO_2$	9.6×10^{12}	0.0	24.0	6-1
$HO_2 + M = H + O_2 + M$	$1.59 \times 10^{15} b_w$	0.0	1.0	6-1, 3-5
$H_2O + M = H + OH + M$	1.17×10^{17}	0.0	0.0	6-3
$N_2 + M = N + N + M$	10^{18}	1.0	0.0	6-5
$NO + M = N + O + M$	6×10^{16}	0.5	0.0	6-5
$O_3 + M = O_2 + O + M$	10^{18}	1.0	0.0	6-6
$H_2O_2 + M = OH + OH + M$	8.4×10^{14}	0.0	5.3	6-1
$NO + H = N + OH$	5.3×10^{11}	-0.5	2.832	6-5
$N_2 + O = NO + N$	1.5×10^{13}	0.0	0.0	6-5
$N_2 + O_2 = NO + NO$	10^{13}	0.0	40.0	6-5
$NO + O = O_2 + N$	1.8×10^{8}	-1.5	3.020	6-5
$H_2O_2 + H = OH + H_2O$	5.6×10^{13}	0.0	77.9	6-1
$H_2O + OH = H_2O_2 + H$	3.18×10^{14}	0.0	9.0	6-1
$H_2O + HO_2 = H_2O_2 + OH$	10^{13}	0.0	1.8	6-1

Backward rate constant $k_b = AT^{-N} e^{\frac{-B}{RT}}$

$$b_w = 5.0\, X_{H_2} + 1.75\, X_{O_2} + 2.15\, X_{N_2} + 1.00\, X_{AR} + 30.0\, X_{H_2O}$$

combustor geometry, and the equivalence ratio. Cookson reports an air total temperature of approximately 1870°K (3366°R) and an air Mach number of 1.98 at the combustor inlet. The air and fuel static temperature apparently were about 1176°K (2117°R) and 290°K (523°R) respectively. Preliminary calculations were made using $\phi = 0.50$. This is slightly above the highest value ($\phi = 0.45$) given by Cookson.

6.1 RESULTS

At an initial mixed fuel-air temperature of 1150°K, the calculations indicated a chemical efficiency of over 60 percent in the 0.75 degree all-diverging combustor. At an initial temperature of 1130°K the chemical efficiency calculated was less than 1 percent for the same geometry.

For the 30-in. duct with a 5-in. constant-area section and a 1-deg divergence angle, the calculated chemical efficiency was 60 percent or greater for temperatures of 1115°K and above. This indicated that the calculations with initial temperatures in the band of approximately 1115°-1135°K (2007°-2034°R) agreed qualitatively with Cookson's results in one respect; combustion occurred in the duct having a 5-in. constant-area section, and did not occur in the all-diverging combustor.

To avoid choking in the theoretical model at an equivalence ratio of 0.5, the initial temperature had to be more carefully selected. Raising the initial temperature just a few degrees above 1115°K could lead to choking in the divergent portion following the constant-area section.

A few calculations were made for an equivalence ratio of 0.33 using both Zupnik's and Frey's programs, with an initial temperature of 1115°K and the two different sets of rate constants listed in Table 3.1-2 and 6.0-1. The initial conditions are listed in Table 6.1-1. Both programs again predicted the result found by Cookson--that combustion would occur in the combustor with a constant-area section followed by a 1-deg divergence, but not in the combustor having a constant divergence angle of 0.75 deg. Furthermore, when a constant-area combustor was specified, the calculation indicated choking. This apparently is in agreement with Cookson's observation that a shock would form in the constant-area combustor.

The computed axial temperature profiles for the two diverging combustor cases are shown in Figures 6.1-1 and 6.1-2. In the case with no combustion (Figure 6.1-2) the temperature profiles from the two programs were very nearly identical and only one curve is shown.

Disagreement between the results from the two computer programs is due to the differences in rate constants which were used rather than the differences in mathematical method. The curves are labeled with the program name only for convenience.

One of the conspicuous features of the case with no combustion is the decrease in (OH) concentration which occurs in the results from both programs and begins well along the combustor length, as shown in Figure 6.1-3. (A decrease in (O) concentration begins farther downstream; see Figure 6.1-4.)

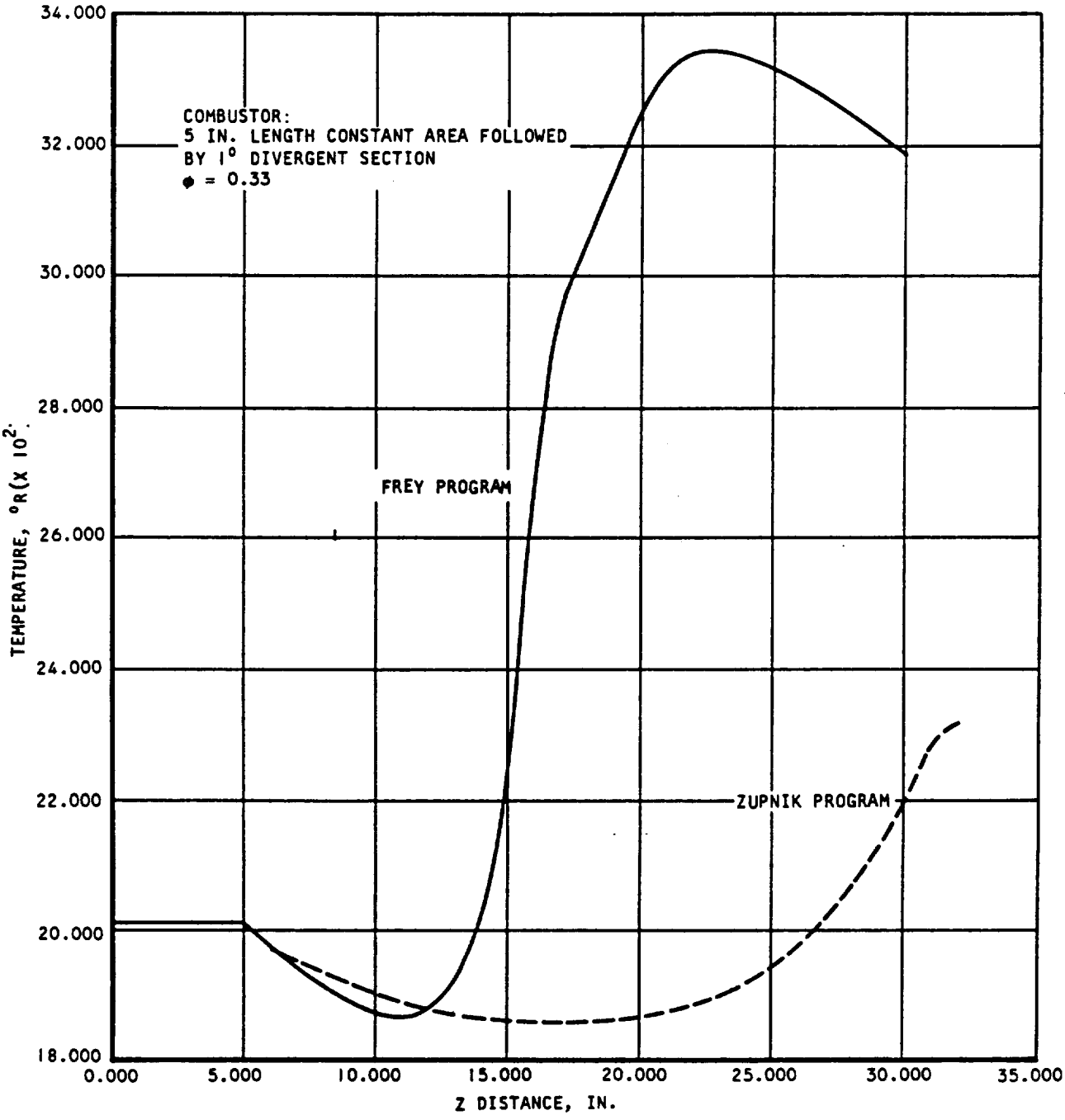

S-53943

Figure 6.1-1. Chemical Kinetics Simulation of Cookson's Experiment

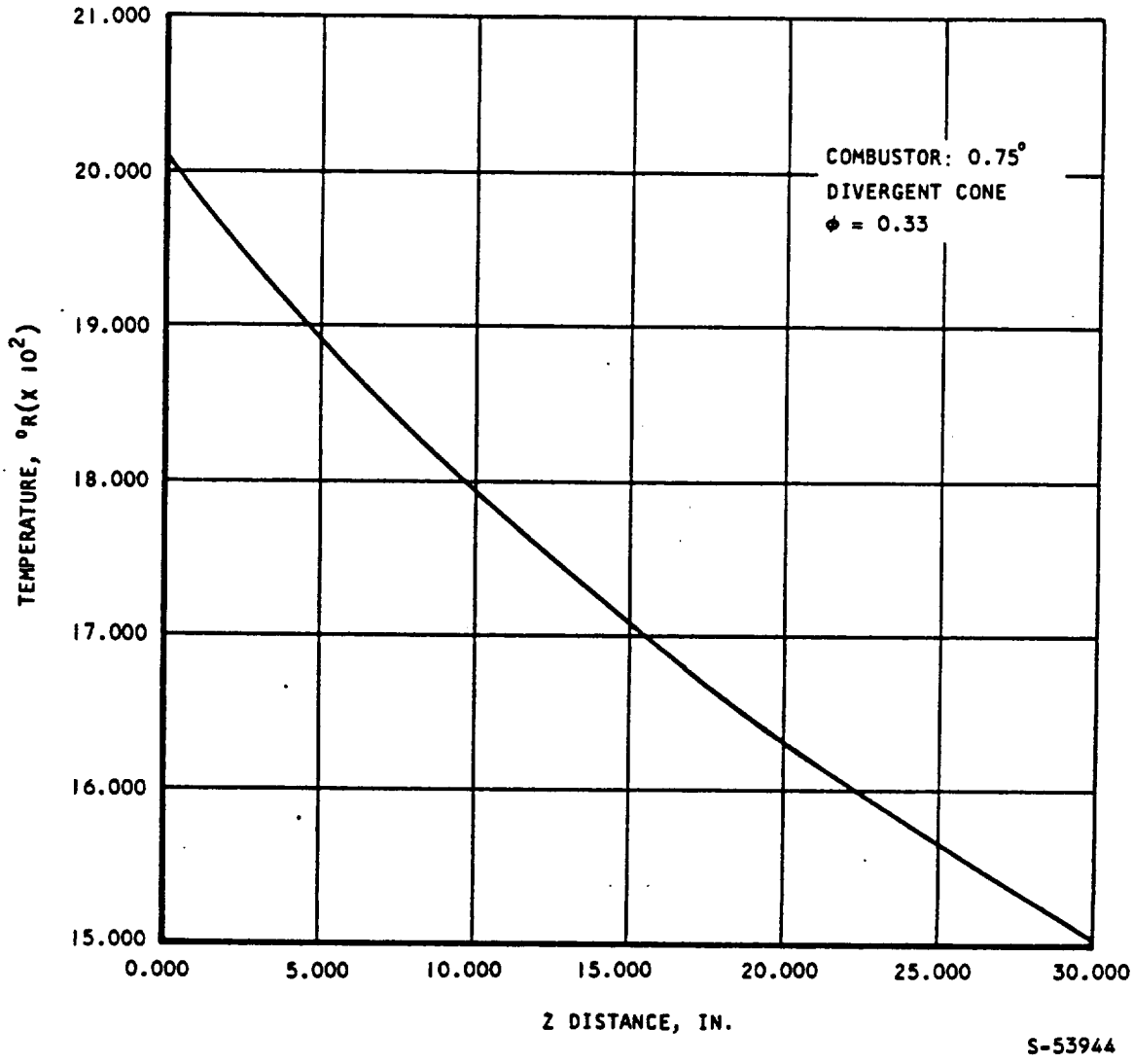

Figure 6.1-2. Chemical Kinetics Simulation of Cookson's Experiment

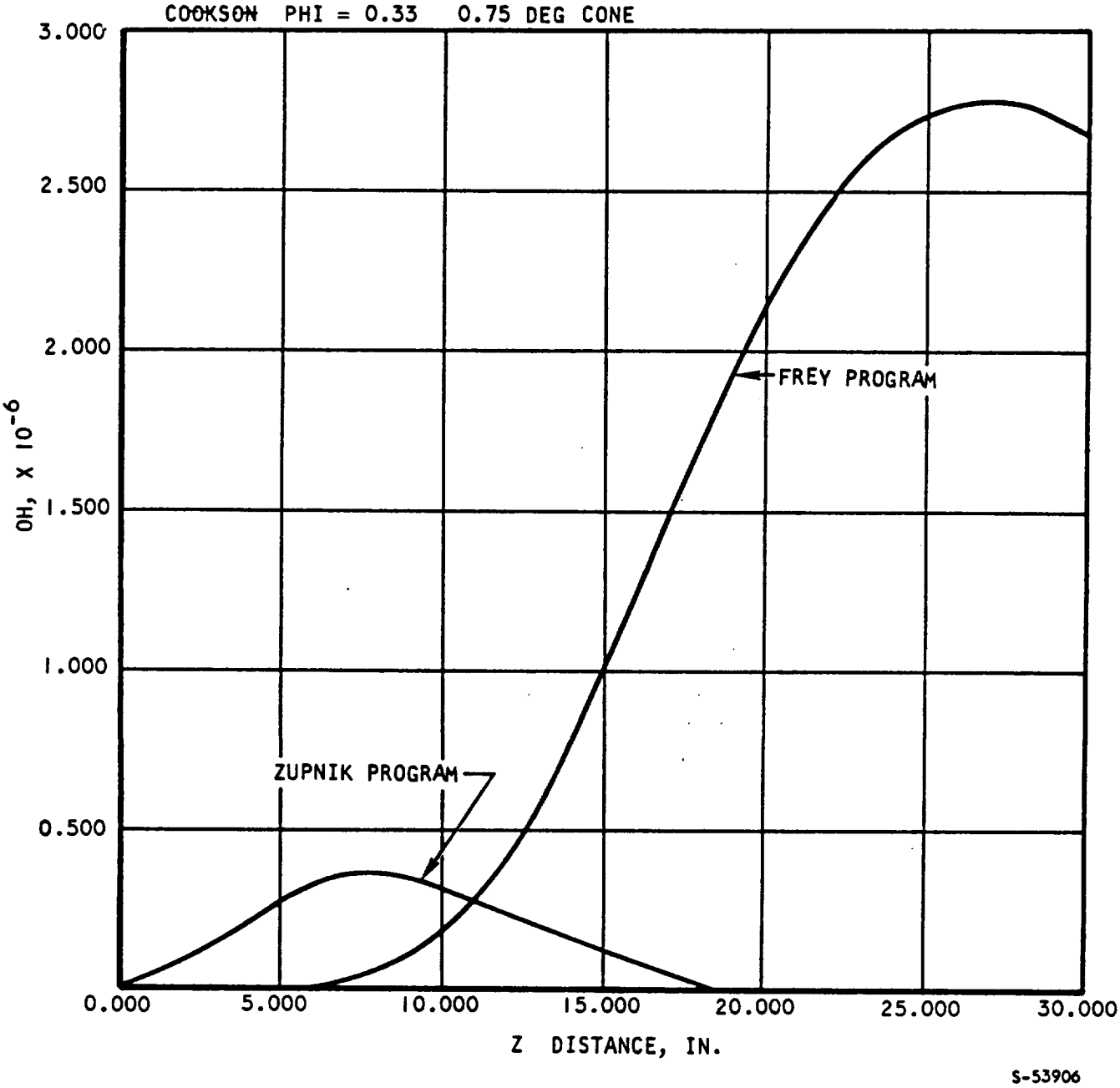

Figure 6.1-3. Chemical Kinetic Simulation of Cookson's Experiment Mole Fraction OH vs Z

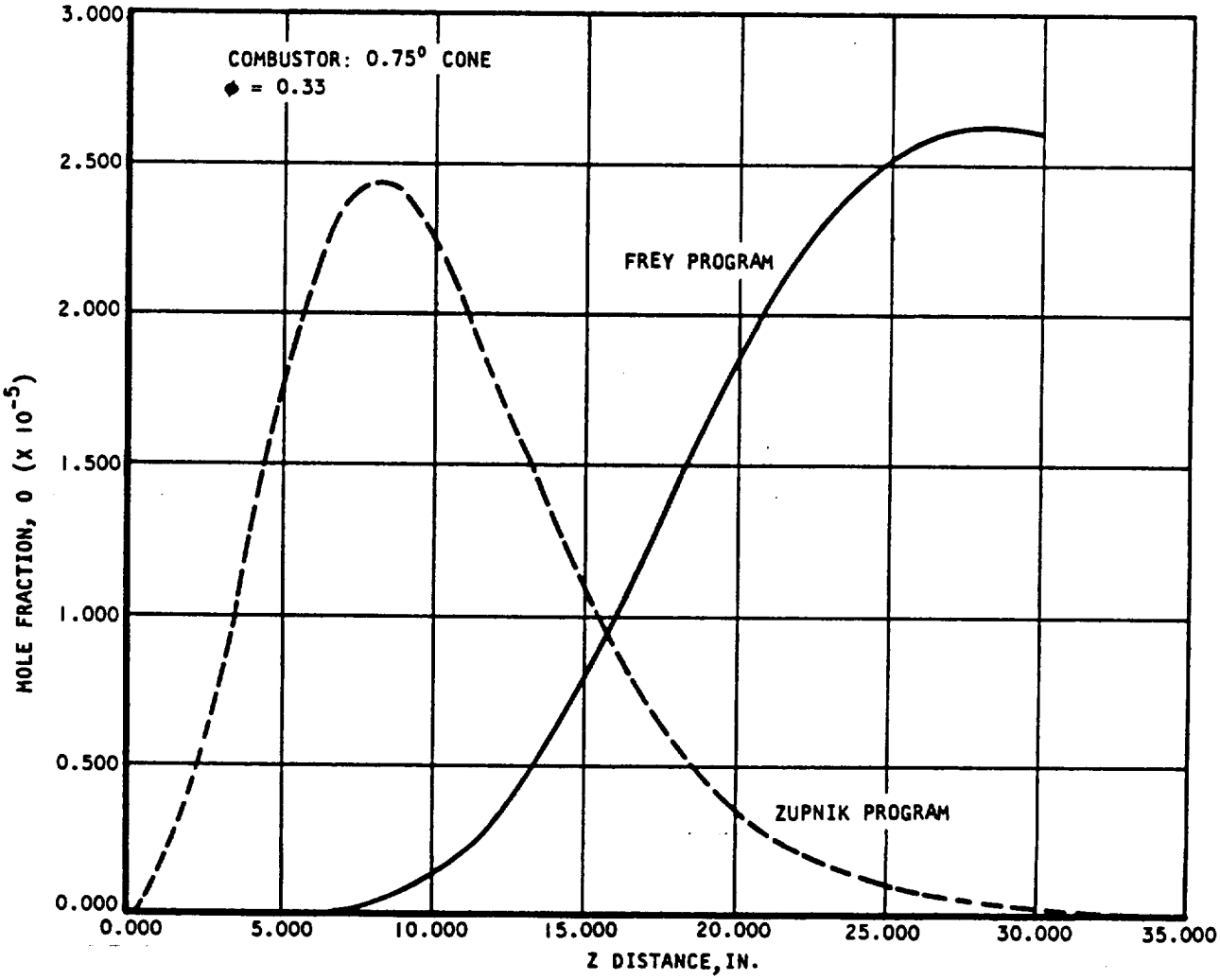

Figure 6.1-4. Chemical Kinetic Simulation of Cookson's Experiment

TABLE 6.1-1

INITIAL CONDITIONS ASSUMED FOR COOKSON'S COMBUSTOR
MASS FRACTIONS

Species	Zupnik Program	Frey Program
H	10^{-9}	0.0
O	10^{-9}	0.0
N_2	0.761	0.761
H_2	0.00958	0.00958
O_2	0.230	0.230
OH	10^{-9}	0.0
H_2O	10^{-9}	0.0
HO_2	10^{-9}	0.0
H_2O_2	10^{-9}	0.0
NO	Not Applicable	0.0
N	Not Applicable	0.0
O_3	Not Applicable	0.0

Velocity, ft/sec = 4215
Static pressure, psia = 12.81
ϕ = 0.33

Reaction rates from the Frey program indicate that the reversal in the time-derivative of (OH) concentration occurs when the rate of the OH-destroying reaction

$$OH + H_2 \rightarrow H_2O + H \qquad (6\text{-}1)$$

outweighs the combined rates of the two dominant OH-producing reactions

$$O_2 + H \rightarrow OH + O \qquad (6\text{-}2)$$

$$H_2 + O \rightarrow OH + H \qquad (6\text{-}3)$$

The (OH) reversal is apparently only a symptom and not the basic cause of the quenching of combustion in the analytical study. Exploratory calculations showed that when the rate of Reaction (6-1) above was suppressed by lowering its rate constant, the destruction of (OH) was accomplished by the reaction

$$OH + OH \rightarrow H_2O + O \qquad (6\text{-}4)$$

Similarly, when in a further calculation Reactions (6-1) and (6-4) above were both suppressed, two more reactions took their place to cause net destruction of (OH).

It is believed that the quenching observed in the computer programs is due to a decrease in the rates of all the reactions, which is caused simply by the lowering of static pressure and temperature associated with expansion of the gas. The OH reversal seems to be a part of the adjustment of the chemical process to the slower rates. Changing the rate constants of the OH-destroying reactions changes the overall process rate, but apparently does not change the mechanism.

The pressure profile reported by Cookson for $\phi = 0.33$ and those computed by the two chemical kinetic programs for the geometry in which combustion occurred are shown in Figure 6.1-5. Computed profile forms in disagreement with the experimental profile is not surprising; the heat release was spread out due to finite-rate mixing in the experiments, but in the theoretical premixed model the heat release occurred over a short axial distance. Agreement in the constant-area section would probably be improved by considering the effects of mixing and of wall friction.

As previously mentioned, a high frequency factor was assigned to the rate constant for reaction 5 in using the Zupnik program. This frequency factor was about 2.5 times greater than that in the original reference (see Table 3.1-2). Decreasing the frequency factor of this reaction has the effect of increasing the overall heat release rate. When the lower frequency factor in Table 3.1-2 was used, the heat release was accelerated enough to cause choking in the combustor having a constant-area section although the calculation for the conical combustor still indicated no heat release. Thus for a marginal case the results can be very sensitive to the rate of the $H + O_2 + M$ reaction. This rate constant is believed to be known within a factor of two (Reference 6-1).

The temperature chosen for obtaining qualitative agreement with Cookson's results was about 110^0R, or 5 percent lower than the unmixed air inlet static temperature. This is not considered a serious discrepancy in view of the assumption of premixing in the model and the uncertainties in the chemical kinetic rate constants.

It is believed that the qualitative agreement between theory and experiment in this case is sufficient to indicate that the 0.75-deg divergence of the combustor used by Cookson et al. may have had a serious effect on the chemical kinetics, leading to the observation of little or no burning inside the combustor.

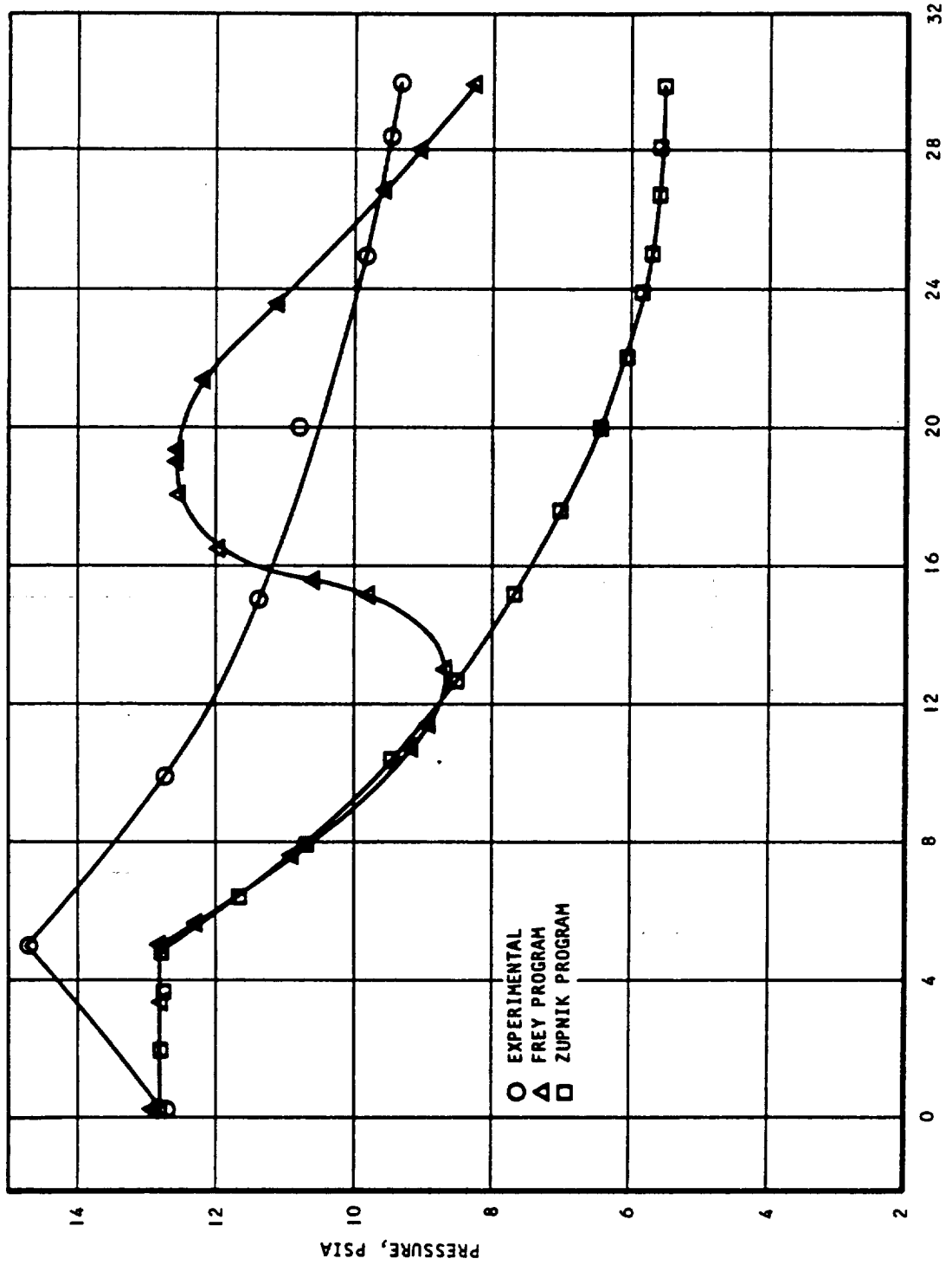

Figure 6.1-5. Pressure Profiles for Cookson Combustor

6.2 CHEMICAL KINETIC SIMULATION OF TWO-DIMENSIONAL COMBUSTOR TESTS

Combustion tests were conducted with a two-dimensional, constant-width combustor having a length of 29 in., an inlet cross section of 0.6 by 6 in. and an exit-to-inlet area ratio of 2.6. The tests were conducted at various test temperatures and injector geometries. Fuel was injected in two stages; the first in a constant area, the second in a diverging area as shown in Figure 6.2-1. High chemical efficiencies were obtained in the first stage (about 90 percent) while second-stage efficiencies were lower (about 60 to 70 percent). A study was made to determine if the second-stage combustion was chemical-kinetics limited or mixing limited. The Zupnik computer program (Reference 3-1) was used in the second-stage combustor to investigate the chemical kinetics, and the Frey computer program (Reference 2-2) was used to investigate both chemical kinetics and mixing in the first- and second-stage combustors.

The first case studied was at a test total temperature of 3000°R with $\phi = 0.68$ injected in the second stage. Entrance conditions to the second stage were calculated from a one-dimensional data reduction program using equilibrium chemistry. In this case, second-stage entrance conditions were determined assuming complete combustion in the first stage.

The Zupnik computer program (Reference 3-1) was used to evaluate second-stage combustion. The calculated air static temperature (from the data reduction program) was averaged with the 1500°R H_2 temperature and resulted in a 2100°R mixed fuel-air temperature at the second stage entrance. Results in Figures 6.2-2 through 6.2-4 indicated no second stage combustion. The OH concentration reached a maximum of 1.47×10^{-8} moles/liter or about 100 times lower than that used to indicate ignition delay, Figure 6.2-4.

Two cases at 3800°R total test temperature were run in a manner similar to that at 3000°R. This time an equivalence ratio of 0.25 was injected in the first stage and $\phi = 0.38$ and 0.78, respectively, were injected in the second stage. Results are shown in Figures 6.2-5 and 6.2-6. In both cases, the fuel started burning about 1-in. from the second-stage entrance.

The static temperature distribution computed for complete mixing was higher than that calculated from the data reduction program. This higher temperature arises because more fuel reacts as shown by the chemical efficiencies in Figure 6.2-7. Also, cooling losses are not accounted for. The maximum reaction rate occurred (Figure 6.2-7) at a point about 2-in. downstream of second-stage injection, a chemical efficiency of 80 percent was attained 5-in. from injection. Several species are plotted in Figures 6.2-8 and 6.2-9 for the stoichimetric and fuel lean cases, respectively. In both cases there was a rapid increase in the concentrations of H, O, OH and HO_2. About 1.5 to 2.5 in. downstream of injection the production rate of OH, HO_2 and H began to decrease.

Therefore with the assumption of complete and instantaneous mixing and no second-stage air-fuel injection disturbance, the second stage fuel reacted

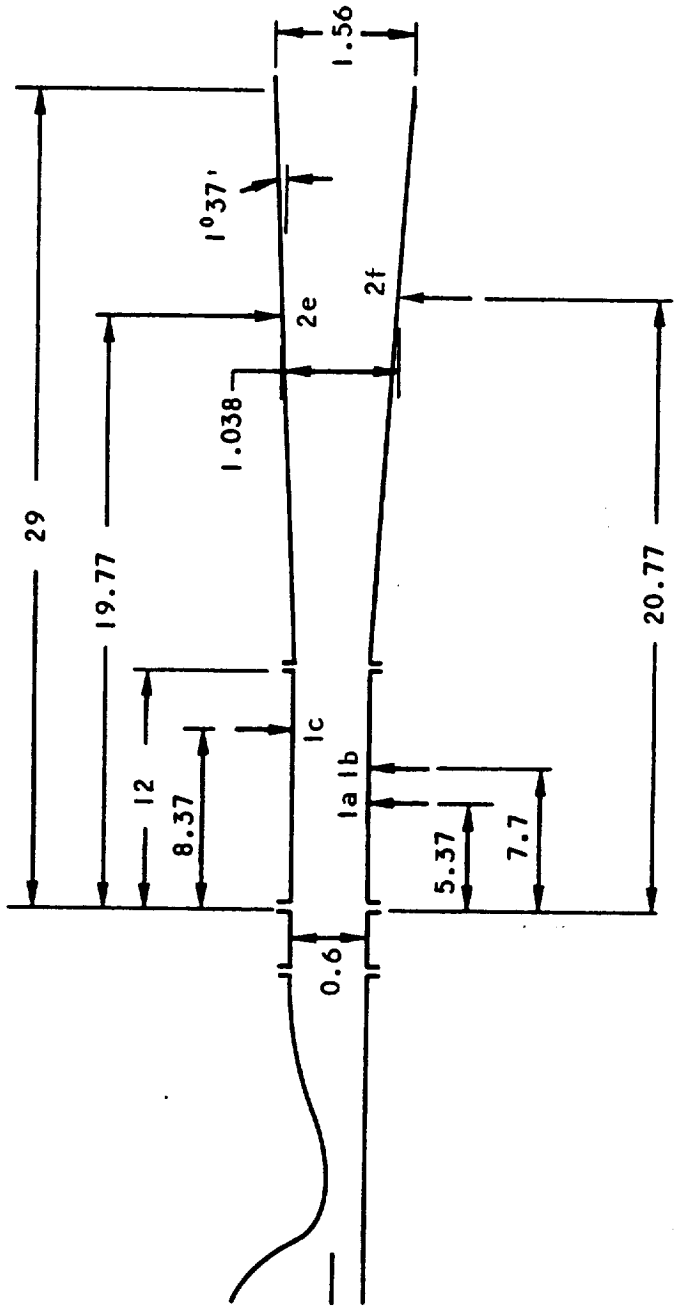

NOTE: ALL DIMENSIONS IN INCHES

Figure 6.2-1. Combustor Configuration Schematic

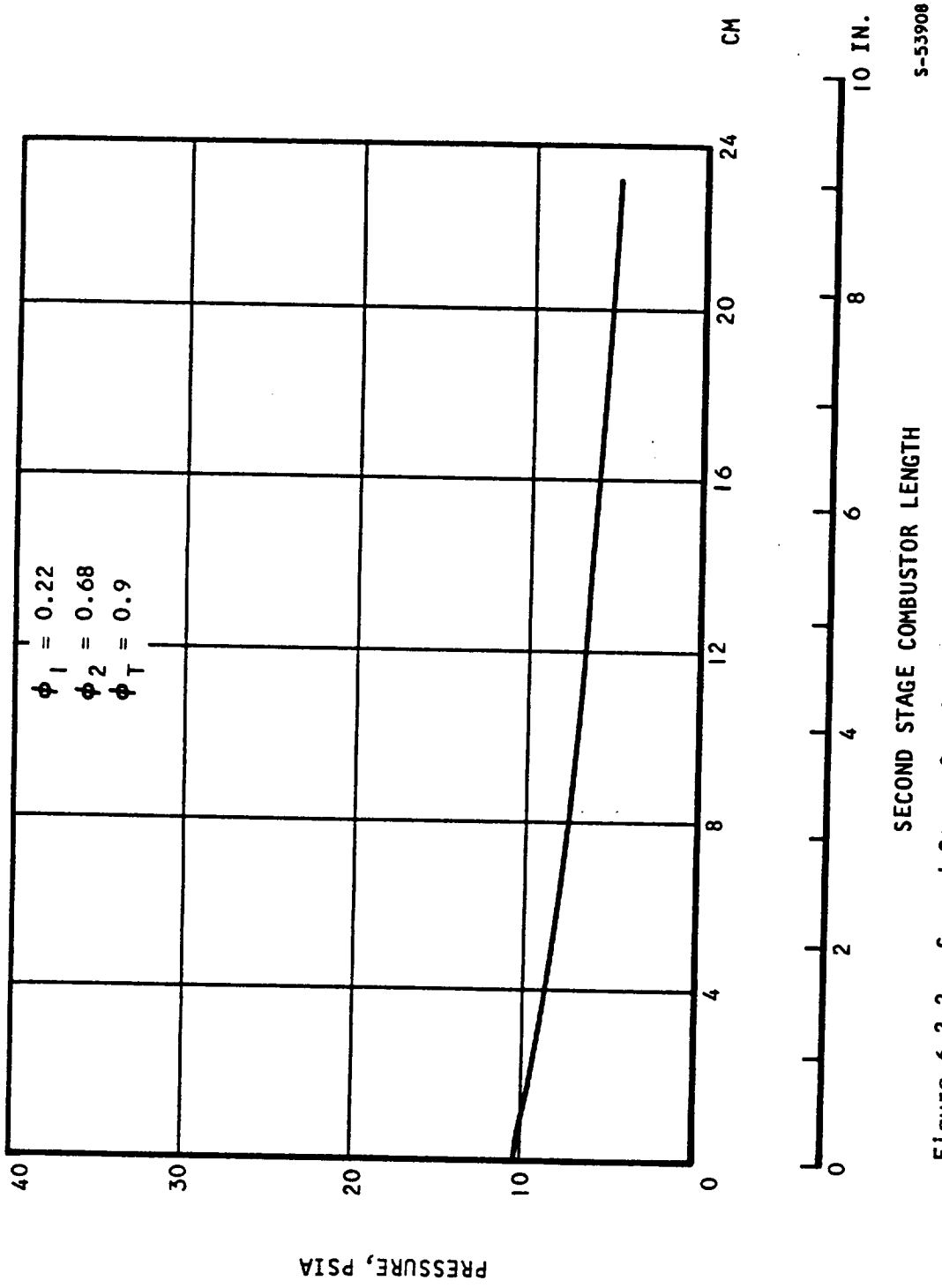

Figure 6.2-2. Second Stage Static Pressure Variation in Two-Dimensional Combustor at $T_{TO.} = 3000^{\circ}R$

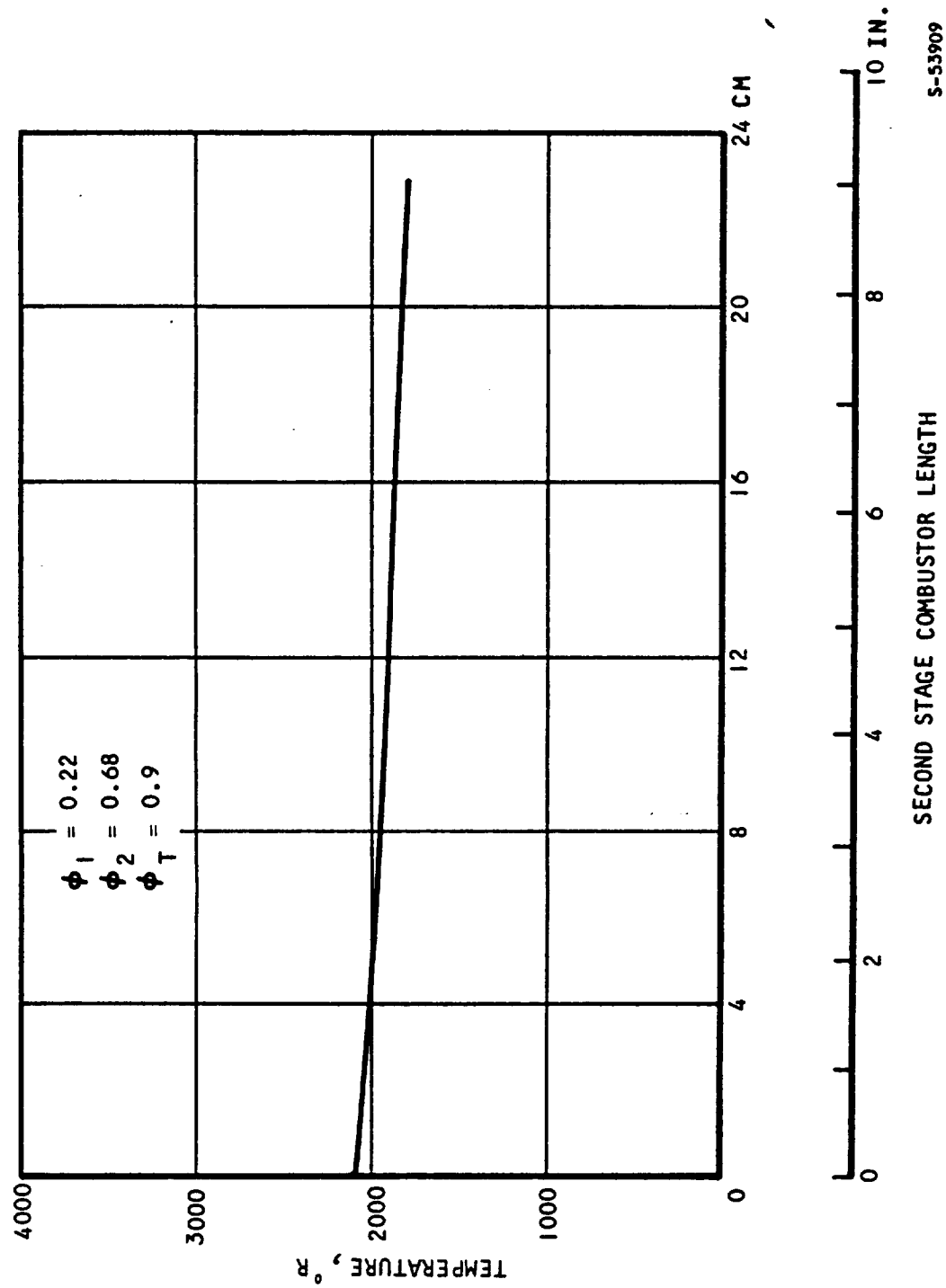

Figure 6.2-3. Second Stage Temperature Variation in Two-Dimensional Combustor at $T_{TO} = 3000^0R$

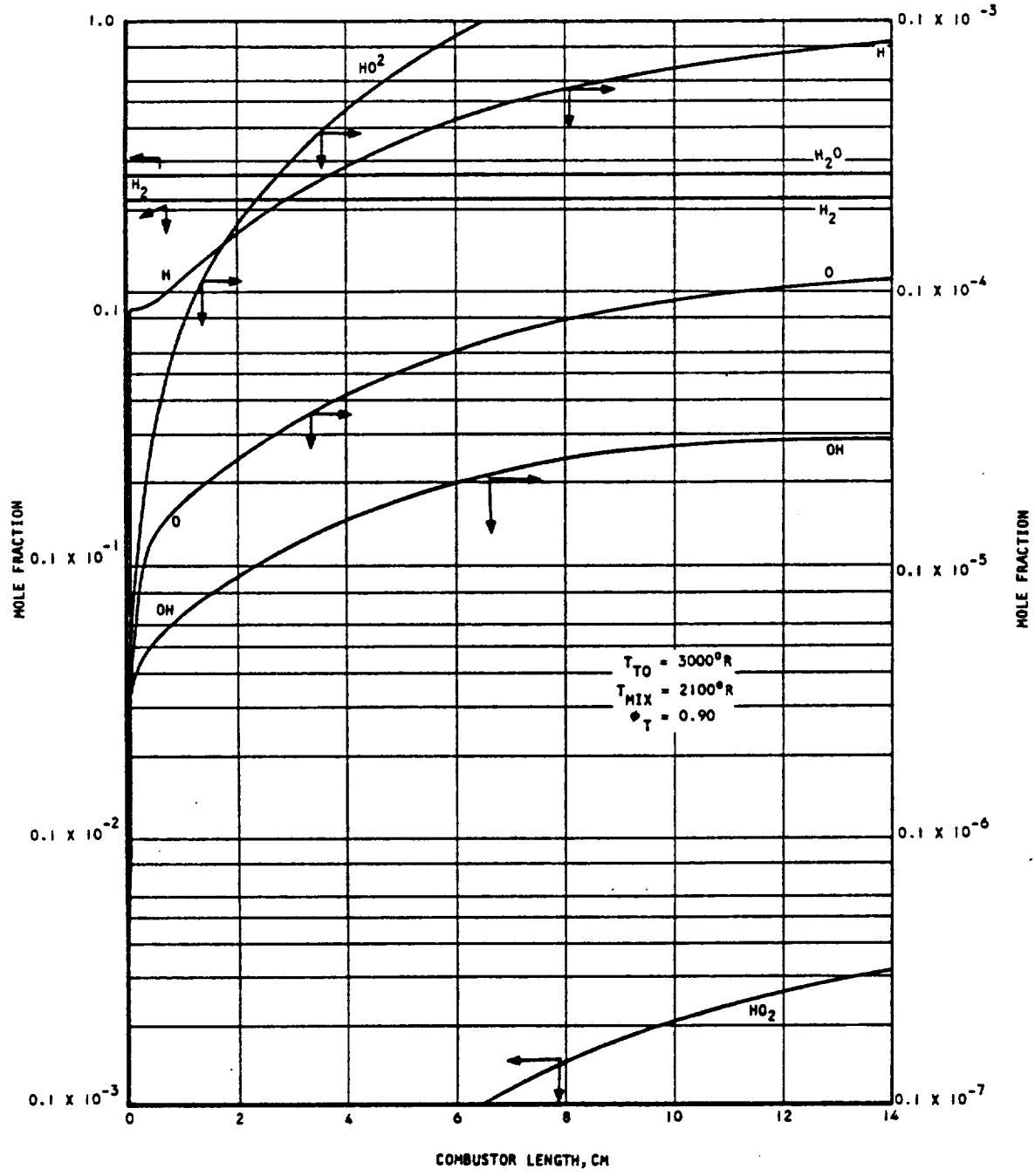

S-53948

Figure 6.2-4. Species Concentration, Two-Dimensional Combustor at T_{TO} = 3000°R

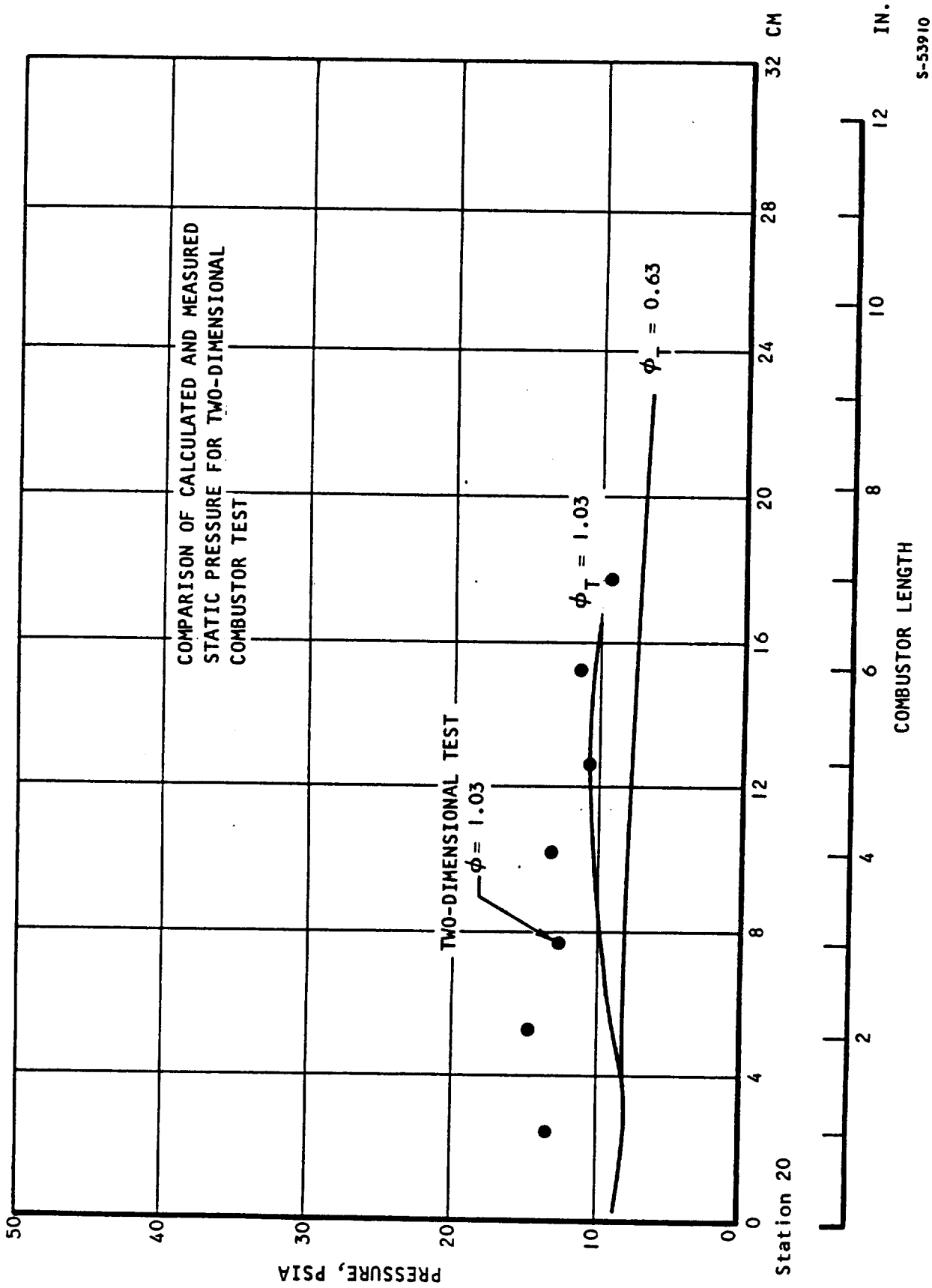

Figure 6.2-5. Comparison of Calculated and Measured Static Pressures for Two-Dimensional Combustor Test at T_{TO} = 3800°R

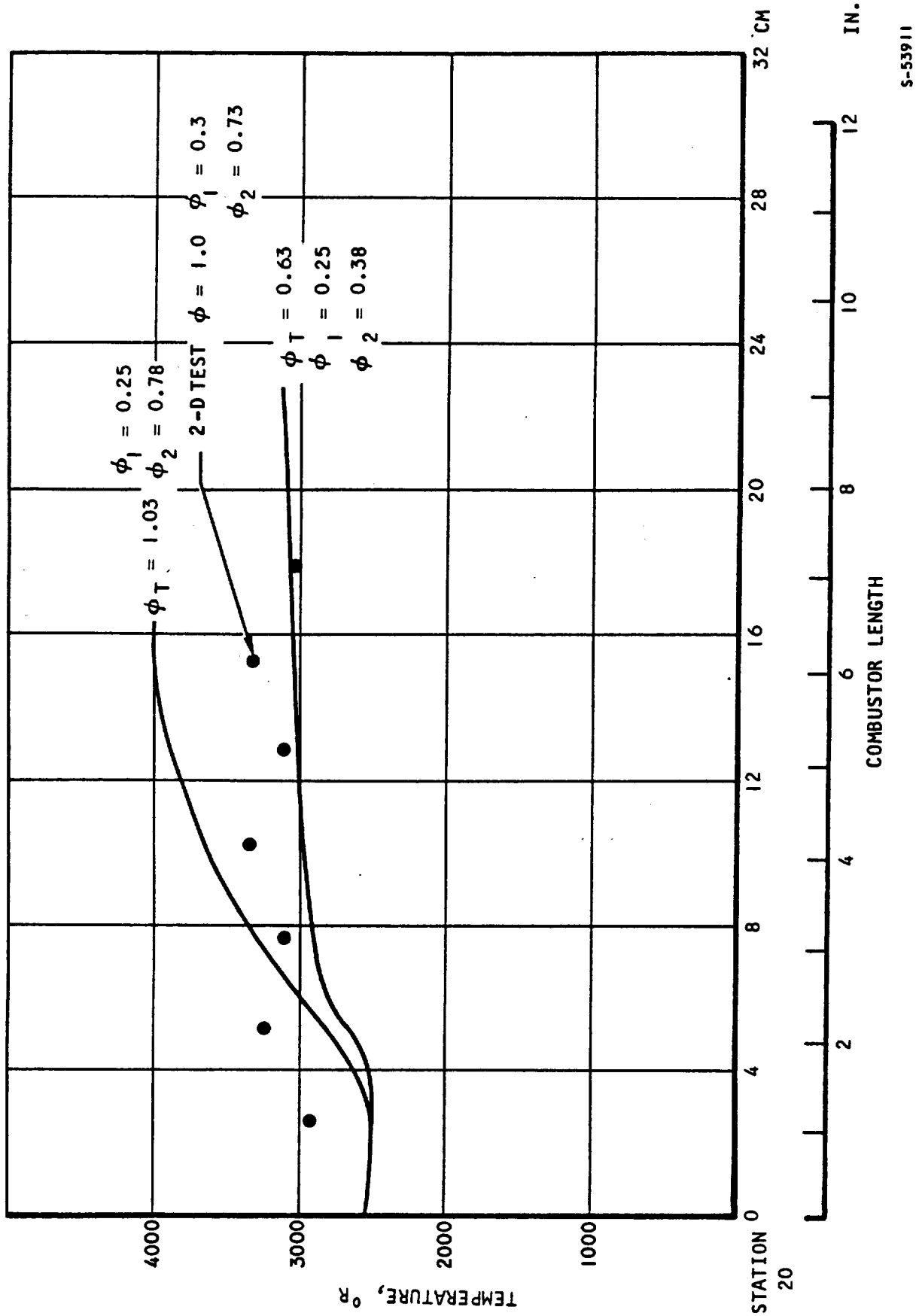

Figure 6.2-6. Static Temperature Comparison for Two-Dimensional Combustor at T_{TO} = 3800°R

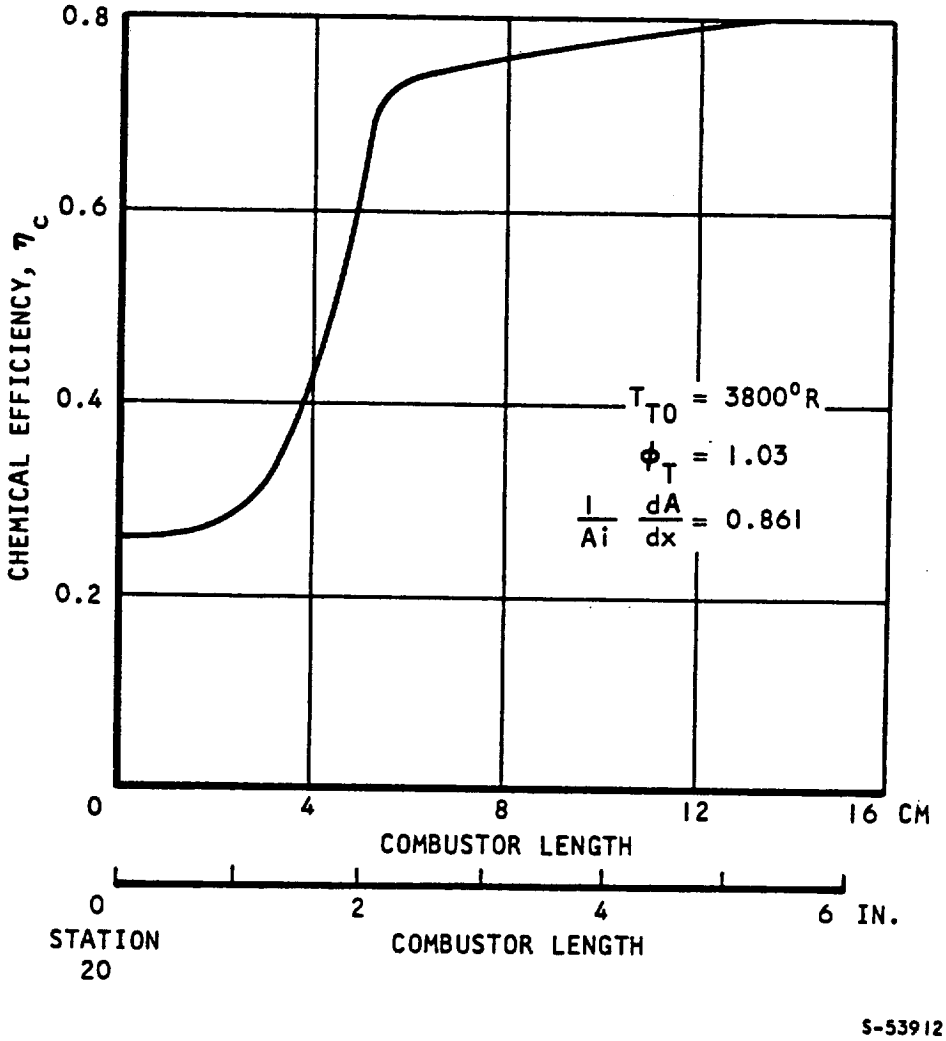

Figure 6.2-7. Chemical Efficiency Variation at T_{TO} = 3800°R

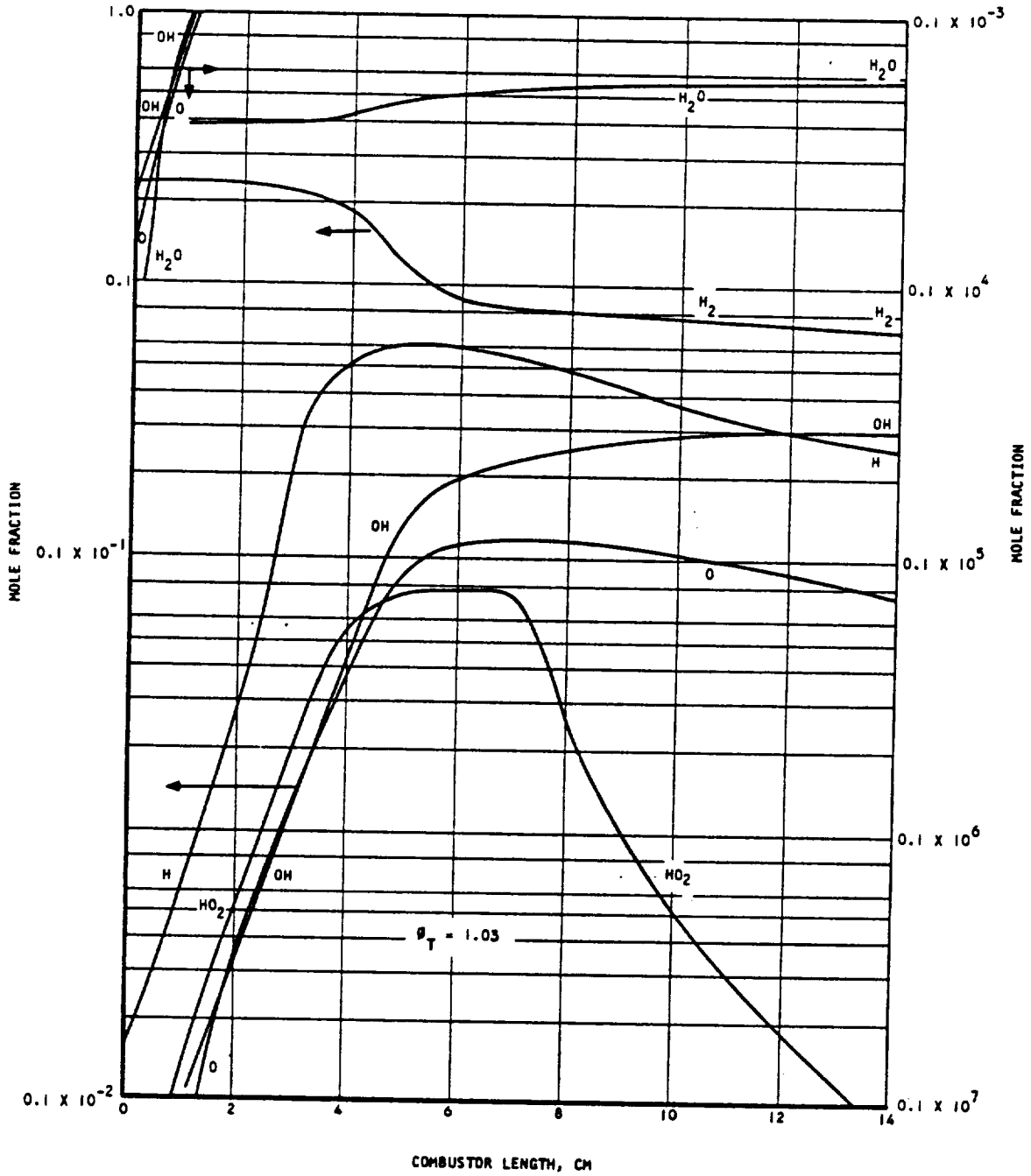

S-53949

Figure 6.2-8. Species Concentration, Two-Dimensional Combustor Study at $T_{TO} = 3800^{\circ}R$

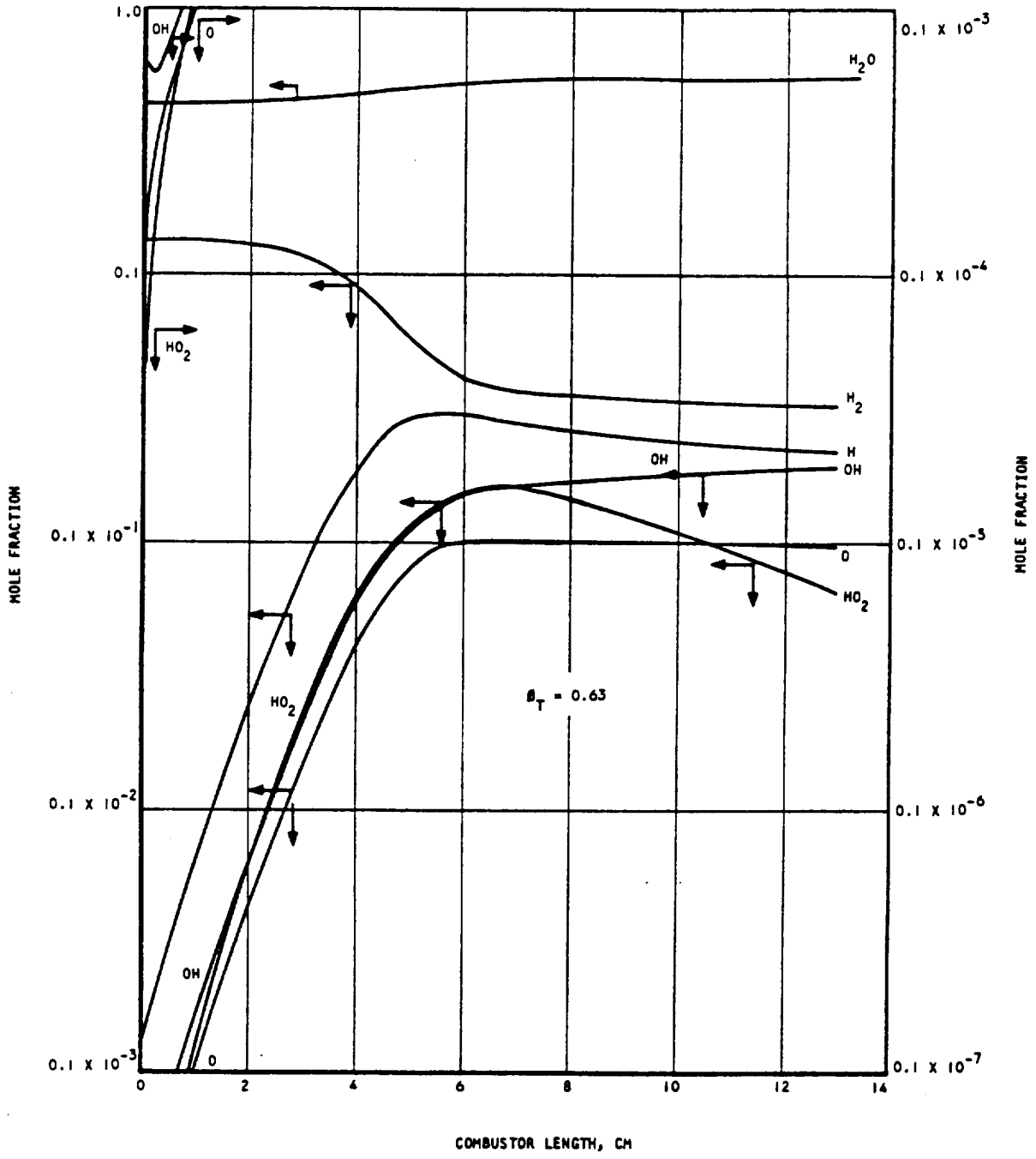

S-53950

Figure 6.2-9. Species Concentration, Two-Dimensional Combustor Study at T_{T0} - 3800°R

rapidly at 3800°R total temperature and did not react at all at 3000°R total temperature. At 3800°R about 80 percent of all fuel injected reacted which was higher than that calculated from the one-dimensional data reduction program. A more realistic study at both temperatures was made with another computer program. Measured static pressures, cooling, mixing, and friction losses were included in the model. The results of that study follow.

Two of the two-dimensional combustor tests were simulated in the Shear Layer Combustion Computer Program (Reference 2-2) developed by Dynamic Science. This program permits the analysis of complex chemical kinetic systems with arbitrary gas phase reactions and species using a one-dimensional (area or pressure defined) stream-tube model. Unique features of this program are (1) its ability to integrate the differential equations governing the chemical kinetic system with complete numerical stability using an implicit integration technique (Reference 6-2), and (2) its ability to add (or extract) mass momentum, energy, and species at any position along the stream tube.

The simulation of the tests was based on the assumption of two limiting conditions. The first of these conditions assumed that the combustor efficiencies calculated from test data represented chemical efficiencies (100 percent mixing efficiency). The second assumed that the combustor efficiencies represented the mixing efficiencies.

The several mixing models used with the two limiting conditions were implemented by the concept of an inert hydrogen molecule denoted by the symbol HZ_2. This inert hydrogen molecule participated in the flow dynamics, but was not permitted to dissociate or react with other species. Mixing was done by replacing inert hydrogen (HZ_2) with active hydrogen (H_2) using the species-addition feature of the computer program.

The three basic mixing models are shown in Figure 6.2-10. Model 1 produced early mixing, Model 2 produced a maximum mixing rate at the mid-point of the mixing length, and Model 3 produced late mixing. Further variation within each mixing model was obtained by varying both the mixing length and the amount of hydrogen mixed at the injectors.

The two tests chosen for this simulation are listed in Table 6.2-1 along with their nominal test parameters.

TABLE 6.2-1

	Run 238	Run 242	
Time (sec)	520.30	682.55	
φ	0.6049	1.0267	
T_T (°R)	2838	3575	Station 7.3
T (°R)	1897	2158	Station 7.3
Combustor Efficiency	60 percent	60 percent	

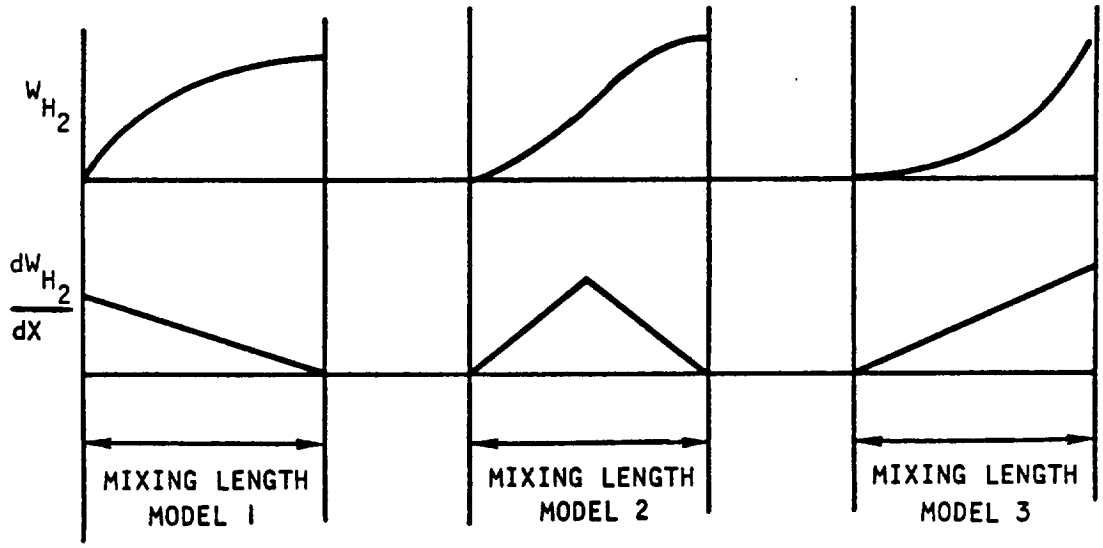

Figure 6.2-10. Mixing Models

The chemical kinetics calculations were started at Station 7.3, just ahead of the first stage injectors, using equilibrium concentrations of the species. The energy and momentum defects due to heat transfer and wall friction were distributed linearly along the combustor, while the energy, momentum, and mass addition due to fuel injection were input at the appropriate injectors. The pressure-defined stream tube model was employed using measured static pressures from the two tests (see Figure 6.2-11).

The results obtained from imposing the two limiting conditions on the simulation of run 238 in the Shear Layer Combustion Computer Program are presented in Figures 6.2-12 through 6.2-14, where the areas, mixing efficiencies, and chemical efficiencies were plotted as a function of axial position. In all cases 100 percent mixing efficiency (η_m) was assumed in the first stage combustor using mixing model 2 with 50 percent mixing at the injectors and complete mixing at station 12. Examination of the calculated areas in Figure 6.2-12 indicated a reasonable blockage (30 percent) in the constant-area portion and reattachment of the flow near the entrance of the divergent portion of the first stage combustor. The first stage results demonstrated chemical efficiencies of 95 percent at station 13 and nearly 100 percent beyond station 17 (see Figure 6.2-14).

The first limiting condition (100 percent overall mixing efficiency) was imposed on the second-stage combustor using both a 50-percent local mixing efficiency at the injectors with mixing Model 2 and a 0 percent local mixing efficiency at the injectors with mixing Model 3. An overall mixing efficiency of 100 percent was set at station 29 with both mixing models-- the former simulating early mixing; the latter, late mixing.

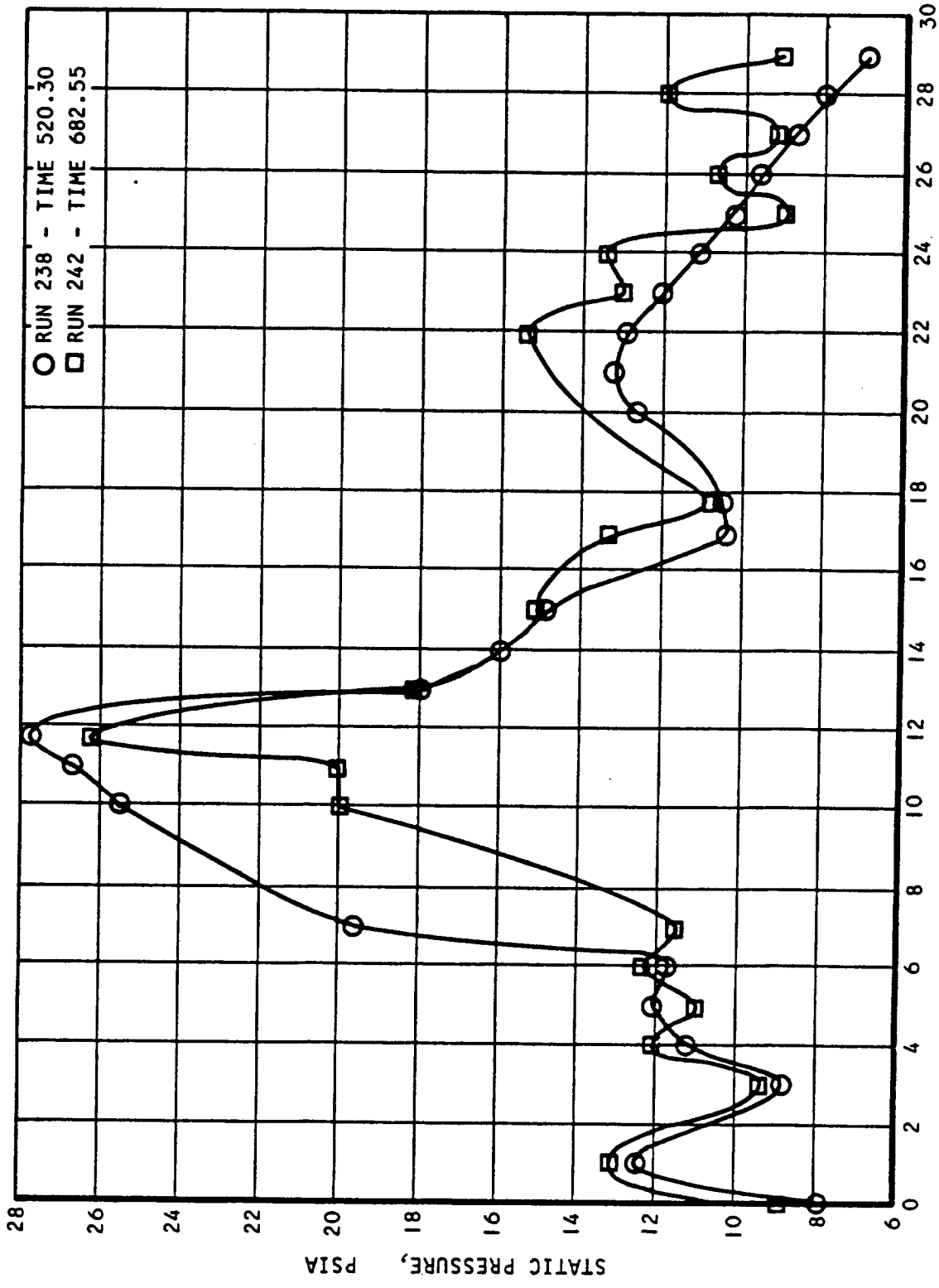

Figure 6.2-11. Measured Static Pressures - Tests 238 and 242

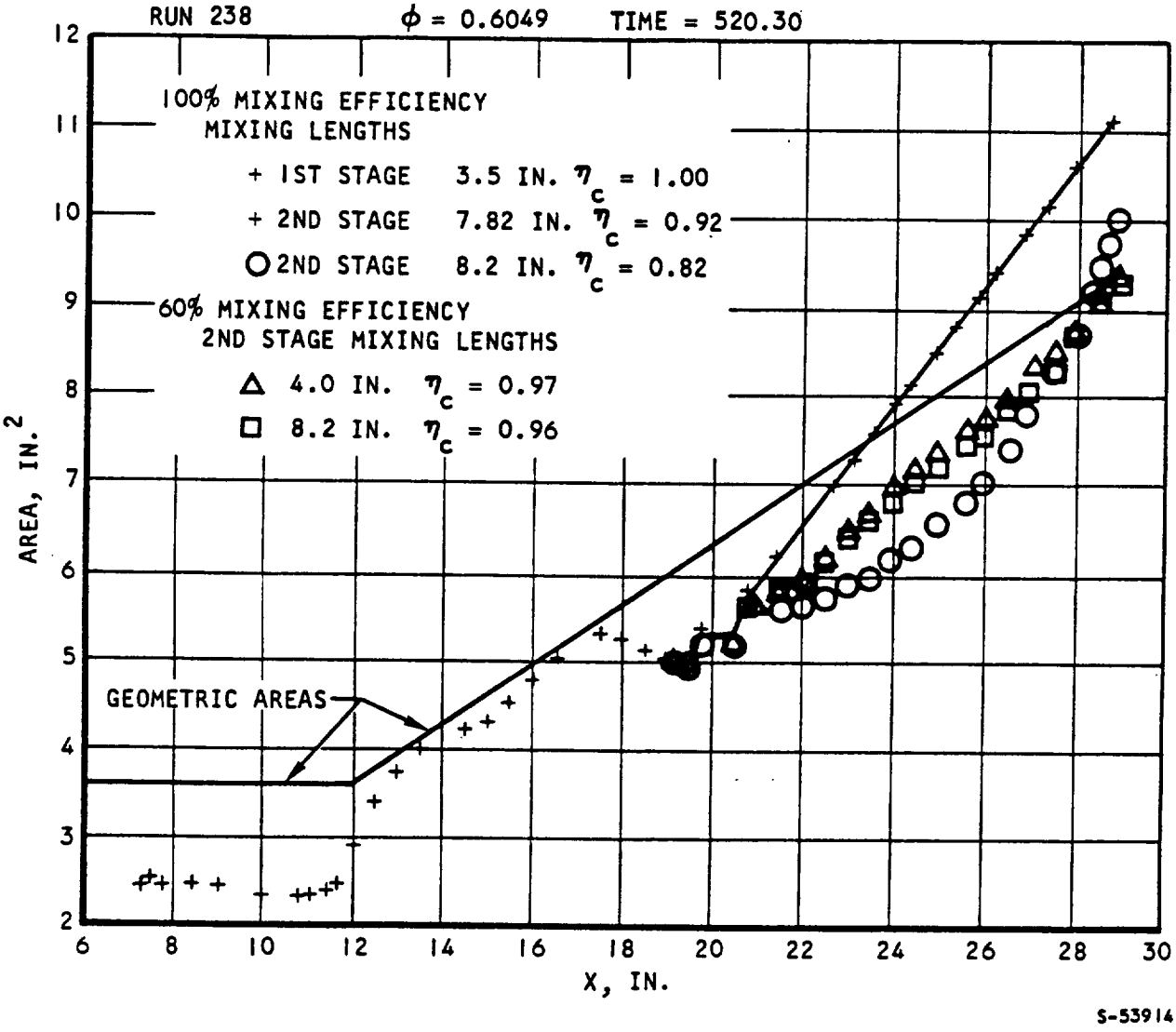

Figure 6.2-12. Geometric and Calculated Areas vs Axial Position

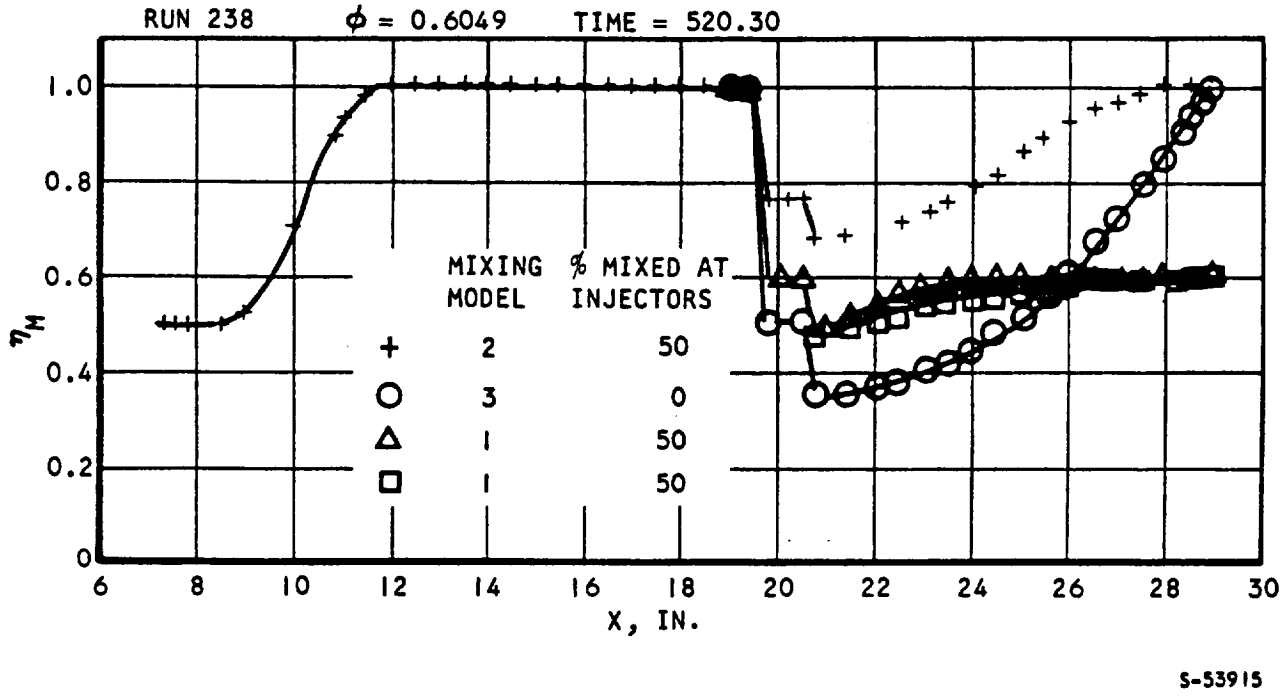

Figure 6.2-13. Mixing Efficiency vs Axial Position - Run 238

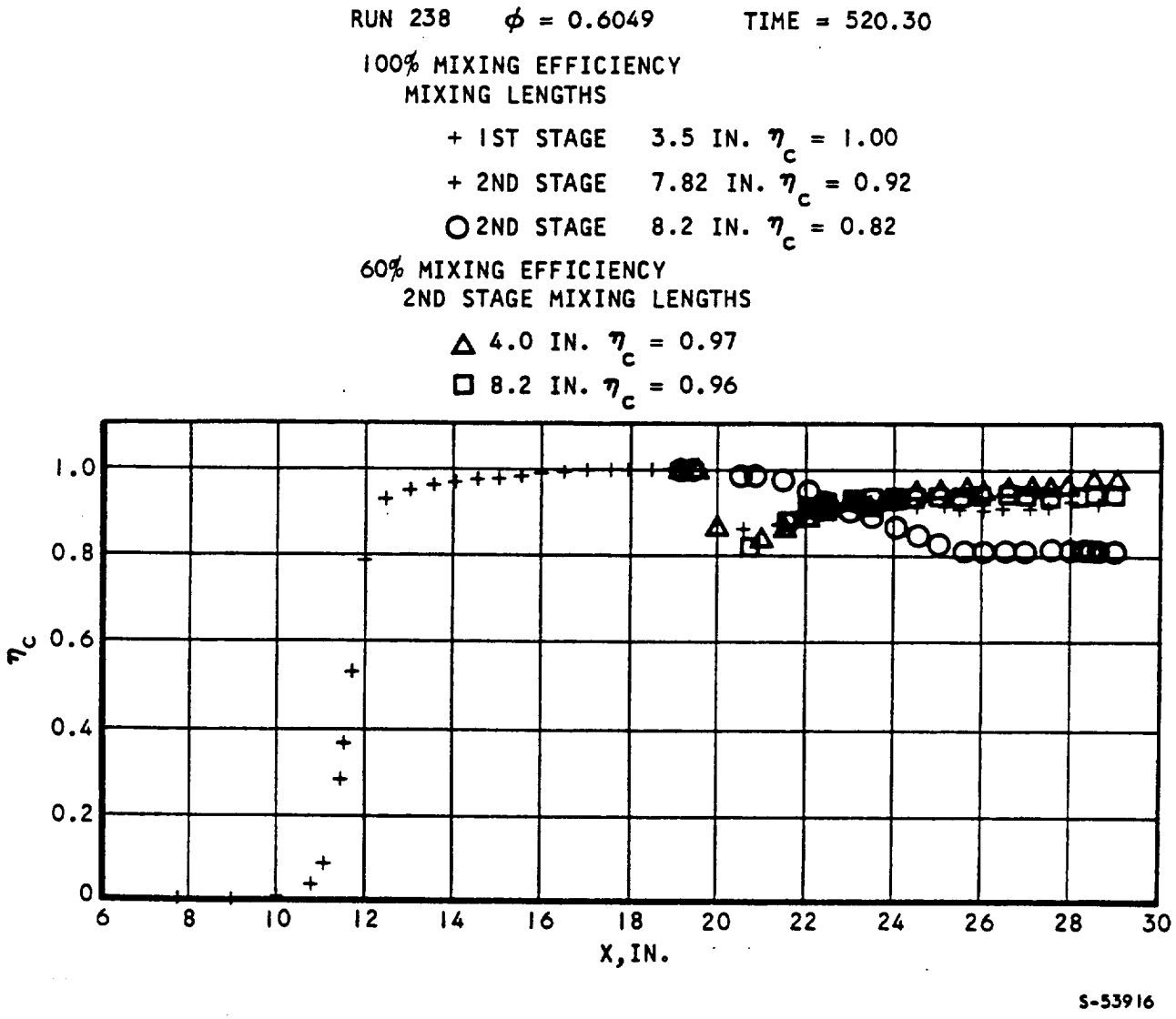

Figure 6.2-14. Chemical Efficiency vs Axial Position

Examinations of the calculated areas (symbols + and ⊙) in Figure 6.2-12 indicated a reasonable blockage (15 percent) at the second-stage injectors, however both mixing models eventually required flow areas greater than the geometric areas. Since such flows would be impossible to attain with the measured pressures from run 238, the assumption that the combustor efficiency equalled the chemical efficiency with 100-percent mixing was in error. This argument was further substantiated from the chemical efficiencies in Figure 6.2-14 where values were 92 percent for early mixing and 82 percent for late mixing, compared with the value of 60 percent required to match the test data.

Therefore, the other limiting condition (combustor efficiency = mixing efficiency) was imposed on the second-stage combustor. A 50-percent local mixing efficiency at the injectors with mixing Model I (early mixing) was assumed. An overall mixing efficiency of 60 percent was set at 4.0- and 8.2-in. downstream of the injectors (second stage) as shown in Figure 6.2-13.

Again, as shown in Figure 6.2-12, the calculated flow areas indicated a reasonable blockage in the vicinity of the second-stage injectors, with the blockage gradually decreasing to zero as the flow approached the combustor exit. The mixing length of 4 in. produced flow areas which closely matched the geometric areas and resulted in a chemical efficiency of 97 percent.

The two limiting conditions were imposed on the simulation of run 242 using the same mixing models as in run 238 with the exception that time did not permit the late mixing case to be run. The flow areas, mixing efficiencies, and chemical efficiencies were plotted as a function of axial distance and presented in Figures 6.2-15 through 6.2-17. Examination of the areas in Figure 6.2-15 again indicated that the first limiting condition (chemical efficiency = combustor efficiency, 100 percent mixing) was in error and that the flow areas resulting from the second limiting condition more closely matched the test conditions. The fluctuating flow areas near the exit of the combustor (Figure 6.2-15) were due to pressure fluctuations (see Figure 6.2-10).

While it appeared that the second limiting condition, i.e., incomplete mixing produced the correct flowfields, the true condition could be found somewhere between the two limiting conditions, quite close to the second. If the chemical efficiency is denoted by η_c combustor efficiency by η and, mixing efficiency by η_m, the relationship.

$$\eta = \eta_m \cdot \eta_c \qquad (6\text{-}5)$$

could be used to iterate on a mixing efficiency to produce flows which would more closely match the test results. For example, the next value of mixing efficiency in the iteration for run 238 would be obtained from

$$\eta_m^{(n+1)} = \frac{\eta}{\eta_c^{(n)}} = \frac{0.60}{0.97} = 0.62$$

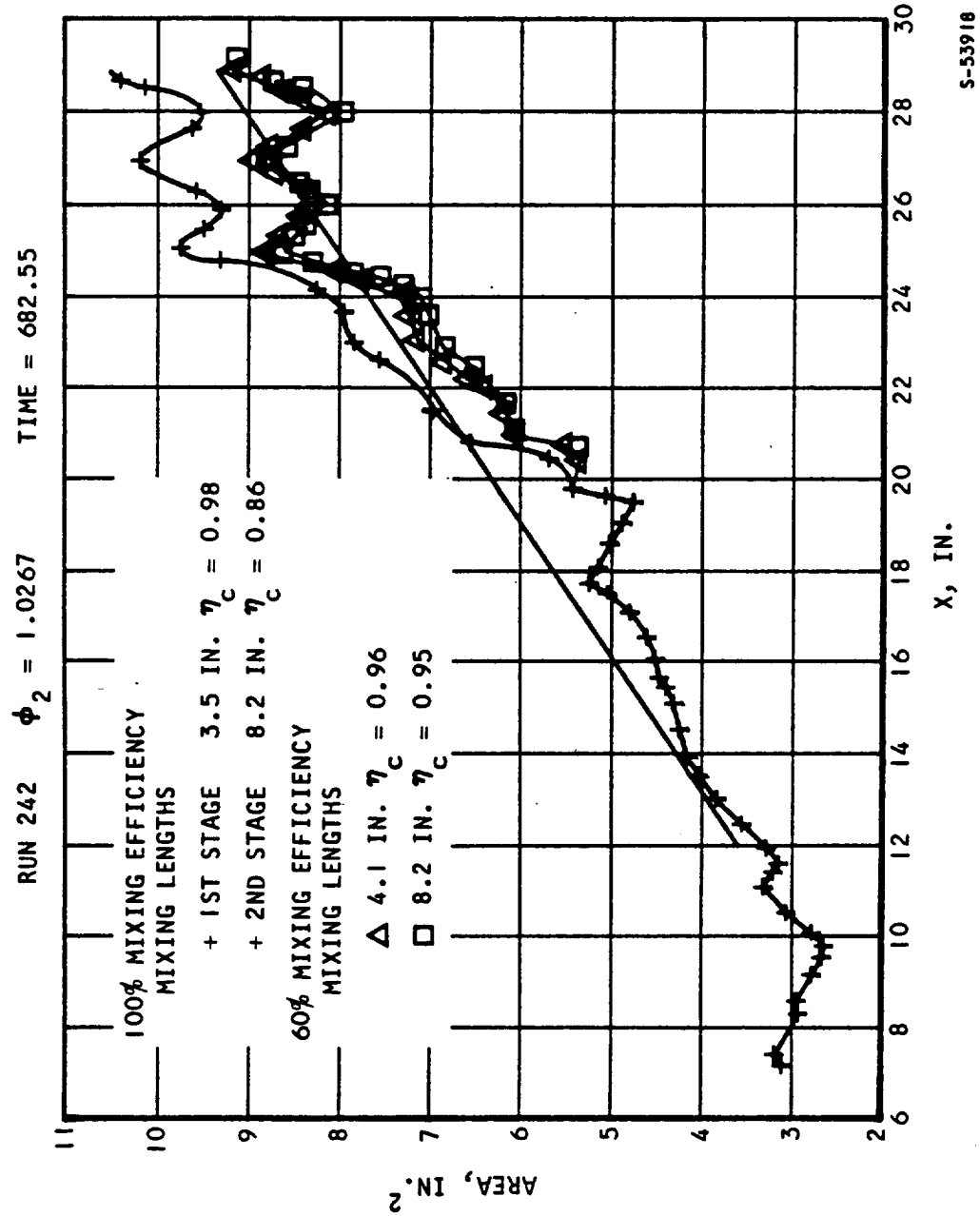

Figure 6.2-15. Mixing Efficiency vs Axial Position - Run 242

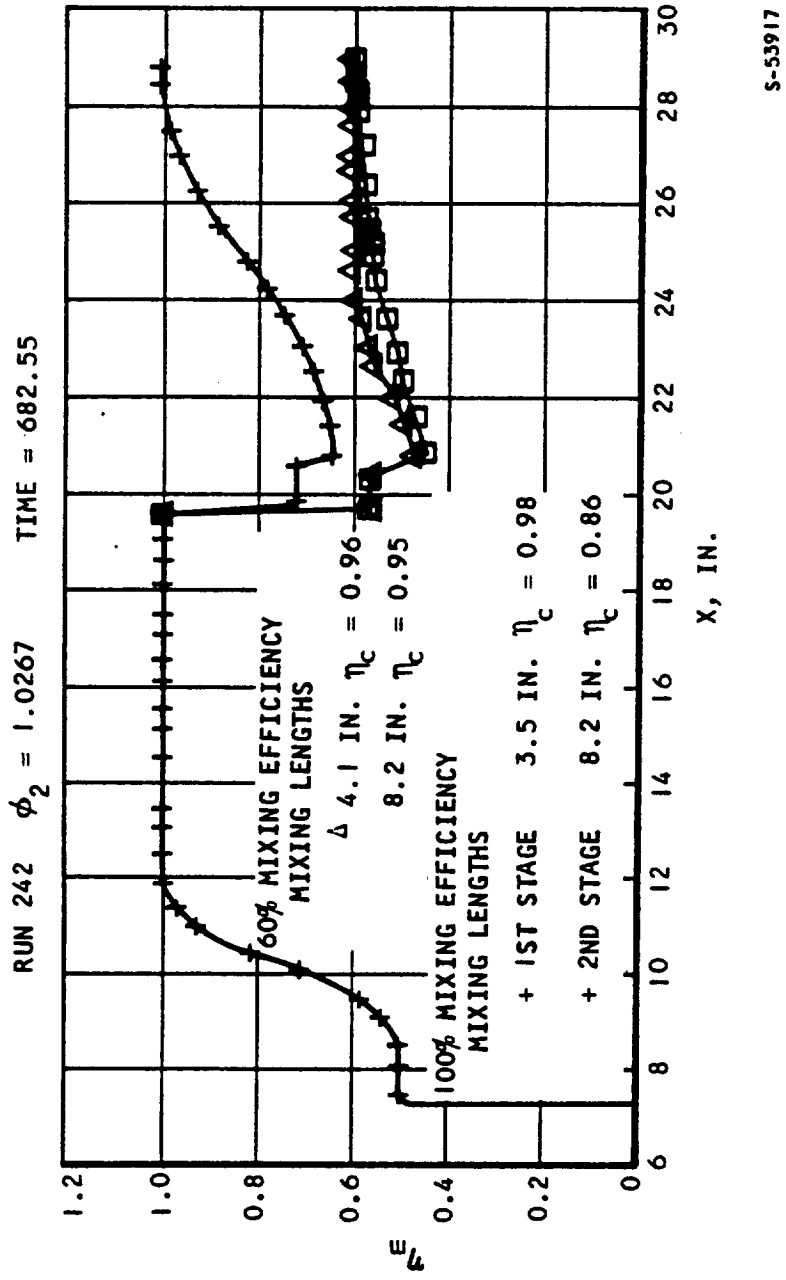

Figure 6.2-16. Geometric and Calculated Areas vs Axial Position - Run 242

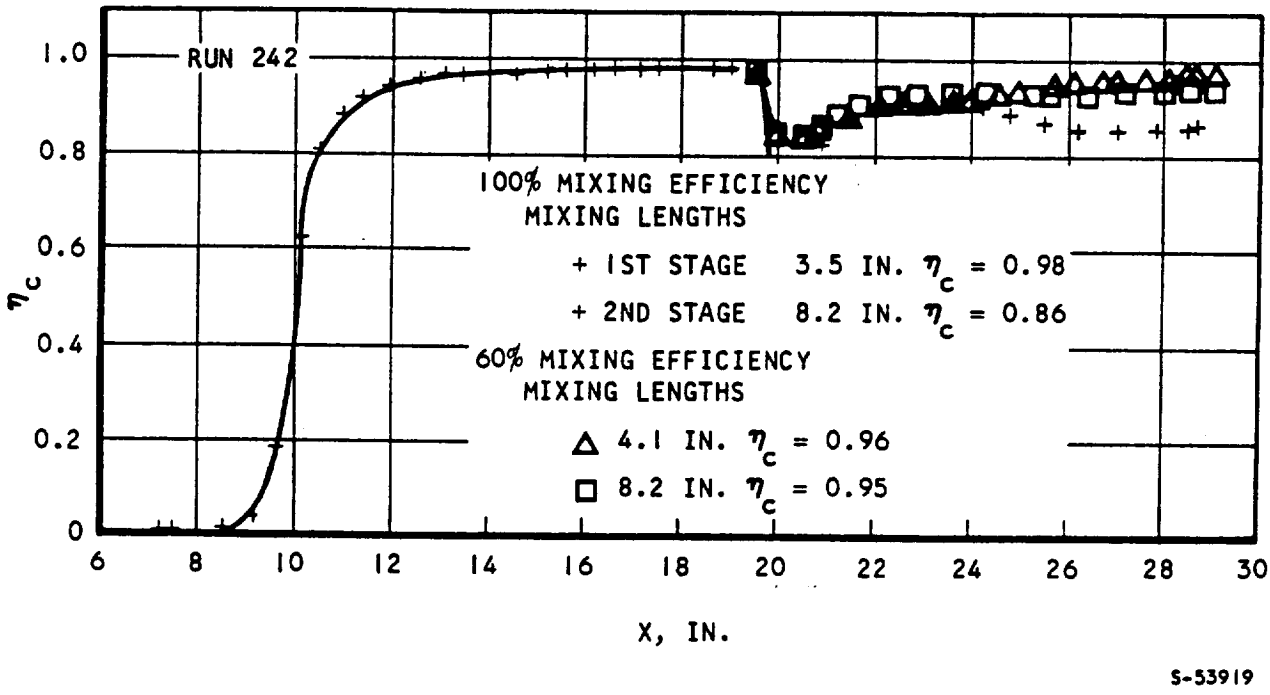

Figure 6.2-17. Chemical Efficiency vs Axial Position

The results from the above test simulations support the conclusion that the low combustor efficiencies experienced in the two-dimensional combustor tests were due to poor mixing in the second stage.

The detailed results from the chemical-kinetic simulation of runs 238 and 242 are presented in Appendixes I and 2.

7. AIM ENGINE

7.1 ANALYSIS

In the AIM combustor, fuel is injected from several locations as shown below:

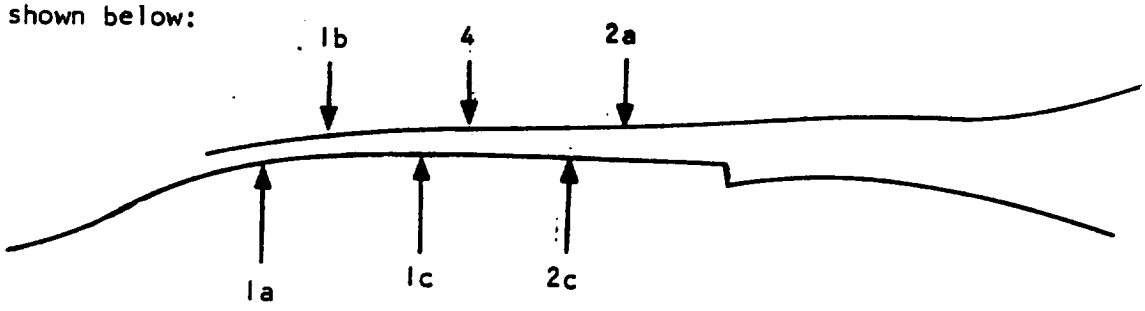

The first stage injectors (1a, and 1b) are located in a slightly diverging section; the second stage injectors (1c, 4 and 2a, 2c) at greater divergence. Fuel flow requirements in the first stage are set to prevent inlet unstart and thermal choking. The second stage fuel flow schedule was to be determined from cycle analysis and mixing studies.

A simulation of both stages was made in a two-dimensional combustor test. Testing demonstrated high chemical efficiency (near 90 percent) for the first stage injectors. The second stage injectors, which were located in a diverging area, gave much lower efficiencies (near 60 to 70 percent). A study was made of the present AIM combustor to see if these low efficiencies were inherent in the design due to chemical kinetics.

It was assumed that combustion would be temperature-controlled. Thus complete mixing was assumed. The Zupnik computer program was used to determine whether the second stage combustor could have a high chemical efficiency.

The first case studied was Mach 7 total temperature at 1000 psia total pressure to simulate test conditions for future AIM tests. It was assumed that an equivalence ratio of 0.4 would be injected from the first stage and that the second stage would begin midway between injectors 2a and 2c. A chemical efficiency for the first stage was based on two-dimensional combustor test results which indicated that at least 80 percent chemical efficiency should be obtained in the first stage combustor at an equivalence ratio of 0.4.

The engine cycle program was used to determine second-stage entrance conditions. This program uses equilibrium chemistry. Using the output static

temperature from the engine cycle program and assuming 900°R H_2 fuel at an equivalence ratio of 0.6 gave a mixed fuel-air temperature of 3000°R. This H_2 temperature included second stage cooling losses. Using this mixed temperature at 19 psia and 4800 ft/sec as the first stage exit conditions, the static pressure and temperature profiles for the second stage combustor were calculated in the Zupnik chemical kinetics program as shown in Figure 7.1-1 and 7.1-2. Examination of these profiles indicated a very short ignition delay period at mixed temperature of 3000°R. At a distance of 2.7 cm downstream of the second-stage entrance, the flow thermally choked after 85 percent of all fuel injected in both stages (ϕ = 1.0) had reacted. Instantaneous complete mixing was assumed at the second stage entrance. Actually, mixing will take some finite length with mixing and reaction occurring simultaneously over a portion of the combustor. Therefore, whether choking would actually occur cannot be determined using this model. However, with the assumption of complete and instantaneous mixing it does appear that at Mach 7 conditions there will be no chemical kinetics problem in the second stage combustor of the AIM engine. When the first stage chemical efficiency was reduced to 50 percent, which produced a mixed temperature of 2400°R, the fuel reacted less rapidly as indicated in Figure 7.1-2. In this case, a chemical efficiency of 83 percent was attained at a distance of 8.3 cm from the second stage entrance. Since the Mach number was about 1.6 at this point, it is improbable that thermal choking would have occurred had the calculation been continued.

Combustion occurred when species H and OH produced from first stage combusion were removed at the second-stage entrance (see Figure 7.1-2). There is, however, a large ignition delay with about 33 percent of the second-stage fuel reacted 19.2 cm from the entrance. This case is not very realistic, but was conducted to demonstrate that, at Mach 7, there is no combustion problem due to temperature alone.

An idea of how the mole fractions of several species varied with combustor length is presented in Figures 7.1-3 and 7.1-4. At a mixed temperature of 3000°R (see Figure 7.1-3) the concentrations of H, O, OH and HO_2 increased rapidly, but after 1 cm the concentrations of H, O, and HO_2 decreased. The buildup of OH and H_2O became less rapid after 1 cm, and OH started to de-decrease just before thermal choking occurred. Similar trends were observed at a mixed temperature of 2400°R (see Figure 7.1-4). It appeared that the production rate of H_2O started to decrease at 6 cm of combustor length and that the reaction of H_2 proceeded very slowly beyond 7 cm. In the AIM combustor there is about 5-times as much length compared with the two-dimensional combustor so slower reaction should not be a problem. The variation of second stage chemical efficiencies are shown in Figure 7.1-5. The chemical efficiencies were approximated from the change in weight fraction of H_2. This is not exact since even if the chemical reaction were to go to equilibrium, some H_2 would remain. It does indicate, though, a rapid increase in chemical efficiency near 80 percent with a slow rise thereafter.

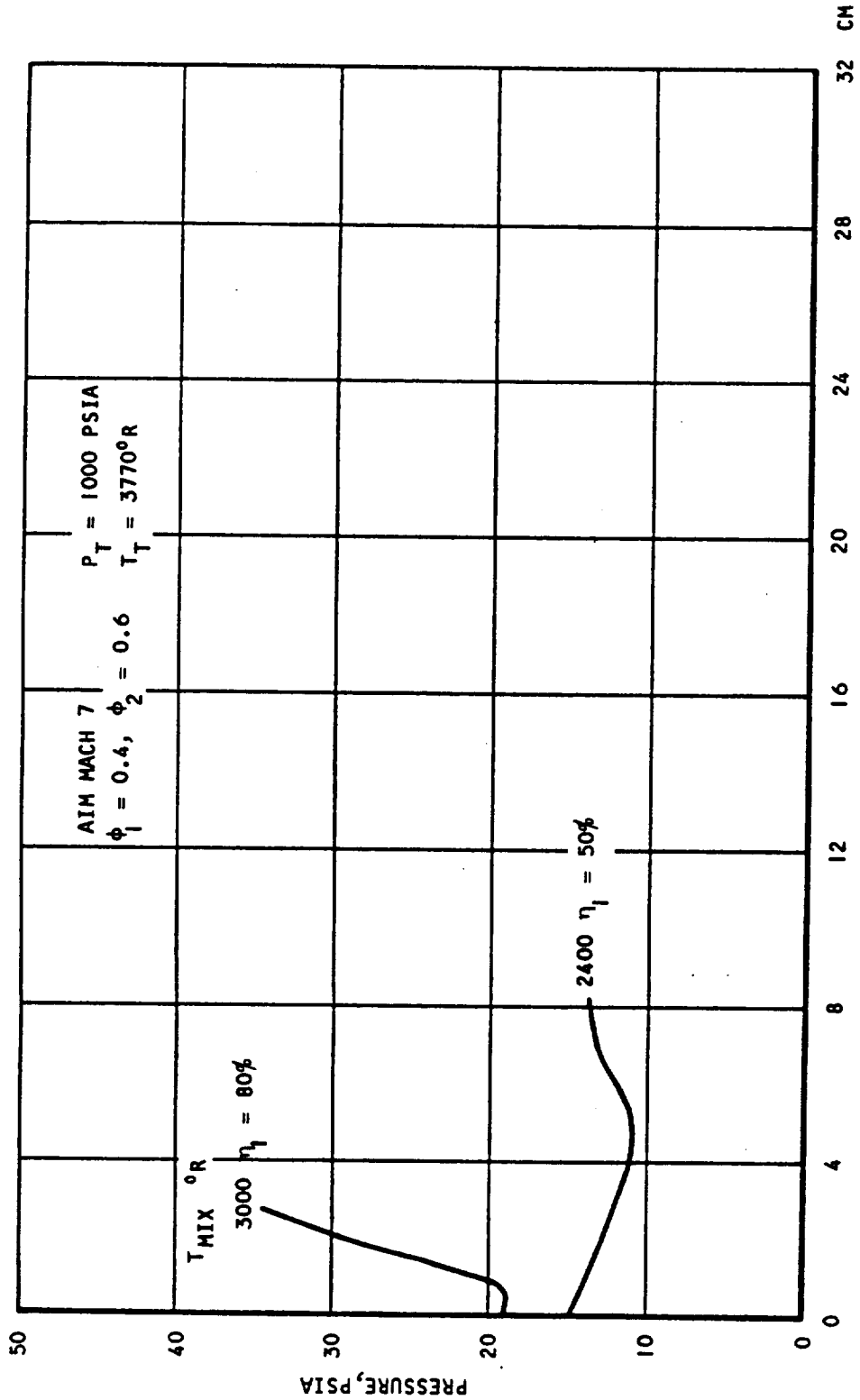

Figure 7.1-1. Static Variation at Mach 7 - AIM Combustor (U)

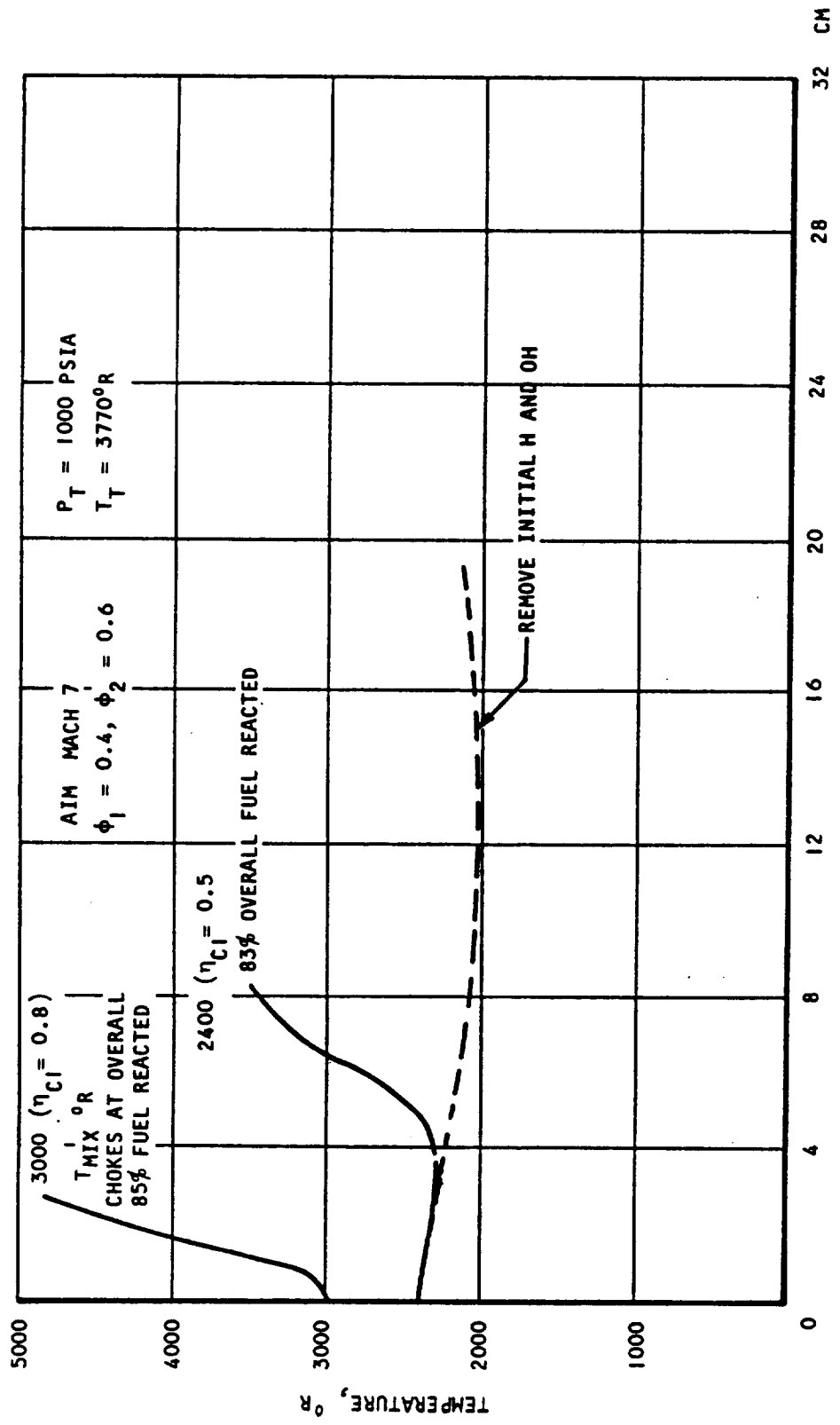

Figure 7.1-2. Static Temperature Variation at Mach 7 - AIM Combustor (U)

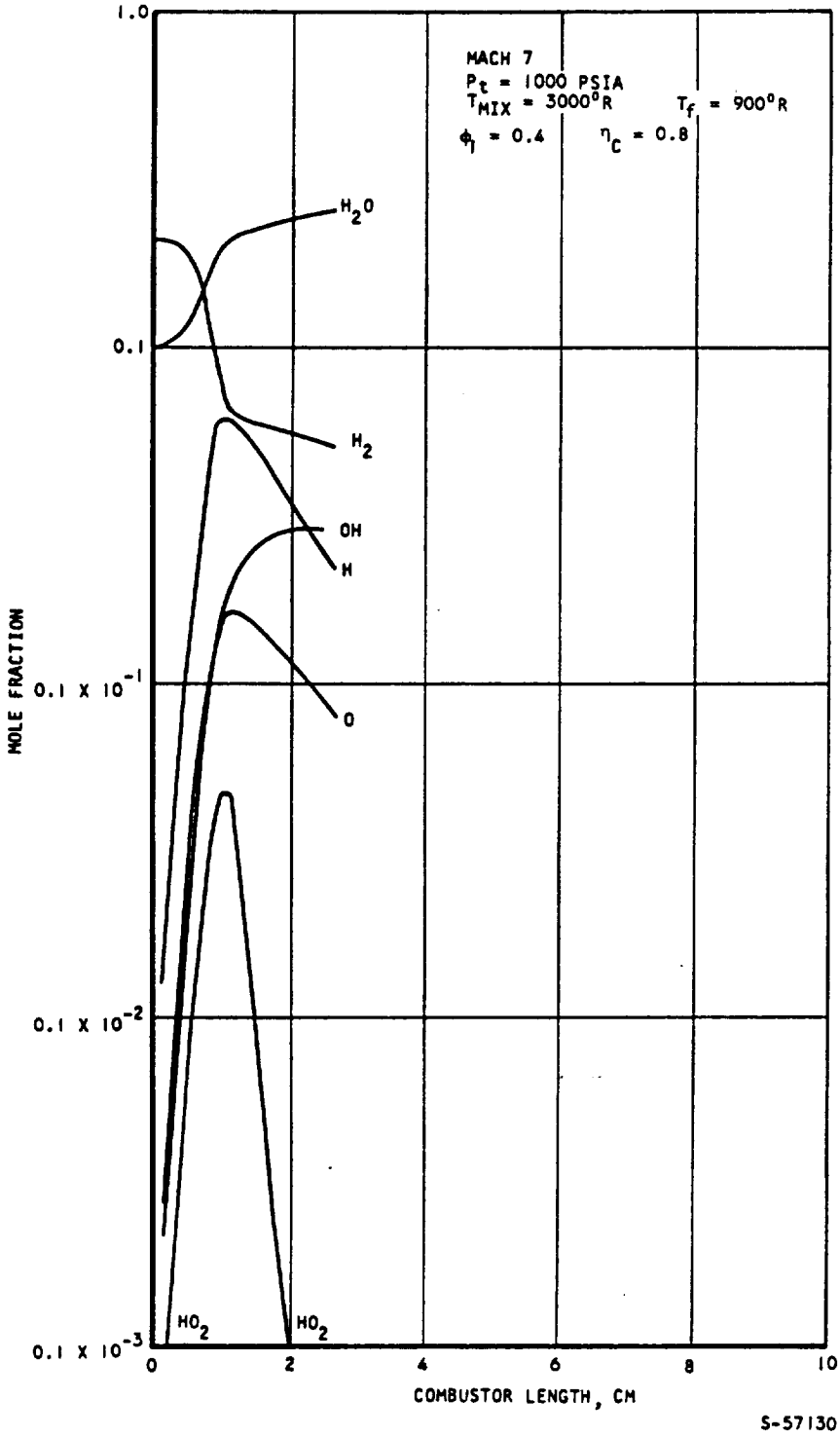

Figure 7.1-3. Species Concentration of Mach 7 - AIM Combustor (U)

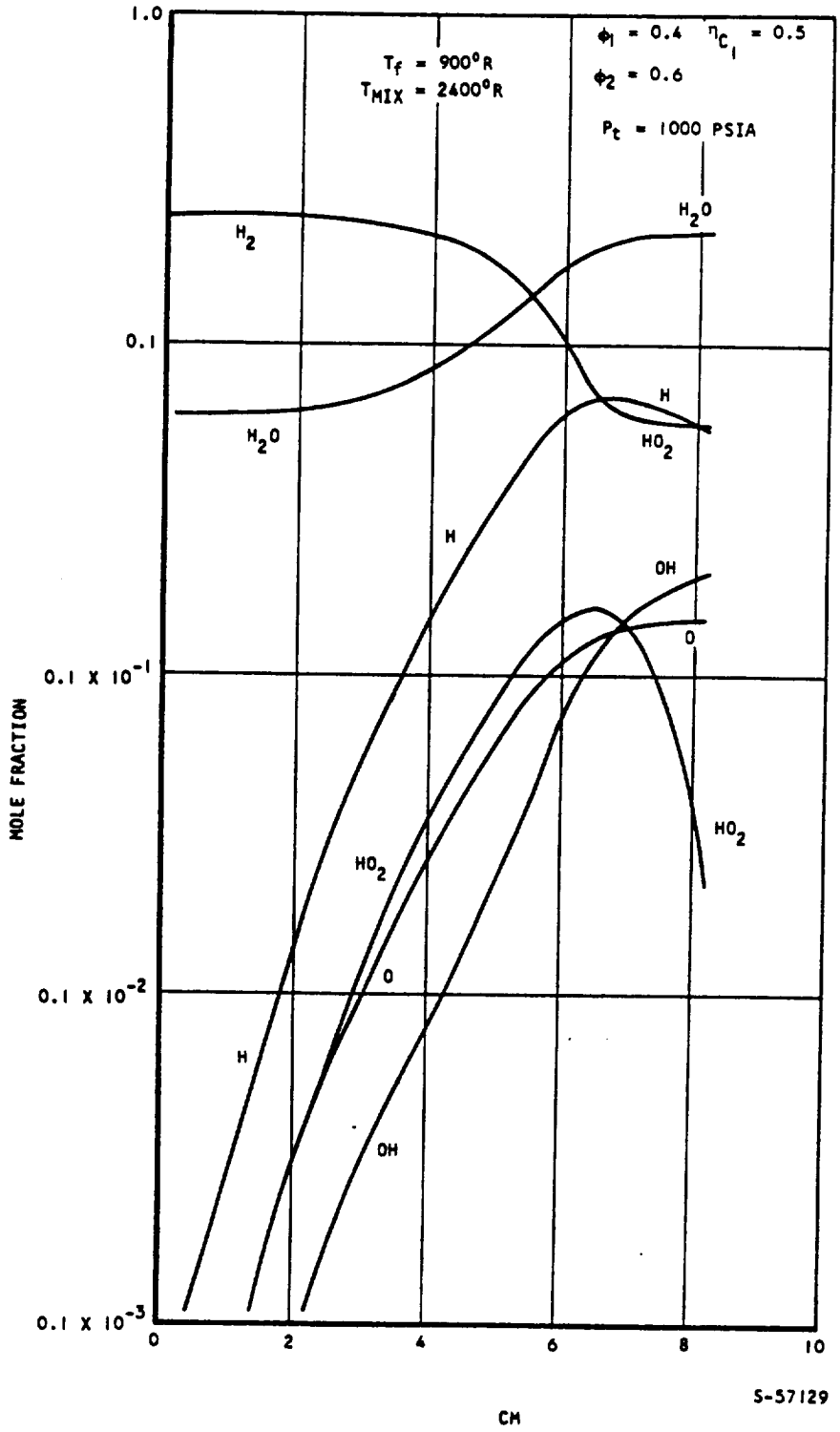

Figure 7.1-4. Species Concentration at Mach 7 - AIM Combustor (U)

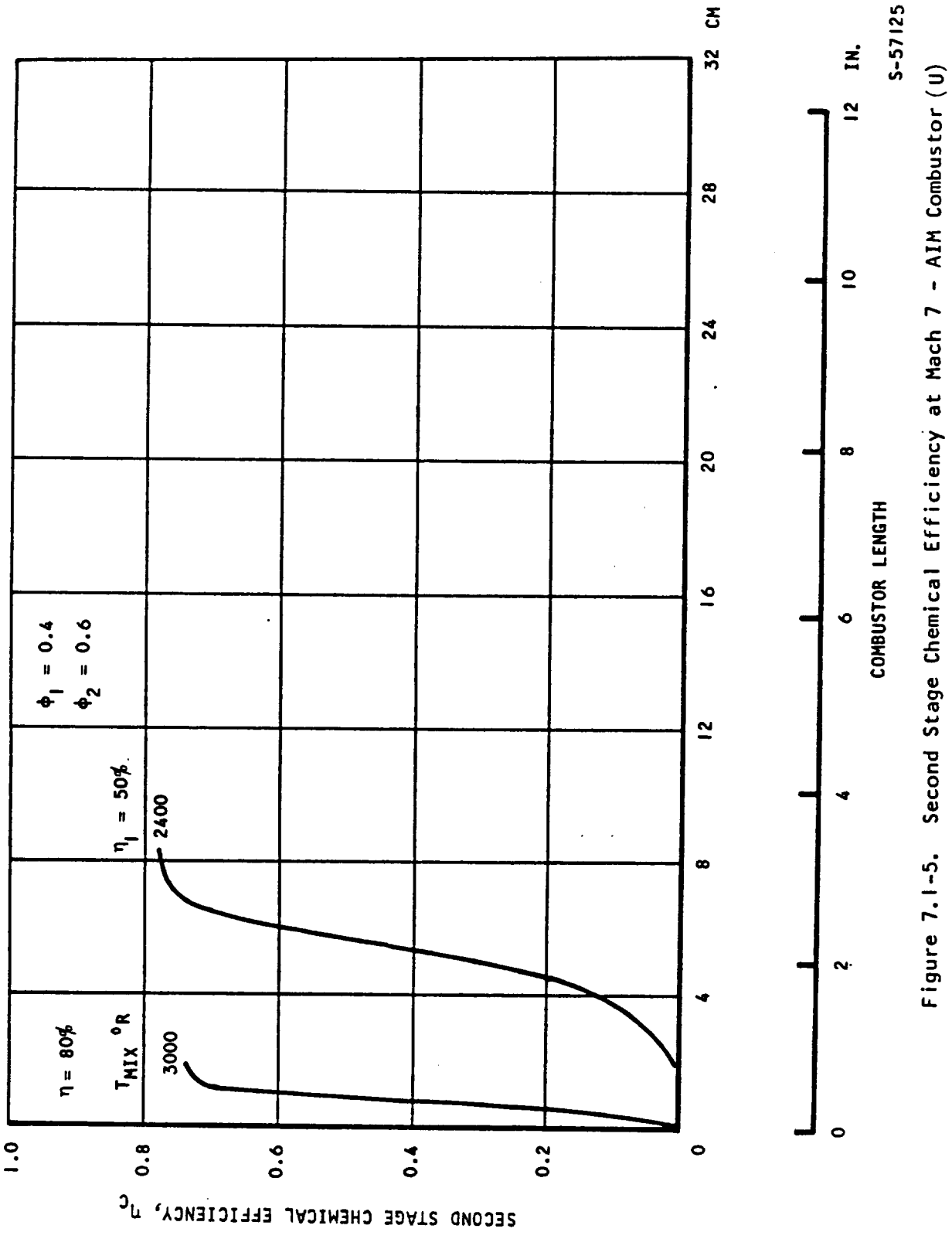

Figure 7.1-5. Second Stage Chemical Efficiency at Mach 7 - AIM Combustor (U)

The second case simulated Mach 6 flight conditions. The manner in which the study was conducted was the same as at Mach 7. This time an equivalence ratio of 0.2 was assumed for the first stage with a chemical efficiency of 80 percent at a point midway between injectors 2a and 2c. The second-stage equivalence ratio was 0.8, and several fuel temperatures from 900°R to 1500°R were used. The results obtained from the finite kinetics program are shown in Figures 7.1-6 and 7.1-7. At a fuel temperature of 900°R, the mixed fuel-air temperature was 2150°R and no temperature rise was observed; at 1500°R fuel temperature or 2270°R mixed fuel-air temperature the fuel burned rapidly. A mixed temperature between these two was run (2200°R) and in this case the fuel also reacted. Thus using species concentrations based on equilibrium chemistry for second-stage entrance conditions showed that a change of 50°R mixture temperature would produce a go or no-go situation. When the H and OH produced from the first stage combustion were removed at a mixed temperature of 2200°R, no temperature rise was observed, as shown in Figure 7.1-7. This was not the case at Mach 7 at a mixed temperature of 2400°R. At a mixed temperature of 2270°R, about 70 percent of all fuel injected (ϕ = 1.0) reacted before thermal choking occurred, while at 2200°R mixed temperature 60 percent reacted before computer cut-off time was reached (flow did not choke). The chemical efficiencies for these cases are shown in Figure 7.1-8. When the fuel reacted it did so rapidly. The chemical efficiencies continued to rise at both mixed temperatures.

Several species were plotted in Figures 7.1-9 to 7.1-12 for cases with fuel reacting and without fuel reacting. The OH concentration for a mixed temperature of 2150°R reached a maximum of 2×10^{-7} moles/liter at about 6 cm downstream of the second stage injection as shown in Figure 7.1-11. At this point the static temperature had dropped to about 1950°R with a static pressure of 20 psia. The parametric studies seemed to indicate that once the static temperature became less than about 2000°R in a divergent duct and the OH concentration had not reached 10^{-6} moles/liter by then, combustion did not occur. Thus, results from chemical kinetics simulation of the AIM configuration were consistent with the parametric study in Section 3 of this report. For the cases with combustion (Figures 7.1-9 and 7.1-10) an OH concentration of 10^{-6} moles/liter was always reached before the static temperature was reduced to 2000°R. As shown in Figure 7.1-12, the 50°R difference in static temperature between the go and no-go cases caused an increased production rate of OH starting at about 0.05 cm from the second stage entrance. Thus the OH concentration was able to reach 10^{-6} moles/liter before the temperature became too low due to divergence.

For a mixed temperature of 2200°R, an OH concentration of 10^{-6} moles/liter was reached in about 3 cm. This corresponded to an ignition delay time of about 25 μsec. By this time the temperature had dropped to 2100°R. If one had assumed expansion with friction at a mixed temperature of 2150°R, the variation of static temperature with time would have been as shown in Figure 7.1-13. With a friction coefficient of 0.006, at 25 μsec, the static temperature would be close to 2100°R. Thus, had friction been included in the model,

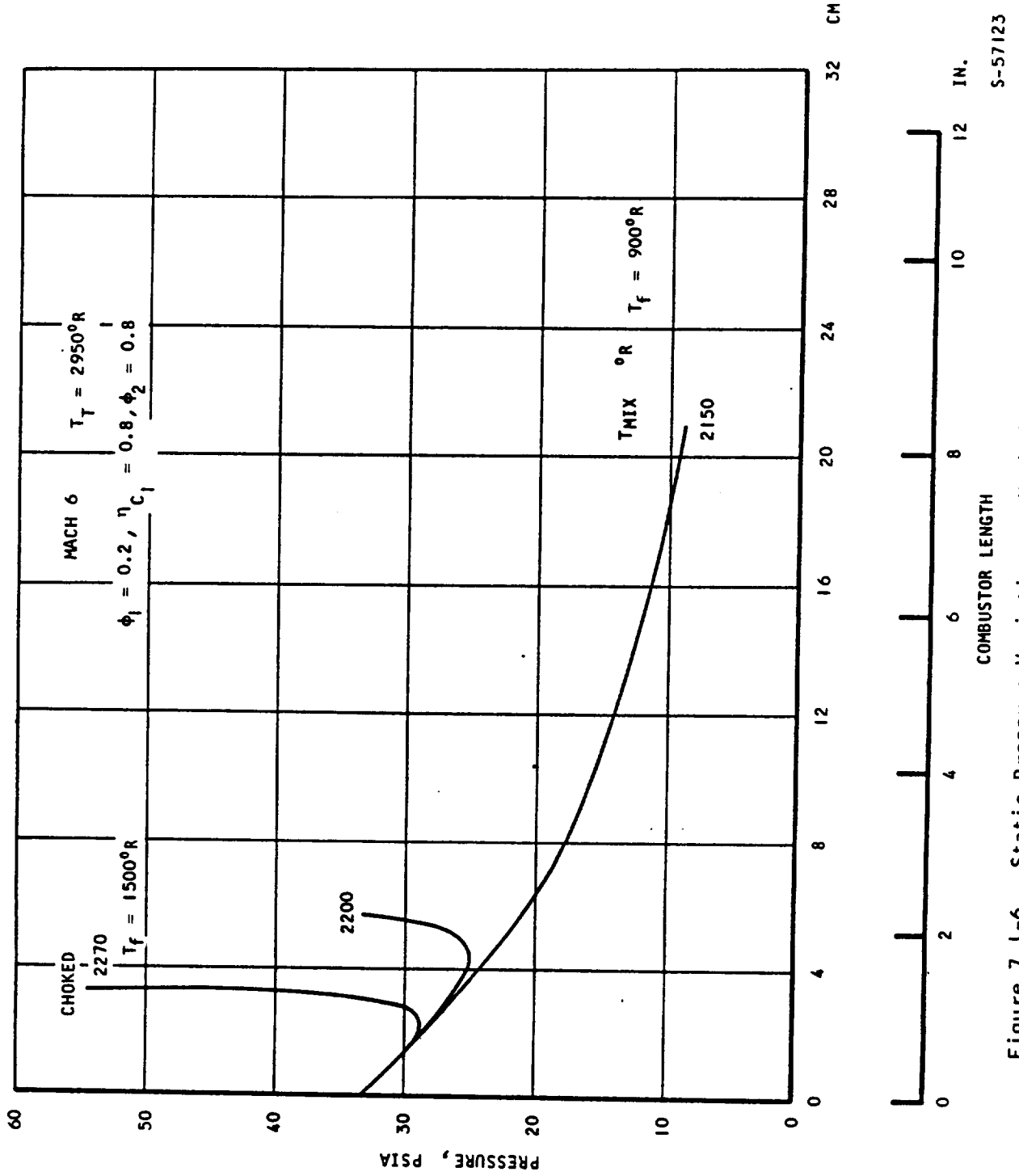

Figure 7.1-6. Static Pressure Variation at Mach 6 - AIM Combustor (U)

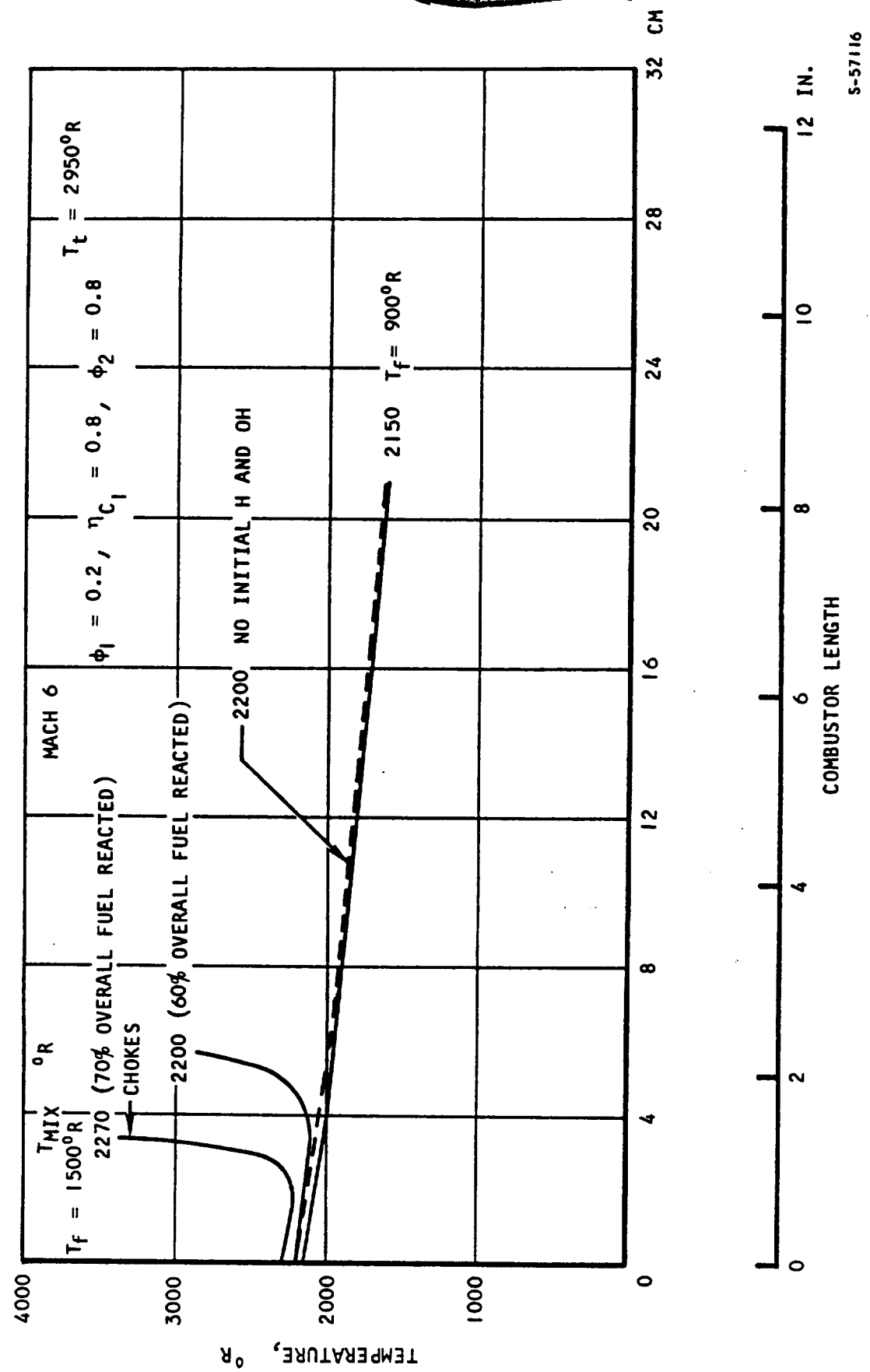

Figure 7.1-7. Static Temperature Variation at Mach 6 - AIM Combustor (U)

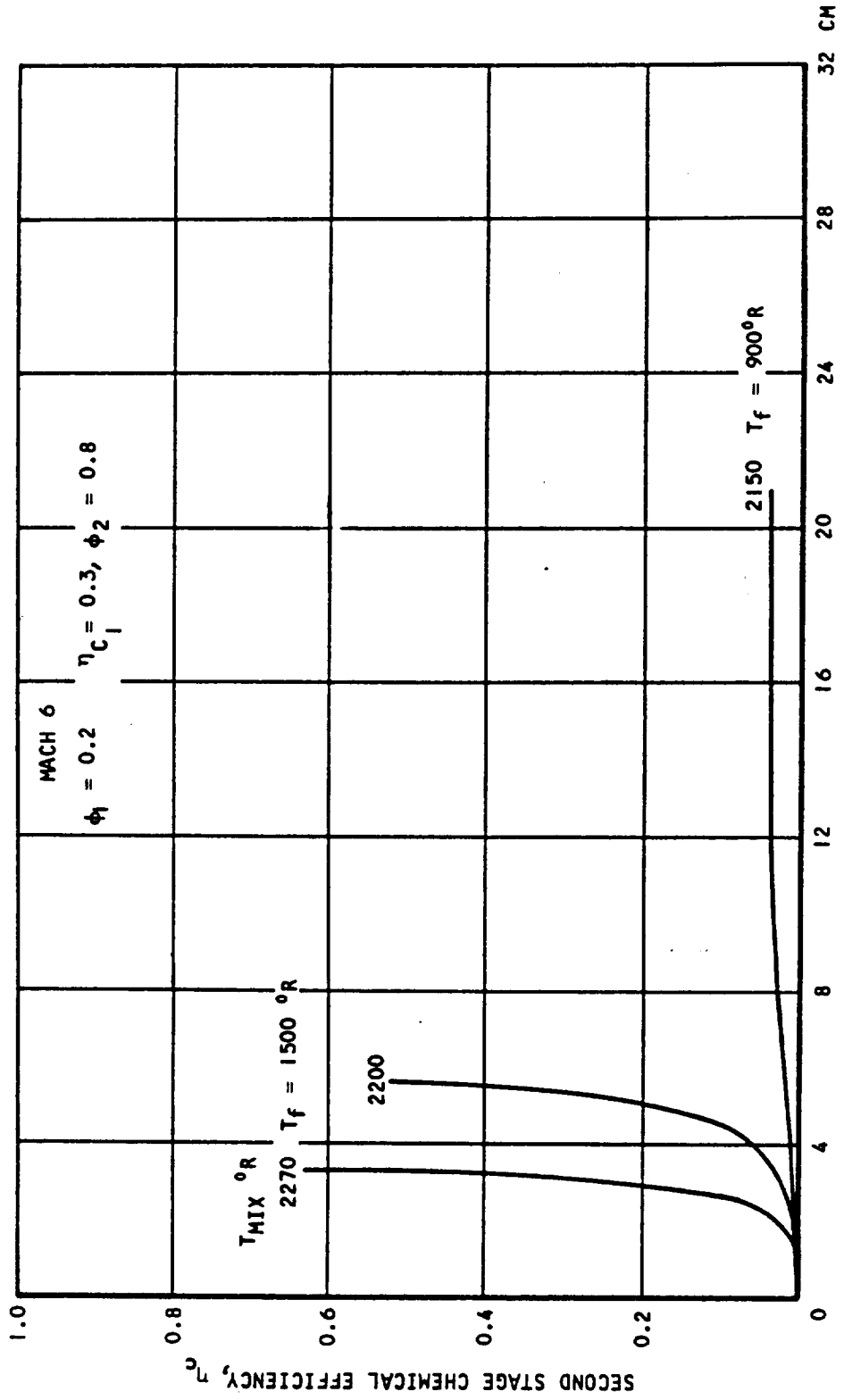

Figure 7.1-8. Second Stage Chemical Efficiency at Mach 6 - AIM Combustor (U)

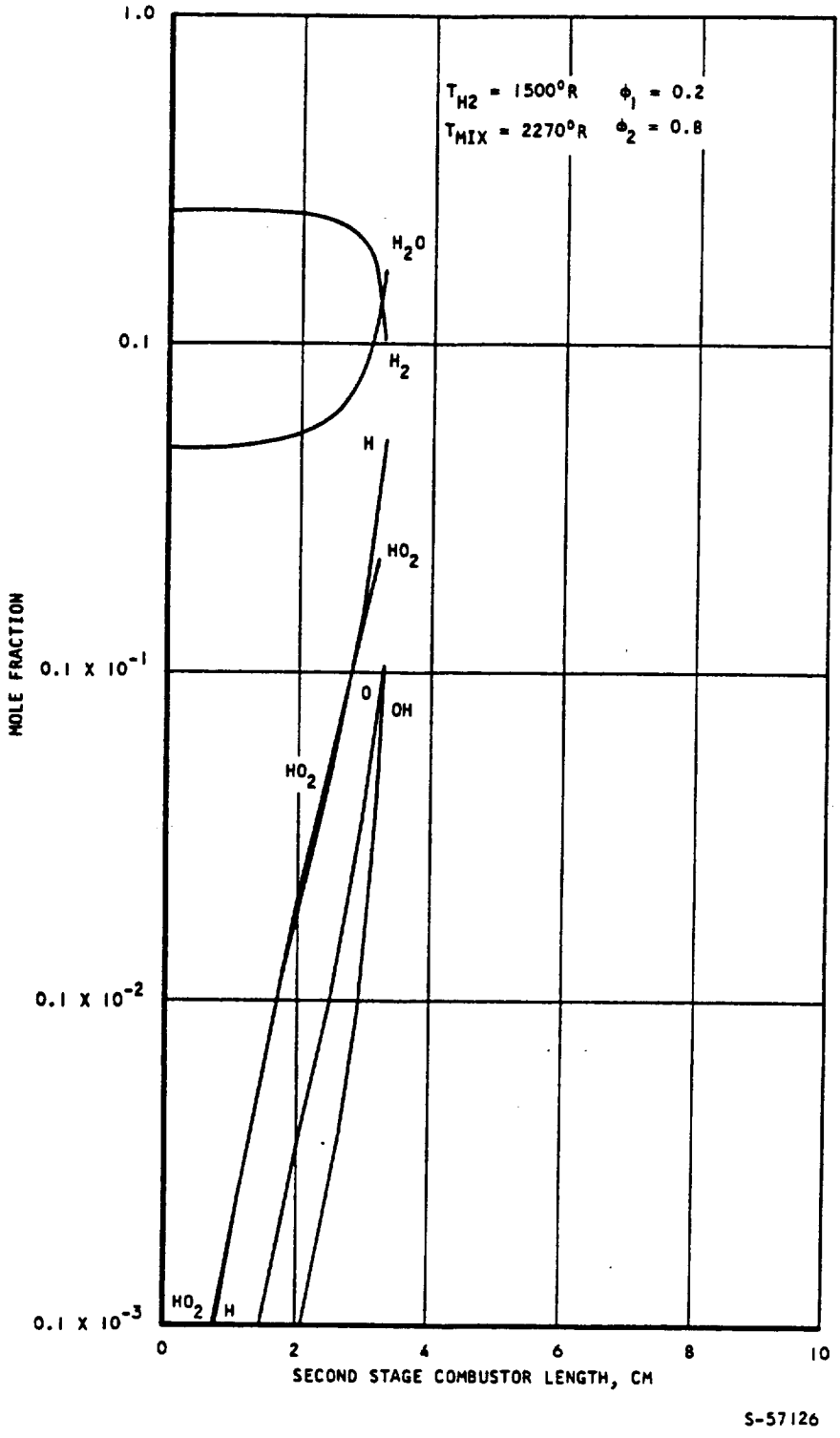

Figure 7.1-9. Species Concentration at Mach 6 - AIM Combustor (U)

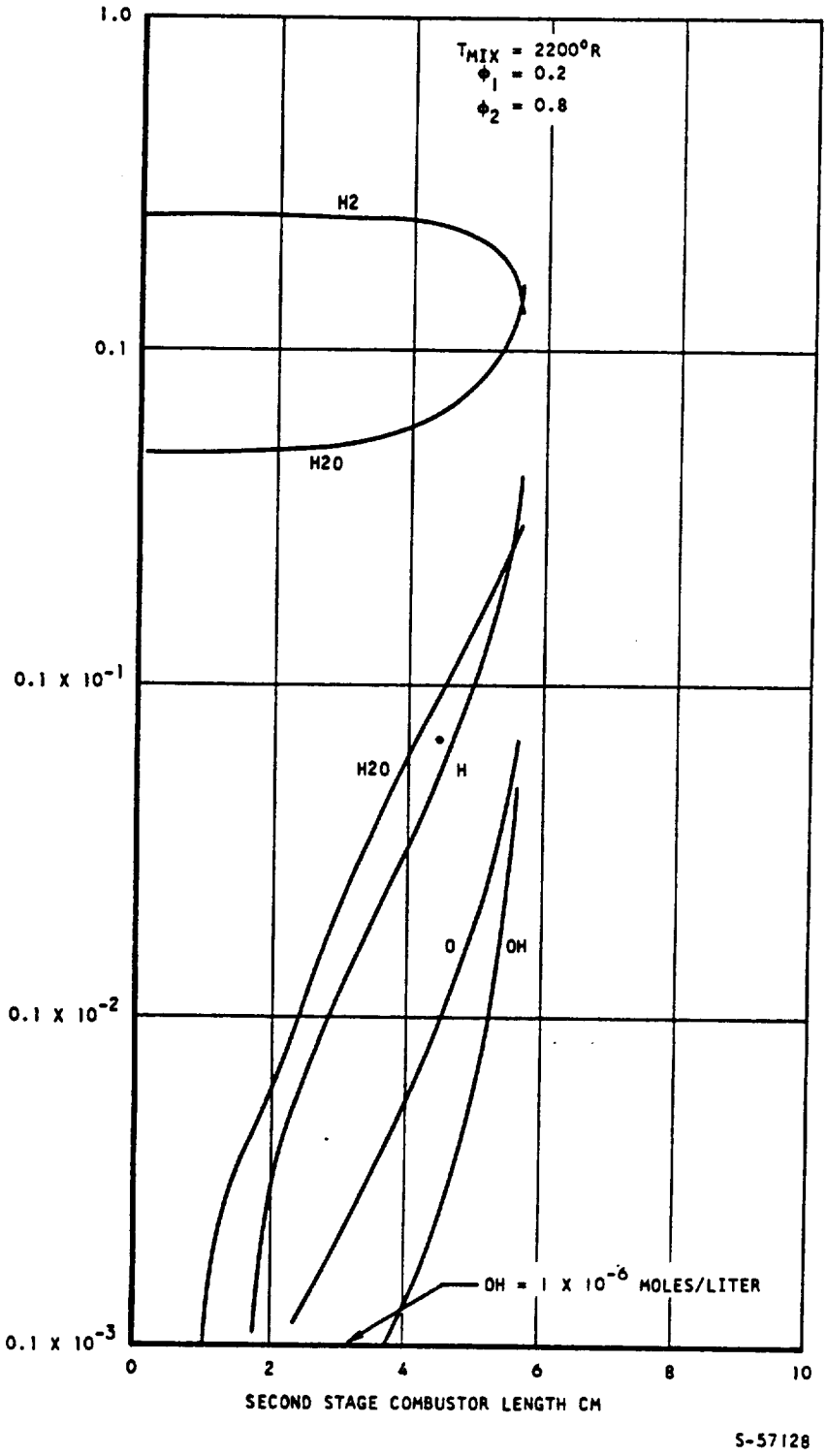

Figure 7.1-10. Species Concentration at Mach 6 - AIM Combustor (U)

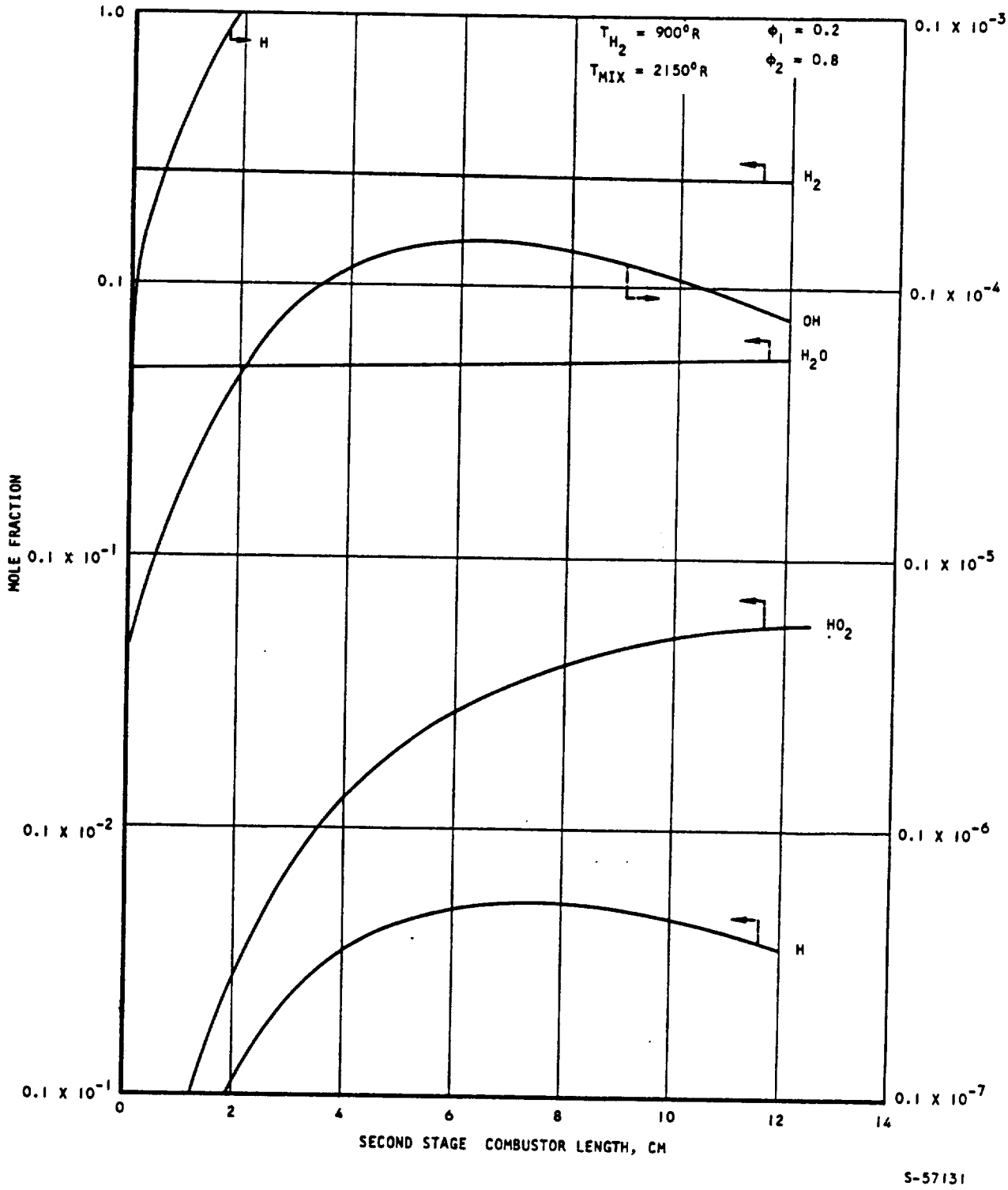

Figure 7.1-11. Species Concentration at Mach 6 - AIM Combustor (U)

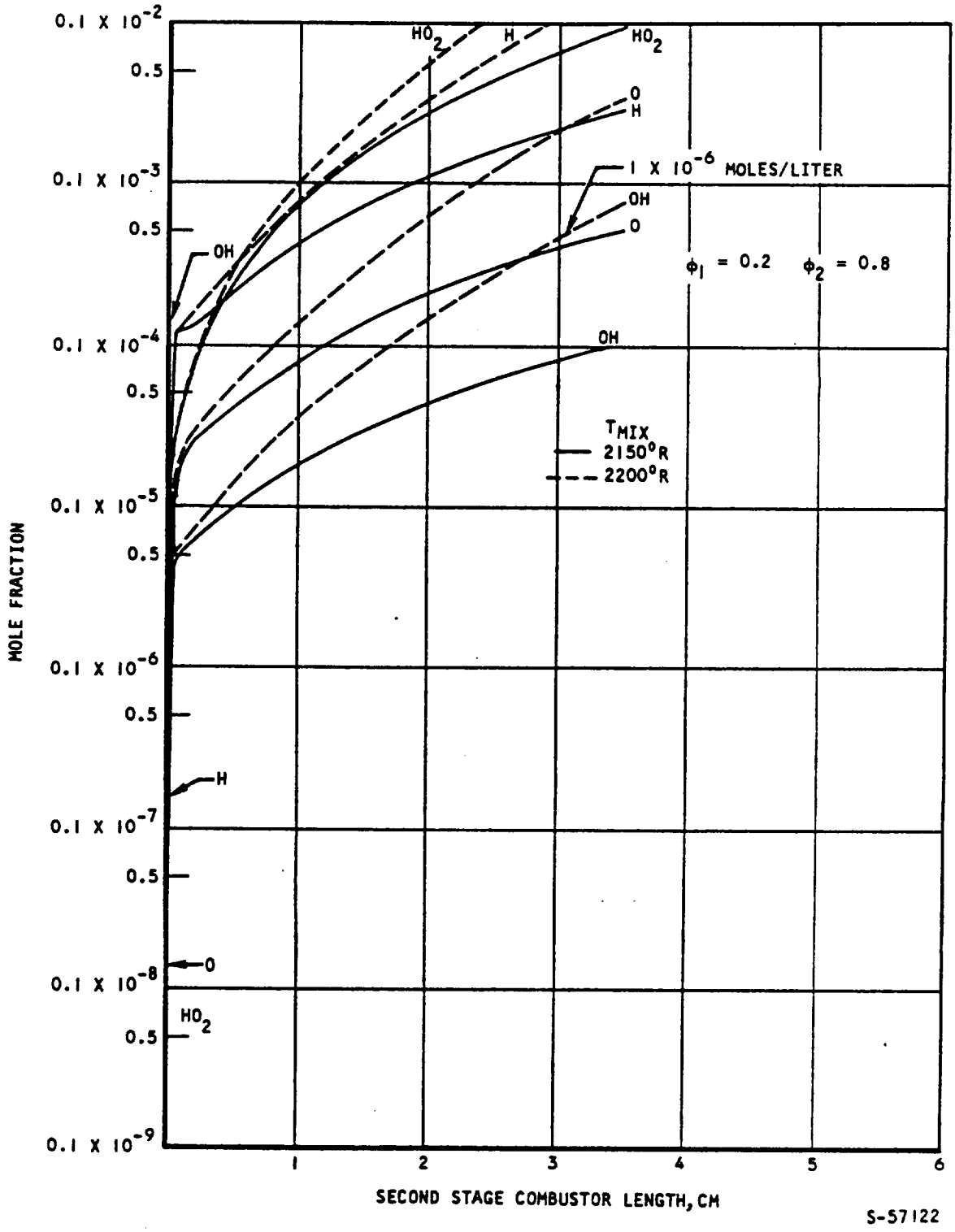

Figure 7.1-12. Comparison of Species Concentration for Different Mixed Temperatures at Mach 6 - AIM Combustor (U)

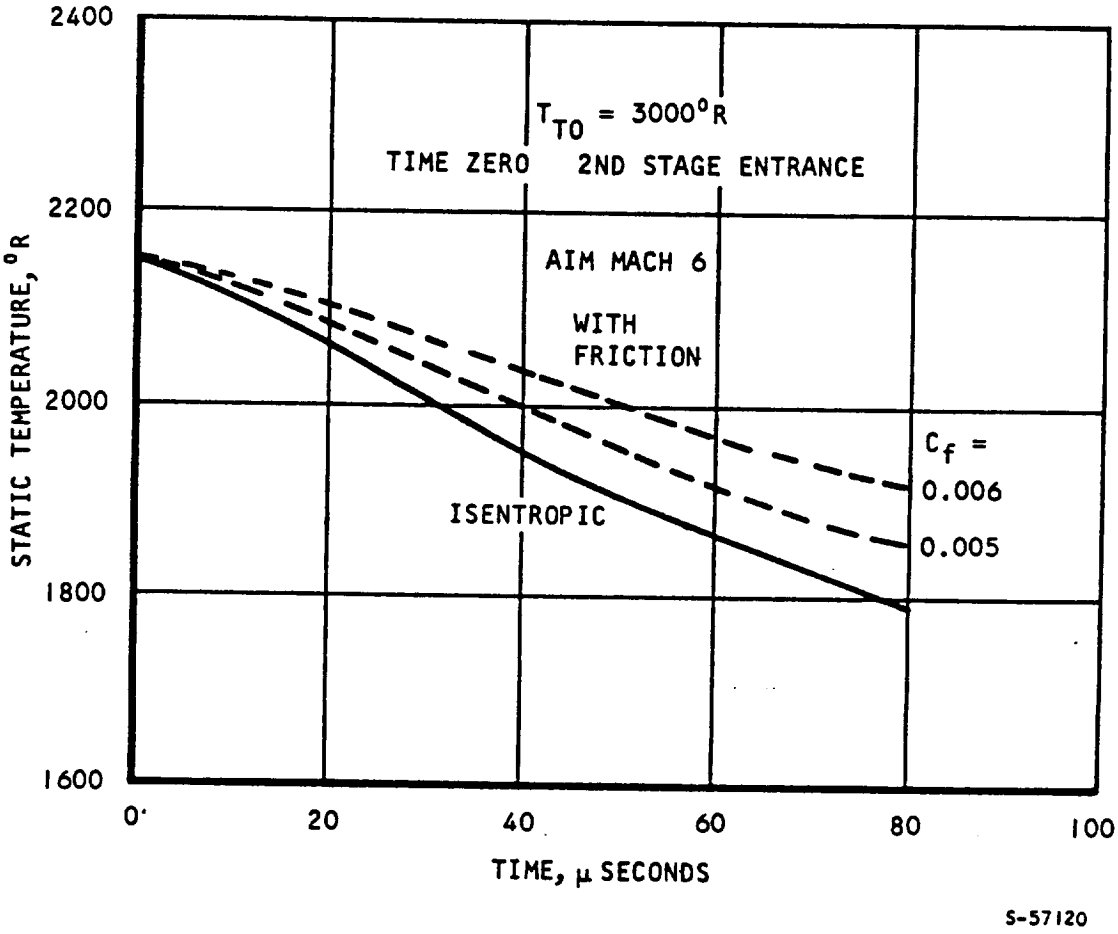

Figure 7.1-13. Temperature Vs Time, Second Stage (U)

combustion at a mixed temperature of 2150°R would probably have occurred. Also, the model did not include any temperature rise from fuel disturbance which would have helped initiate combustion.

The above study indicated that second stage combustion was very sensitive to the first-stage chemical efficiency, fuel temperature, and skin friction.

Second-stage entrance conditions (including the concentrations of all major species) were determined from an engine cycle program which used equilibrium chemistry. Therefore, a study was made to determine whether application of a chemical kinetics solution in both stages would affect the combustion characteristics of the second stage. The results showed that it would.

The first-stage entrance static temperature at Mach 6 is about 1300°R. At this temperature the finite kinetics program would indicate no combustion. To simulate the air shock due to fuel injection, an air static temperature of 2000°R was chosen as the first stage entrance condition. An equivalence ratio of 0.2 was assumed and combustion at a constant area was specified to insure that the fuel would react. In this manner it was hoped that at the same amount of fuel reacted (in a constant area), static temperature, pressure and velocity would match that from the engine cycle computer program. Thus the only difference in second stage entrance conditions (if any) would be the concentration of the individual species.

The first stage was defined to be halfway between injectors 1c and 4 at a chemical efficiency of 50 percent. With 900°R H_2 fuel, the mixed fuel air temperature was 1800°R. As shown in Figure 7.1-14, reaction took place almost immediately, and the flow choked about 1 cm downstream of injection. In this case the initial concentration of OH at the entrance of the second stage combustor was 3×10^{-5} moles/liter, or 30-times that concentration used to define the ignition delay time. This OH concentration was also 100 times that obtained from the cycle program output which used equilibrium chemistry (Figures 7.1-9 to 7.1-12). As shown in Table 7.1-1, the values of carriers O, H, HO_2 and H_2O_2 also changed significantly.

Therefore with finite rate kinetic chemistry, second stage combustion occurred at a mixed temperature of 1800°R, whereas with equilibrium chemistry a mixed temperature of 2200°R was required for combustion. This indicated that at Mach 6, second stage combustion would not be chemical kinetics-limited. Thus at both Mach 6 and 7 there should be no combustion problem if complete mixing is assured.

Since combustion was shown to be very sensitive to initial specie concentration, an investigation was made varying the percent of fuel reacted in the first stage in order to determine the effect on combustor length. To simplify results the first stage was run at constant area and the second stage at a constant divergence. An equivalence ratio of 0.2 was used in the first stage at 2000°R, 20 psia and 4400 ft/sec mixed conditions. An equivalence ratio of 0.8 was used for the second stage. The effect of varying the percentage of first stage fuel reacted on combustor length is shown in Figure 7.1-15.

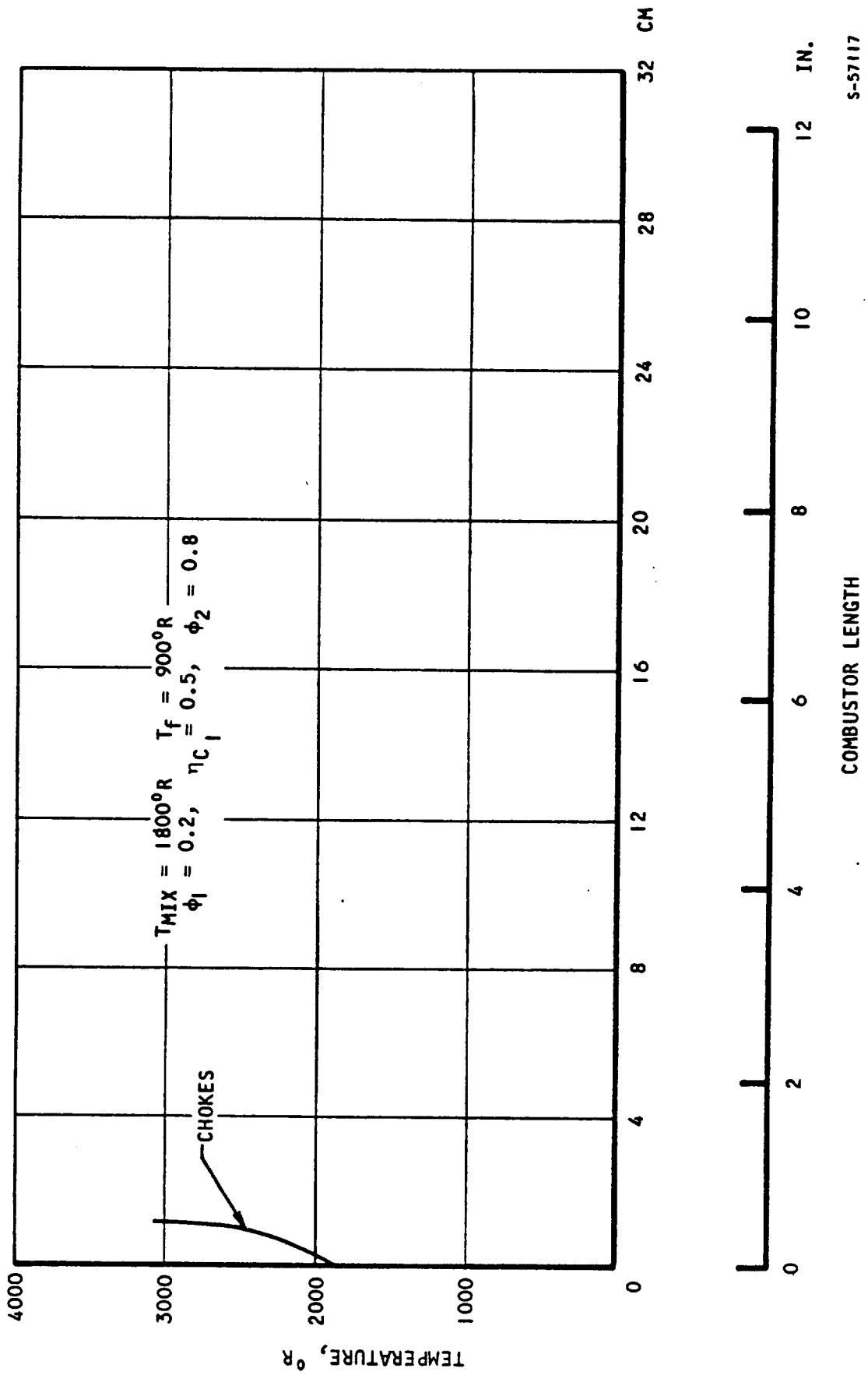

Figure 7.1-14. Static Temperature Variation at Mach 6 - AIM Combustor (U)

TABLE 7.1-1

COMPARISON OF INITIAL MASS FRACTIONS USED IN AIM STUDY AT SECOND STAGE ENTRANCE* (U)

Specie	Equilibrium Chemistry 1st Stage $\eta c_1 = 0.5$	Finite Kinetics Chemistry 1st Stage $\eta c_1 = 0.5$	Equilibrium Chemistry 1st Stage $\eta c_1 = 0.8$ Used in Figs. 7.1-6 Thru 7.1-12
H	$< 10^{-10}$	0.24267×10^{-3}	1×10^{-9}
O	$< 10^{-10}$	0.35479×10^{-2}	1×10^{-9}
N_2	0.74674	0.746219	0.74711
H_2	0.02550	0.025491	0.02383
O_2	0.20243	0.190273	0.18854
OH	4.02×10^{-7}	0.95006×10^{-3}	0.11×10^{-4}
H_2O	0.02533	0.0188078	0.04051
HO_2	$< 10^{-10}$	0.0144648	1×10^{-9}
H_2O_2	$< 10^{-10}$	0.2592×10^{-5}	1×10^{-9}

*$\phi_1 = 0.2$, $\phi_2 = 0.8$

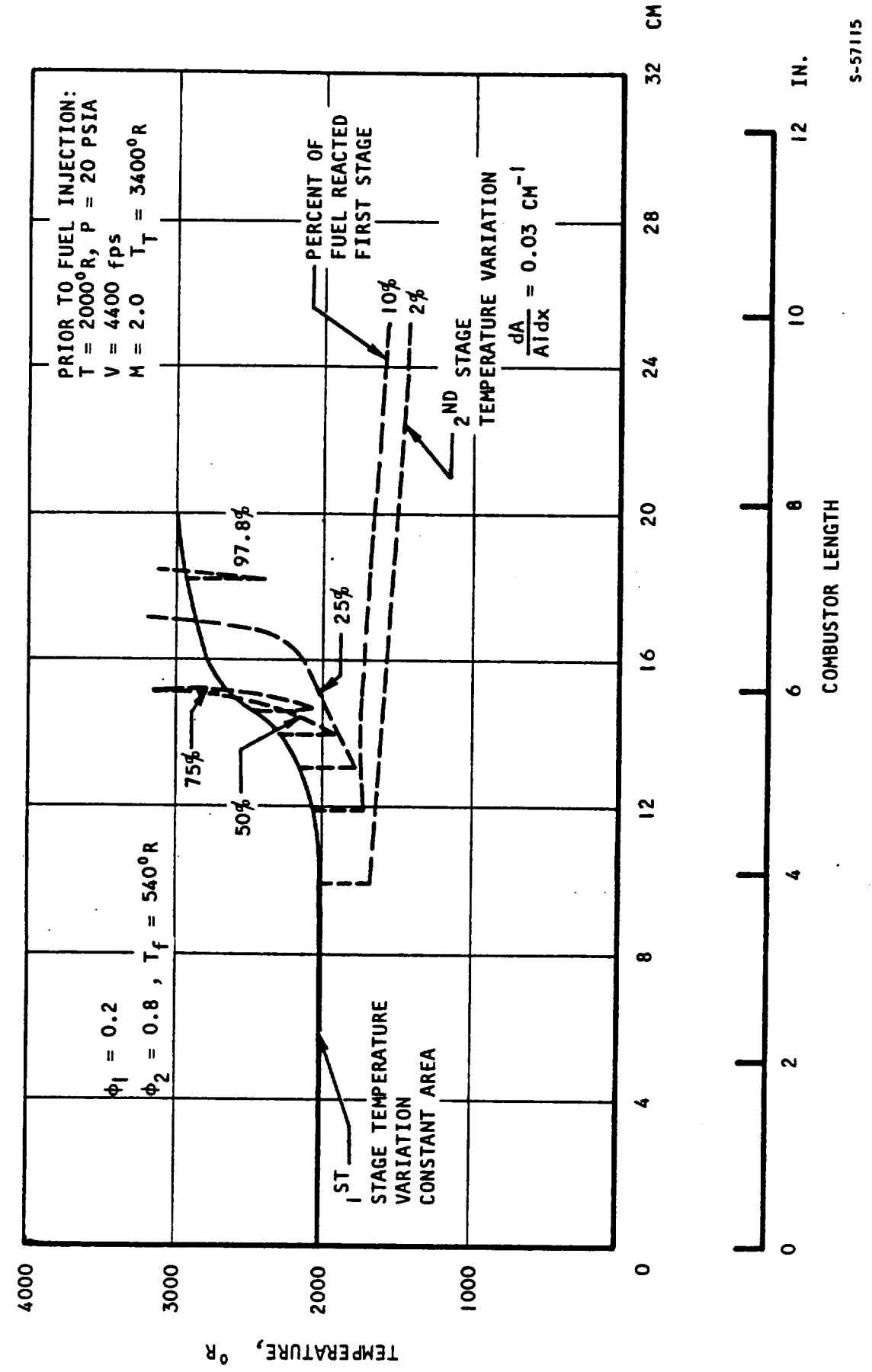

Figure 7.1-15. Effect of First Stage Efficiency on Second Stage Temperature(U)

In a length of 10 cm, 2 percent of the first stage fuel reacts while it takes about 18 cm for 97.8 percent of the fuel to react. Mixing the temperature of output air with 540°R fuel shows that about 25 percent of the first stage fuel must react in order for combustion to occur in the second stage at a divergence ($dA/A_1 dx$) of 0.03 cm^{-1}. No combustion occurred in the second stage for values of less than 10 percent of fuel reacted in the first stage. However, the overall combustor length does not necessarily decrease as the percentage of first-stage fuel reacted increases. The reason is that first stage combustor length increases much more rapidly than the second stage length. This is more clearly shown in Figure 7.1-16. In fact a minimum occurs near 60 percent of first stage fuel reacted. The overall length is shown at a constant H_2 mole fraction of 0.15 or at a constant overall chemical efficiency of about 53 percent. This efficiency was the highest reached without choking the second stage with 97.8 percent of fuel reacted in the first stage. A similar minimum occurred when the divergence was doubled to 0.06 cm^{-1} (Figure 7.1-17). This indicated that making the first stage of the combustor less efficient might decrease the overall combustor length.

In summary,

(1) Equilibrium chemistry and finite kinetics chemistry in the first-stage combustor did not predict the same combustion characteristics for the second stage of the AIM combustor.

(2) Finite-rate chemistry assuming complete mixing indicated no second stage combustion problems at both Mach 6 and 7.

(3) Shorter combustor lengths might occur with less efficient first stages.

7.2 AIM KINETICS AT MACH 6

Model T inlet test data indicate that at Mach 6 the static temperature for undisturbed flow at the first injection station of the AIM will be approximately 1290°R, the local Mach number being about 2.8. This static temperature is too low for autoignition. Some exploratory chemical kinetic calculations were made, using the Shear Layer One-dimensional Combustion Program, (Reference 2-2) to ascertain what strength of flow disturbance might be needed at the first injection station in order to initiate combustion. A further calculation was made for the second stage with no flow disturbance other than that from simple mass and energy addition (no boundary layer separation).

For all these calculations certain constant conditions were assumed. The first-stage total equivalence ratio was set at 0.2, the fuel being equally split between the two first stage injectors (1a and 1b). The second-stage total equivalence ratio was 0.8, split equally between injectors 2c and 2a. The igniters, about 1 in. downstream of the first-stage injectors, were assumed to contribute 0.0413 lb/sec of hydrogen-oxygen combustion products

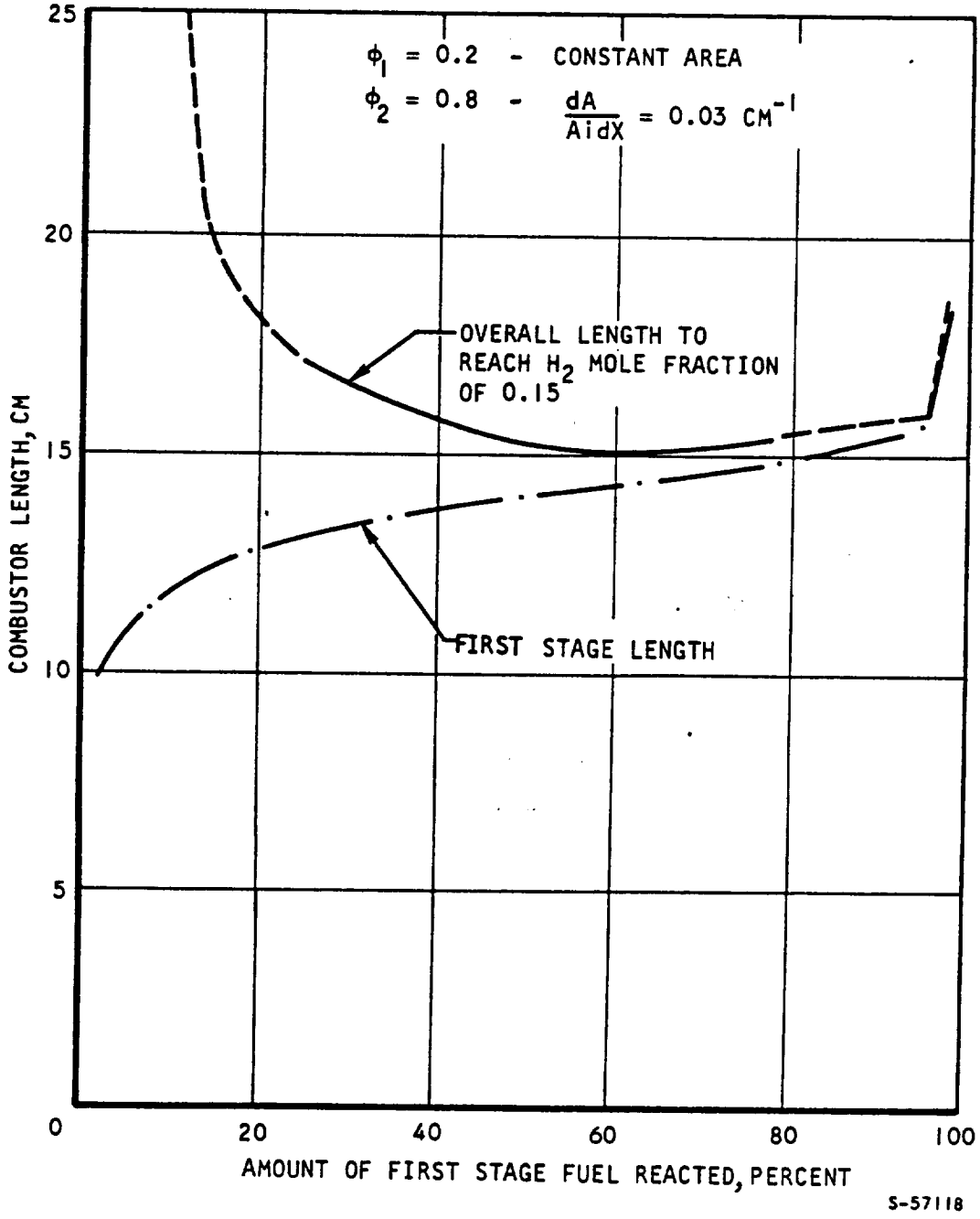

Figure 7.1-16. Combustor Length vs Amount of First Stage Fuel Reaction (U)

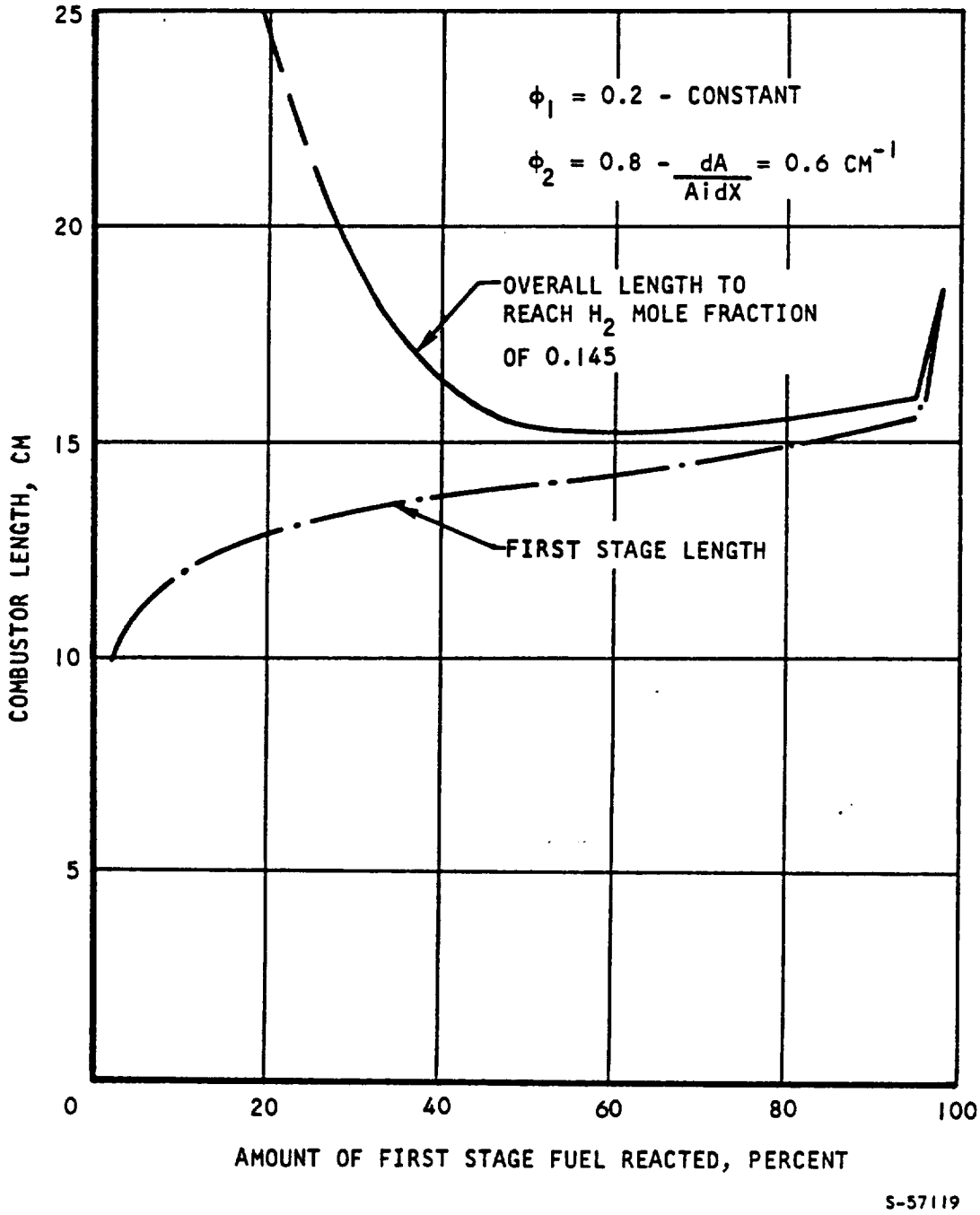

Figure 7.1-17. Combustor Length vs Amount of First Stage Fuel Reaction(U)

at an overall igniter equivalence ratio of 1.6. The igniters' combustion efficiency was taken to be 23 percent, giving a mixed igniter exit gas temperature of 3050°R. The composition of the igniter gases was taken from quasi-equilibrium calculations using the above chemical efficiency.

A uniform frictional force of 18.7 lbf/in. along the combustor's length was assumed. Estimated local heat losses were used; these varied between 109 Btu/in. sec. and 234 Btu/in. sec. and were specified as a function of axial distance.

The fuel temperature was assumed to be 1440°R, and the total air flow was taken to be 34.6 lb/sec. The fuel and the igniter gases were assumed to be injected normal to the engine axis, and to mix completely and instantaneously with the main flow. The fuel was injected over a length of 0.2 inches at each injector.

The disturbances assumed for the flow ahead of the first injection station corresponded roughly to those produced by two-dimensional flow over a wedge. Thus the strength of the disturbance can be described by specifying a wedge angle.

Results

Assuming a 15-deg wedge angle ahead of the first injection station gave a Mach number of 2.1, a static pressure of 47 psia, and a static temperature of 1740°R just upstream of the first injector. An effective flow area reduction of 47 percent was used in order to satisfy continuity. In the first calculation using these conditions, the effective flow area was kept constant for a distance of 2 in., then linearly increased to the actual duct area at a point 8 in. downstream of the first injector. Fuel injection and igniter gas injection produced static temperature rises in the constant-area section (see Figure 7.2-1), but the maximum temperature was less than 1800°R. Ignition did not occur. The computed pressure profile is shown in Figure 7.2-2, and Figure 7.2-3 shows the concentration of OH.

A second calculation was made using the same initial conditions but with the assumption that the pressure along the combustor was constant. In this case fuel injection produced a slight drop in static temperature, and the effect of the igniter on static temperature was negligible (see Figure 7.2-4). Again, ignition did not occur.

Increasing the wedge angle to 20 deg gave an initial static temperature of 1940°R, a pressure of 61.7 psia, and an effective area reduction of 51 percent. A chemical kinetic calculation using constant pressure indicated complete combustion in the first stage. The temperature profile is shown in Figure 7.2-5. The area expansion of the gas stream at the equivalence ratio of 0.2 (see Figure 7.2-6) was not sufficient to fill the actual cross-sectional area of the AIM duct. Consequently, the calculation was re-started at a point near completion of first stage combustion (Z = 45; see Figure, 7.2-5). From this point on, an assumed effective flow area (rather than constant pressure) was specified. The initial area was that determined by the first stage constant

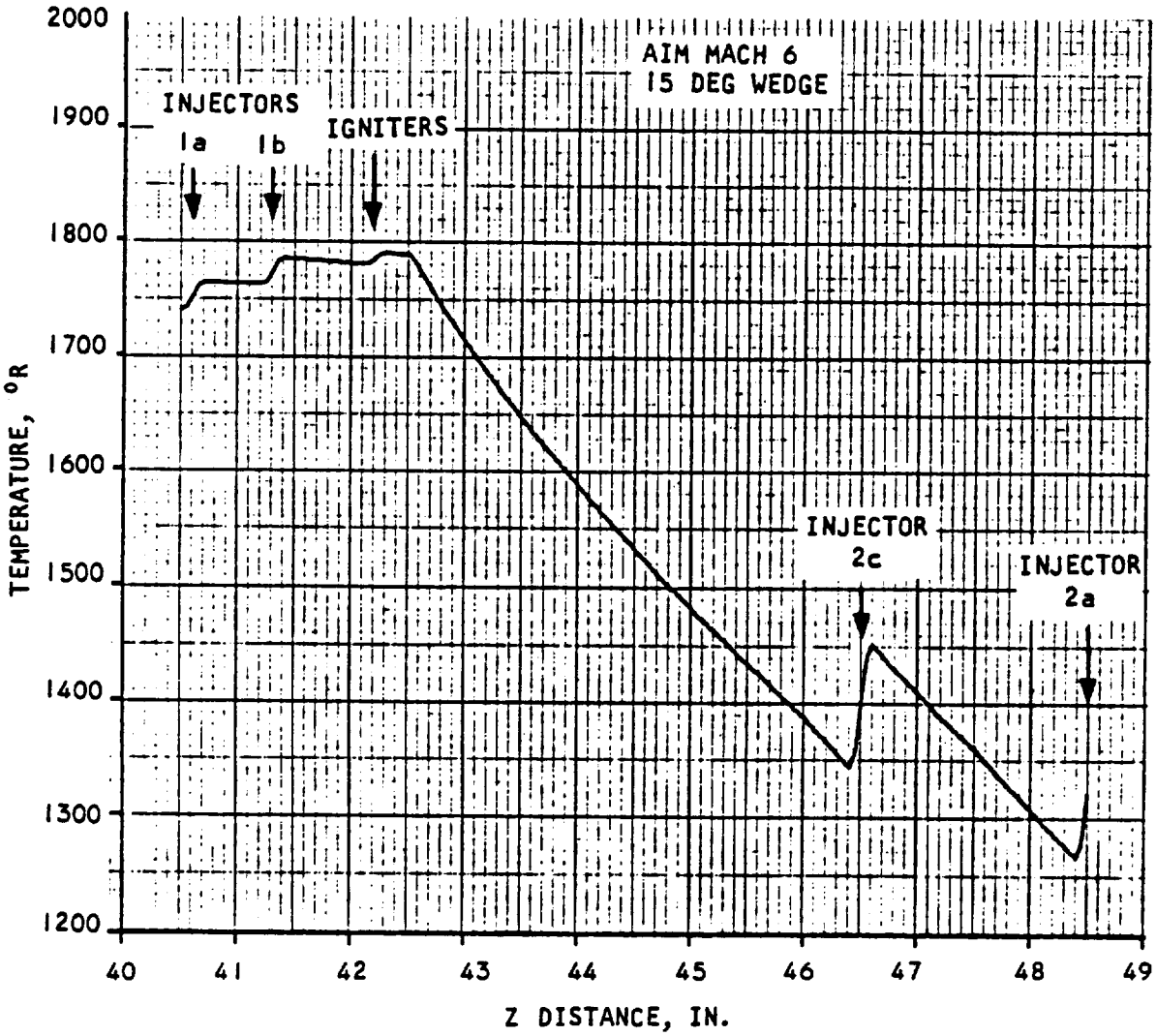

Figure 7.2-1. Static Temperature in a Constant Area Section (U)

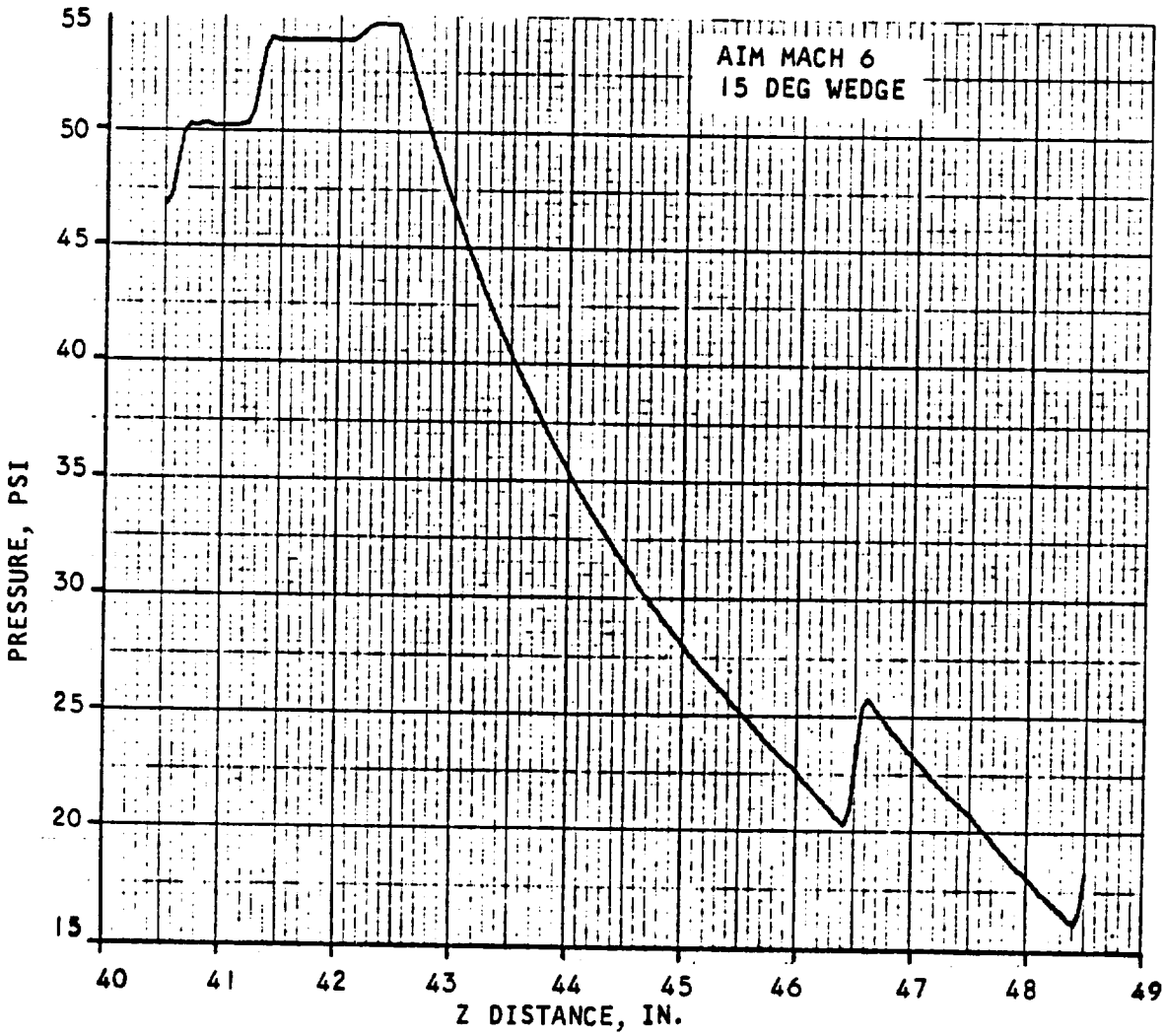

Figure 7.2-2. Computed Pressure Profile(U)

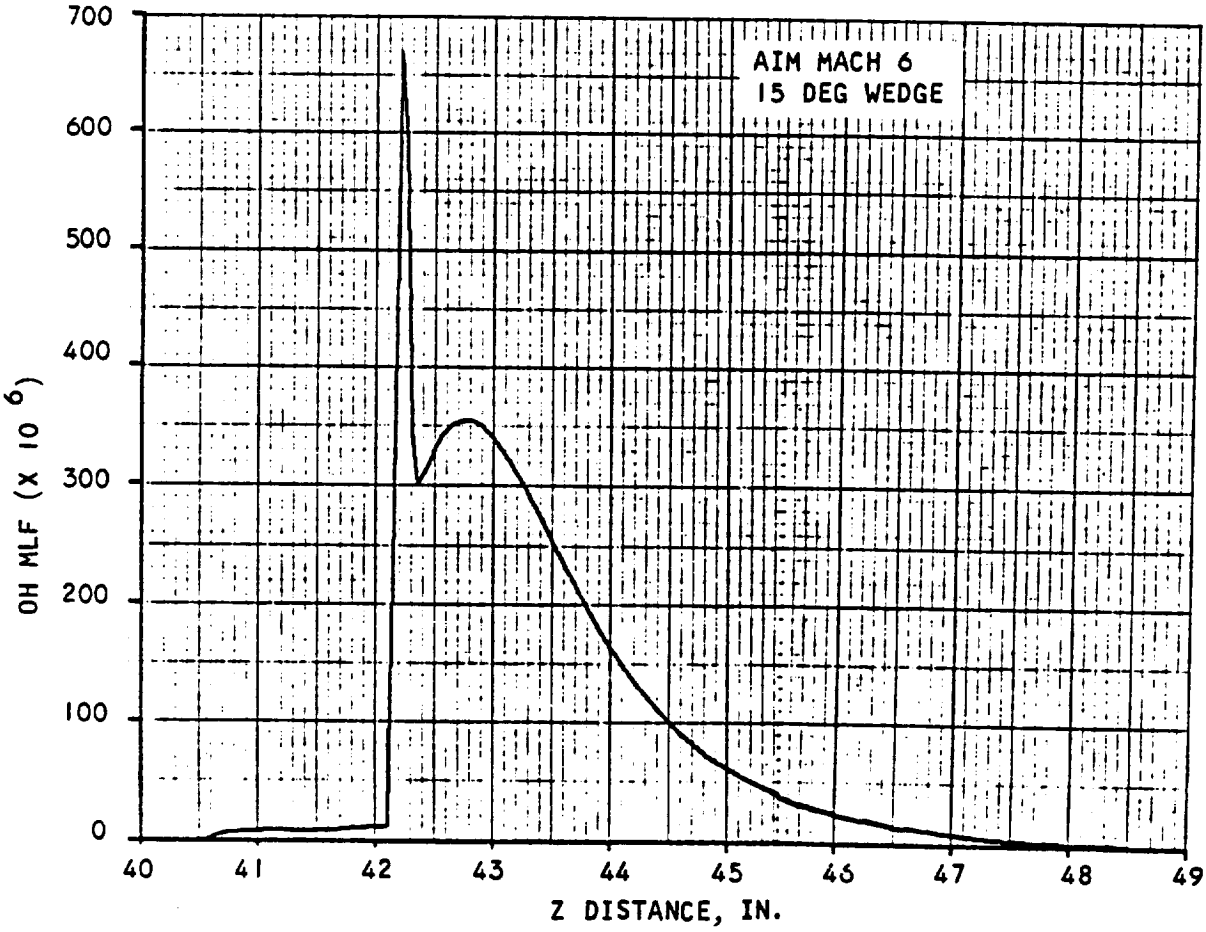

Figure 7.2-3. Concentration of OH (U)

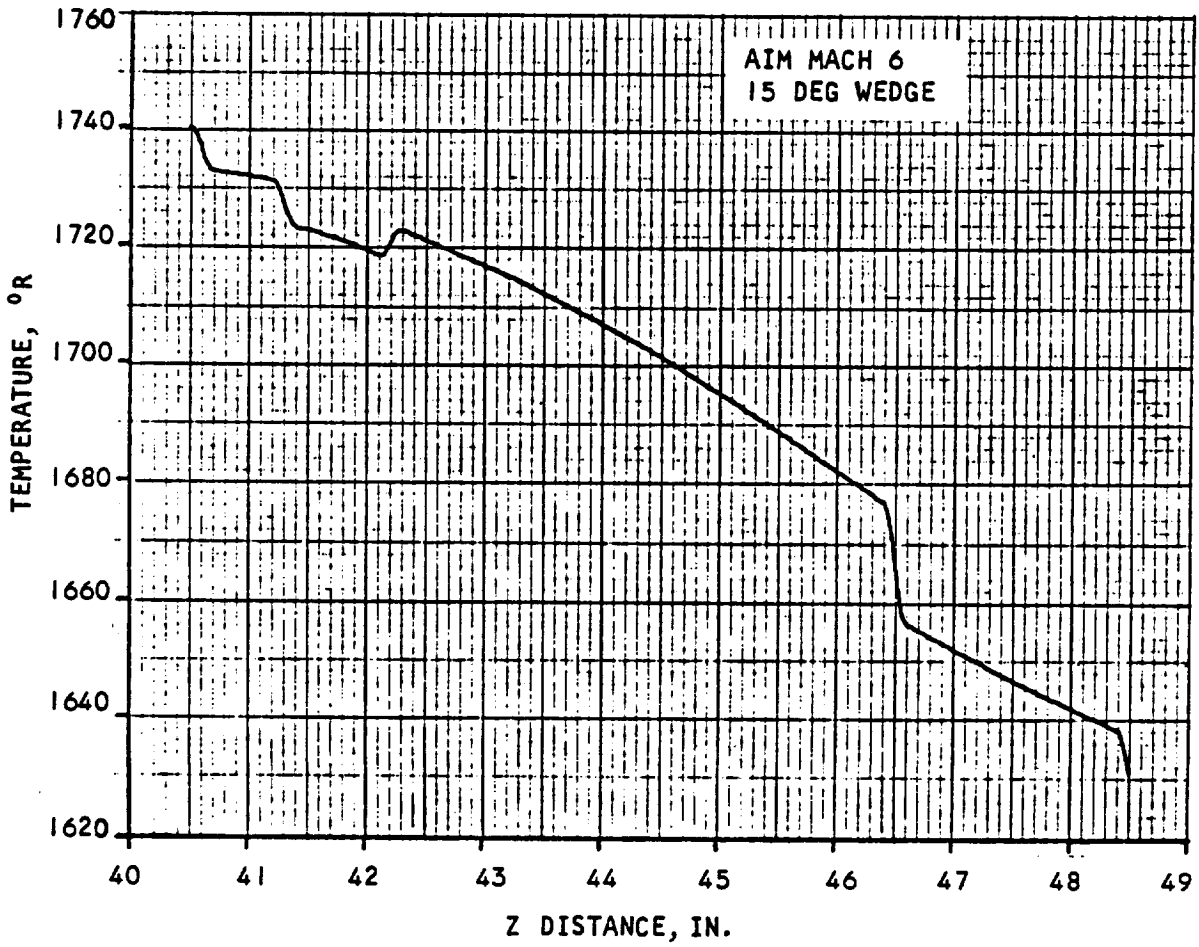

Figure 7.2-4. Effect of Igniter on Static Temperature(U)

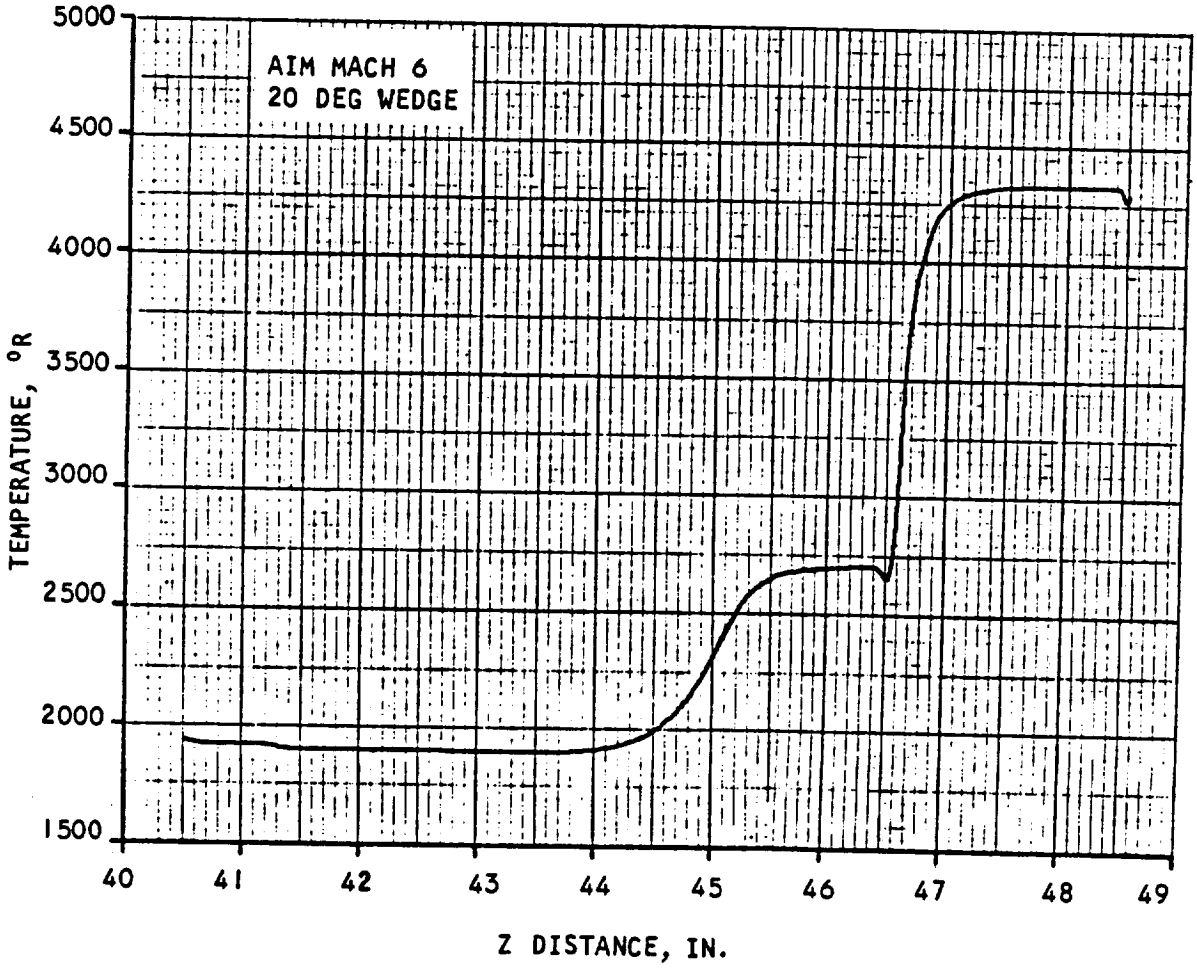

Figure 7.2-5. Temperature Profile(U)

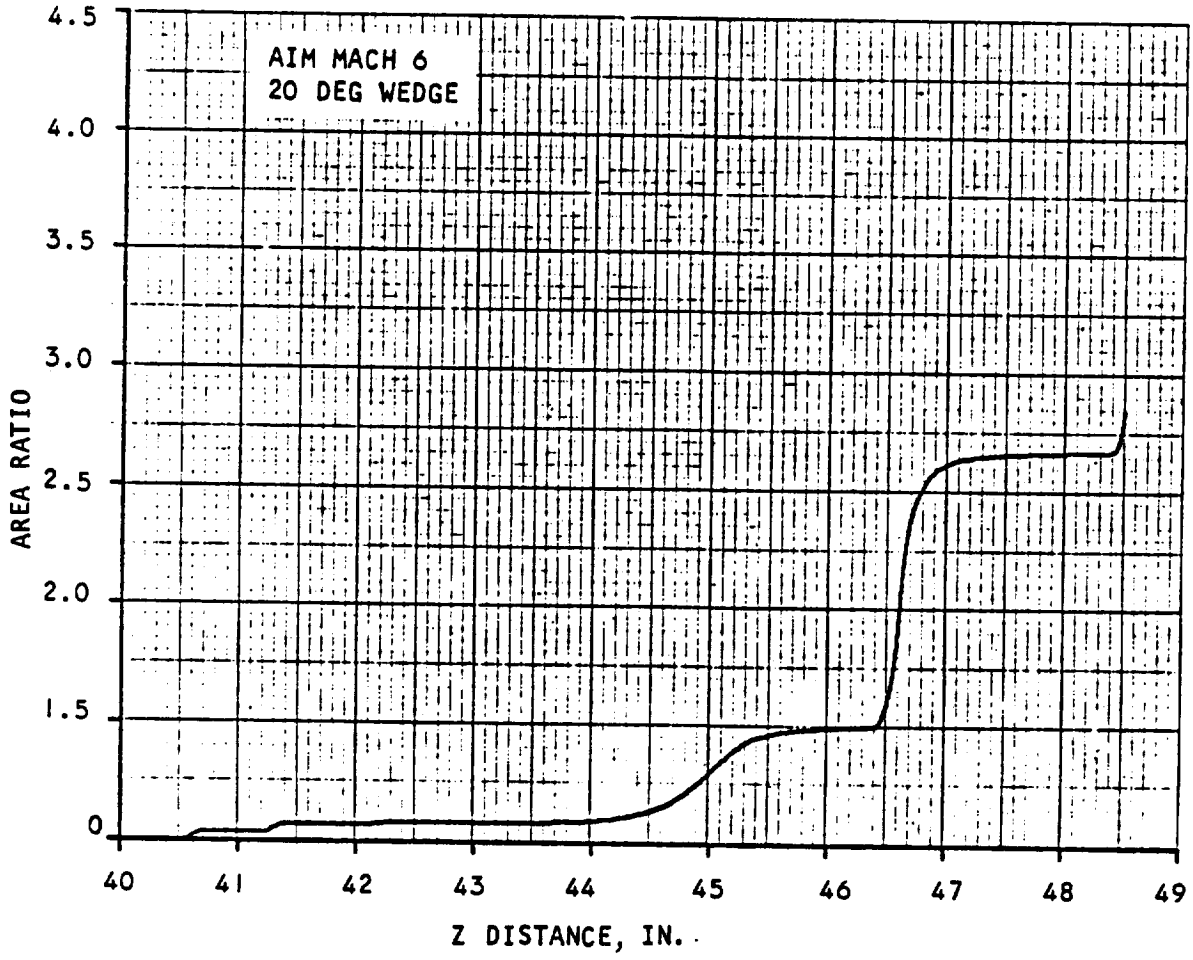

Figure 7.2-6. Gas Stream Area Expansion(U)

pressure calculation; the effective area was then increased linearly until it matched the actual duct area just downstream of the first injector of the second stage. At the entrance of the second stage, the computed gas temperature was over 2300°R. The calculation indicated that the fuel from the first injector of the second stage would burn in a very short distanoe and cause choking of the flow.

7.3 DISCUSSION

Time limitations prevented the investigation of any mixing model other than instantaneous mixing for the AIM. With respect to the mixing model, the calculation must be considered optimistic. Also, it is not known whether anything approximating a constant-pressure profile can be sustained over a length of 4.5 in. in the AIM's diverging first stage geometry.

The strength of the flow disturbance (pressure ratio of almost 4 to 1) required to produce combustion in the theoretical calculations is probably excessive; it is unlikely that this pressure ratio can be induced in the AIM (at some equivalence ratio) without unstarting the inlet. However, it may be possible to initiate combustion with smaller disturbances because of localized igniter effects.

Treating fuel and igniter gas injections one-dimensionally undoubtedly neglects some of the most beneficial effects of these processes. The igniter gases, for instance, are known to be poorly mixed; the igniters' design is in fact based on film cooling by unmixed oxygen. The core of the igniter streams therefore contains zones which have higher temperatures, and correspondingly higher concentrations of labile species, than indicated by the fully-mixed igniter model.

The effectiveness of the igniters is also considerably increased because the hot gases mix only with part of the mainstream. The assumption used in the calculations, namely that mainstream gas is mixed with igniter gases in a mass ratio greater than 800 to 1, leads to the unrealistic result that the igniters' effect on local static temperature is negligible. For Mach 5 test conditions the igniter used in the two-dimensional combustor was effective with a static temperature (before boundary layer separation) of approximately 1000°R. The undisturbed static temperature in the AIM is 1290°R; hence, it seems possible that combustion can be initiated in the AIM by use of the igniters even if the flow disturbance is small. Also, the prediction of choking at the second injection station might be negated by use of a reasonable finite-mixing model.

The conclusion from this AIM study is that with instantaneous mixing and for the conditions assumed in the 20 deg wedge angle case, the second stage of the AIM would not be kinetically limited at the Mach 6 test condition.

8. DISCUSSION AND RECOMMENDATIONS

8.1 DISCUSSION

The analytical studies have indicated that chemical kinetics problems would not be present in the AIM engine at Mach 6 and 7 flight conditions. Inadequate mixing was considered to be the major contributing factor for the low combustor efficiencies in the two-dimensional combustor tests. In order to substantiate these theoretical findings, it is recommended that future research programs be directed to better understanding the mixing process, particularly in a confined, favorable pressure gradient system.

As discussed in the fifth oral review, Reference 8-1, the mixing process in a supersonic combustor may be classified in three distinct phases; (1) jet penetration, (2) turbulent mixing, and (3) molecular diffusion. Among these, the turbulent mixing is least understood. The function of jet penetration is to properly distribute the fuel sources into the combustor by means of jet momentum. The turbulence either existing in the airstream or generated by jet penetration and combustion is to break up the fuel sources into many small lumps stirring up the fuel and air. Finally, mixing is completed by molecular diffusion which brings hydrogen and oxygen molecules into intimate contact. The molecular diffusion process is slow, therefore, in order to shorten the mixing length, it is necessary to generate strong turbulence and small eddies at the molecular level to reduce the distance in which the molecules diffuse for complete combustion.

Since turbulent mixing theory is still in an early stage of development, it cannot be applied to the solution of this problem at present. Therefore, future solution of this problem will have to rely on experiment.

8.2 FUTURE WORK RECOMMENDATIONS

The following items are recommended for future work to extend and compliment present efforts in solving potential problems in supersonic combustion.

8.2.1 Analytical Approach

The analytical study may be best summarized by Swithenbank's paper, Reference 8-2. In general, the low-wave-number end of the turbulent energy spectrum depends on the geometry of the turbulence-producing device, while the high-wave number region of the spectrum is almost isotropic and independent of the source of eddy formation. The smaller eddies are very important in the turbulent mixing process in which two gases are stirred together, to the molecular level. Since the high-wave-number eddies contain about 80 percent of the total turbulent energy, the ability of different systems to achieve mixing

will depend largely upon the total turbulent energy in each particular system. In general, the ability of a turbulent mixing system to mix two gases will depend upon

(a) Intensity of turbulence

(b) The scale of turbulence

(c) Mixing region length

(d) Lateral distances through which the injected fluid must travel

(e) Velocity of gas through the mixing system.

To obtain a semi-quantitative analysis of the mixing process, we need to know the relation between these five various quantities, and the effect of the chamber geometry.

The analytical study should provide guidance in conducting a well defined experimental effort.

8.2.2 Experimental Approach

The fuel mixing process is strongly influenced by the levels of intensity of turbulence. The one-dimensional chemical kinetics program has indicated that the separation bubble in the first stage is in the order of 30 to 40 percent of the duct area, while in the second stage, only 15 percent of flow area is blocked. This points to a low level of turbulence, and poor mixing in the second stage. General Electric's Report, Reference 1-1, stated: "The constant-area section provides maximum pressure disturbances for given fuel injection and burning; a necessary situation if high-Mach efficiency is to be good". Since the quoted statement was based on experiments, no detailed explanation was given in that report. The static pressure distributions from this test are reproduced in Figure 8.2-1 for reference. The implication was two-fold. First because the "high-Mach" referred to was Mach 9.5, where burner inlet static pressure and temperature were approximately 4.8 PSIA and 2500°F respectively, the chemical kinetic problem was absent. The calculated ignition delay time was at most 50 μsec. The divergence parameter $\frac{1}{A_i}\frac{dA}{dX}$ was 0.0139 cm^{-1} at the initial point. Second, because of the high static temperature, the static pressure rise due to combustion is lower; this results in less flow separation, less turbulence and poorer mixing. The latter is considered to be the basic problem in future high-Mach number flight conditions.

In view of the above discussion, the future research program should be directed toward the following:

(a) To correlate turbulence produced by external sources with mixing, such as the effects of boundary layer thickness, shock strength, size of separation bubble, combustor geometry, pressure gradient and combustion. Particular emphasis should be placed on a confined geometry with favorable pressure gradients.

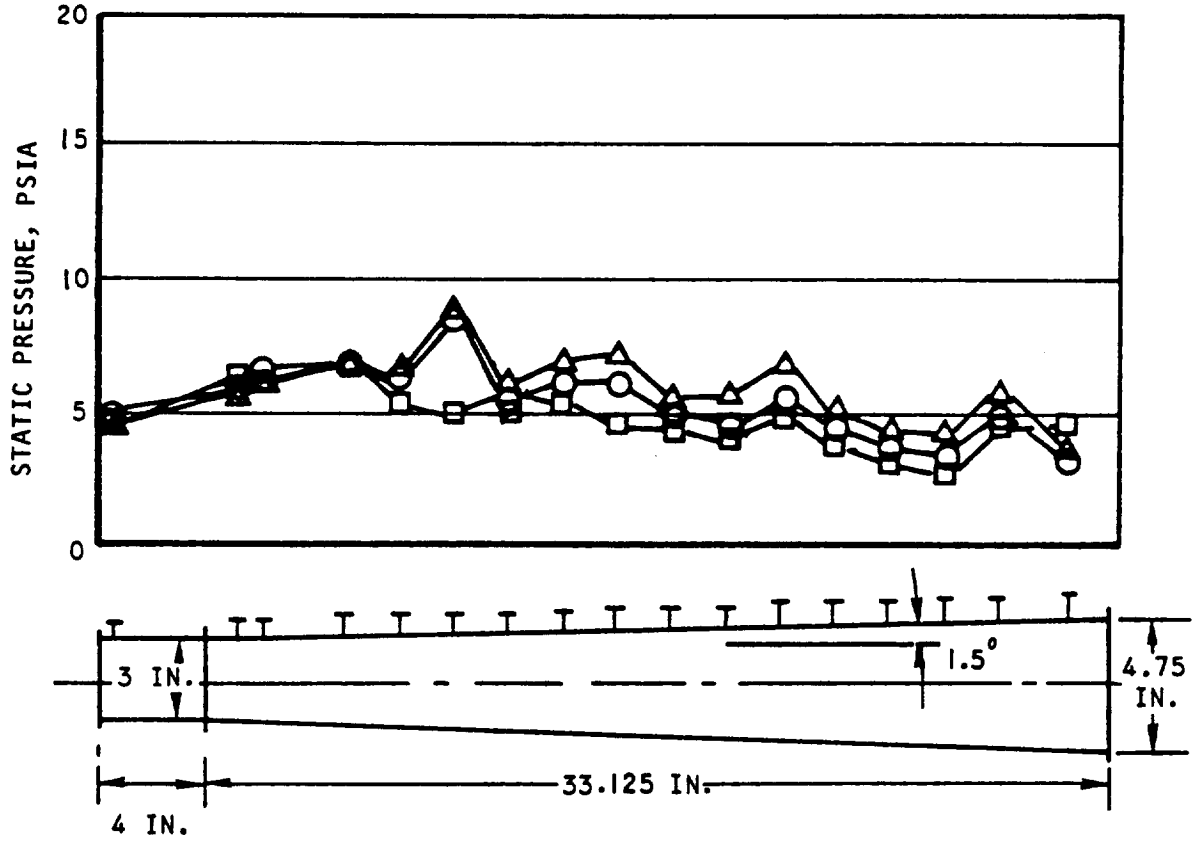

SYMBOL	H_{T2}	ER	M_p	RDG
○	1777	0.96	9.5	12A
△	1814	1.19	9.6	9
□	1856	0.59	9.7	12C

S-53920

Figure 8.2-1. General Electric Test Data(U)

(b) To develop a turbulence generation method. Swithenbank argued that the distance to generate turbulence in a swirling jet is about 1/3 the distance required by a nonswirling jet. Furthermore, the intensity of the turbulence in the developed region is higher in a swirling jet, because for a given axial velocity of the jet there is an additional tangential velocity representing an increase in the jet kinetic energy.

(c) One of the difficulties in experimental work on turbulent mixing is the accurate measurement of the mixing process. The measured quantities are averages of the instantaneous values because the turbulence is a random, fluctuating flow and the flow is three-dimensional. The mixing is not as complete as that indicated by the time-averaged measurements taken over a period of time using a gas-sampling probe. The sampling probe mixes rich and lean regions to indicate an average composition. This may explain the low combustor efficiencies in the two-dimensional combustor tests, in which gas-sampling measurements indicated uniform mixed flow at the exit. This phenomenon was also reported in Reference 8-3 and requires further exploration.

8.2.3 Methods to Improve Mixing

A sudden rearward-facing step in a combustor will promote mixing, however, it would result in lower pressure forces on the combustor wall. In other words, the rearward-facing step will produce higher chemical efficiency, but lower total pressure. The tradeoff between these two should be closely examined.

At high-flight Mach numbers where thermal choking is not likely to occur, a converging burner which would enhance flow separation cannot be ruled out as a potential solution.

The effects of surface roughness were clearly demonstrated in the Phase I boilerplate engine. In the paper presented at the 3rd AIAA Propulsion Specialist Meeting, it was stated that "The Hastelloy-X-coated engine demonstrated quite different characteristics from the pure nickel-coated engine." The high pressure at the fuel injection station indicated spontaneous combustion, the flow was nearly choked, the ignition temperature was lowered about 300°F and the slope of the pressure curve was much steeper. This phenomenon may be due to a combination of the effects of (1) the higher surface temperature, (2) the increased thickness of Hastelloy X coating, which reduces the flow area and increases the static pressure and temperature, (3) the greater area contact with the airstream of the Hastelloy X, which contains 50 percent nickel, and (4) turbulence produced by the rough surface coating. In order to further examine these effects, the surface was smoothed from the throat to a distance approximately 12 to 14 in. downstream of the throat. The test results indicated that there was no significant difference between the rough- and the smooth-surfaced engines. The smoothed surface was later verified by laboratory check as having an average roughness of 300 microinches.

Examination of the methods discussed above indicates the surface coating to be most adaptable to the AIM engine.

9. CONCLUSION

The results of this study lead to a number of conclusions with regard to chemical kinetics in a supersonic combustor. One broad conclusion obtained is that chemical kinetics is very sensitive to the divergence of the combustor. Basically, this is attributed to the low stream static temperature which "freezes" the species in a manner very similar to that in nozzle flow.

The detailed chemical-kinetic simulation of the HRE two-dimensional combustor test results indicated that low combustor efficiencies in the second stage were due to mixing. In the extreme case of late but complete mixing, the chemical efficiency approached 82 percent which indicated that the second-stage flow was not overly kinetics-limited due to the decreasing temperature in the divergent duct.

For the AIM engine at Mach 6 flight conditions, with second-stage fuel injected at stations 2a and 2c, calculations indicated that combustion was not chemical-kinetics limited. Assuming that the fuel was completely mixed with air at the injection station, the second-stage flow was choked.

REFERENCES

1-1. General Electric Co. Evendale, Ohio, Analytical and Experimental Evaluation of the Supersonic Combustion Ramjet Engine (U), Technical Report AF APL-TR-65-103, Vol. II, "Component Evaluation."

1-2. United Aircraft Research Laboratories, Mach 5 Test Results of Hydrogen-Fueled Variable-Geometry Scramjet (U), Technical Report AFAPL-TR-68-116.

2-1. Cookson, R. A., P. Flanagan, and G. S. Penney, A Study of Free-Jet and Enclosed Supersonic Diffusion Flames, Twelfth Symposium (International) on Combustion, The Combustion Institute, Pittsburgh, Pennsylvania.

2-2. Frey, H. M., J. R. Kliegel, G. R. Nickerson, T. J. Tyson, Shear Layer Combustion Computer Program, Vol. I, Dynamic Science, A Division of Marshall Industries.

3-1. Zupnik, T., E. Nilson, V. Sanli, Investigation of Nonequilibrium Flow Effects in High Expansion Ratio Nozzles (Contract NAS3-2572), NASCAR-54042, United Aircraft Corp.

3-2. Schott, G. L., and J. L. Kinsey, Kinetic Studies of Hydroxyl Radicals in Shock Wave. II. Induction Time in the Hydrogen-Oxygen Reaction, Jour. Chem. Phy., Vol. 29, No. 5, Nov. 1958, pp. 1177-1182.

3-3. Nicholls, J. A., Stabilization of Gaseous Detonation Waves with Emphasis on the Ignition Zone, Thesis for Ph.D., Univ. of Michigan, 1960, Ann Arbor, Michigan.

3-4 Momtchiloff, I. N., E. D. Taback, and R. F. Buswell, An Analytical Method of Computing Reaction Rates for Hydrogen-Air Mixture, Paper presented at the Ninth International Meeting of the Combustion Institute, Cornell Univ., August 1962.

3-5. Lezberg, E. A., Ignition and Chemical Kinetics in Hypersonic Ramjets, (C) on Hypersonic Aircraft Technology, AME Research Center, May 16-18, 1967.

3-6. Pergament, H. S., A Theoretical Analysis of Non-Equilibrium Hydrogen-Air Reaction in Flow Systems, AF33(657)-7911.

3-7 Brokaw, R. S., Analytical Solutions to the Ignition Kinetics of The Hydrogen-Oxygen Reaction, NASA TN D-2542.

4-1. Just, T. H., F. Schmalz, Measurement of Ignition Delays of H_2-Air Mixture Under Simulated Conditions of Supersonic Combustion Chambers, Institute Fuel Luftstrahlantriebe Forz-Wahn, Germany, July 1968.

5-1. Quau, V., J. E. Melde, J. R. Kliegel, G. R. Muckerson, and H. M. Frey, Kinetic Performance of Barrier-Cooled Rocket Nozzles, of Spacecraft and Rockets, 5, 10 October 1968, pp. 1137-1142.

REFERENCES (Continued)

5-2 Kliegel, J. R., G. R. Nickerson, H. M. Frey, V. Quau, and J. E. Melde, "ICRPG, Two-Dimensional Kinetic Reference Program", Dynamic Science, Irvine, Calif., July 1968.

5-3 Engineering Staff, Hypersonic Research Engine Project-Phase IIA, Combustor Program Second Interium Technical Data Report, AiResearch Report AP-67-2535, September 1967.

6-1 Baulch, D. L., D. D. Drysdale, and A. C. Lloyd, Critical Evaluation of Rate Data for Homogeneous, Gas Phase Reactions of Interest in High-Temperature Systems, Vol. 3, School of Chemistry, The University, Leeds, England.

6-2 Tyson, T., and J. R. Kliegel, "An Implicit Integration Procedure for Chemical Kinetics", AIAA 6th Aerospace Science Meeting, Paper No. 68-180, January 1968.

6-3 Baulch, D. L., D. D. Drysdale, and A. C. Lloyd, "Critical Evaluation of Rate Data for Homogeneous Gas-Phase Reactions of Interest in High-Temperature Systems", Vol. 2, School of Chemistry, The University, Leeds, England.

6-4 Tyson, T. and J. Kliegel, "An Implicit Integration Procedure for Chemical Kinetics," AIAA 6th Aerospace Sciences Meeting, Paper No. 68-180, January 1968.

6-5 Cherry, S.S., "Phase II Final Report Screening of Reaction Rates," TRW Report No. 08832-6002, 1000, TRW Systems Group, Redondo Beach, Calif., 6 Dec 1967.

6-6 Frey, H.M., Dynamic Science, Irvine, Calif. - private communication.

8-1 Fifth Oral Review Technical Presentation (U), Hypersonic Research Engine Project, Phase II by AiResearch Manufacturing Co., Los Angeles, Calif., Report No. AP-69-5696 (CONFIDENTIAL)

8-2 Swithenbank, J., and N. A. Chigier, "Vortex Mixing for Supersonic Combustion," Dept. of Fuel Technology and Chemical Engineering, The University of Sheffield, England. Twelfth Symposium (International) on Combustion.

8-3. Hawthorne, W. S., D. S. Weddell, and H. C. Hattel, "Mising and Combustion in Turbulent Gas Jet". Third Symposium on Combustion Flame and Explosion Phenomena.

APPENDIX A

RESULTS FROM CHEMICAL KINETIC SIMULATION
OF RUN 238, TIME = 520.30 SECONDS.
STOICHIOMETRIC FUEL-AIR RATIO = 0.032568

1. First Stage Combustor - Run 238
   Mixing Model 2, 50 percent mixing at each injector, 100 percent mixing at Station 12.

Station	A(in.^{2})	$\dot{m}$(lb m/sec)	$\dot{m}_{H_2}$ (mixed)	η_m	η_c	$\dot{m}_{H_2} + \dot{m}_{Hz_2}$	ϕ
7.3000	2.450	1.7810	0	0	0		0
7.5212	2.518	1.7881	0.003551	0.50	0.0071	0.007078	0.1220
7.8112	2.483	1.7881	0.003551	0.50	0.0083	0.007078	0.1220
8.5162	2.483	1.7941	0.006561	0.50	0.0000	0.013122	0.2262
9.0012	2.434		0.006830	0.52	0.0002		
10.0462	2.344		0.009121	0.70	0.0041		
10.8462	2.320		0.011693	0.89	0.0443		
11.0912	2.324		0.012234	0.93	0.0937		
11.4887	2.390		0.012839	0.98	0.2856		
11.5887	2.432		0.012938	0.99	0.3668		
11.6887	2.491		0.013015	0.99	0.5361		
12.0337	2.907		0.013119	1.00	0.7912		
12.5337	3.398				0.9306		
13.0212	3.794				0.9552		
13.5737	3.970				0.9660		
14.0287	4.112				0.9713		
14.5112	4.207				0.9750		
15.0062	4.305				0.9779		
15.5562	4.536				0.9997		
16.0562	4.781				0.9998		
16.5562	5.067				0.9998		
17.0500	5.303				0.9998		
17.5500	5.308				0.9998		
17.9950	5.253				0.9998		
18.4950	5.138	↓	↓	↓	0.9998	↓	↓
18.9950	5.032				0.9998		
19.1950	4.992	1.7941	0.013119	1.00	0.9998	0.013122	0.2262

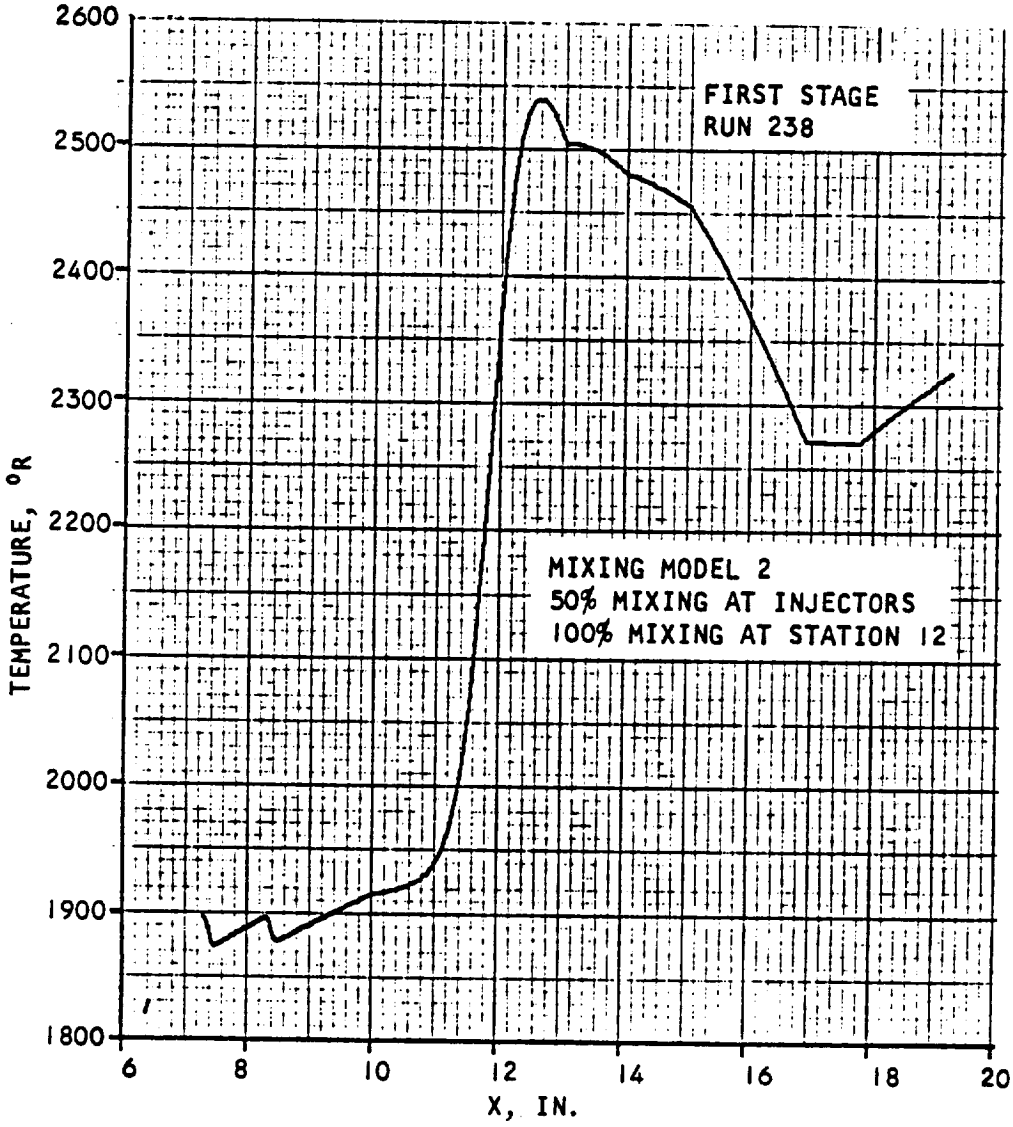

Figure A.1-1. Temperature vs Axial Distance

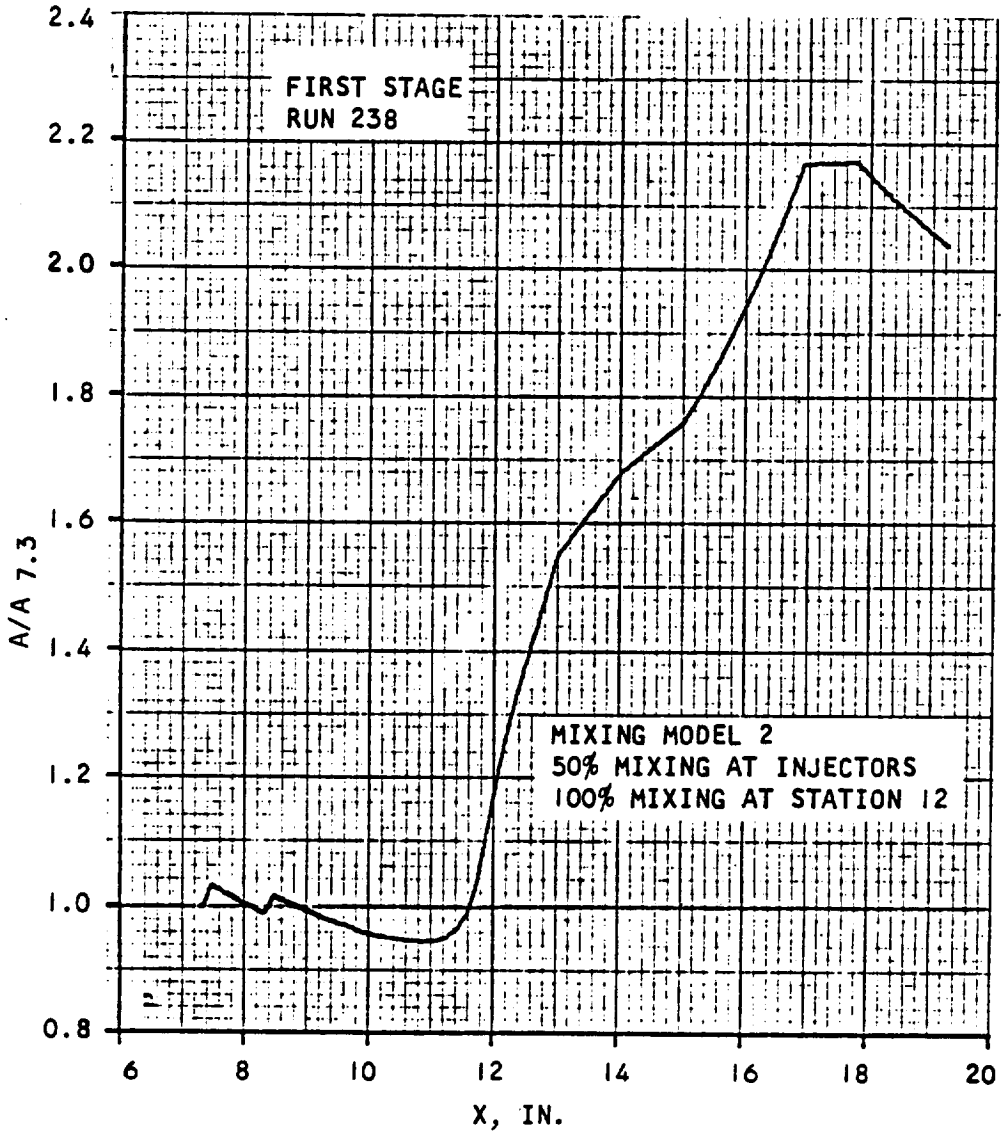

Figure A.1-2. Area Ratio vs Axial Distance

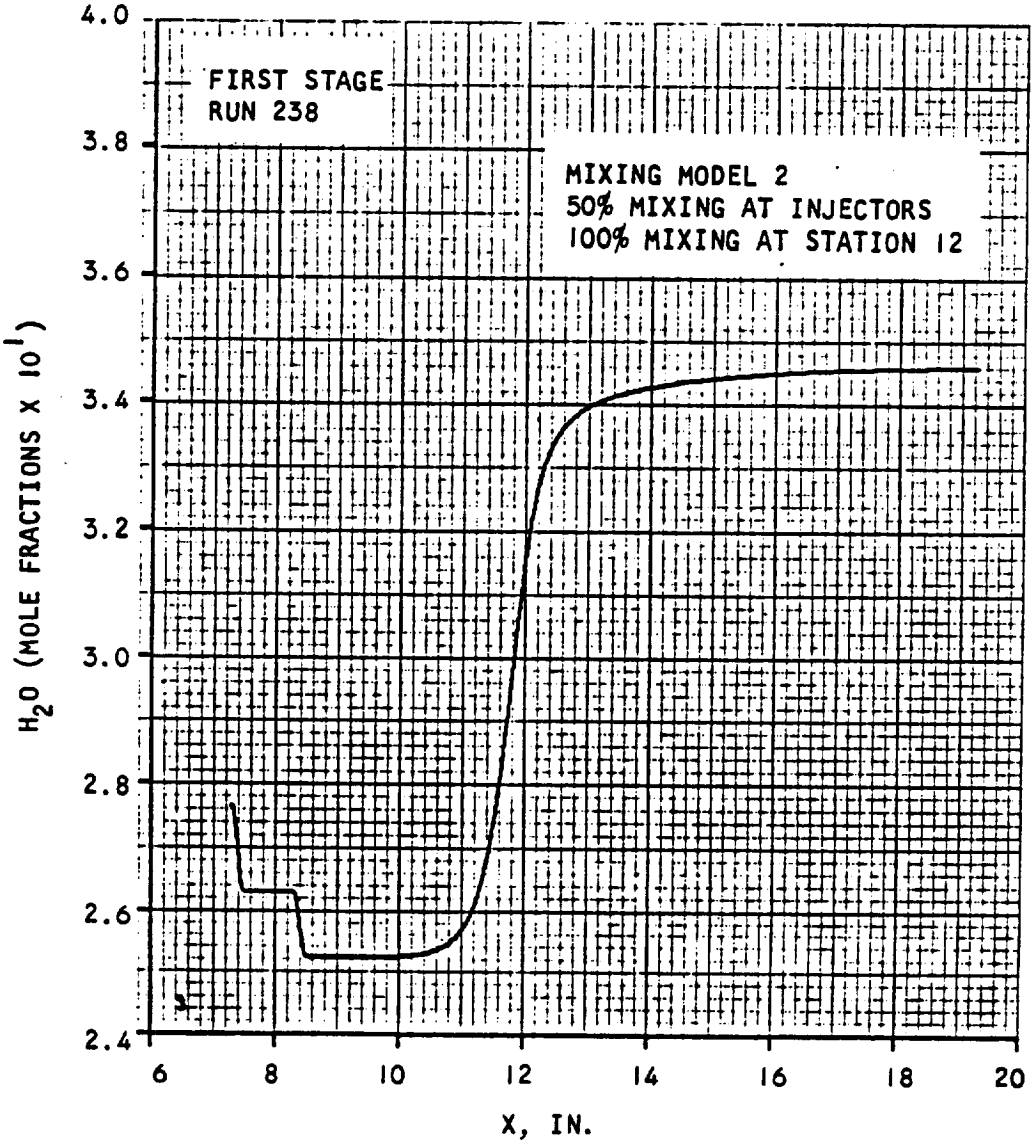

Figure A.1-3. Concentration of H_2O vs Axial Distance

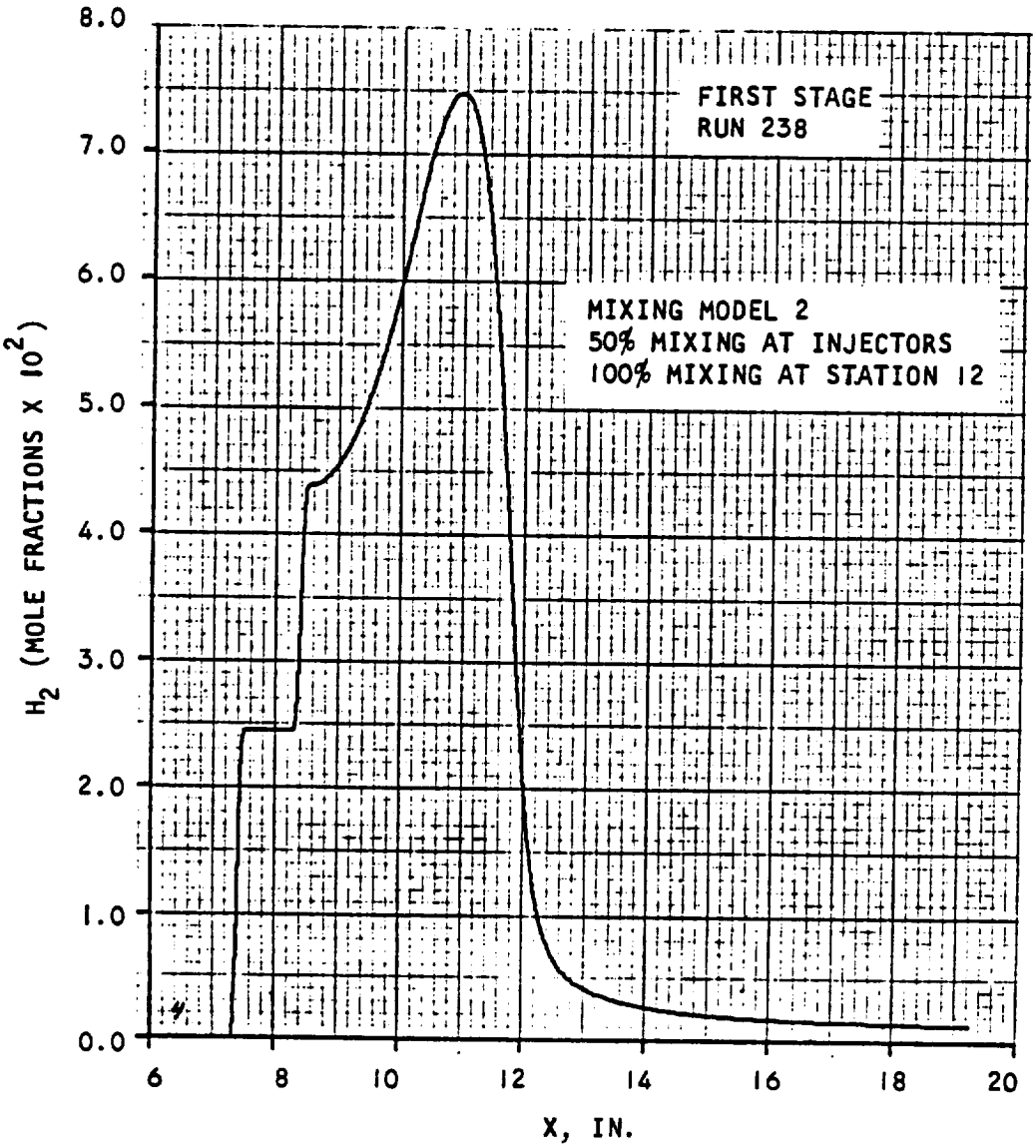

Figure A.1-4. Concentration of H_2O vs Axial Distance

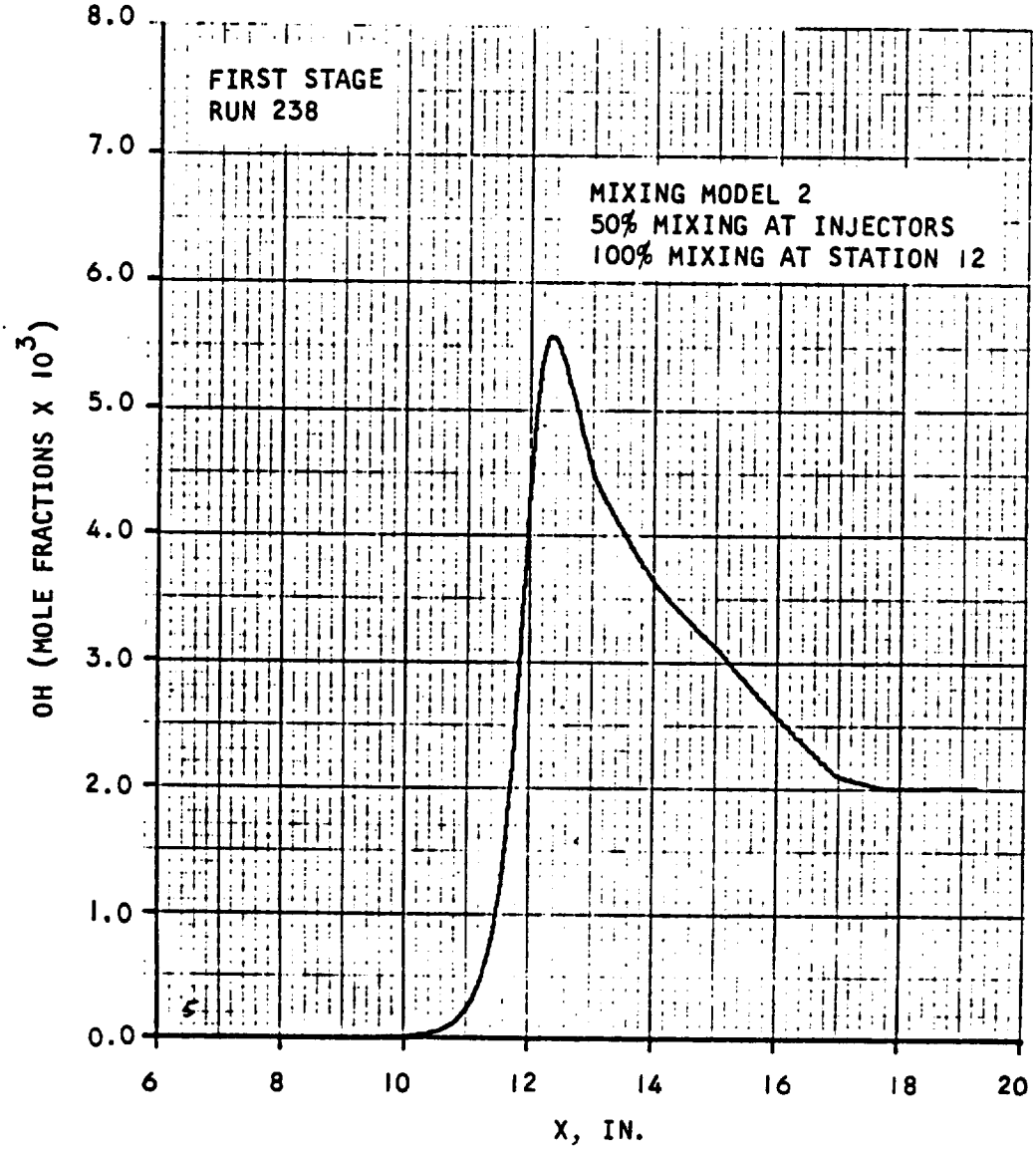

Figure A.1-5. Concentration of OH vs Axial Distance

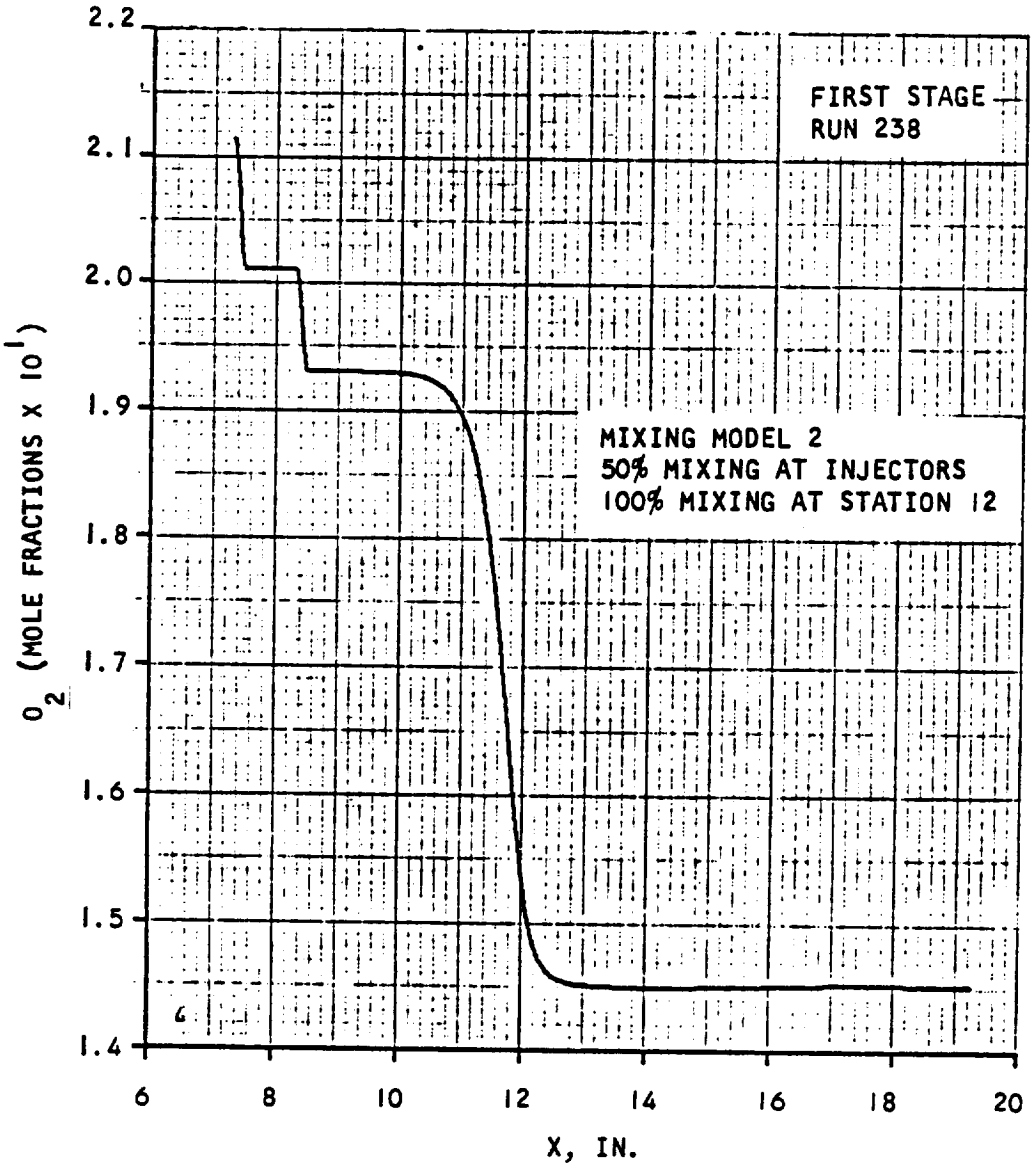

Figure A.1-6. Concentration of O_2 vs Axial Distance

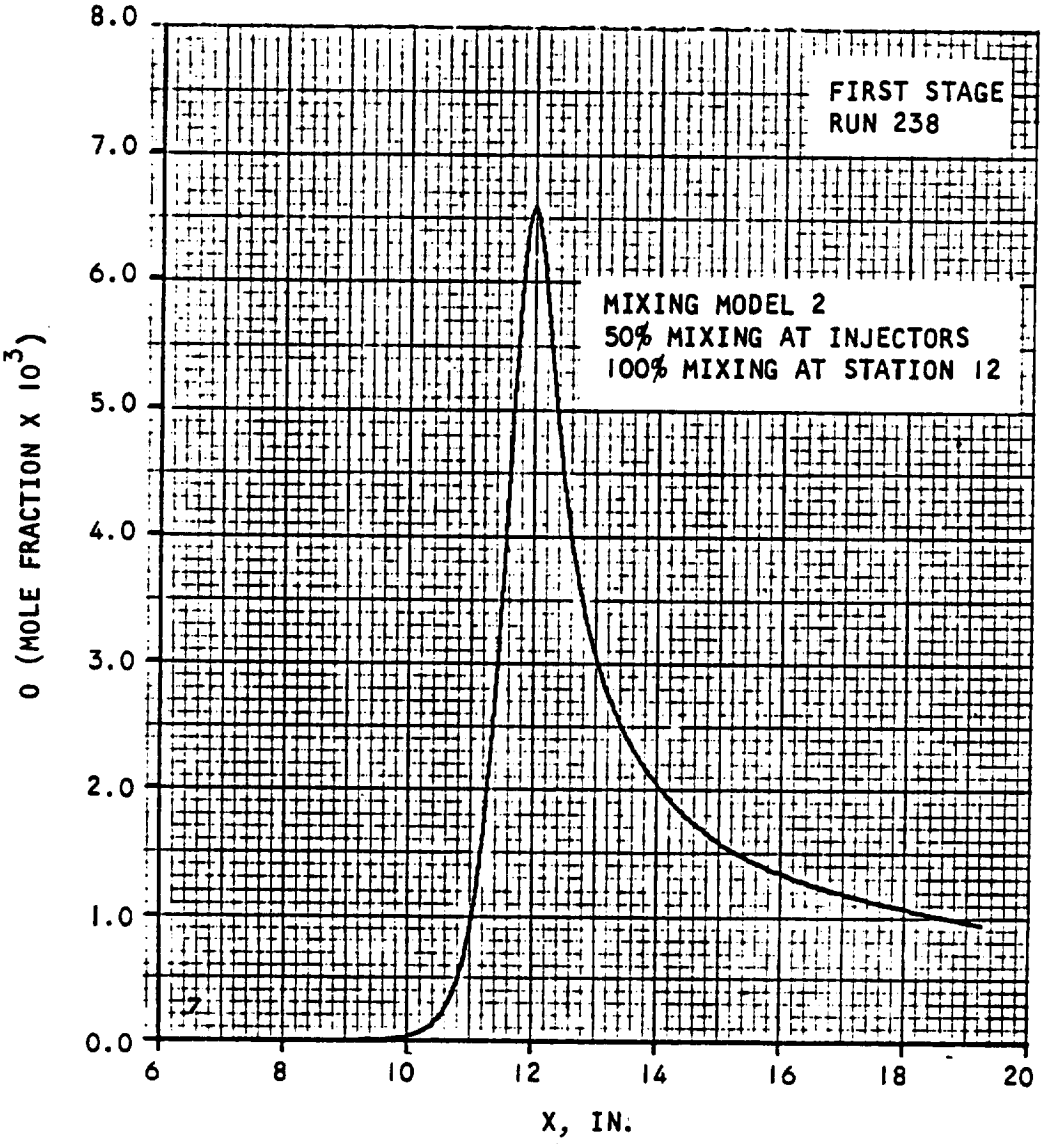

Figure A.1-7. Concentration of O vs Axial Distance

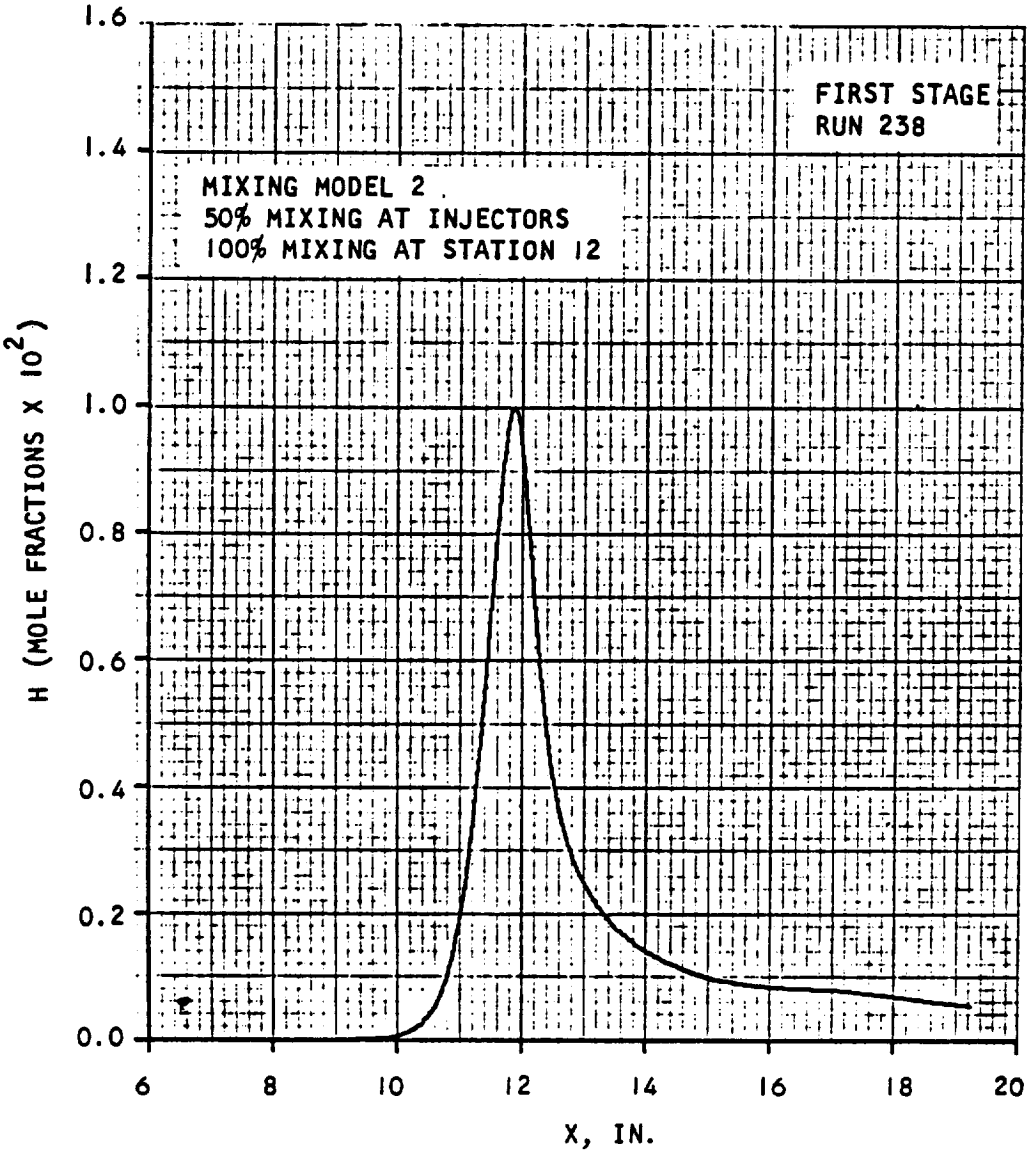

Figure A.1-8. Concentrations of H vs Axial Distance

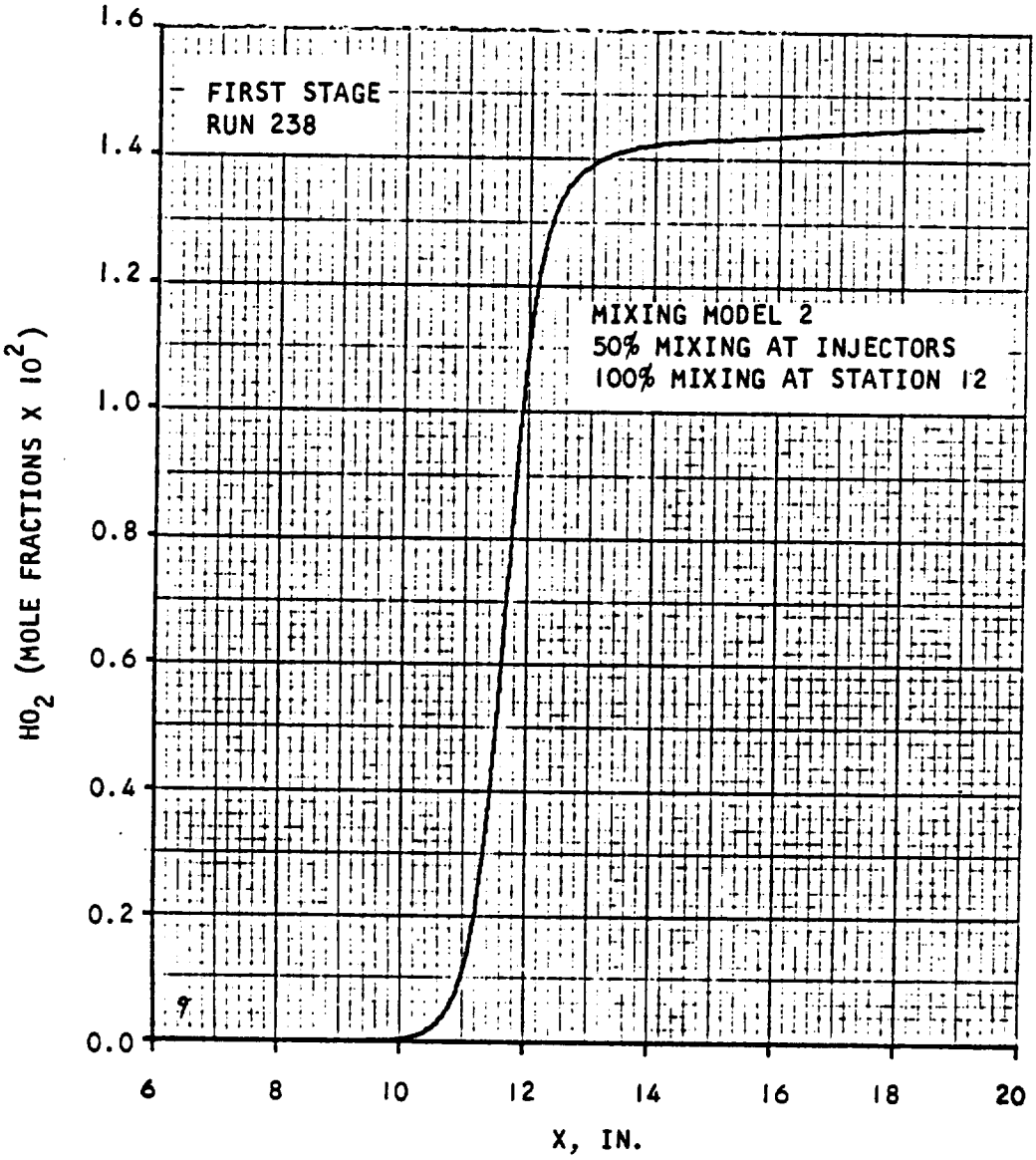

Figure A.1-9. Concentrations of HO_2 vs Axial Distance

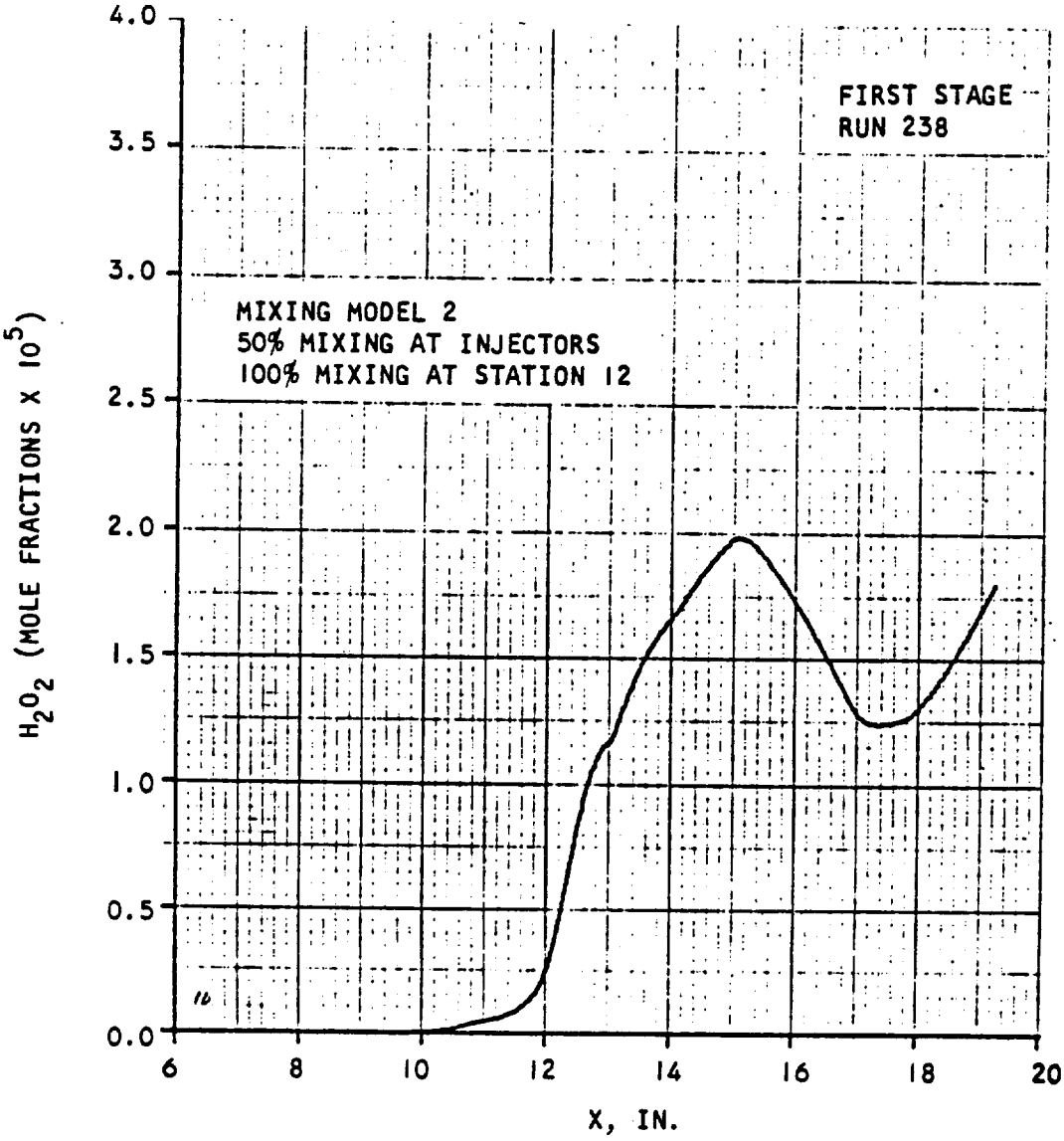

Figure A.1-10. Concentrations of H_2O_2 vs Axial Distance

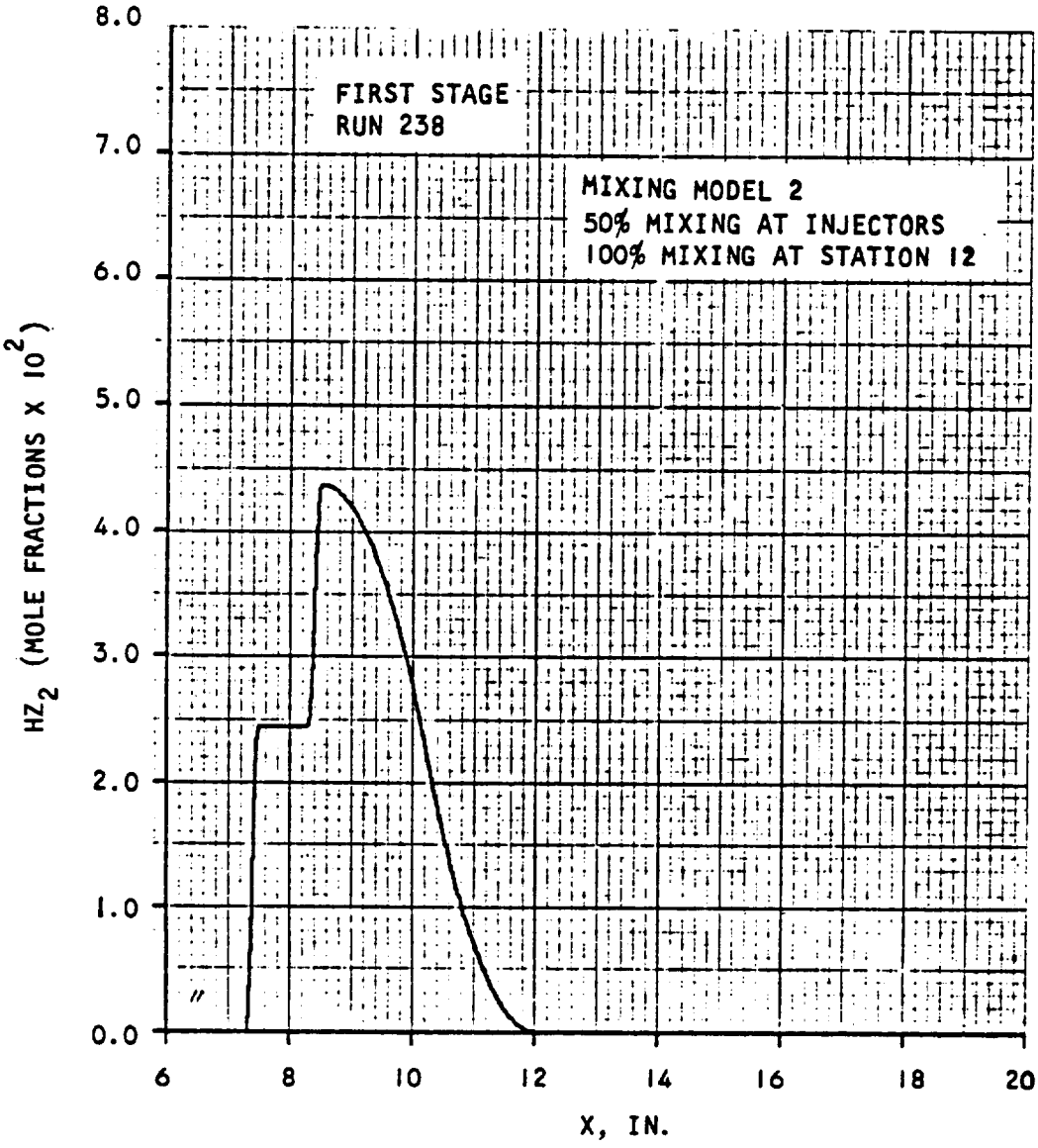

Figure A.I-11. Concentrations of HZ_2 vs Axial Distance

2. Second Stage Combustor - Run 238
Mixing Model 2, 50 percent local mixing at each injector, 100 percent mixing at Station 28.62.

Station	A(in.^{2})	$\dot{m}$(lb m/sec)	$\dot{m}_{H_2}$ (mixed)	η_m	η_c	$\dot{m}_{H_2} + \dot{m}_{Hz_2}$	ϕ
19.1950	4.990	1.7941	0.013119	1.00	0.9998	0.013122	0.2262
19.8550	5.300	1.8068	0.019491	0.755	0.6917	0.025815	0.4443
20.6000	5.326	1.8068	0.022315	0.755	0.8612	0.025815	0.4443
20.8100	5.757	1.8176	0.024931	0.680	0.7209	0.036640	0.6317
21.4150	6.192		0.025068	0.684	0.8774		
22.0150	6.605		0.025461	0.695	0.9150		
22.5600	6.943		0.026041	0.711	0.9257		
23.1600	7.270		0.026928	0.735	0.9284		
23.5600	7.484		0.027662	0.755	0.9272		
24.1600	7.818		0.028977	0.791	0.9230		
24.5600	8.056		0.02998	0.819	0.9191		
25.1050	8.399		0.03150	0.860	0.9142		
25.5050	8.631		0.032516	0.887	0.9132		
26.0750	8.985		0.033765	0.922	0.9135		
26.4750	9.286		0.034509	0.942	0.9142		
27.0750	9.755		0.035420	0.967	0.9159		
27.4750	10.079	↓	0.035891	0.980	0.9175	↓	↓
28.0300	10.547		0.036363	0.992	0.9203		
28.6200	11.065	1.8176	0.036635	1.00	0.9244	0.036640	0.6317

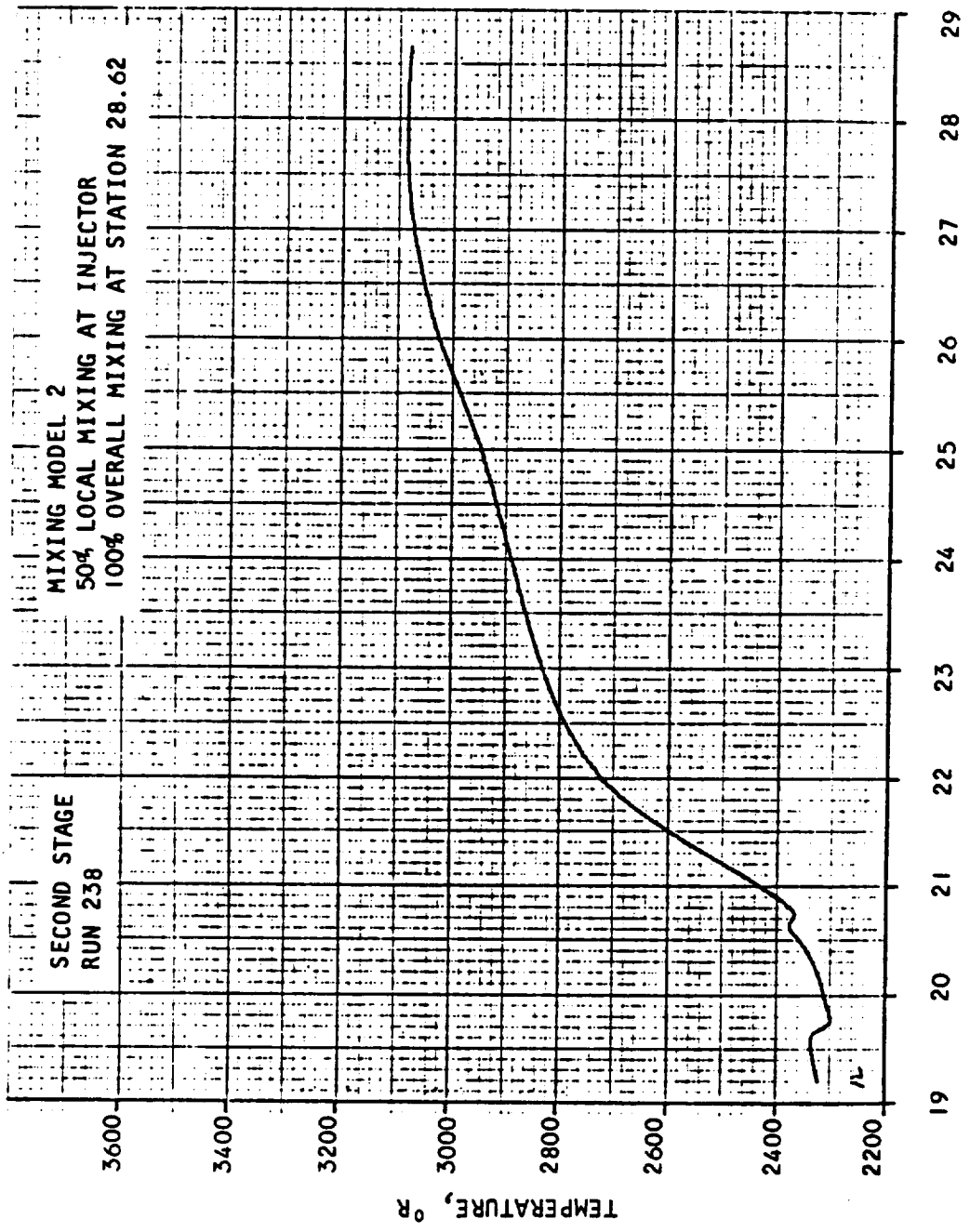

Figure A.2-1. Temperature vs Axial Distance

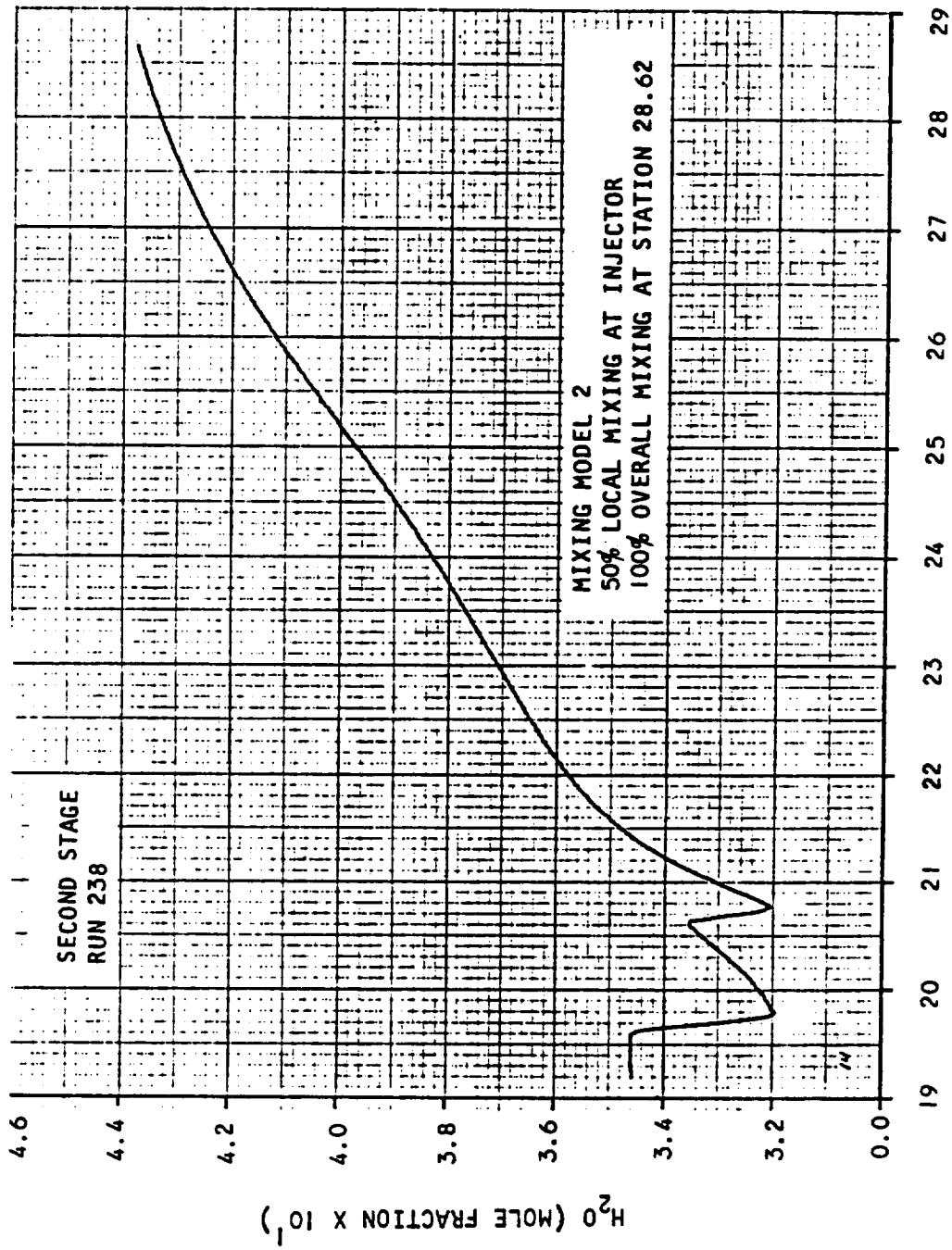

Figure A.2-3. Concentration of H_2O vs Axial Distance

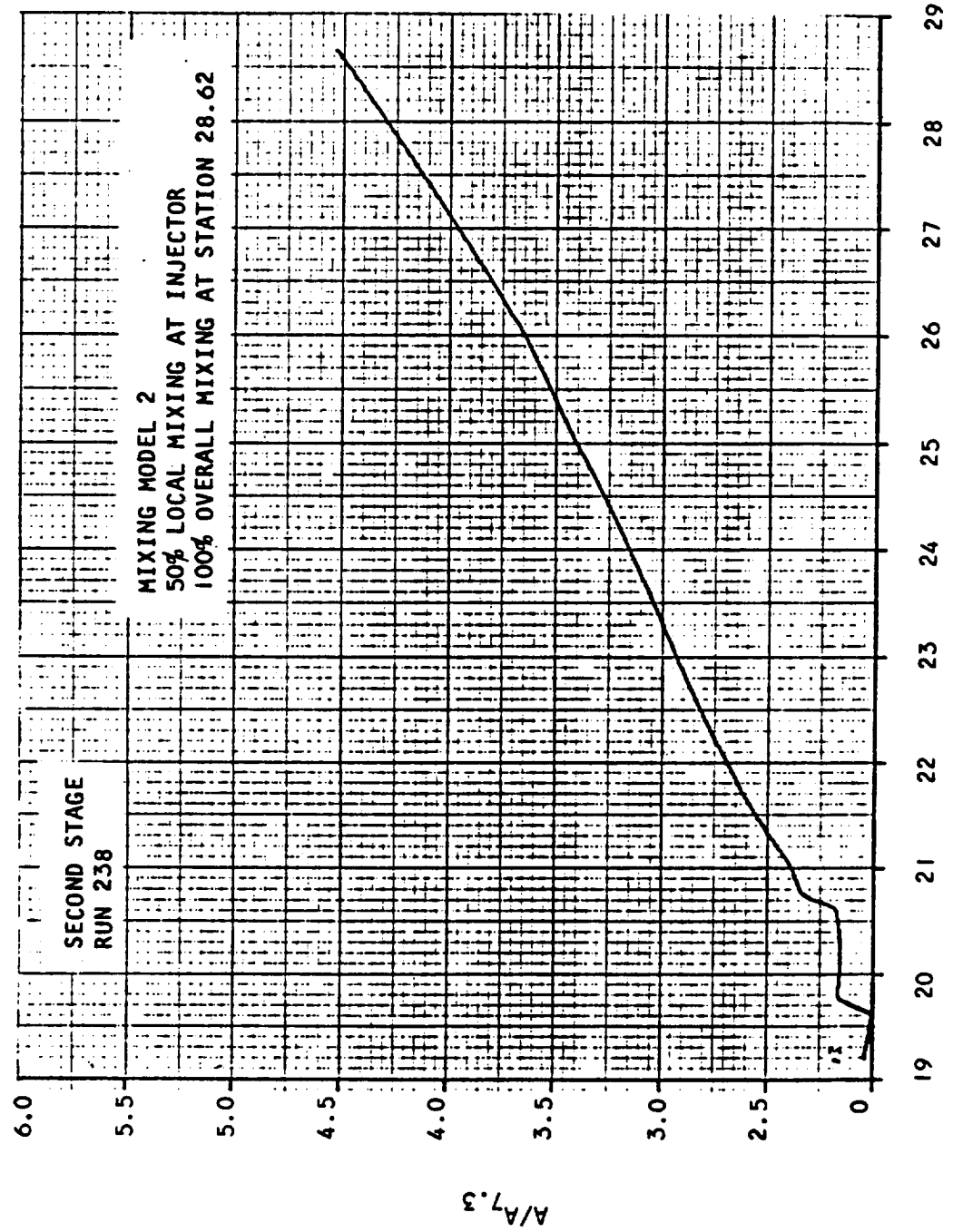

Figure A.2-2. Area Ratio vs Axial Distance

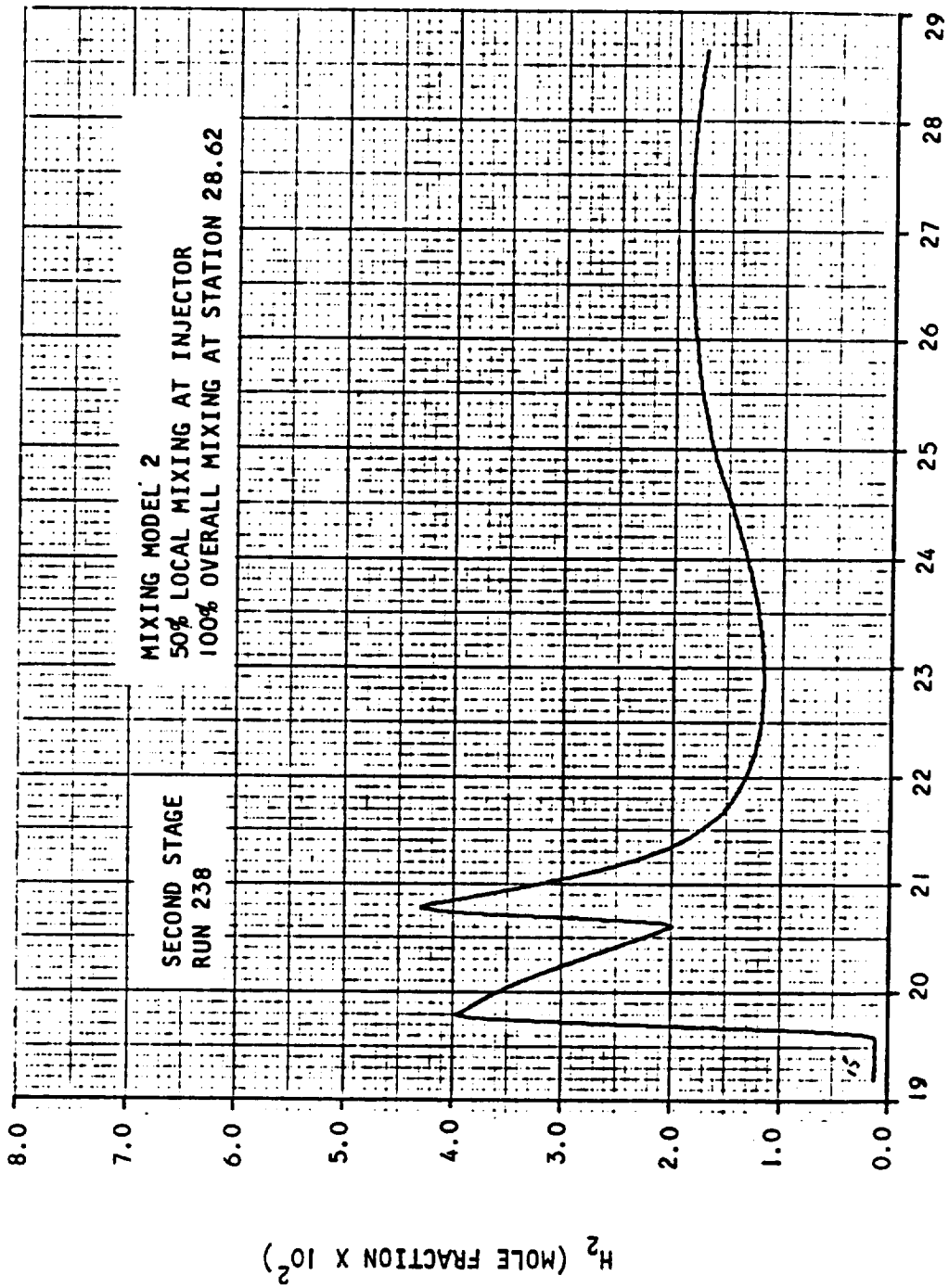

Figure A.2-4. Concentration of H_2 vs Axial Distance

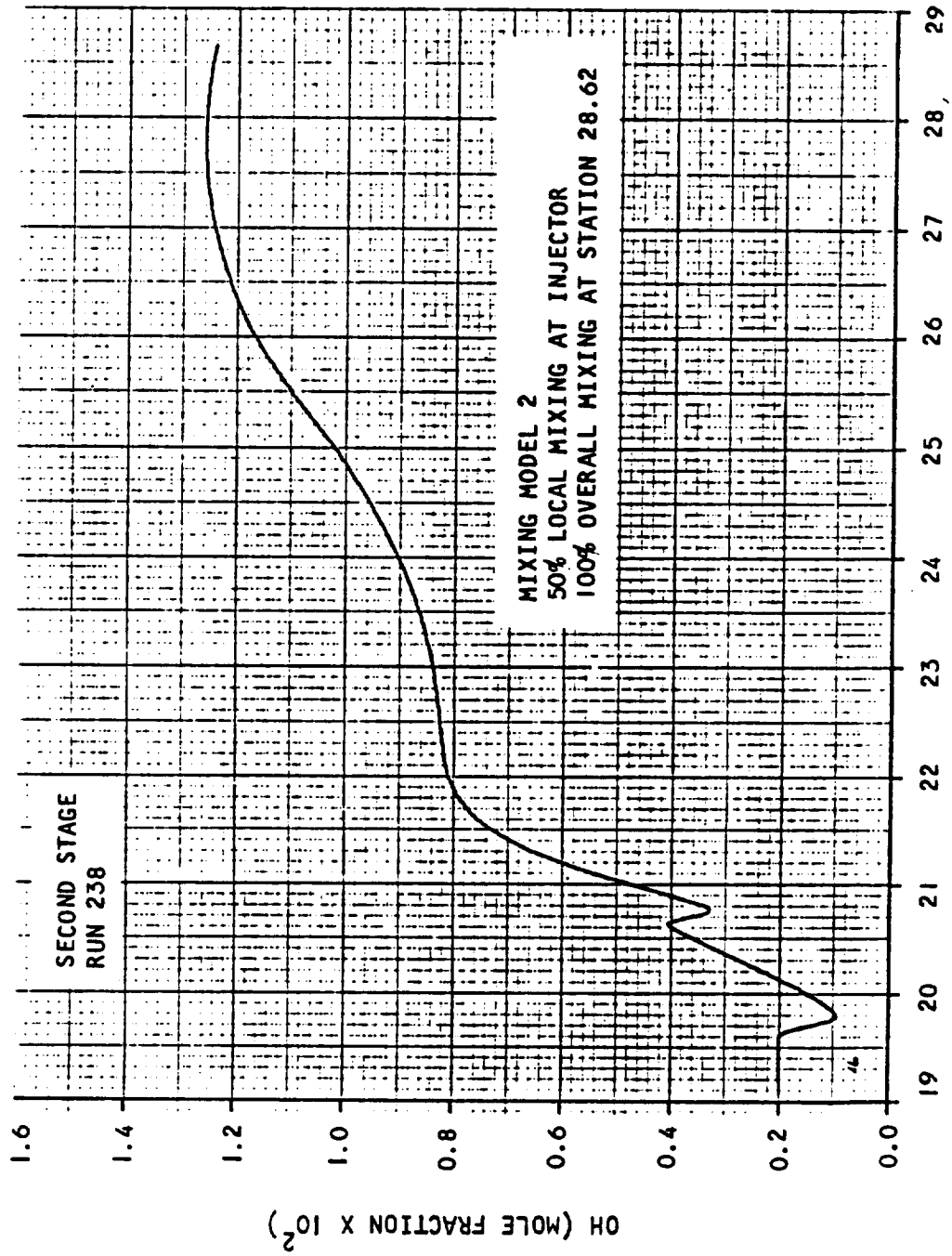

Figure A.2-5. Concentration of OH vs Axial Distance

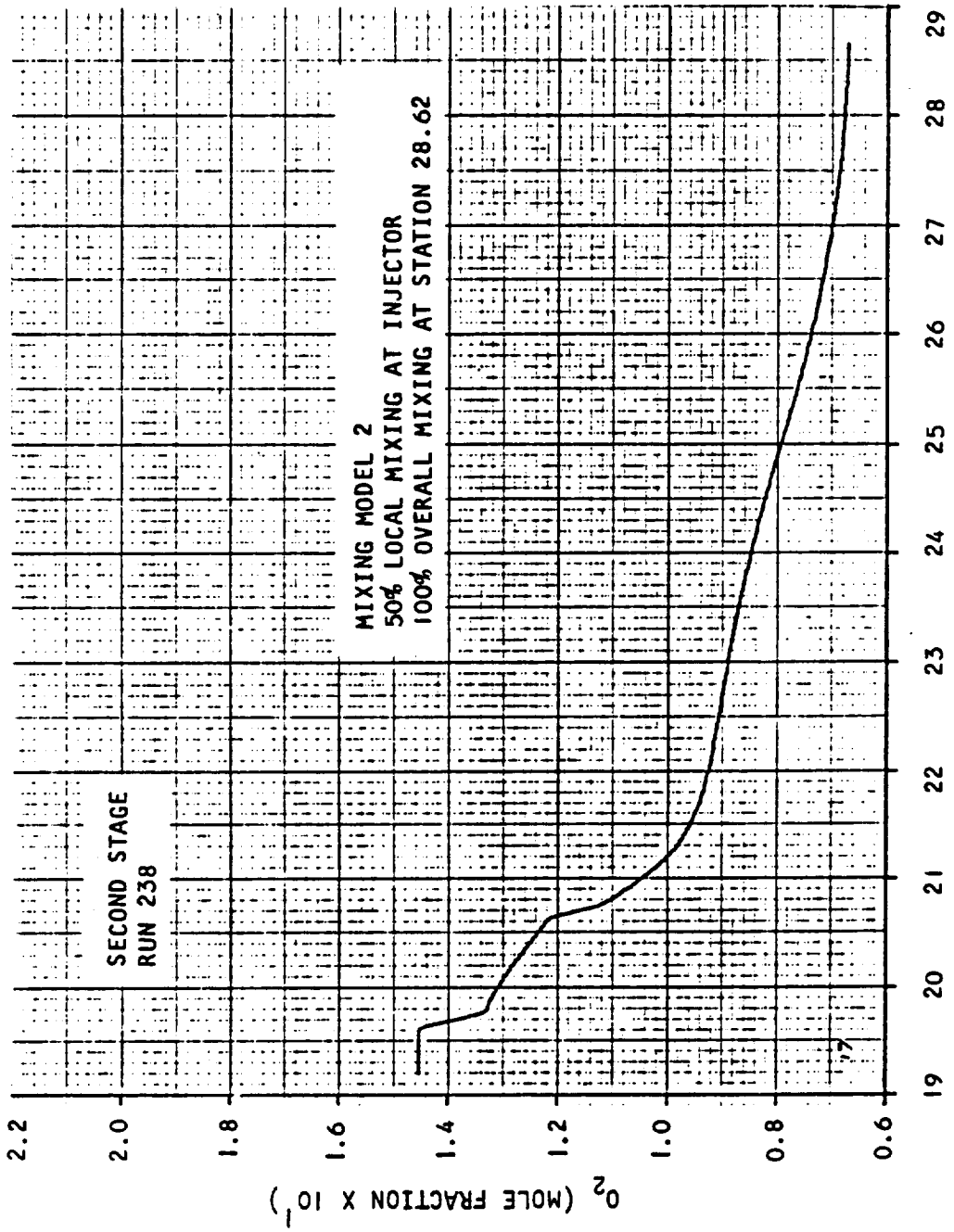

Figure A.2-6. Concentration of O_2 vs Axial Distance

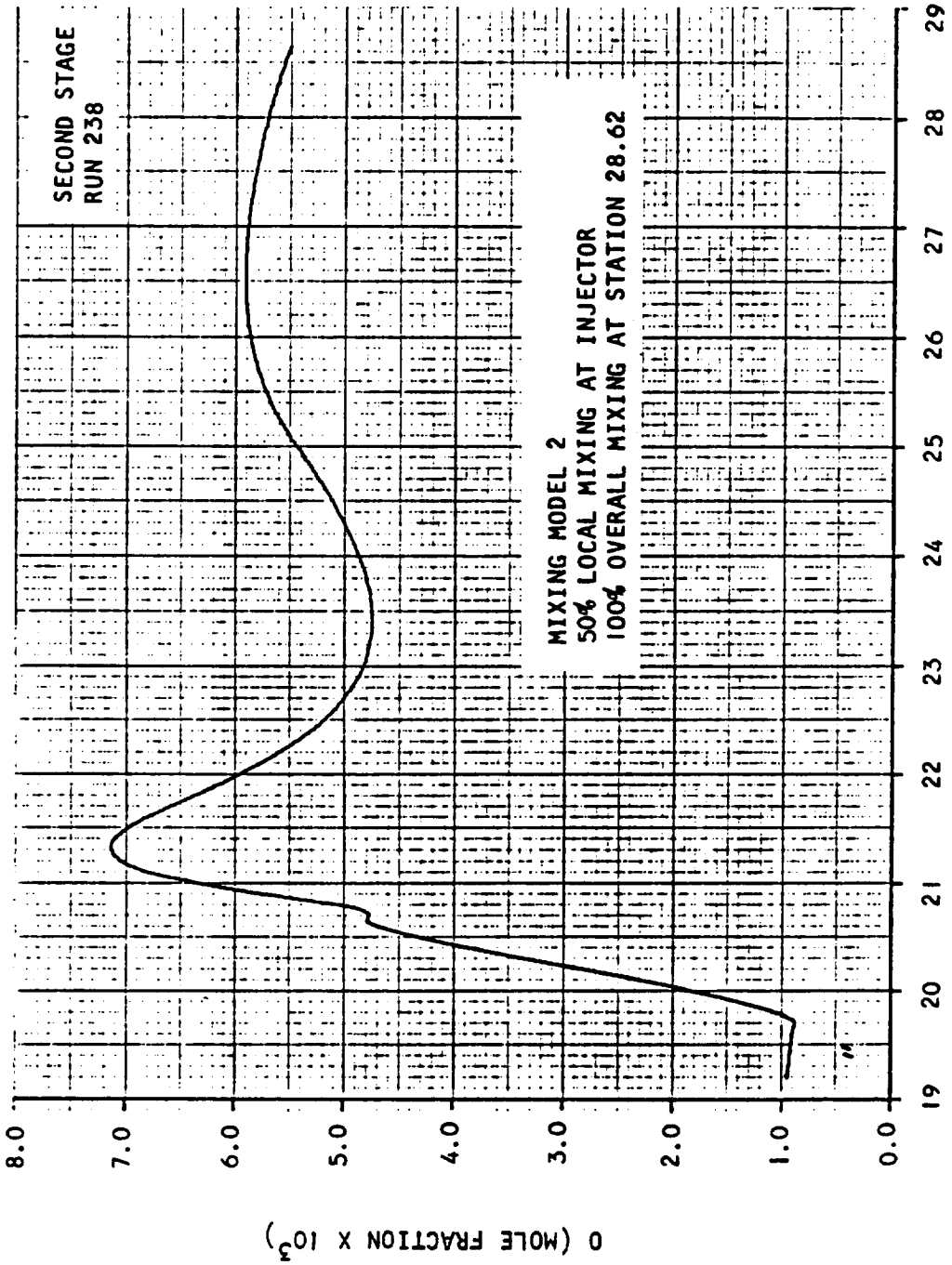

Figure A.1-7. Concentration of O vs Axial Distance

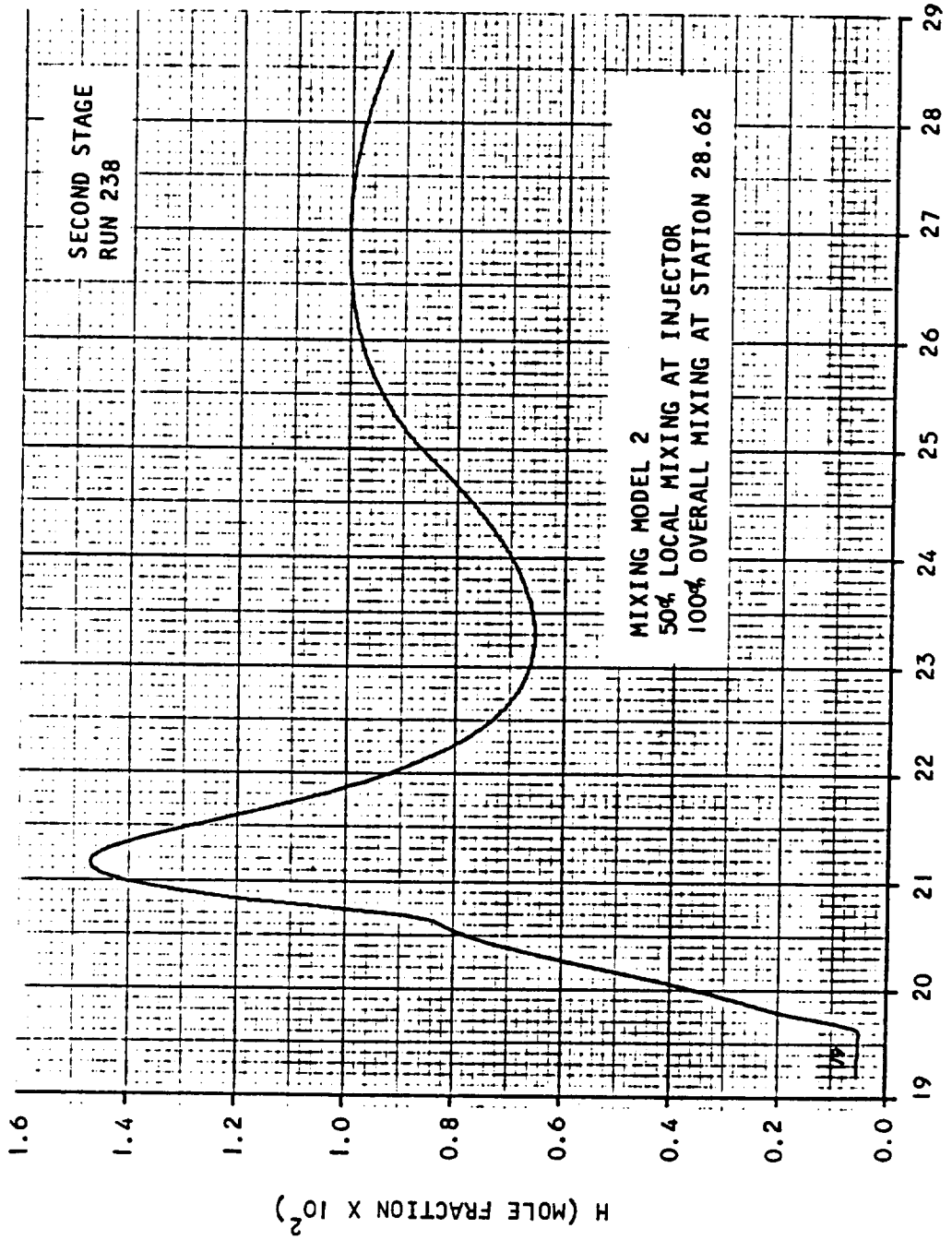

Figure A.2-8. Concentration of H vs Axial Distance

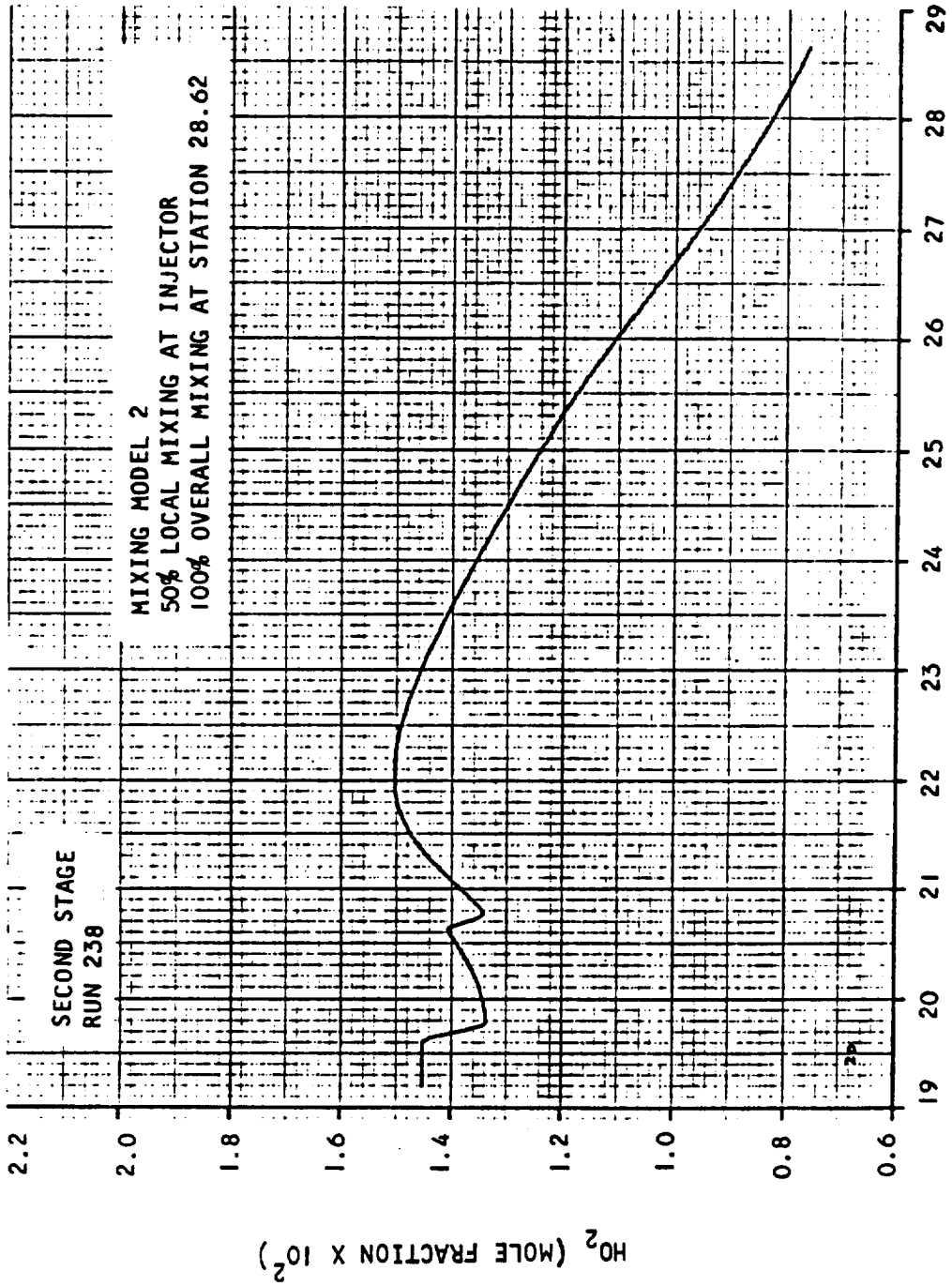

Figure A.2-9. Concentration of HO_2 vs Axial Distance

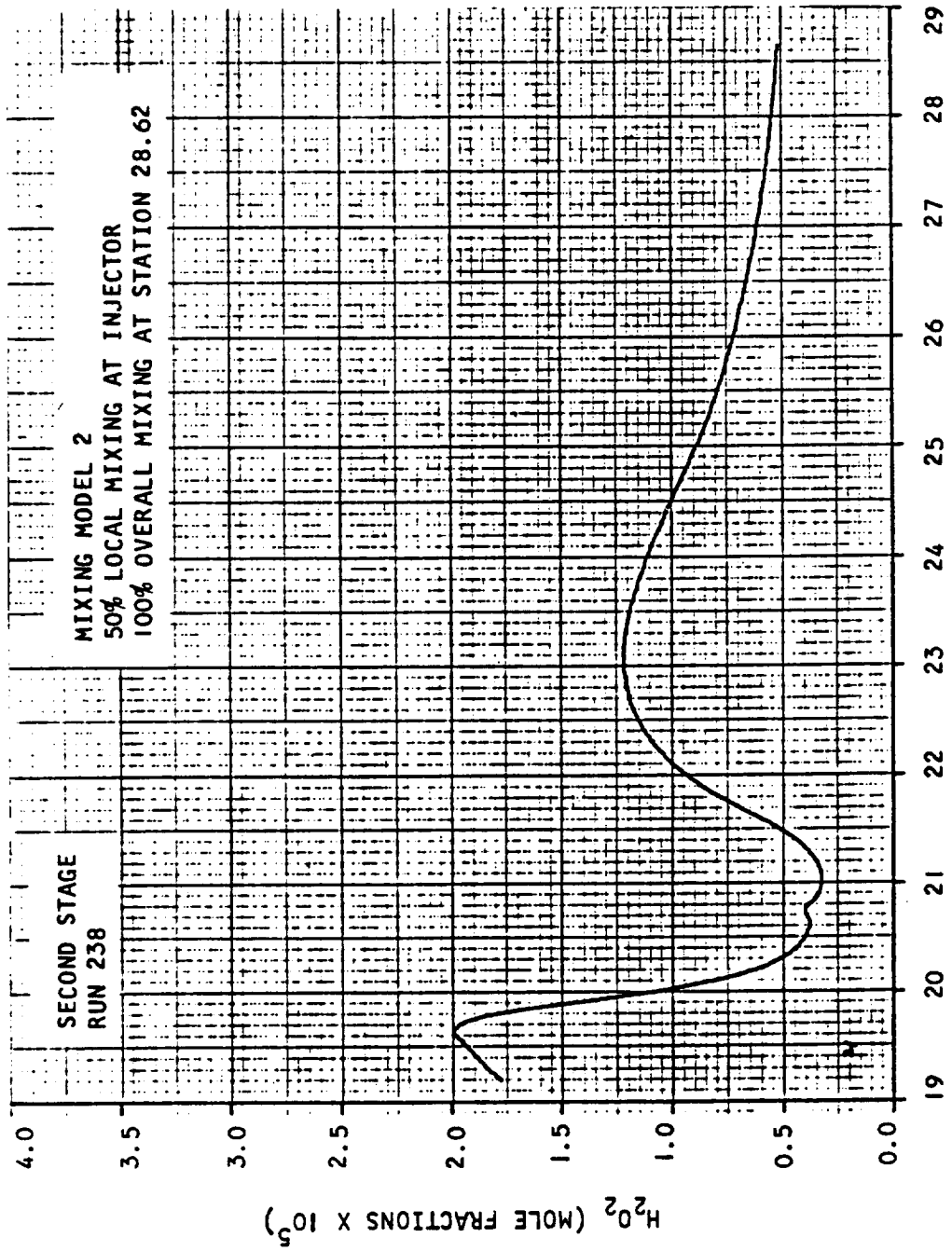

Figure A.2-10. Concentration of H_2O_2 vs Axial Distance

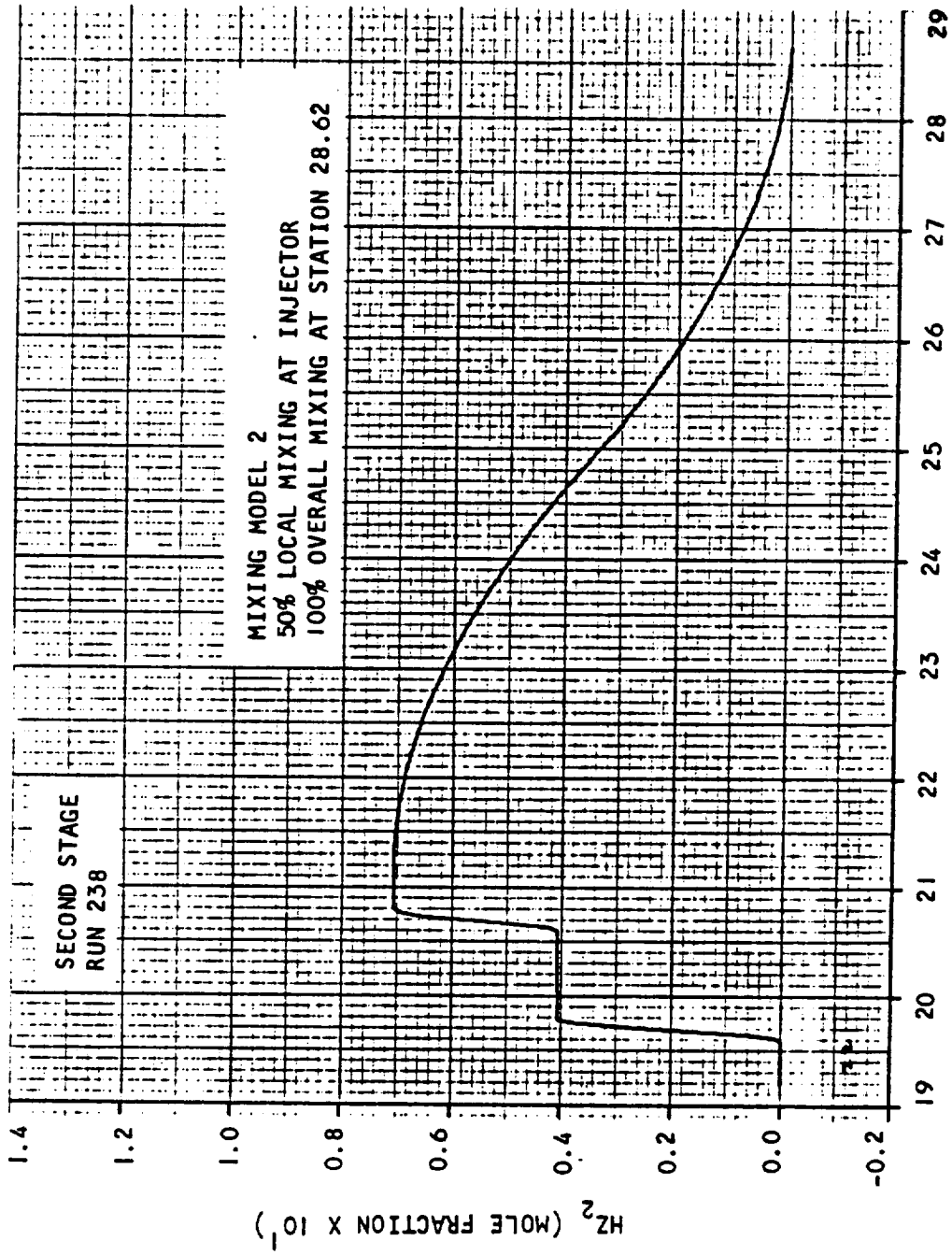

Figure A.2-11. Concentration of HZ_2 vs Axial Distance

3. Second Stage Combustor - Run 238
Mixing Model 3, 0 percent local mixing at injectors, 100 percent mixing at Station 29.

Station	A(in.^{2})	$\dot{m}$(lb m/sec)	$\dot{m}_{H_2}$ (mixed)	η_m	η_c	$\dot{m}_{H_2} + \dot{m}_{Hz_2}$	ϕ
19.1950	4.990	1.7941	0.013155	1.00	0.9998	0.013115	0.2261
19.5437	4.923	1.7941	0.013115	1.00	0.9998	0.013115	0.2261
19.8337	5.296	1.8068	0.013115	0.508	0.9872	0.025815	0.4451
20.5687	5.212	1.8068	0.013115	0.508	0.9881	0.025815	0.4451
20.8387	5.549	1.8176	0.013115	0.358	0.9884	0.036640	0.6317
21.5362	5.580		0.013251	0.362	0.9770		
22.0812	5.367		0.013636	0.372	0.9569		
22.4812	5.725		0.014050	0.383	0.9385		
23.0812	5.872		0.014882	0.406	0.9084		
23.4812	5.982		0.015577	0.425	0.8887		
24.0812	6.172		0.016828	0.459	0.8620		
24.4812	6.319		0.017803	0.486	0.8468		
25.0312	6.551		0.019325	0.527	0.8296		
25.6262	6.795		0.021211	0.579	0.8171		
26.0162	6.985		0.022581	0.616	0.8128		
26.5962	7.385		0.024815	0.677	0.8103		
26.9962	7.706		0.026494	0.723	0.8102		
27.5962	8.263		0.029221	0.798	0.8119		
27.9962	8.689		0.031179	0.851	0.8136		
28.3962	9.157		0.033249	0.907	0.8151		
28.5962	9.409	↓	0.34326	0.937	0.8157	↓	↓
28.7962	9.673		0.035431	0.967	0.8160		
29.0000	9.955	1.8176	0.036586	0.999	0.8162	0.036640	0.6317

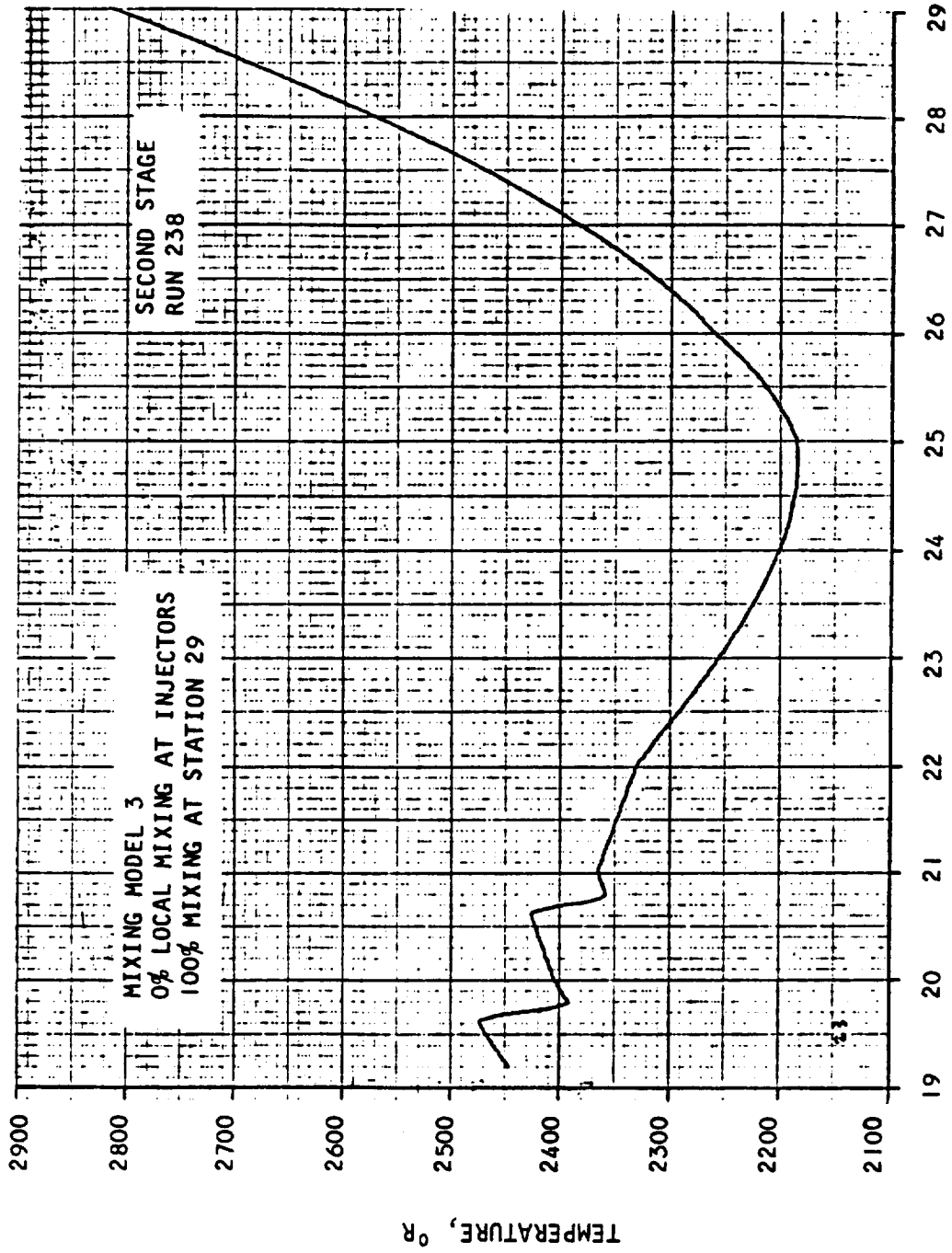

Figure A.3-1. Temperature vs Axial Distance

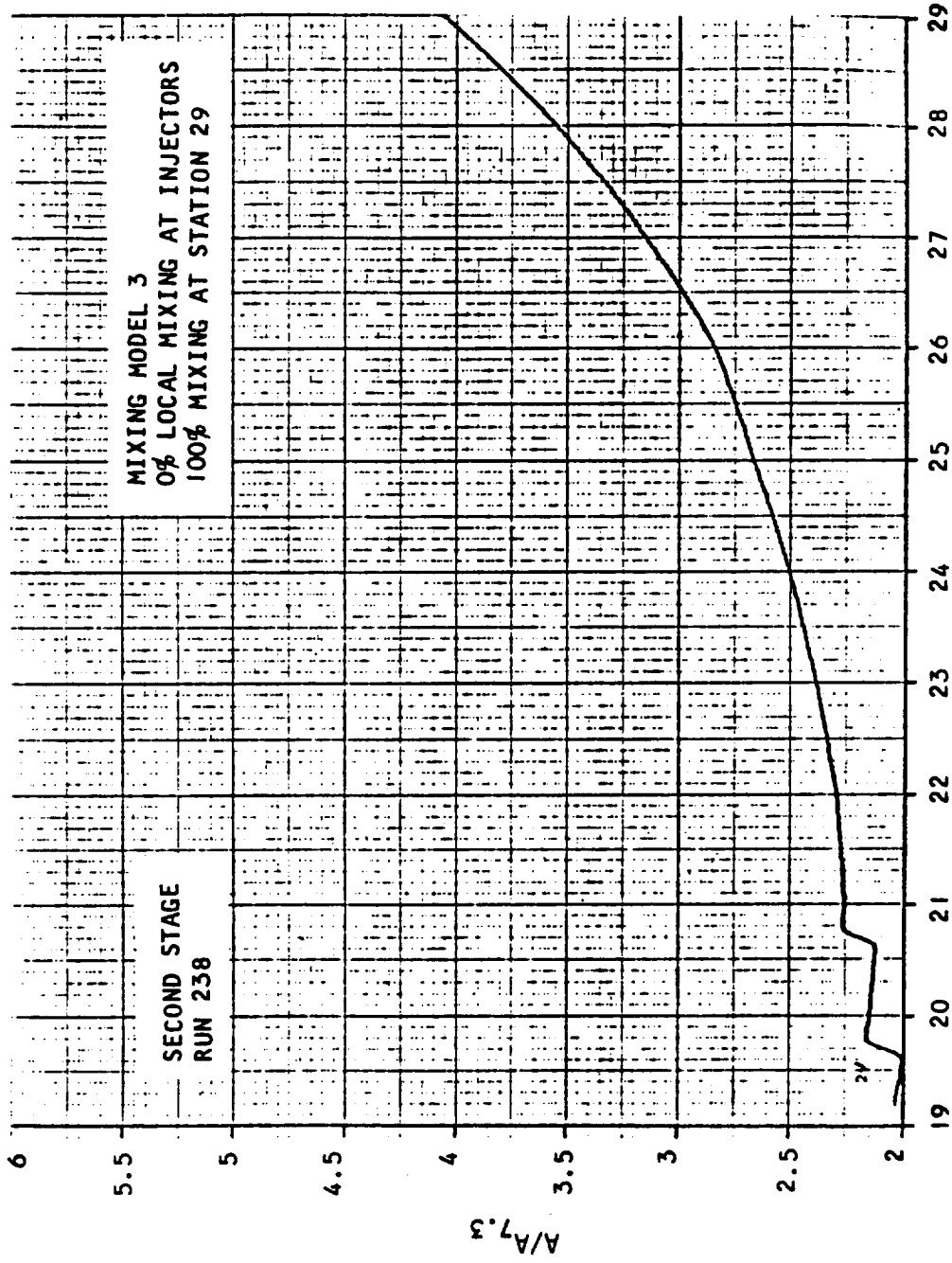

Figure A.3-2. Area Ratio vs Axial Distance

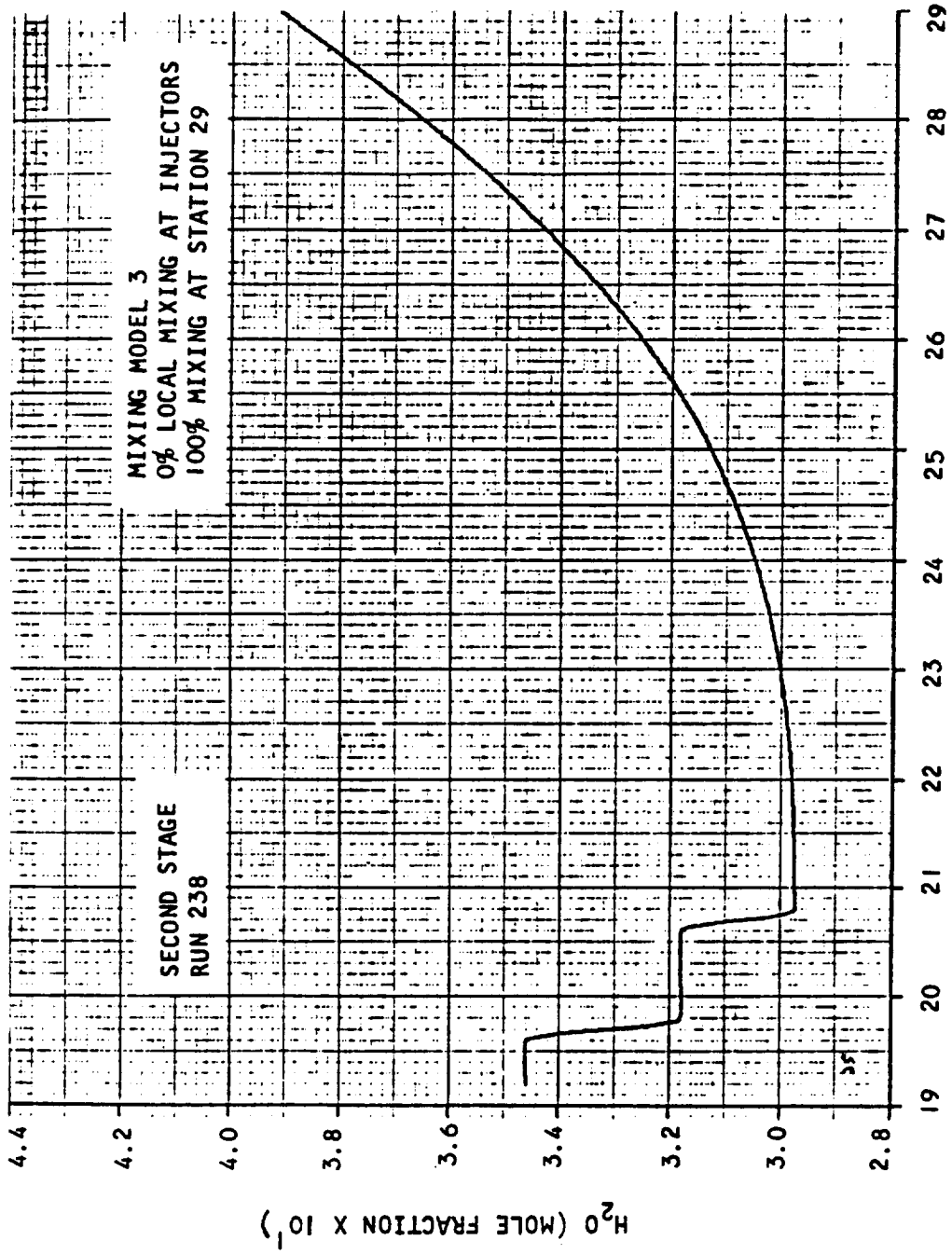

Figure A.3-3. Concentration of H_2O vs Axial Distance

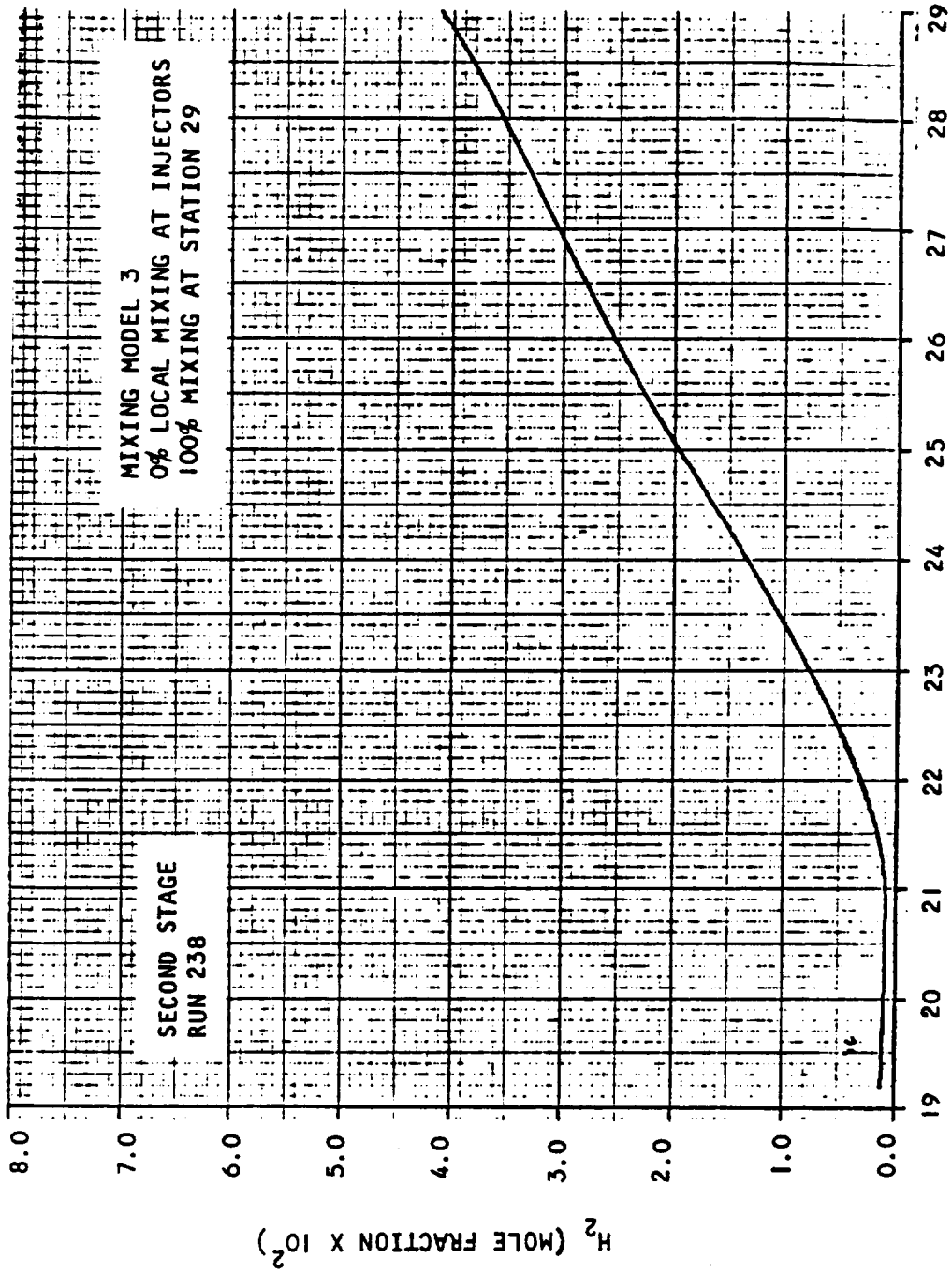

Figure A.3-4. Concentration of H_2 vs Axial Distance

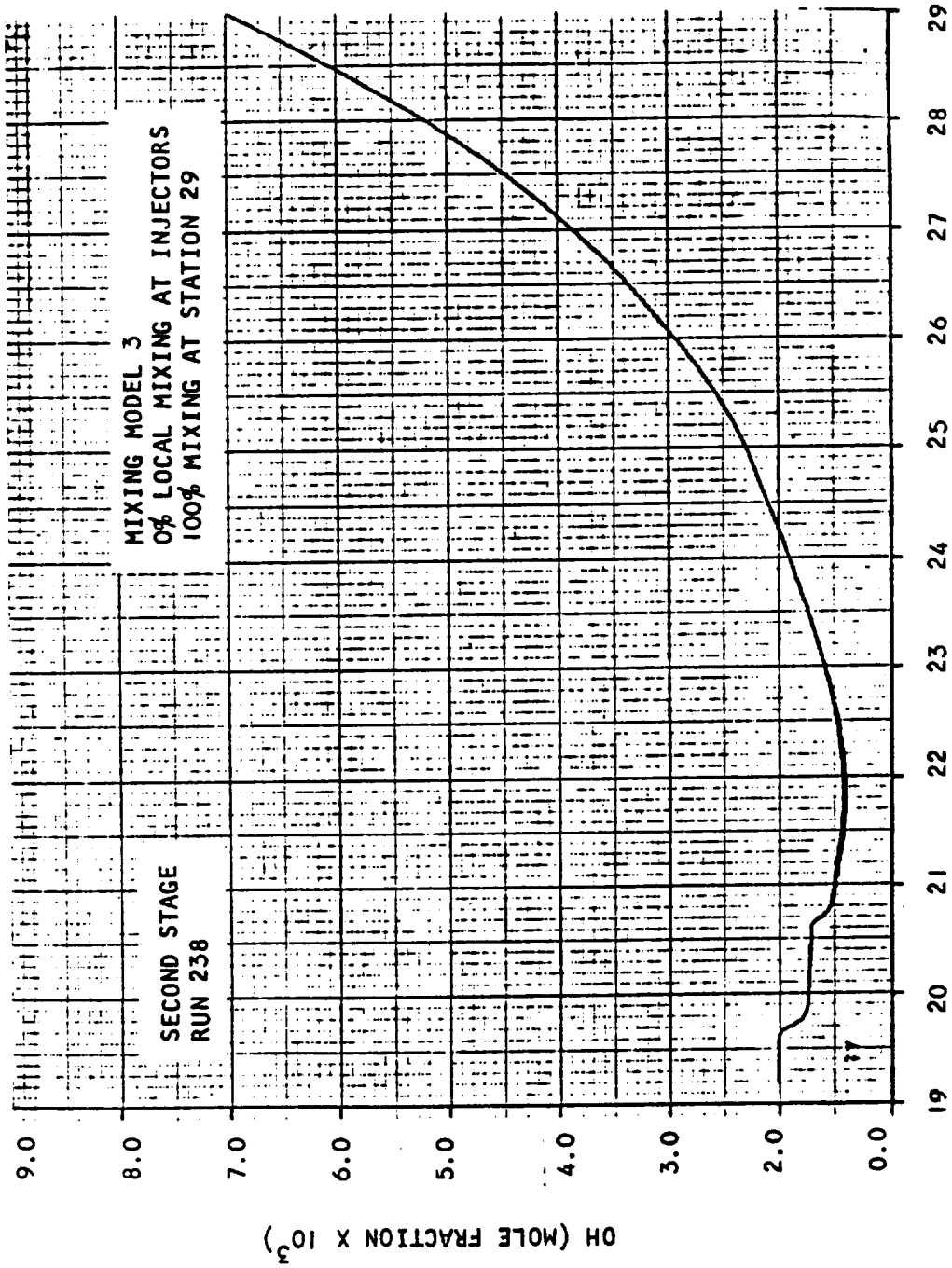

Figure A.3-5. Concentraion of OH vs Axial Distance

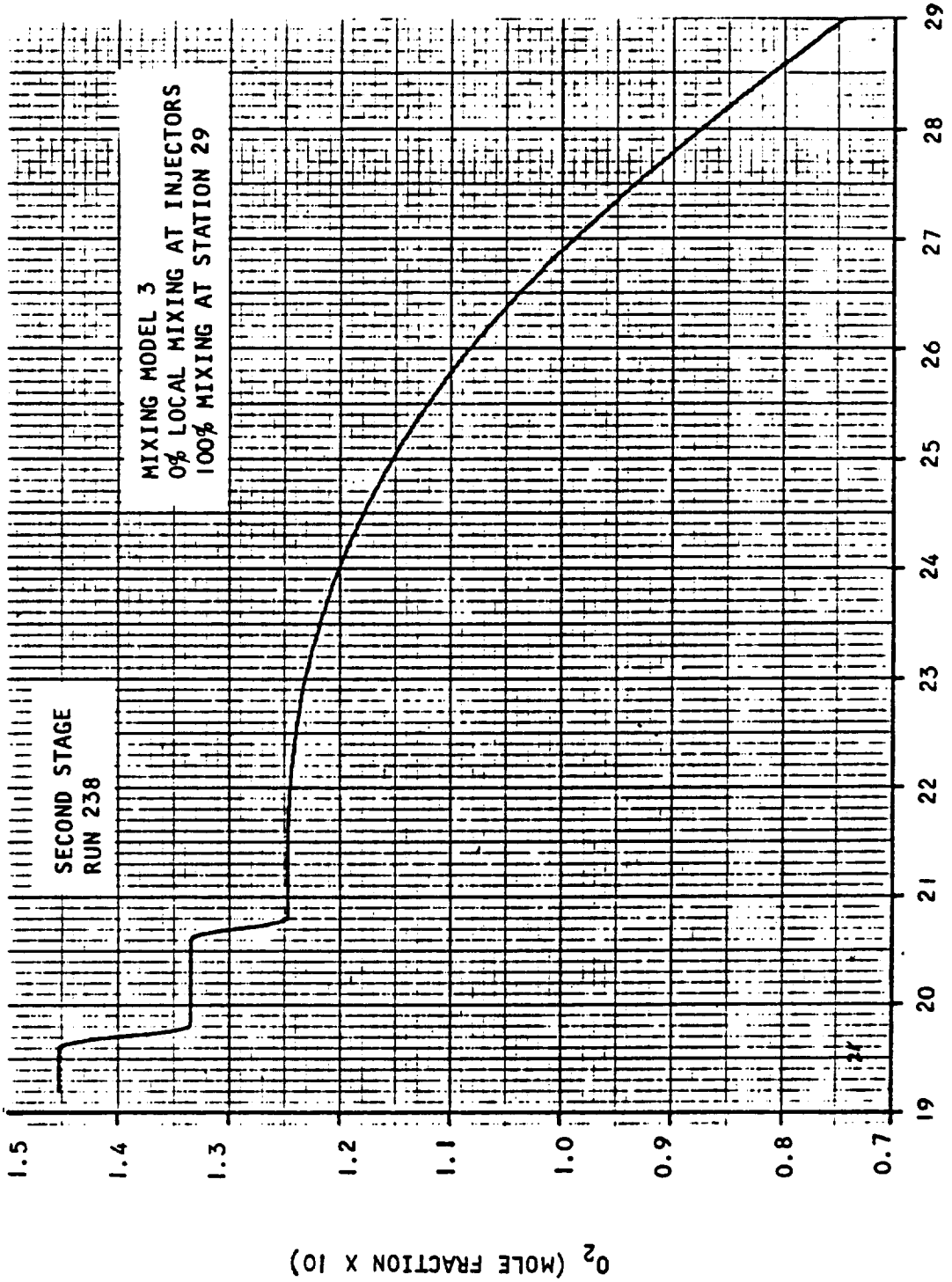

Figure A.3-6. Concentration of O_2 vs Axial Distance

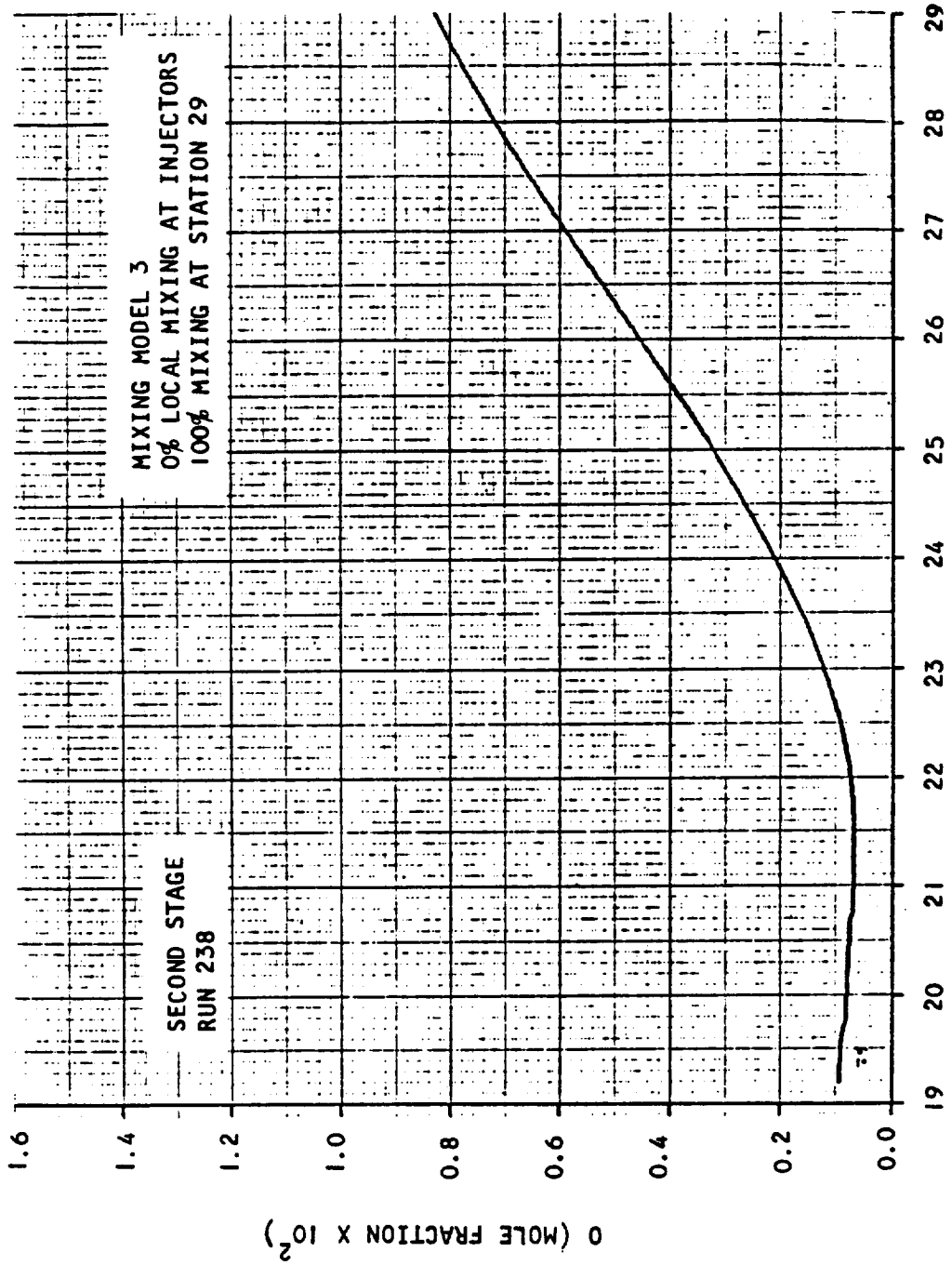

Figure A.3-7. Concentration of O vs Axial Distance

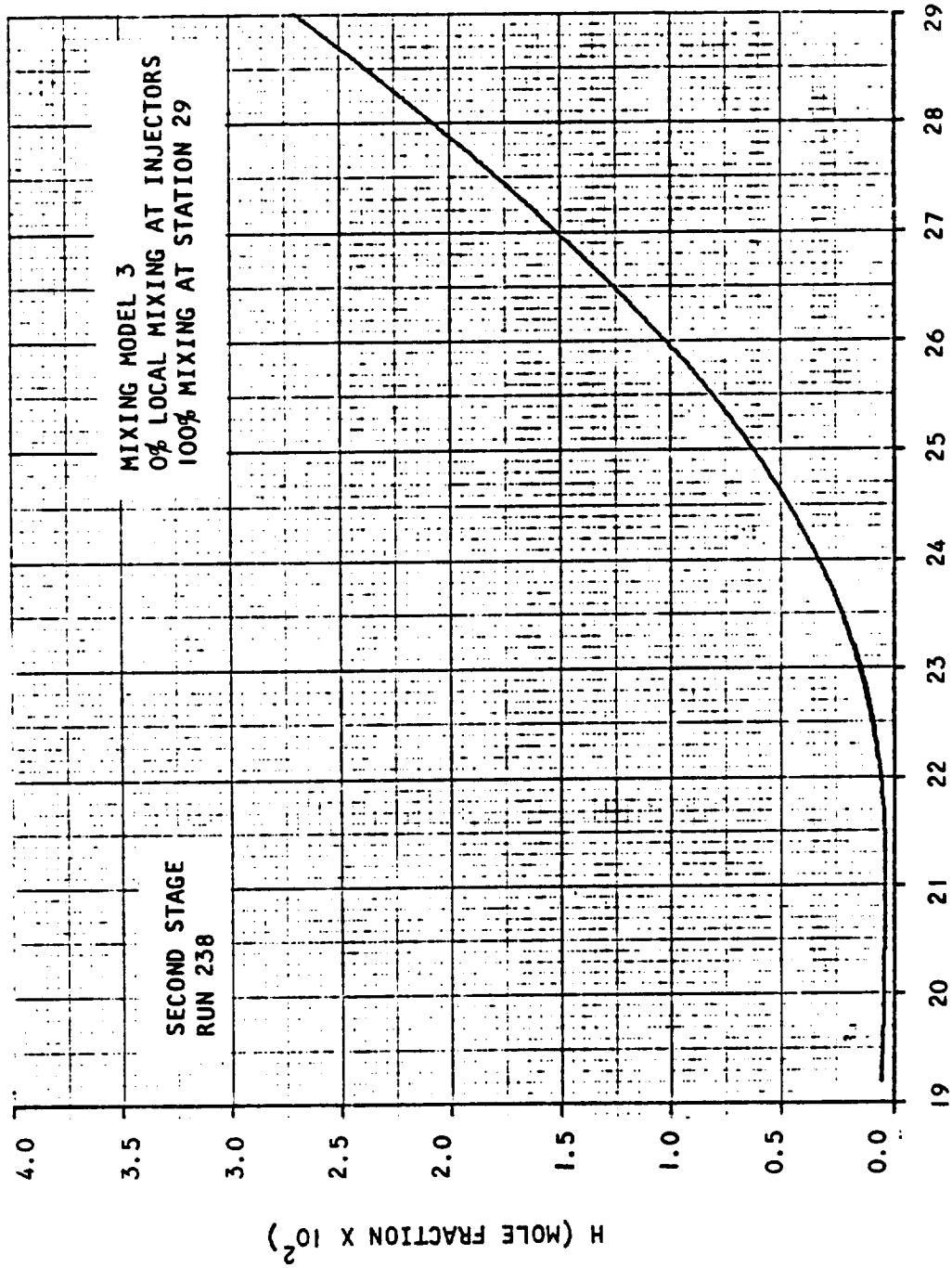

Figure A.3-8. Concentration of H vs Axial Distance

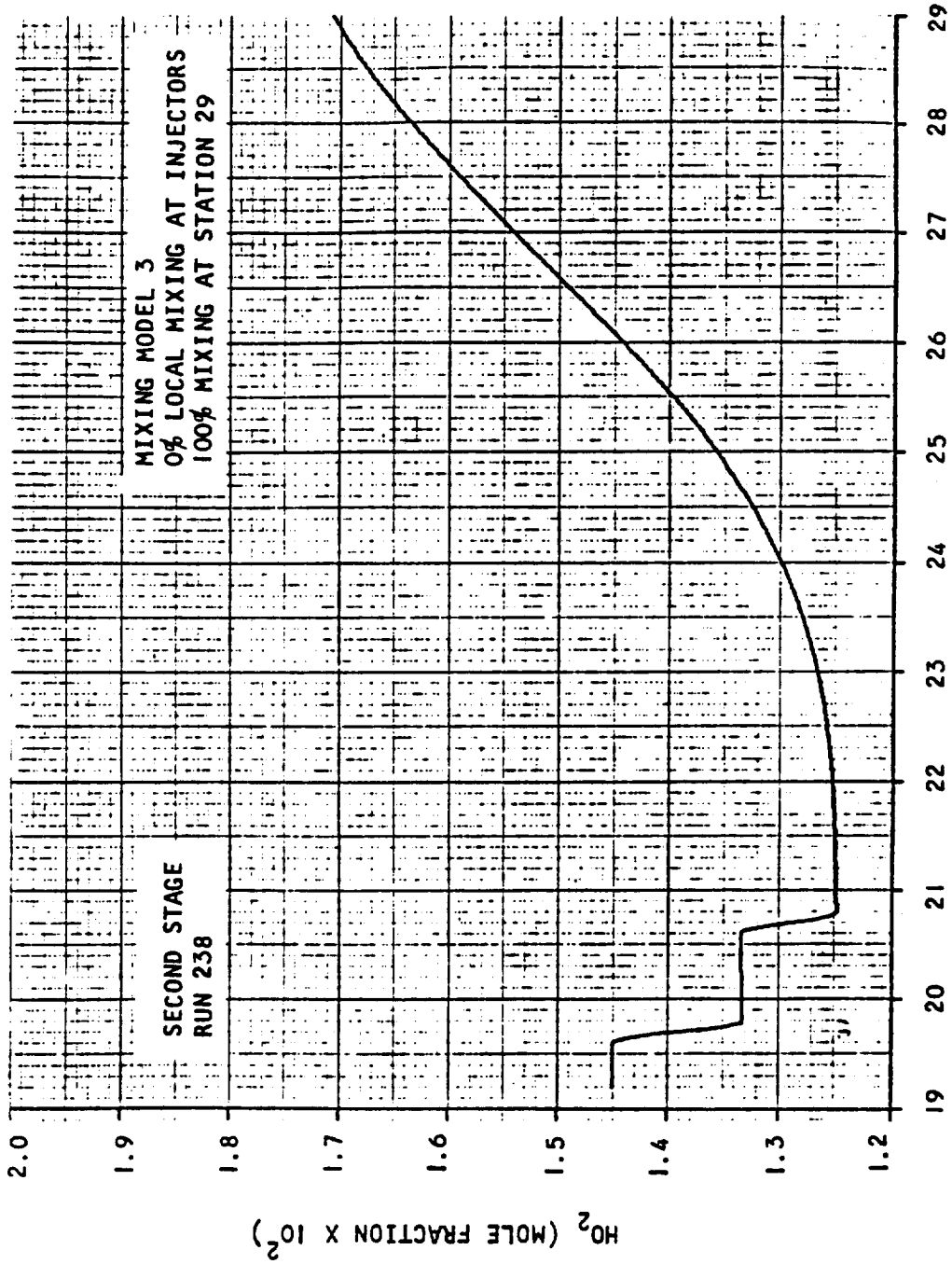

Figure A.3-9. Concentration of HO_2 vs Axial Distance

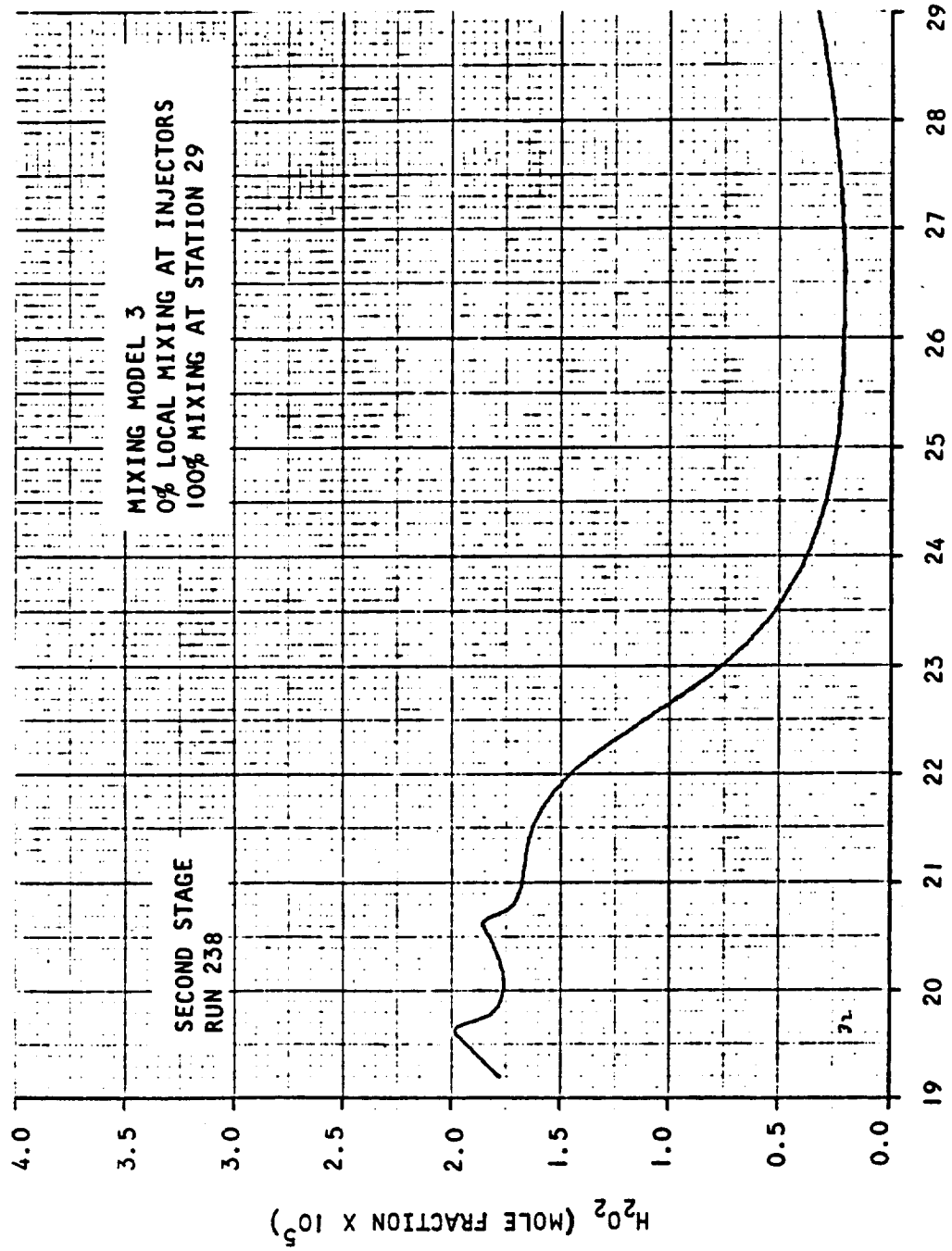

Figure A.3-10. Concentration of H_2O_2 vs Axial Distance

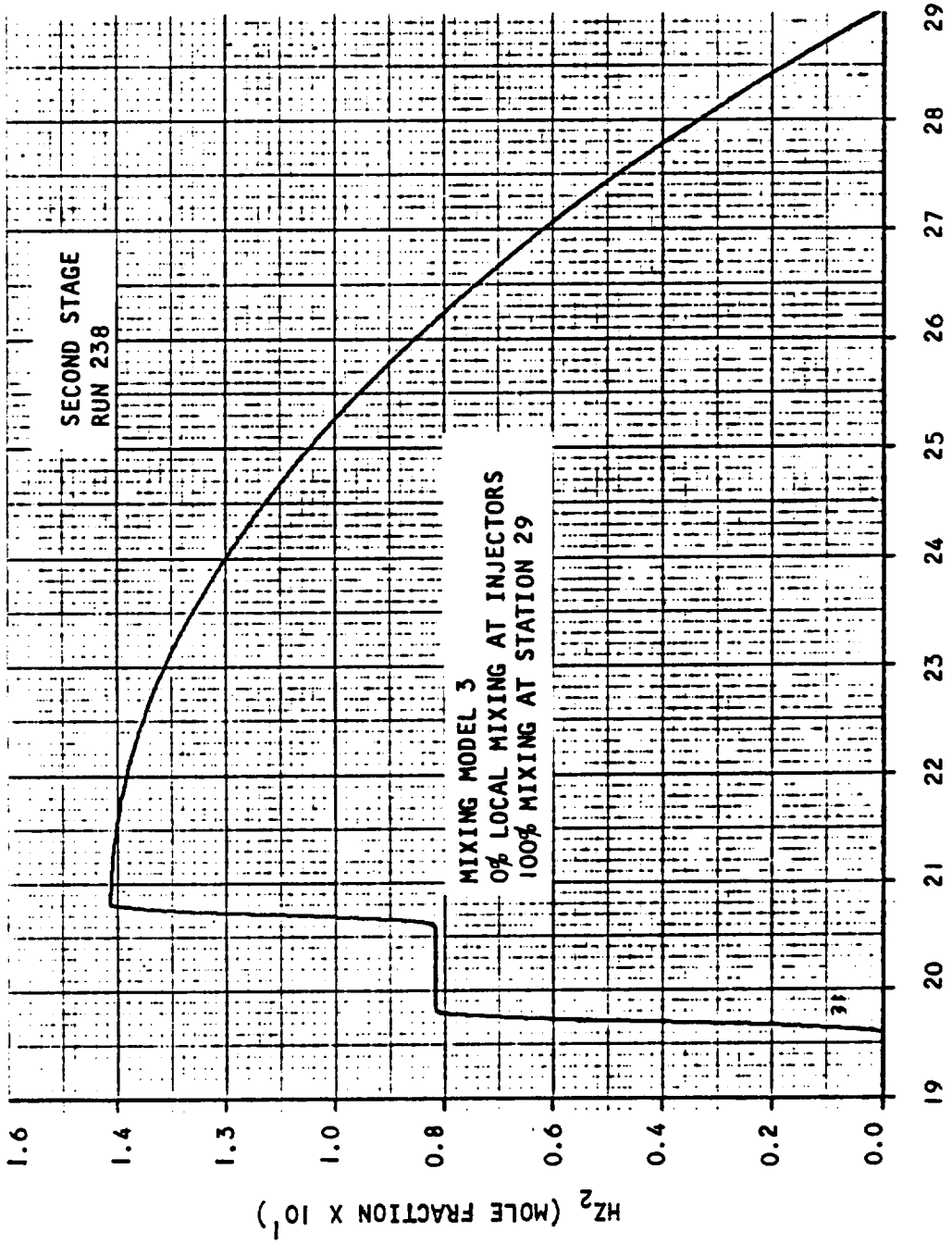

Figure A.3-11. Concentration of HZ_2 vs Axial Distance

4. Second Stage Combustor - Run 238
Mixing Model 1, 50 percent local mixing each injector, 60 percent mixing at Station 24.8.

Station	A(in.^{2})	$\dot{m}$(lb m/sec)	$\dot{m}_{H_2}$ (mixed)	η_m	η_c	$\dot{m}_{H_2} + \dot{m}_{Hz_2}$	ϕ
19.1950	4.990	1.7941	0.013119	1.00	0.9998	0.013122	0.2262
19.5437	4.923	1.7941	0.013119	1.00	0.9998	0.013122	0.2262
20.0137	5.273	1.8068	0.015287	0.59	0.8697	0.025815	0.4451
20.5687	5.243	1.8068	0.015287	0.59	0.9486	0.025815	0.4451
21.0287	5.617	1.8176	0.018020	0.49	0.8376	0.036640	0.6317
21.5612	5.774		0.019055	0.52	0.8706		
22.1062	5.987		0.019951	0.54	0.8954		
22.5062	6.189		0.020504	0.56	0.9070		
23.1062	6.486		0.021167	0.58	0.9202		
23.5062	6.679		0.021498	0.59	0.9272		
24.1062	6.960		0.021828	0.596	0.9367		
24.5062	7.144		0.021938	0.599	0.9429		
25.0437	7.386		0.021962	0.599	0.9511		
25.6437	7.595				0.9570		
26.0212	7.726				0.9598		
26.5887	7.993				0.9630		
27.1887	8.295				0.9658		
27.5887	8.510				0.9672		
27.9887	8.739	↓	↓	↓	0.9684	↓	↓
28.5887	9.106				0.9700		
29.0000	9.382	1.8176	0.021962	0.599	0.9709	0.036640	0.6317

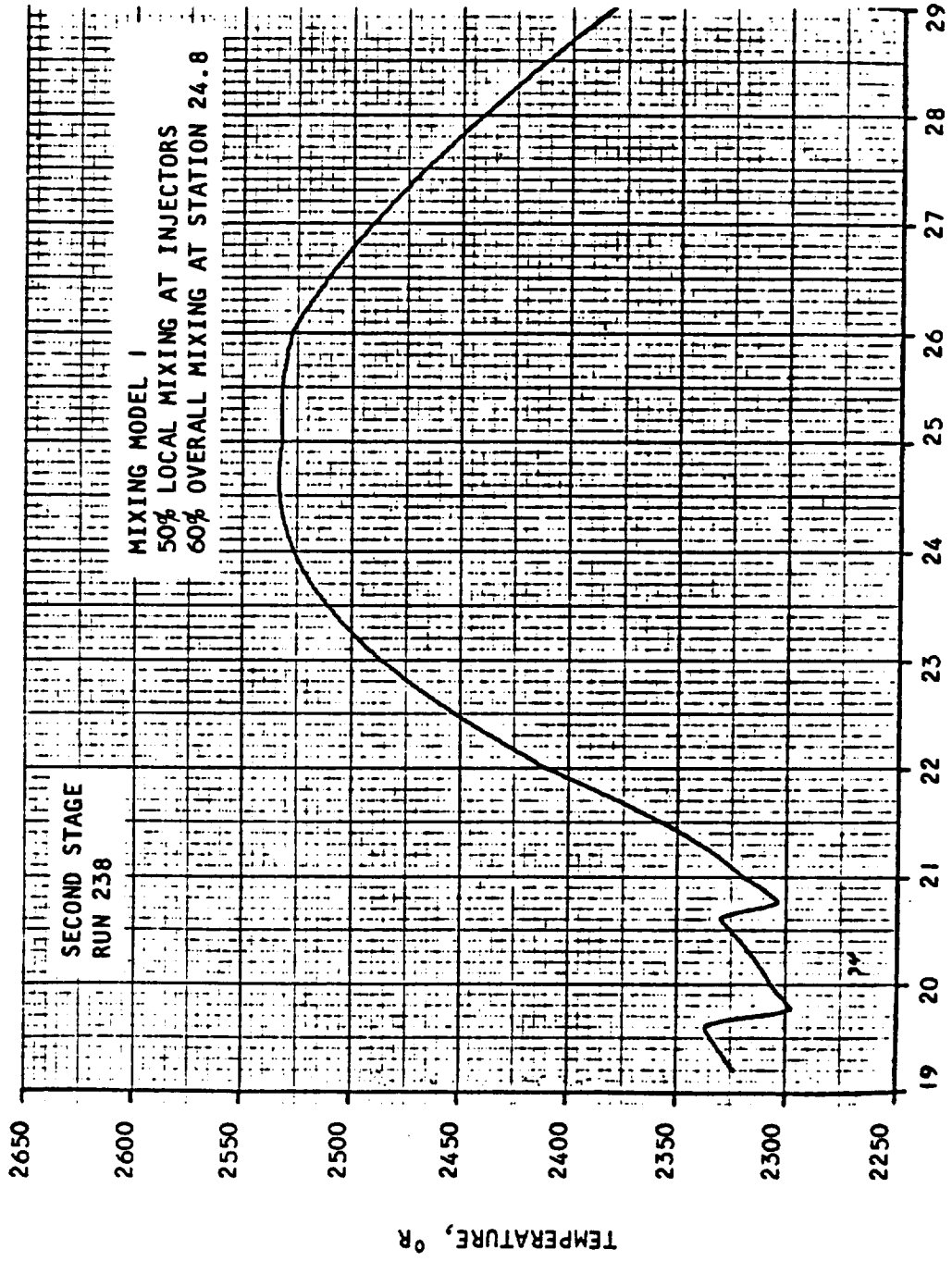

Figure A.4-1. Temperature vs Axial Distance

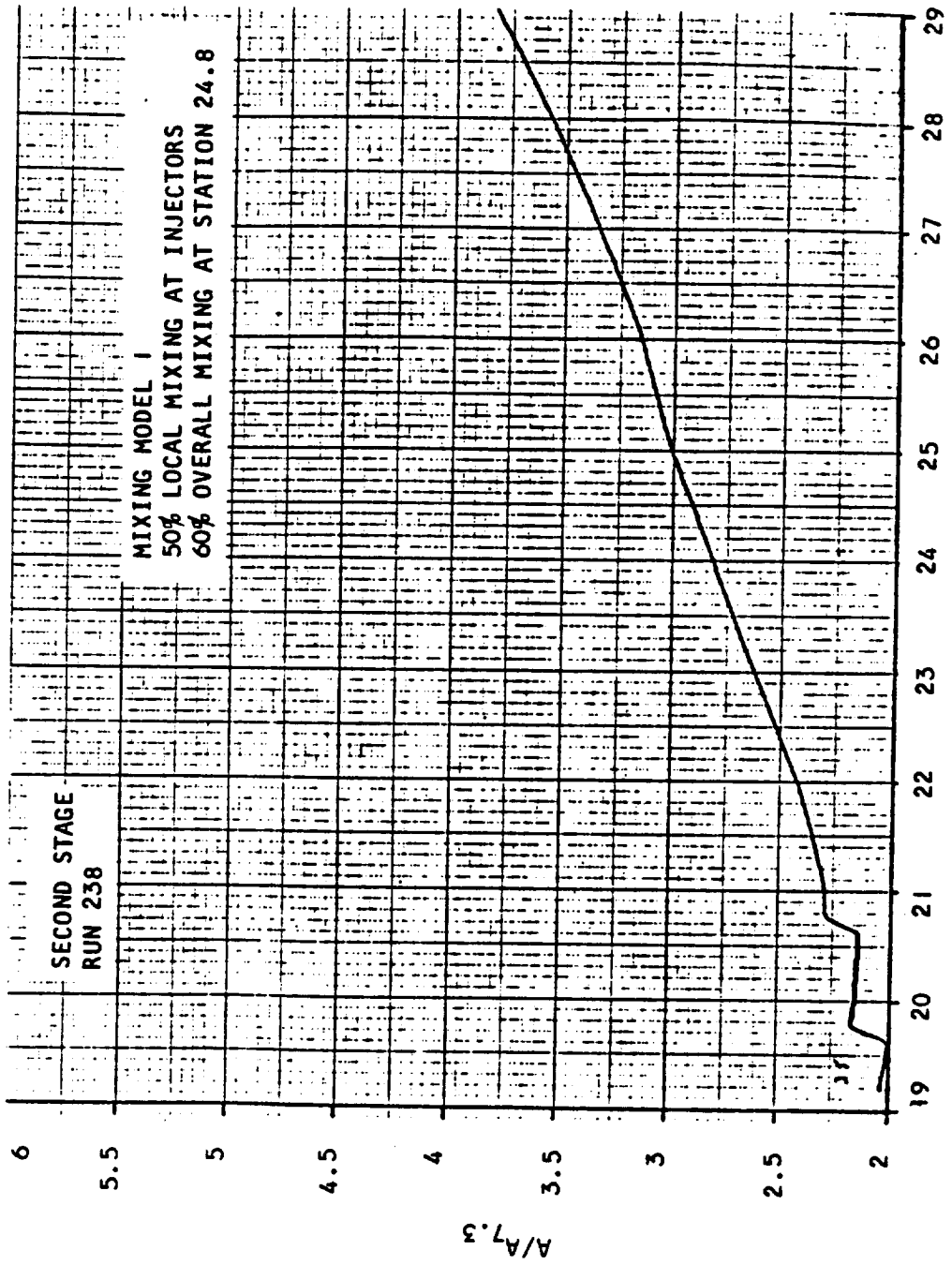

Figure A.4-2. Area Ratio vs Axial Distance

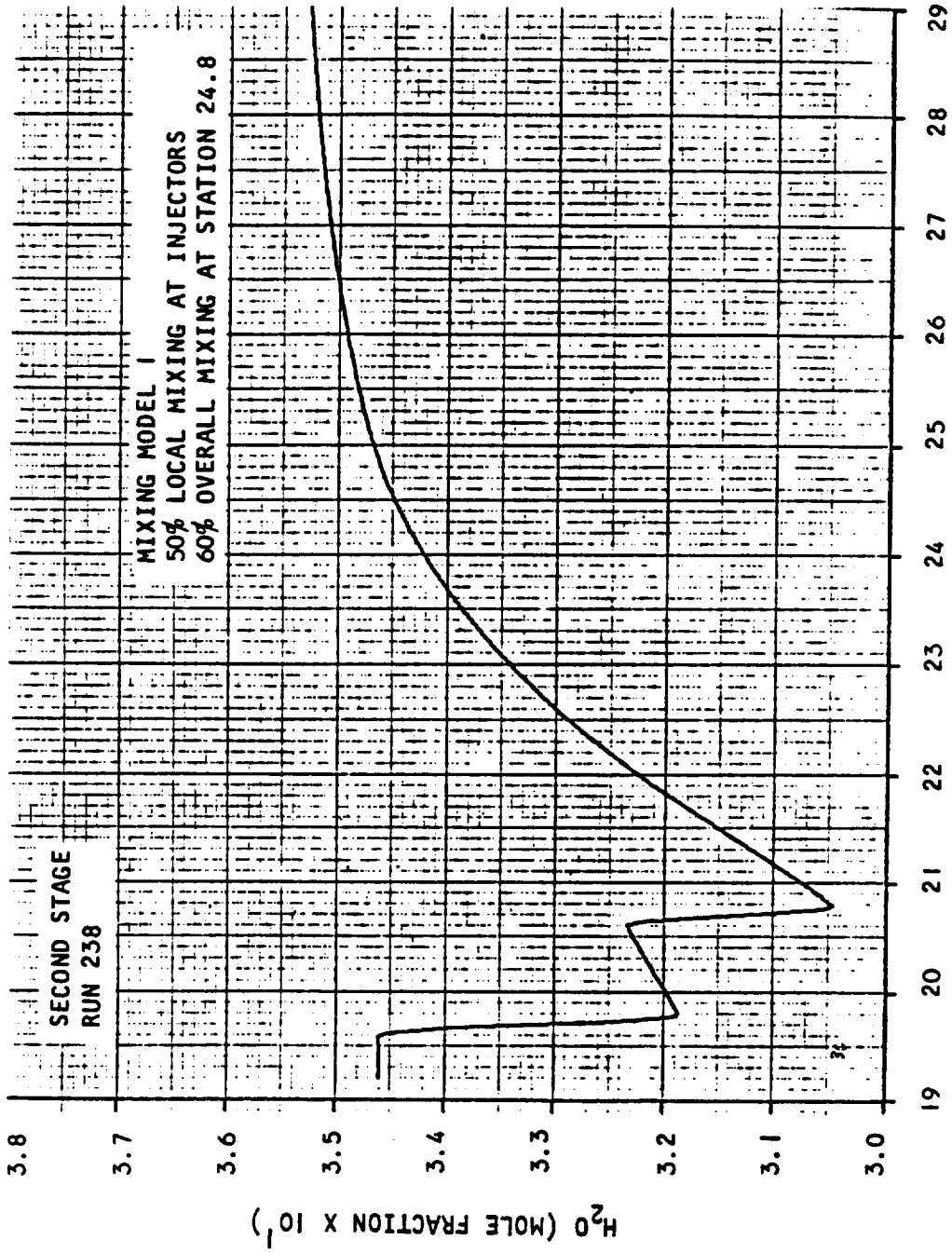

Figure A.4-3. Concentration of H_2O vs Axial Distance

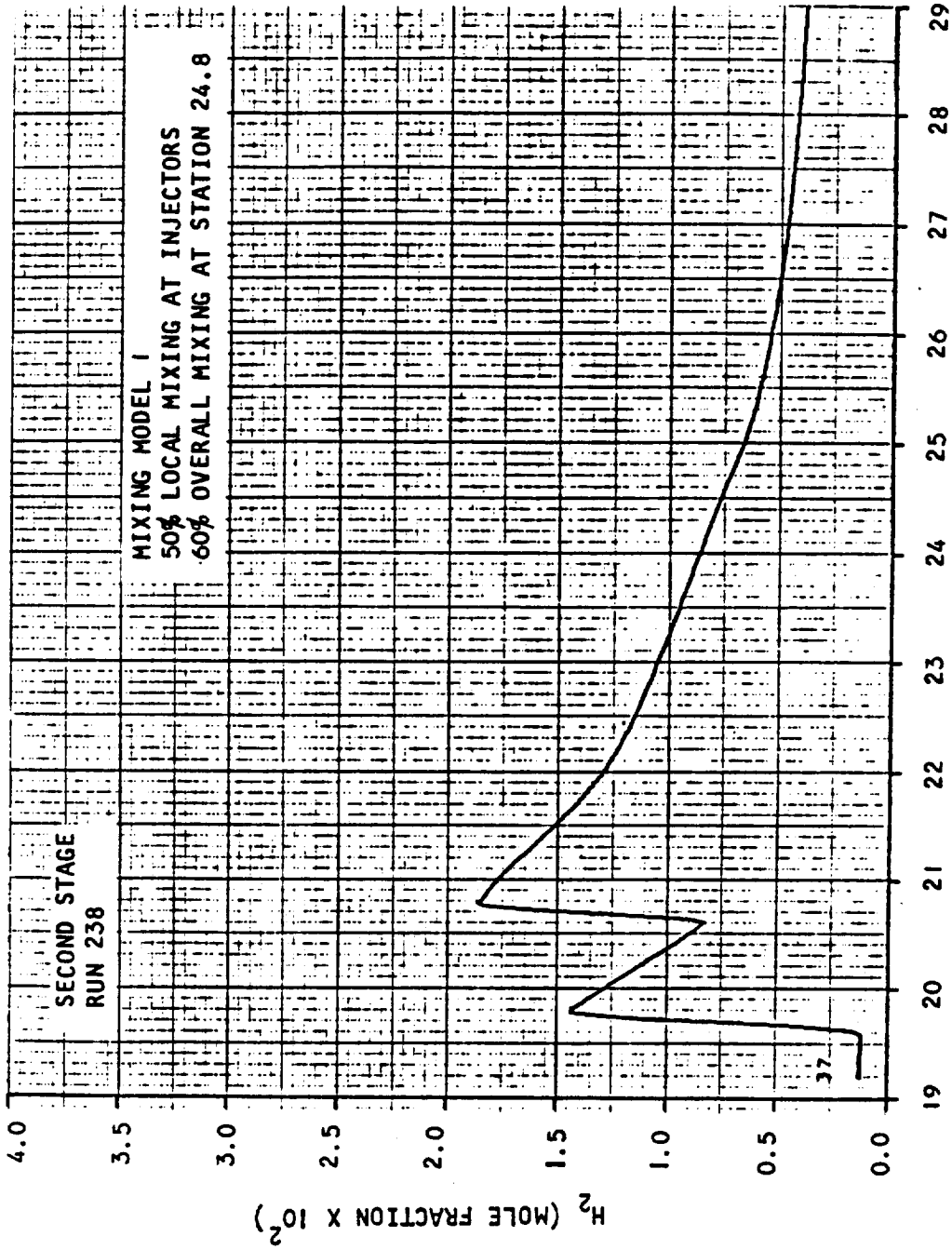

Figure A.4-4. Concentration of H_2 vs Axial Distance

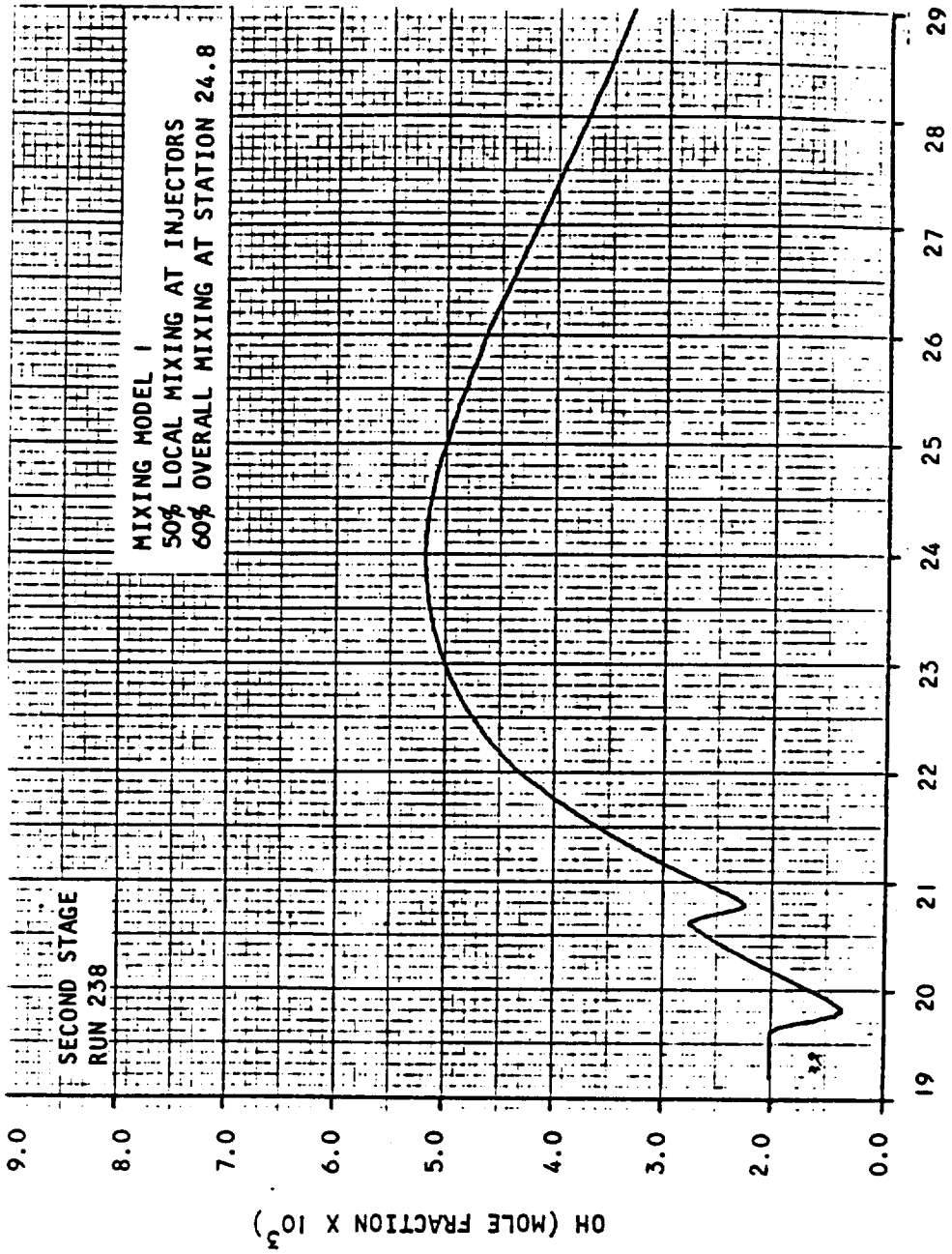

Figure A.4-5. Concentration of OH vs Axial Distance

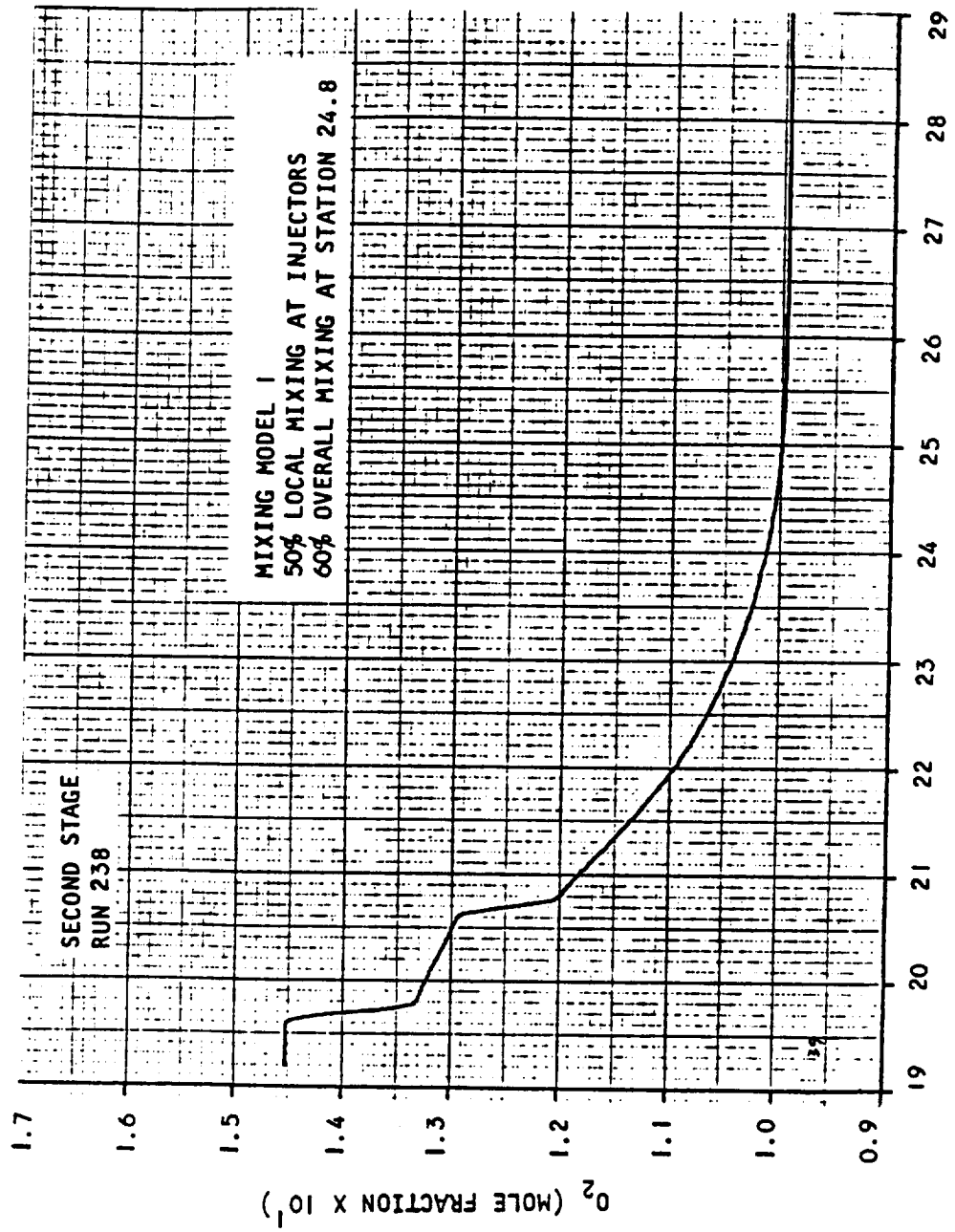

Figure A.4-6. Concentration of O_2 vs Axial Distance

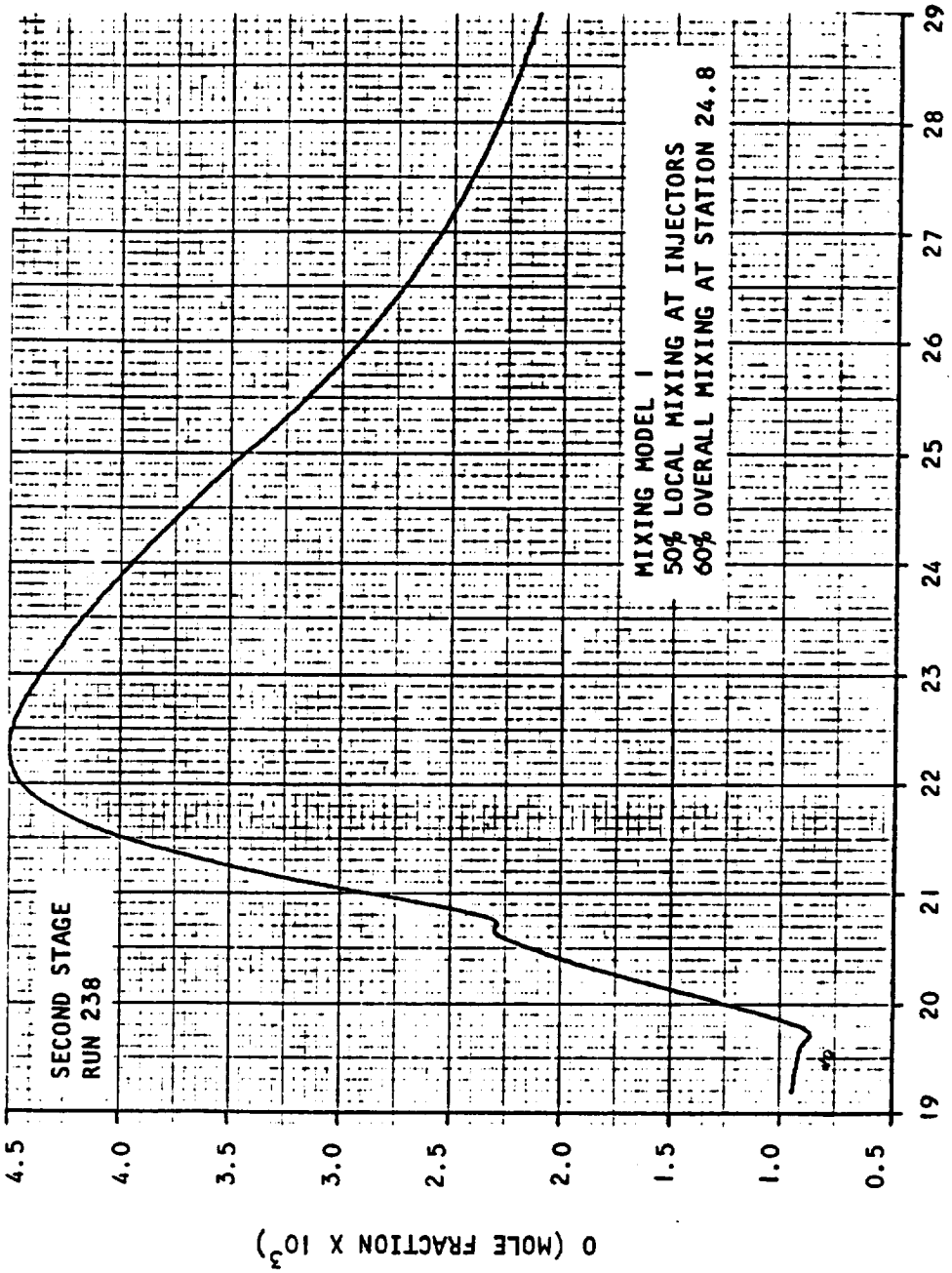

Figure A.4-7. Concentration of O vs Axial Distance

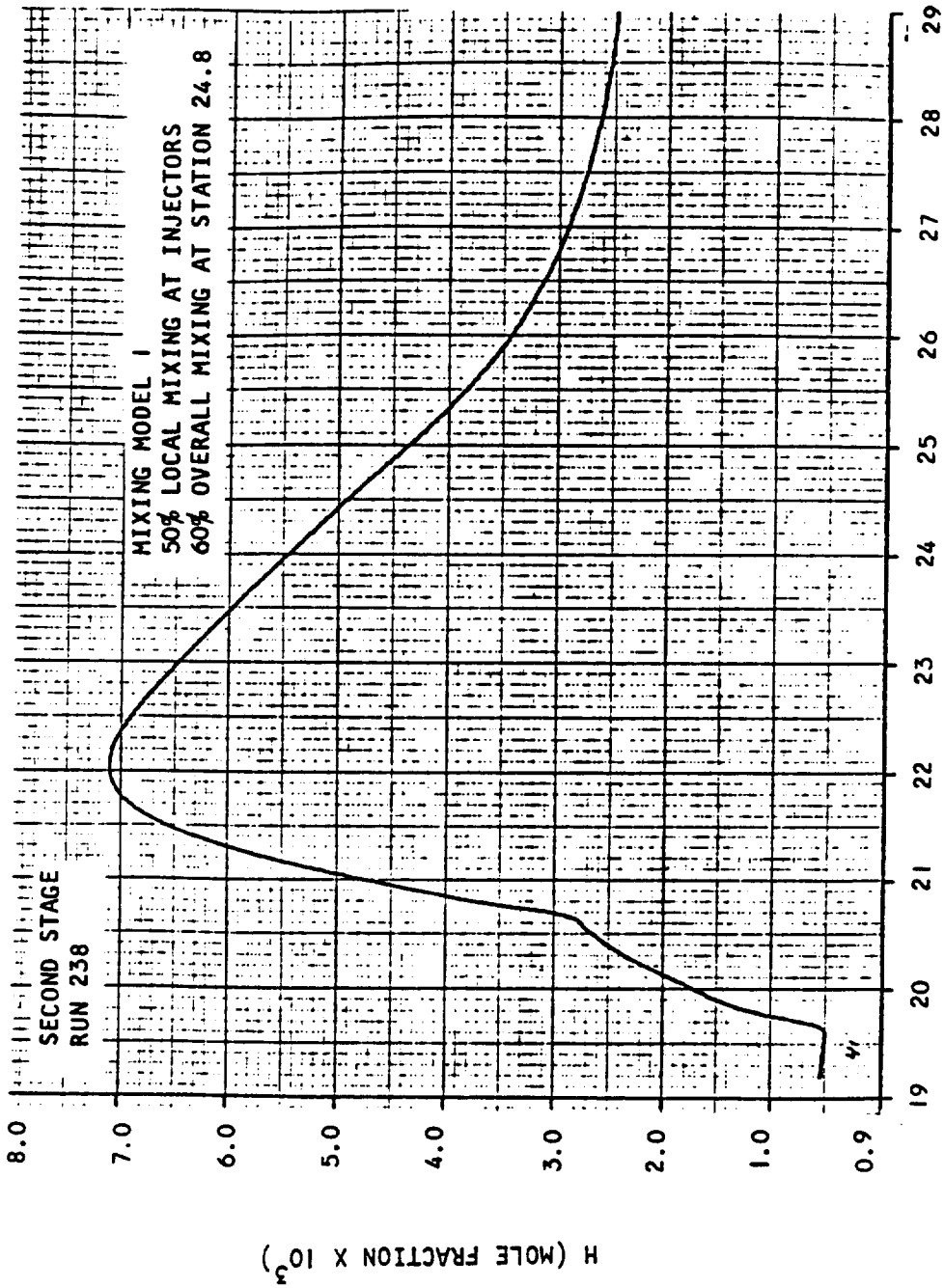

Figure A.4-8. Concentration of H vs Axial Distance

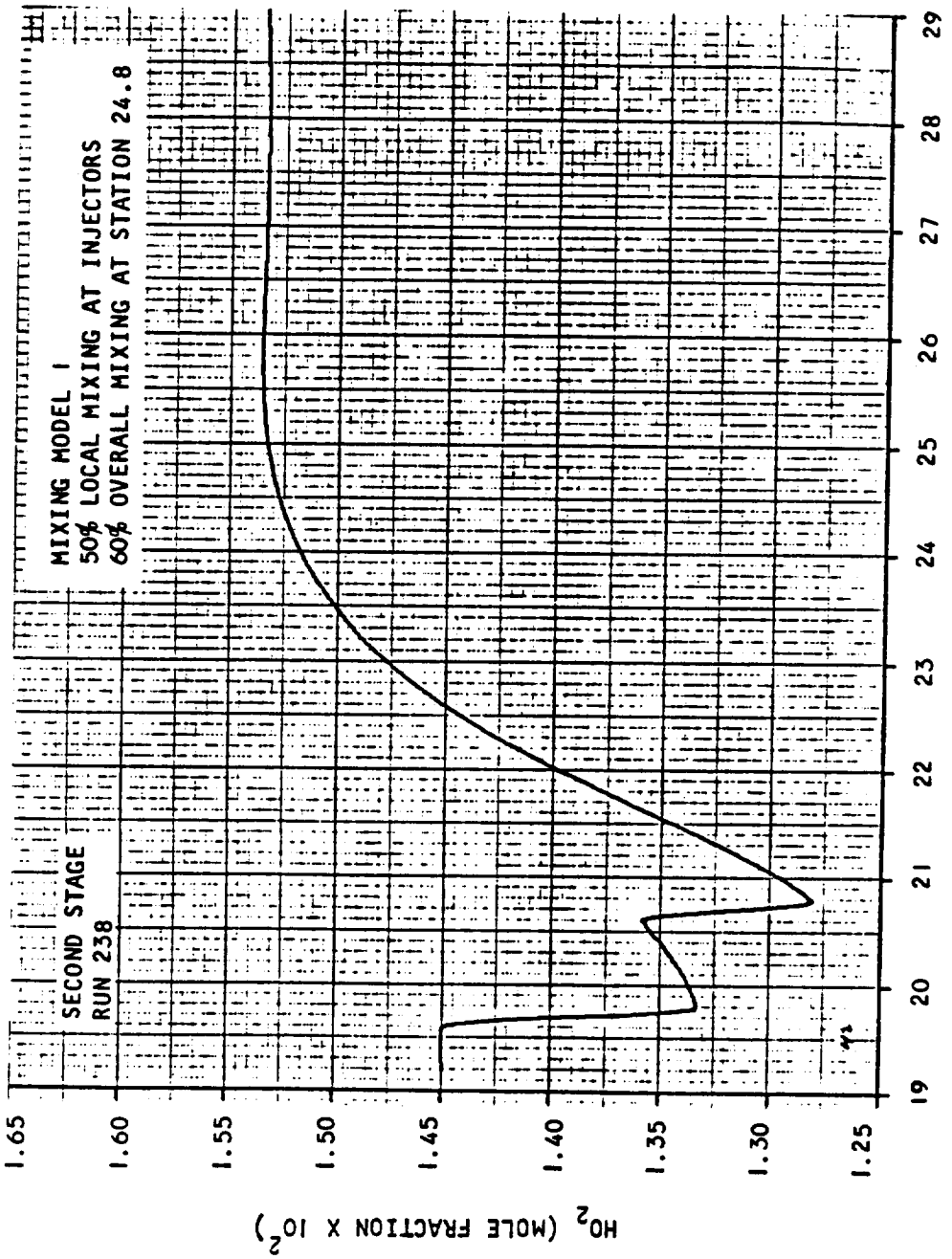

Figure A.4-9. Concentration of HO_2 vs Axial Distance

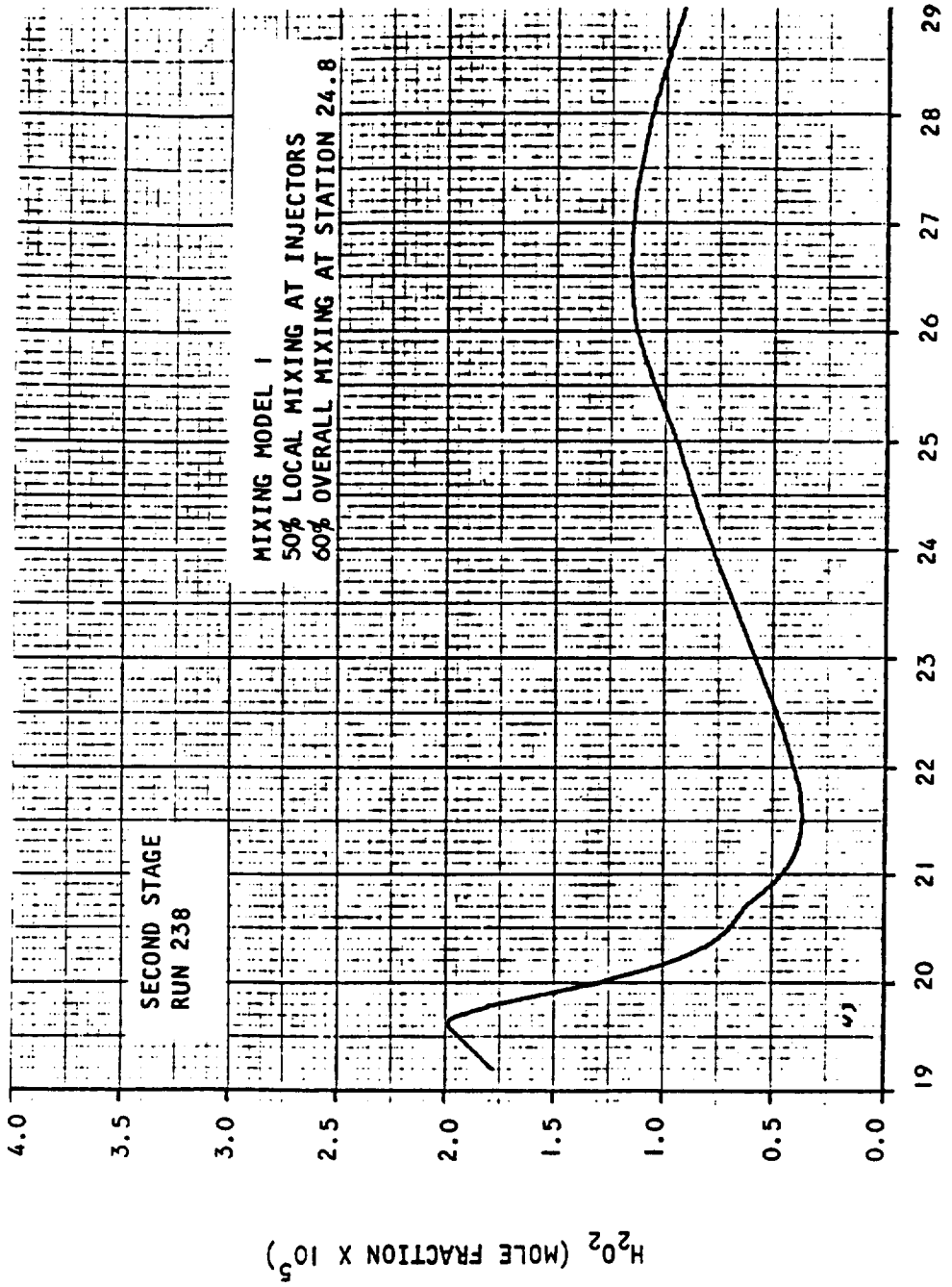

Figure A.4-10. Concentration of H_2O_2 vs Axial Distance

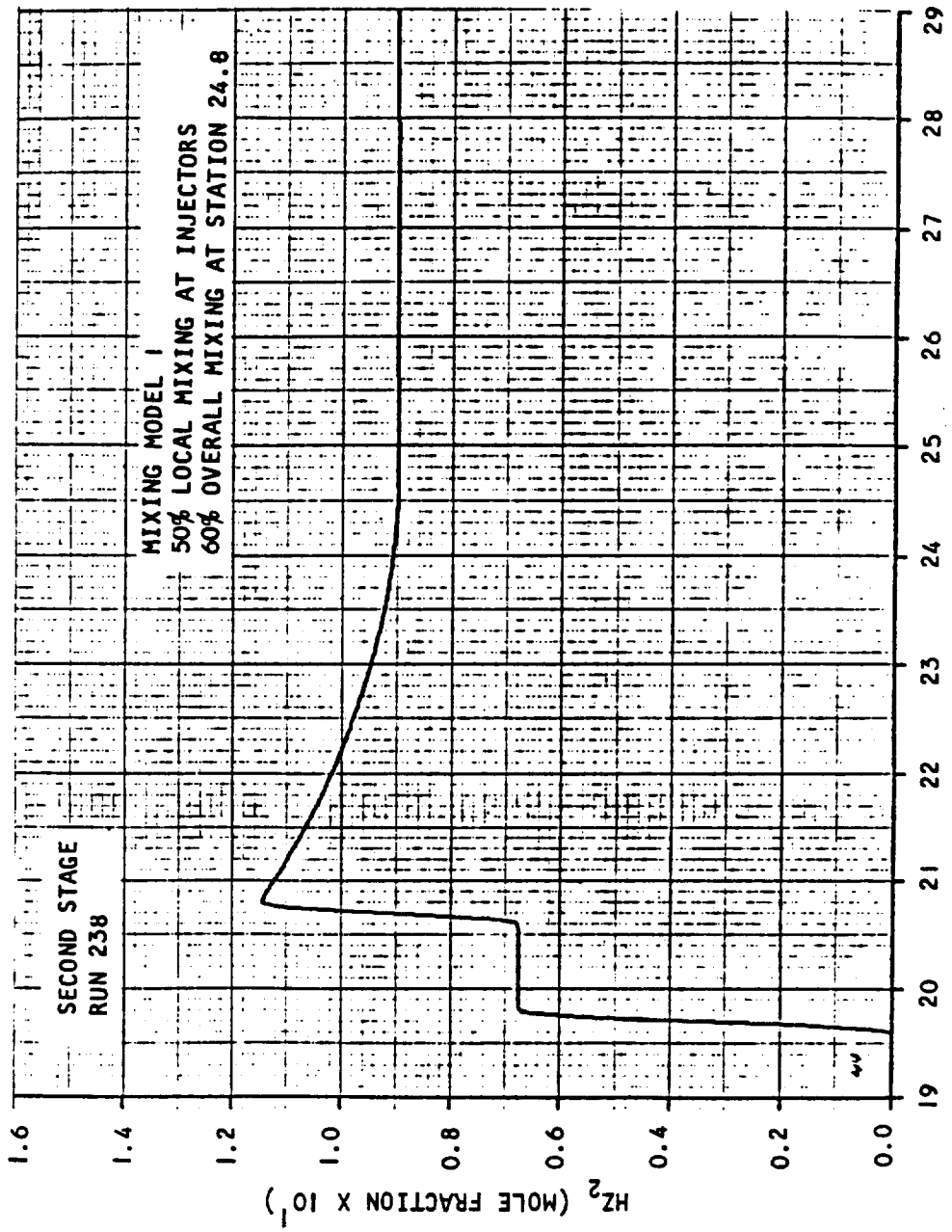

Figure A.4-11. Concentration of HZ_2 vs Axial Distance

5. Second Stage Combustor - Run 238
Mixing Model 1, 50 percent local mixing each injector, 60 percent mixing at Station 29.

Station	A(in.^{2})	$\dot{m}$(lb m/sec)	$\dot{m}_{H_2}$ (mixed)	η_m	η_c	$\dot{m}_{H_2} + \dot{m}_{Hz_2}$	ϕ
20.8587	5.607	1.8176	0.017601	0.48	0.8304	0.036640	0.6317
21.5612	5.764		0.018322	0.50	0.8894		
22.1062	5.947		0.018838	0.51	0.9122		
22.5062	6.120		0.019190	0.52	0.9211		
23.1062	6.374		0.019681	0.54	0.9290		
23.5062	6.541		0.019981	0.55	0.9325		
24.1062	6.794		0.020392	0.56	0.9365		
24.5062	6.965		0.020640	0.56	0.9386		
25.0437	7.198		0.020939	0.57	0.9410		
25.6437	7.408		0.021229	0.58	0.9435		
26.0212	7.545		0.021386	0.583	0.9451		
26.5887	7.822		0.021588	0.589	0.9475		
26.9887	8.028		0.021705	0.592	0.9491		
27.5887	8.358		0.021840	0.596	0.9516		
28.1887	8.717	↓	0.021928	0.598	0.9541	↓	↓
28.5887	8.973		0.020960	0.599	0.9561		
29.0000	9.256	1.8176	0.021972	0.60	0.9583	0.036640	0.6317

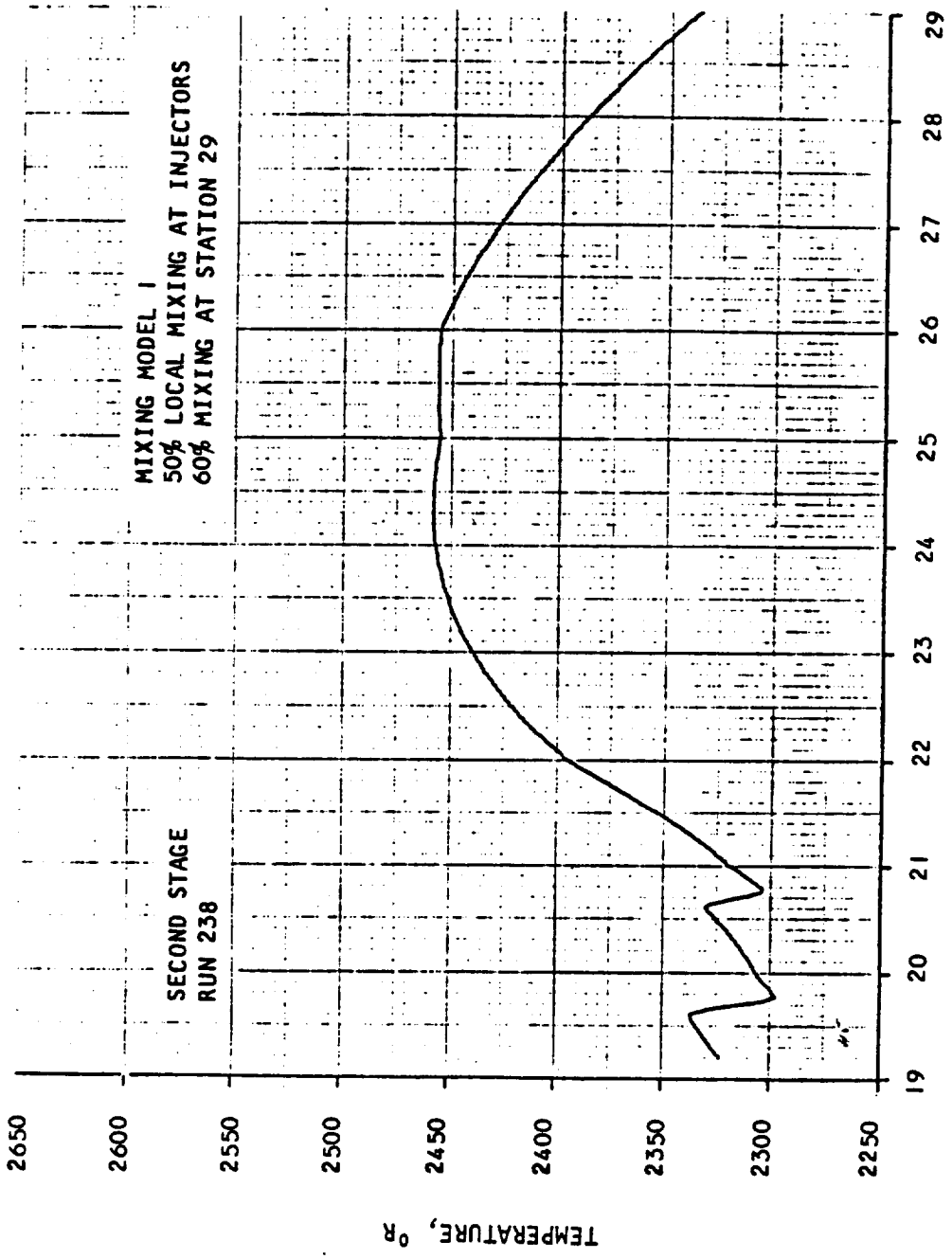

Figure A.5-1. Temperature vs Axial Distance

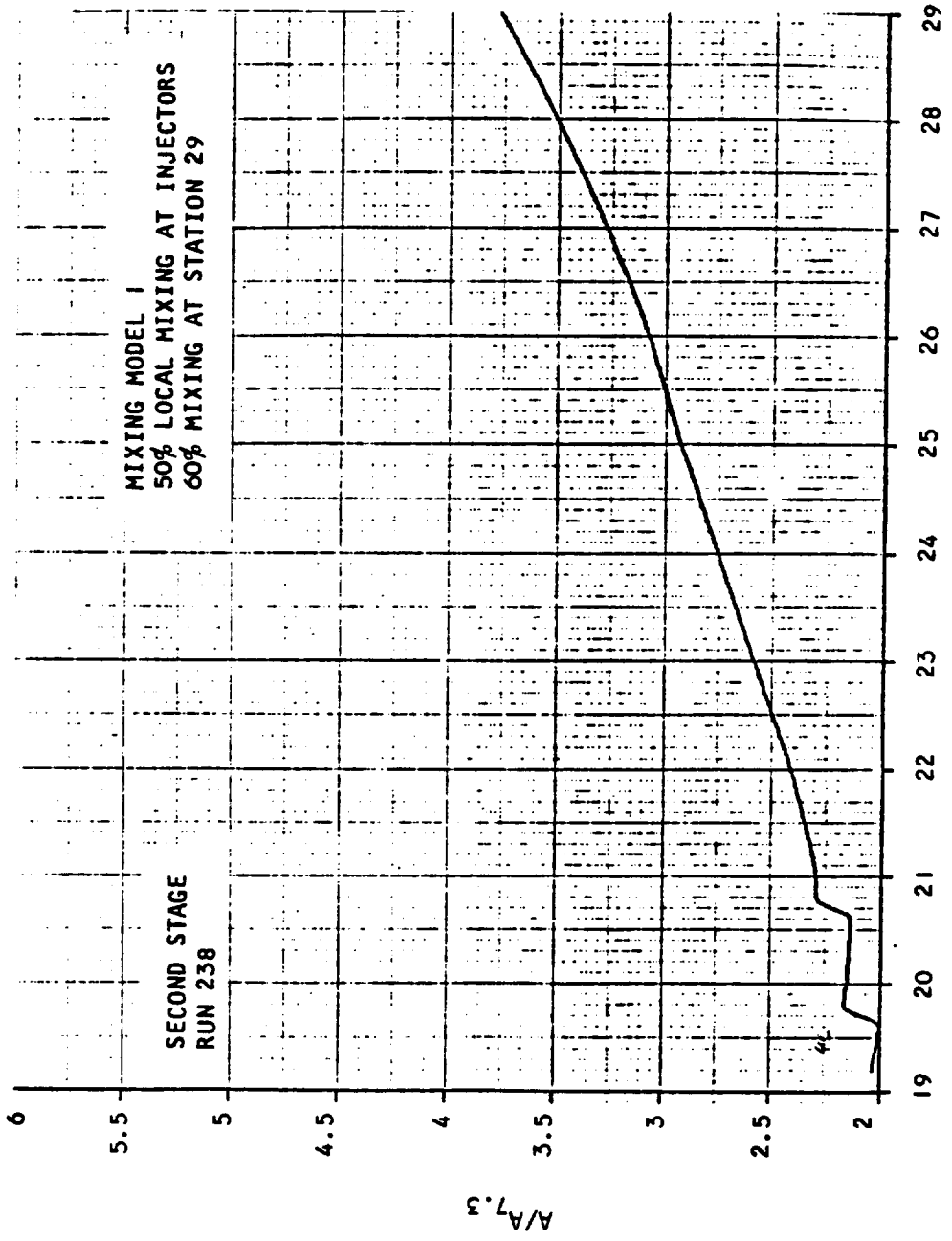

Figure A.5-2. Area Ratio vs Axial Distance

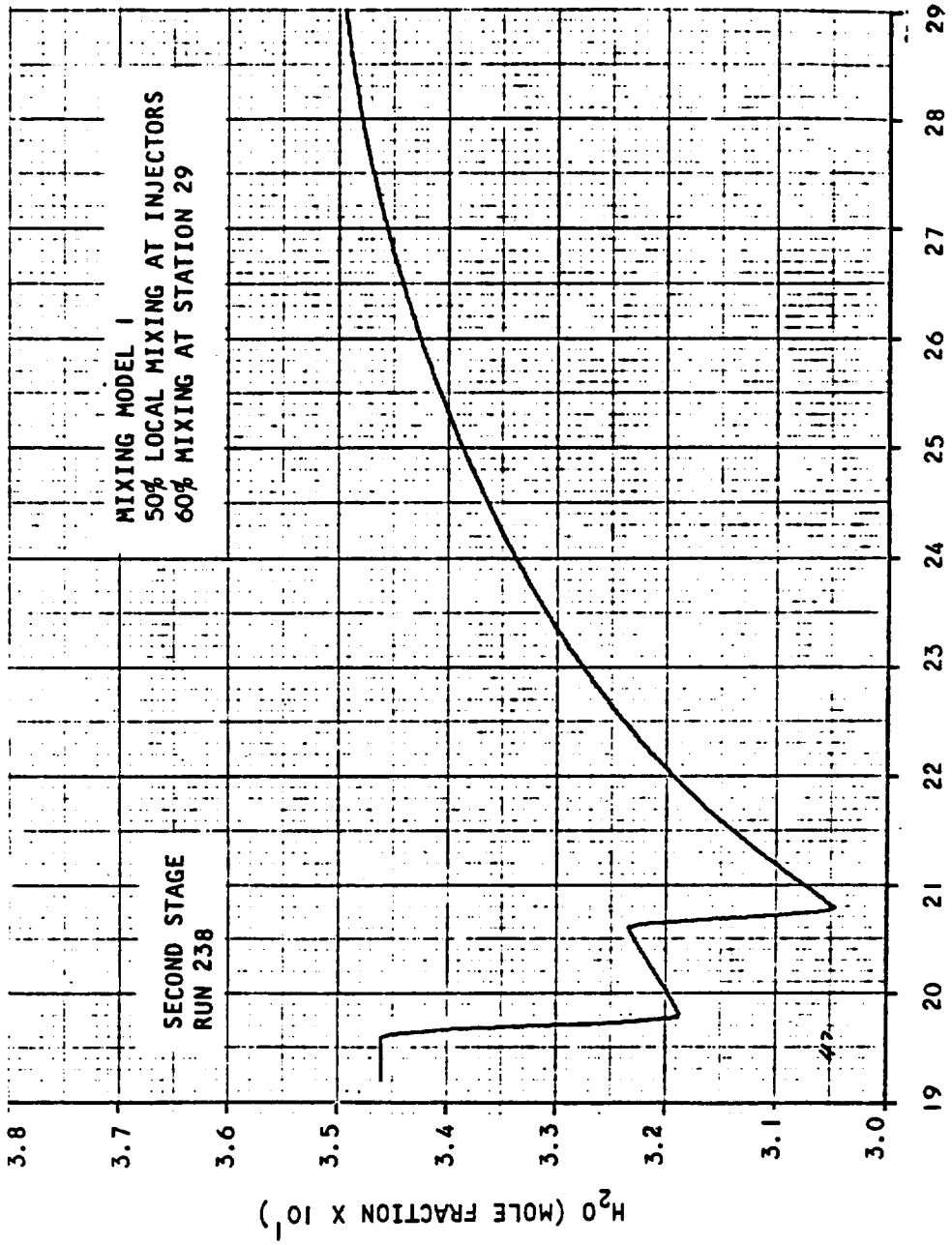

Figure A.5-3. Concentration of H_2O vs Axial Distance

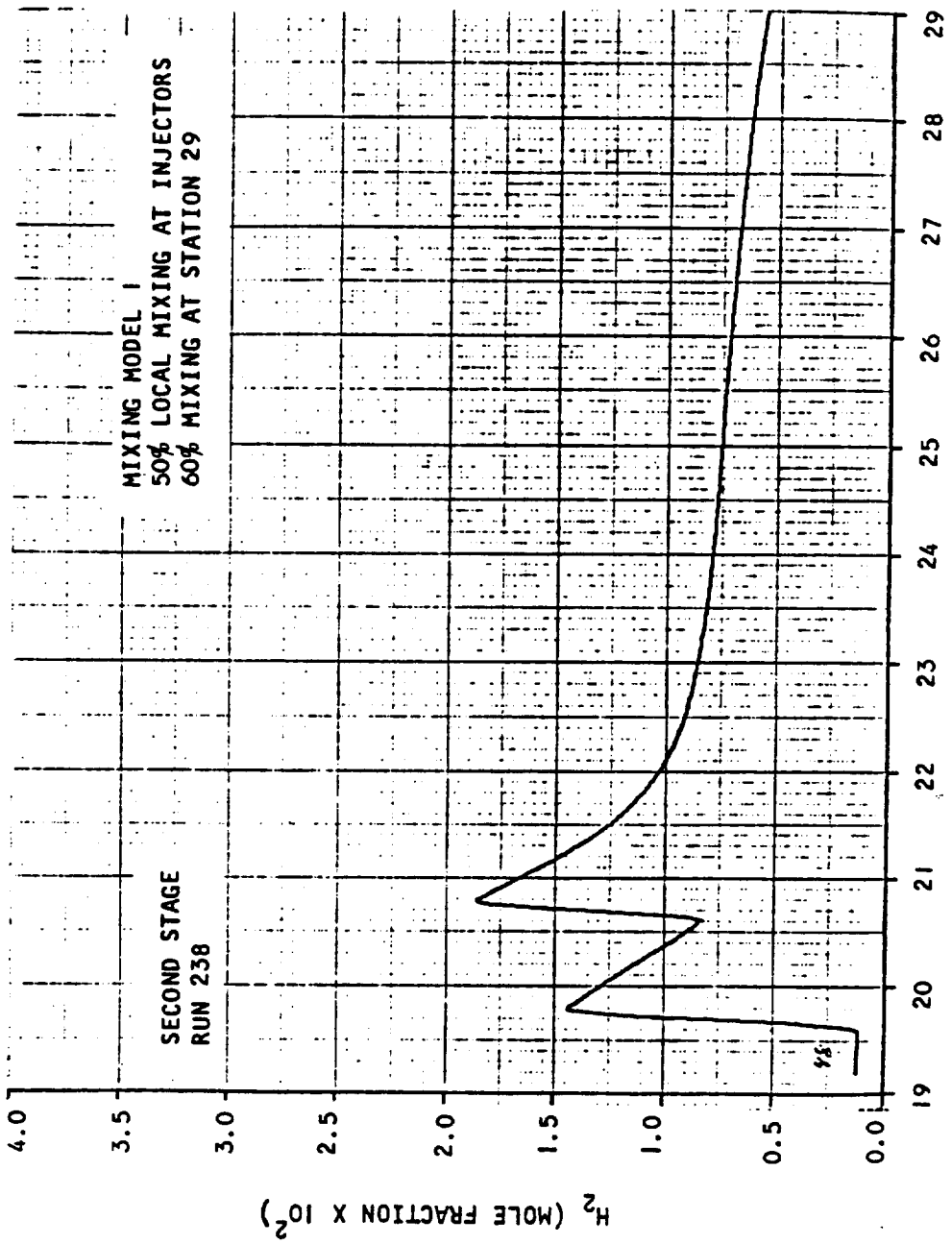

Figure A.5-4. Concentration of H_2 vs Axial Distance

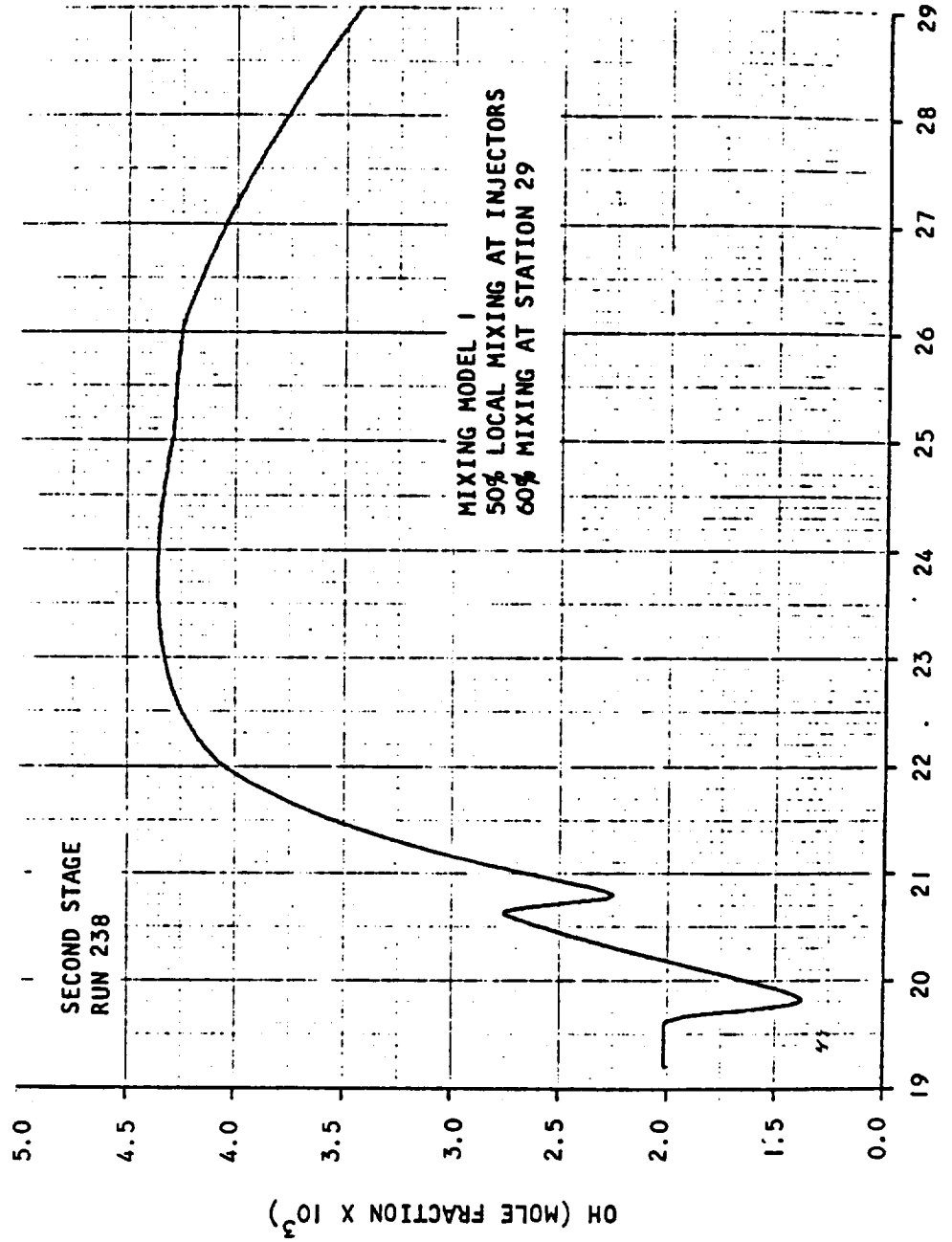

Figure A.5-5. Concentration of OH vs Axial Distance

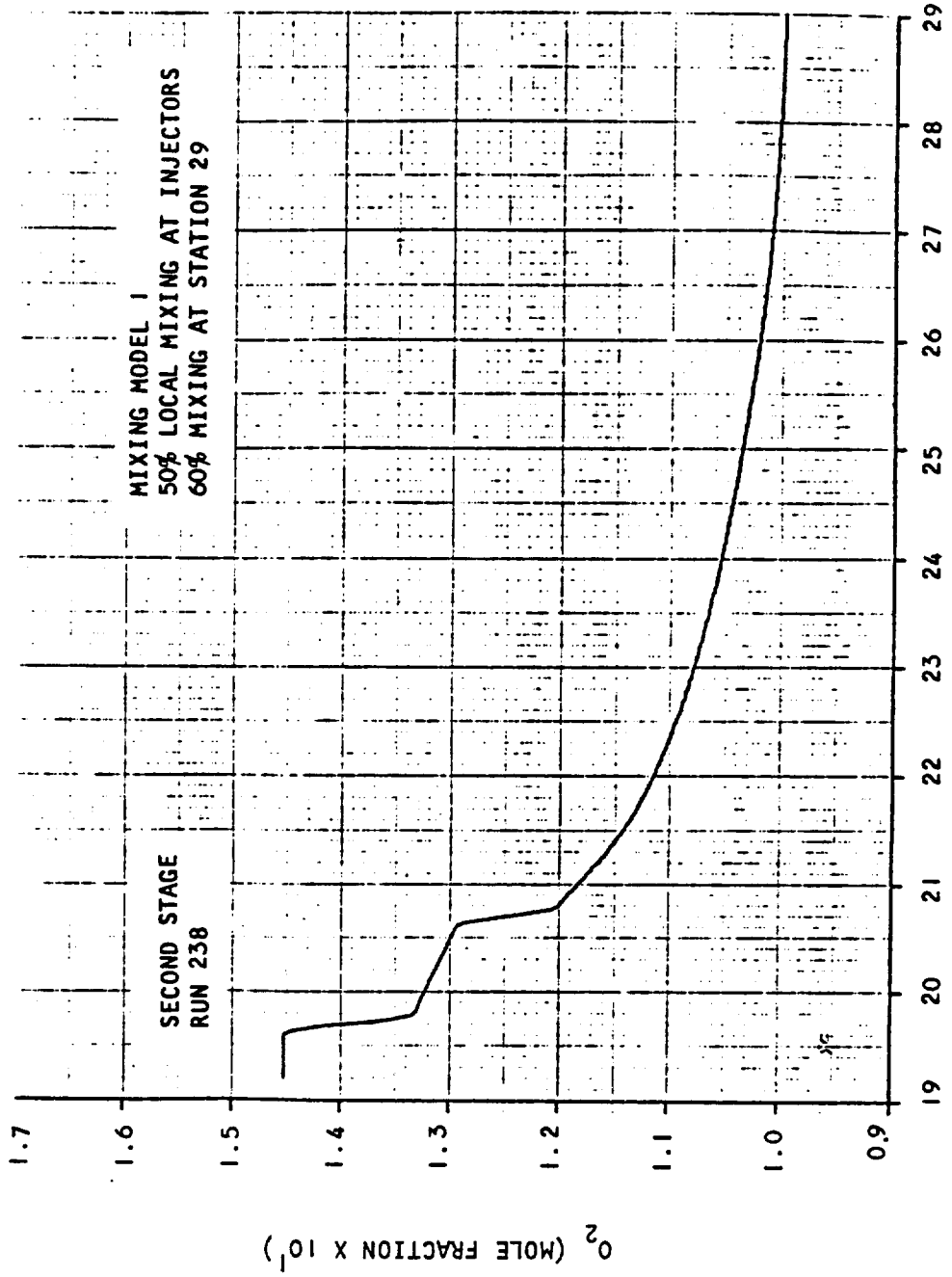

Figure A.5-6. Concentration of O_2 vs Axial Distance

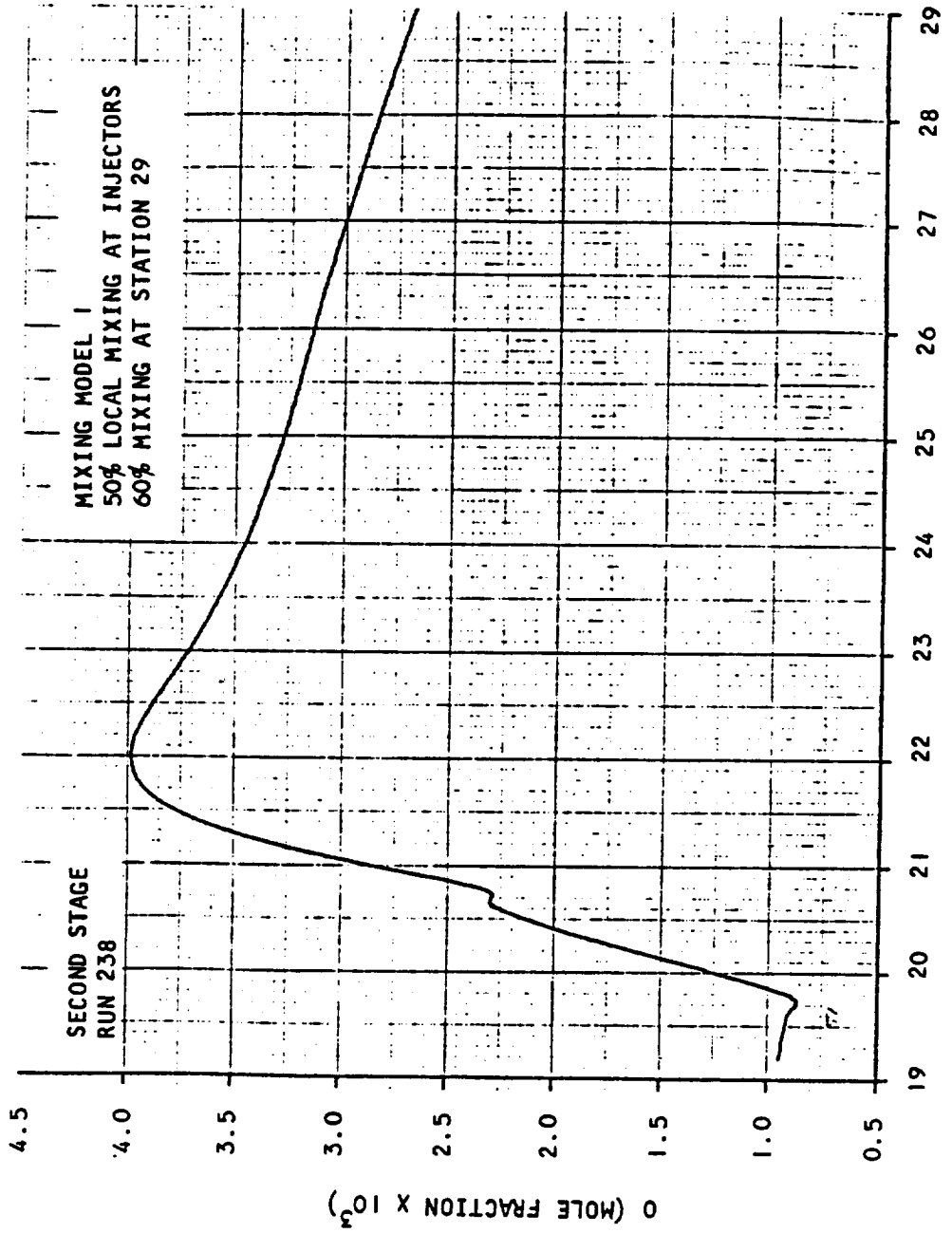

Figure A.5-7. Concentration of O vs Axial Distance

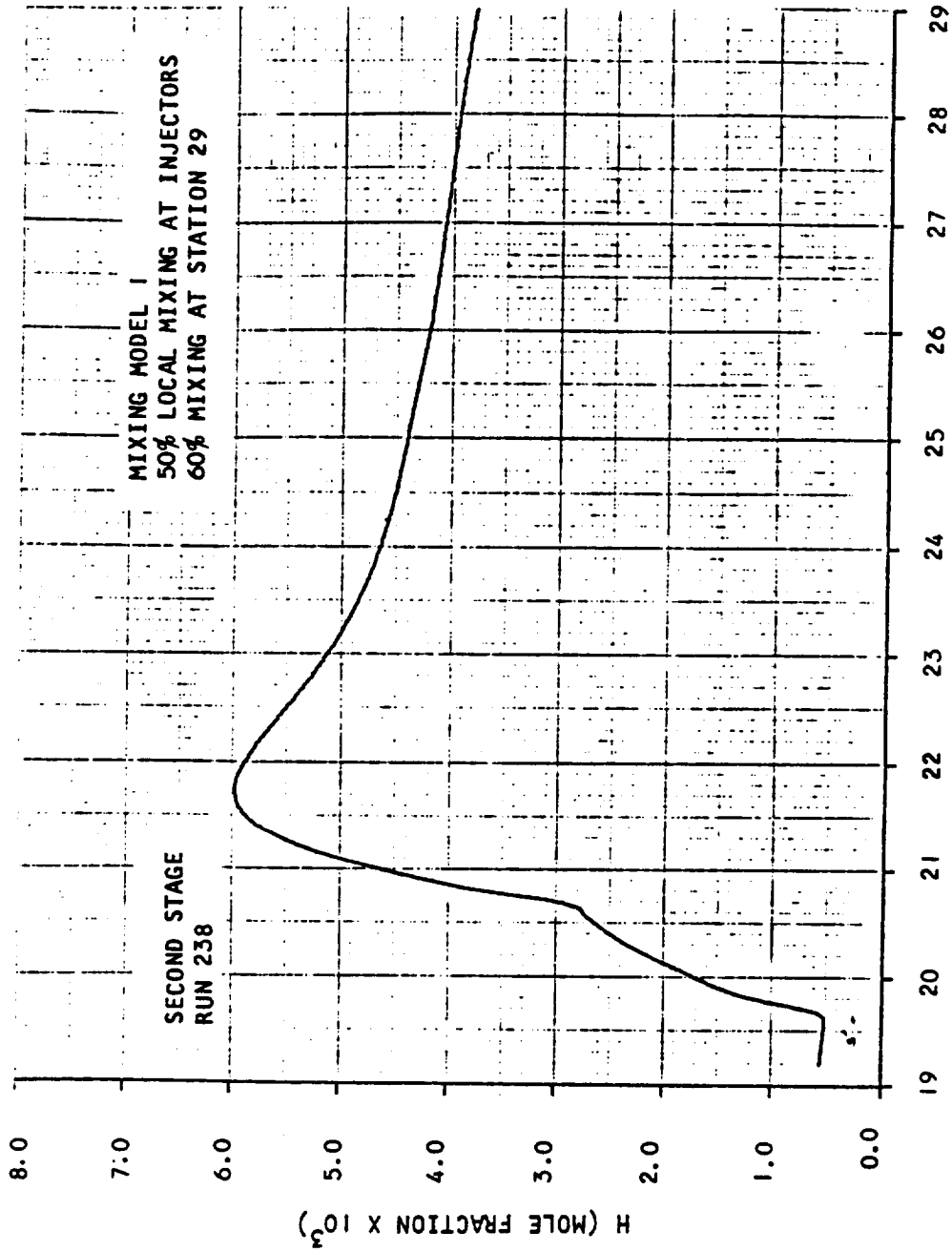

Figure A.5-8. Concentration of H vs Axial Distance

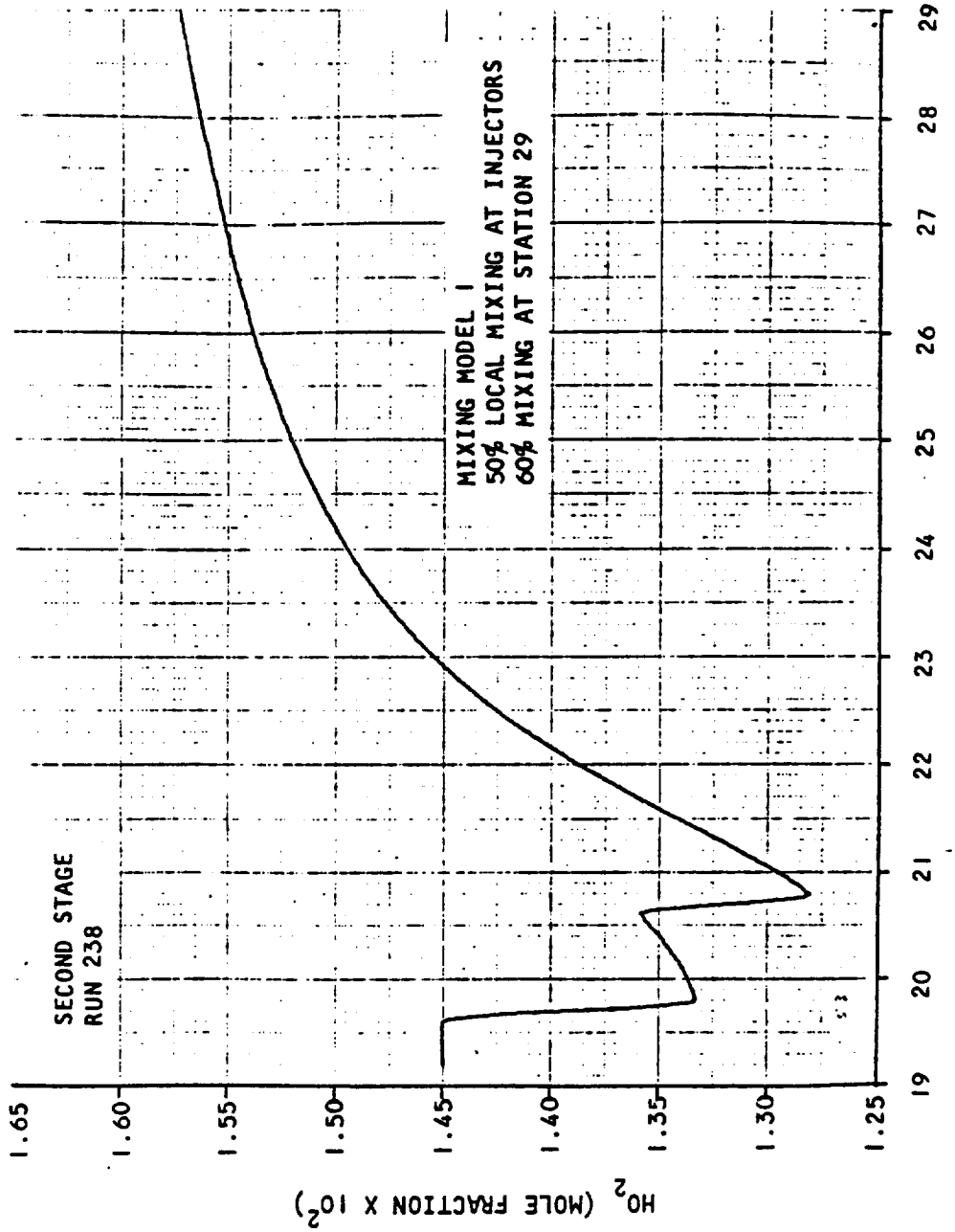

Figure A.5-9. Concentration of HO_2 vs Axial Distance

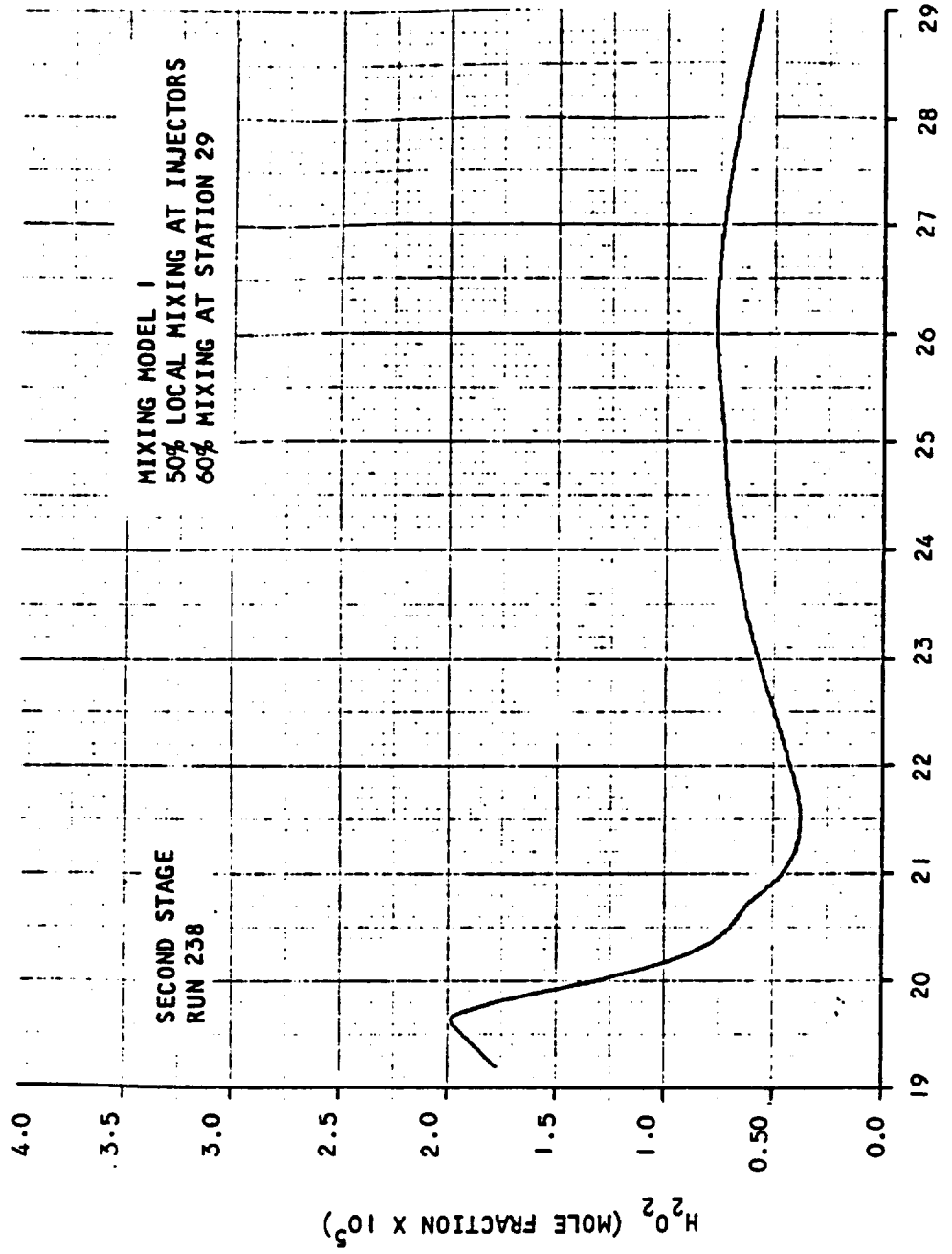

Fogure A.5-10. Concentration of H_2O_2 vs Axial Distance

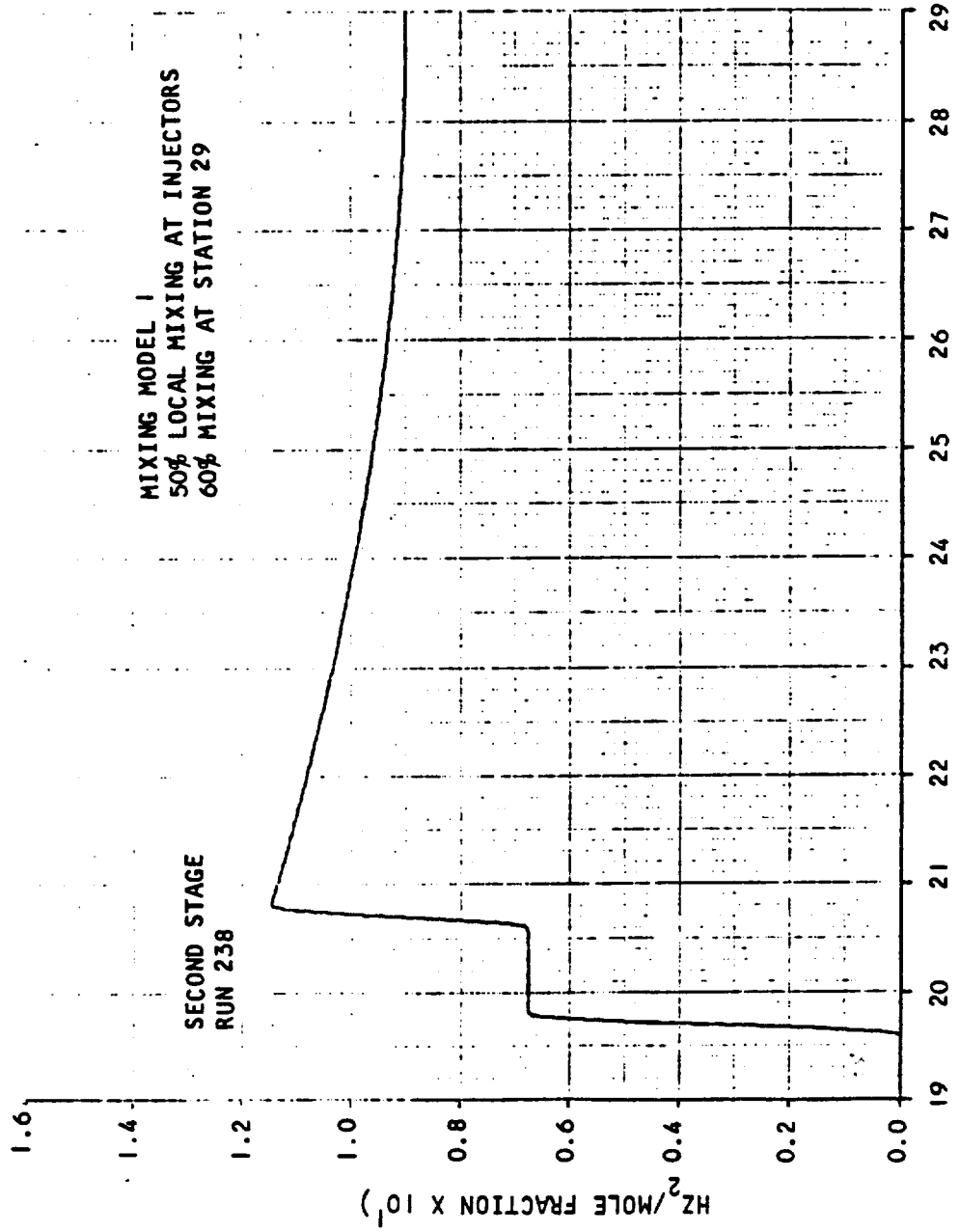

Figure A.5-11. Concentration of HZ_2 vs Axial Distance

APPENDIX B

RESULTS FROM CHEMICAL KINETIC SIMULATION
OF RUN 242, TIME = 682.55 SECONDS.
STOICHIOMETRIC FUEL-AIR RATIO = 0.034746

1. First Stage Combustor - Run 242
   Mixing Model 2, 50 percent mixing at each injector, 100 percent mixing at Station 12.

Station Station	A(in.^{2})	$\dot{m}$(lb m/sec)	$\dot{m}_{H_2}$ (mixed)	η_m	η_c	$\dot{m}_{H_2} + \dot{m}_{Hz_2}$	ϕ
7.3	3.126	1.536	0	0	0	0	0
7.5125	3.203	1.545	0.004415	0.50	0	0.00883	0.1654
8.0925	2.974	1.545	0.004415	0.50	0	0.00883	0.1654
8.5925	2.934	1.5524	0.008211	0.50	0.0026	0.01640	0.3073
9.1925	2.765		0.008841	0.54	0.0353		
9.5925	2.684		0.009797	0.59	0.1874		
10.1000	2.796		0.011626	0.71	0.6259		
10.5000	3.083		0.013387	0.82	0.8092		
11.0450	3.318		0.015178	0.93	0.8831		
11.4450	3.190		0.015986	0.97	0.9155		
11.9525	3.255		0.016396	1.0	0.9436		
12.5525	3.569		0.016400	1.0	0.9586		
13.0900	3.885				0.9770		
13.4900	4.006				0.9673		
14.0375	4.181				0.9704		
14.6275	4.259				0.9729		
15.1975	4.342				0.9749		
15.5975	4.408				0.9761		
16.1975	4.512				0.9776		
16.5975	4.584				0.9784		
17.1425	4.787				0.9794		
17.5425	5.071				0.9798		
18.0800	5.150				0.9801		
18.6800	4.990	↓	↓	↓	0.9809	↓	↓
19.0800	4.893				0.9815		
19.6000	4.776	1.5524	0.016400	1.0	0.9824	0.01640	0.3073
9.7925	2.679						
11.6450	3.139						
17.7425	5.234						

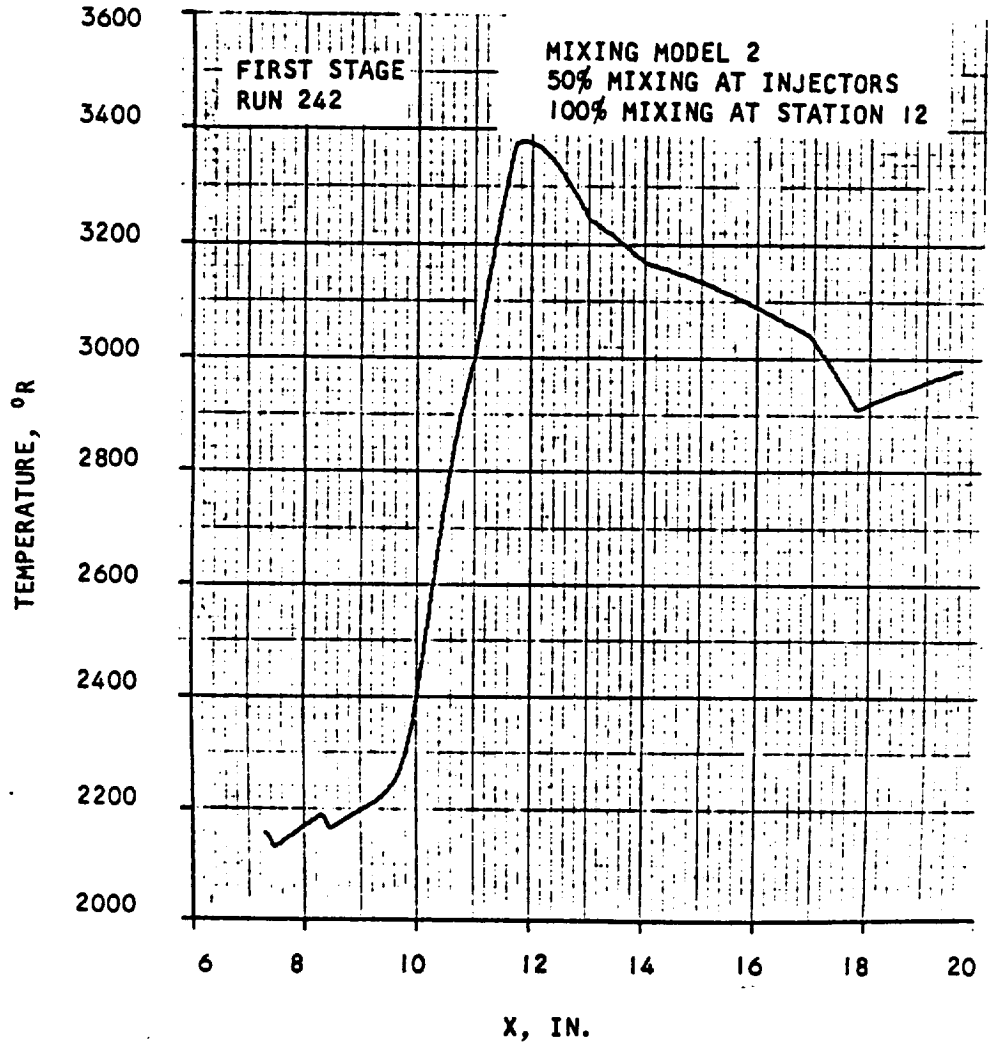

Figure B.1-1. Temperature vs Axial Distance

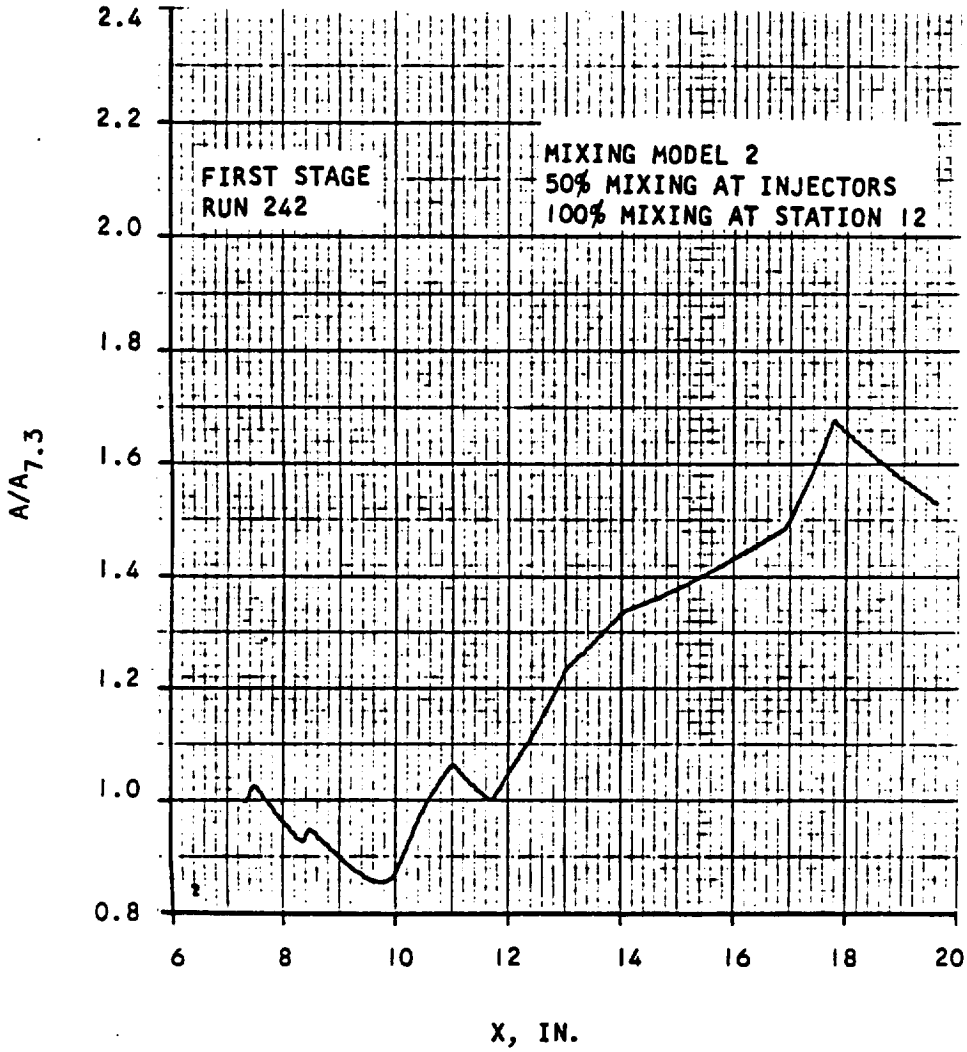

Figure B.1-2. Area Ratio vs Axial Distance

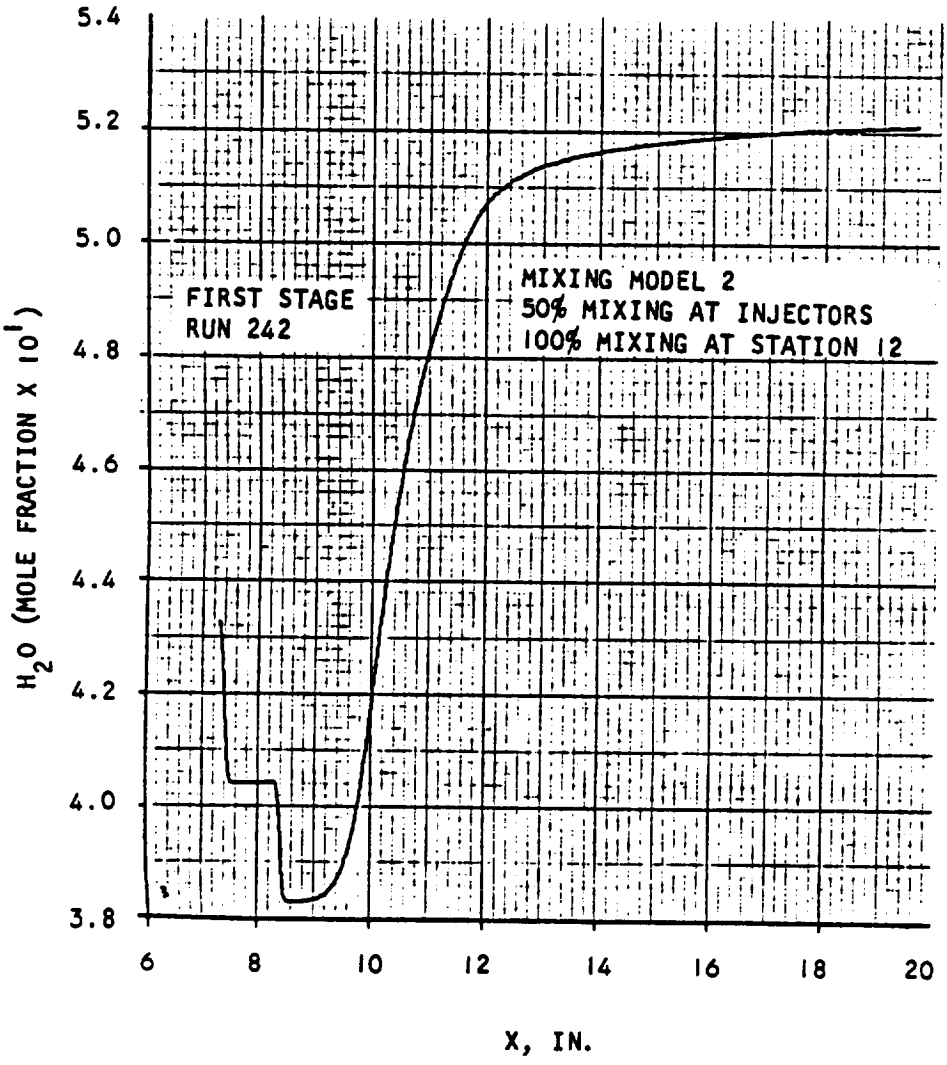

Figure B.1-3. Concentration of H_2O vs Axial Distance

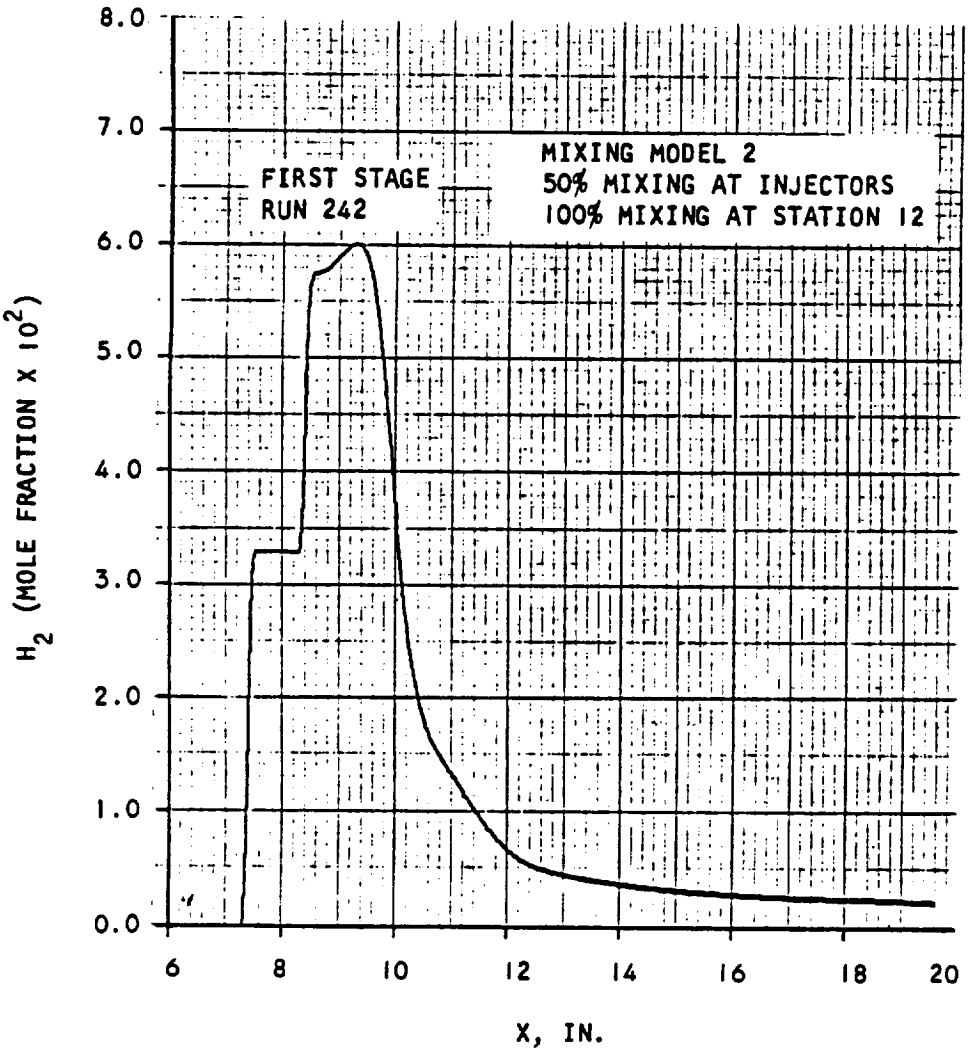

Figure B.1-4. Concentration of H_2 vs Axial Distance

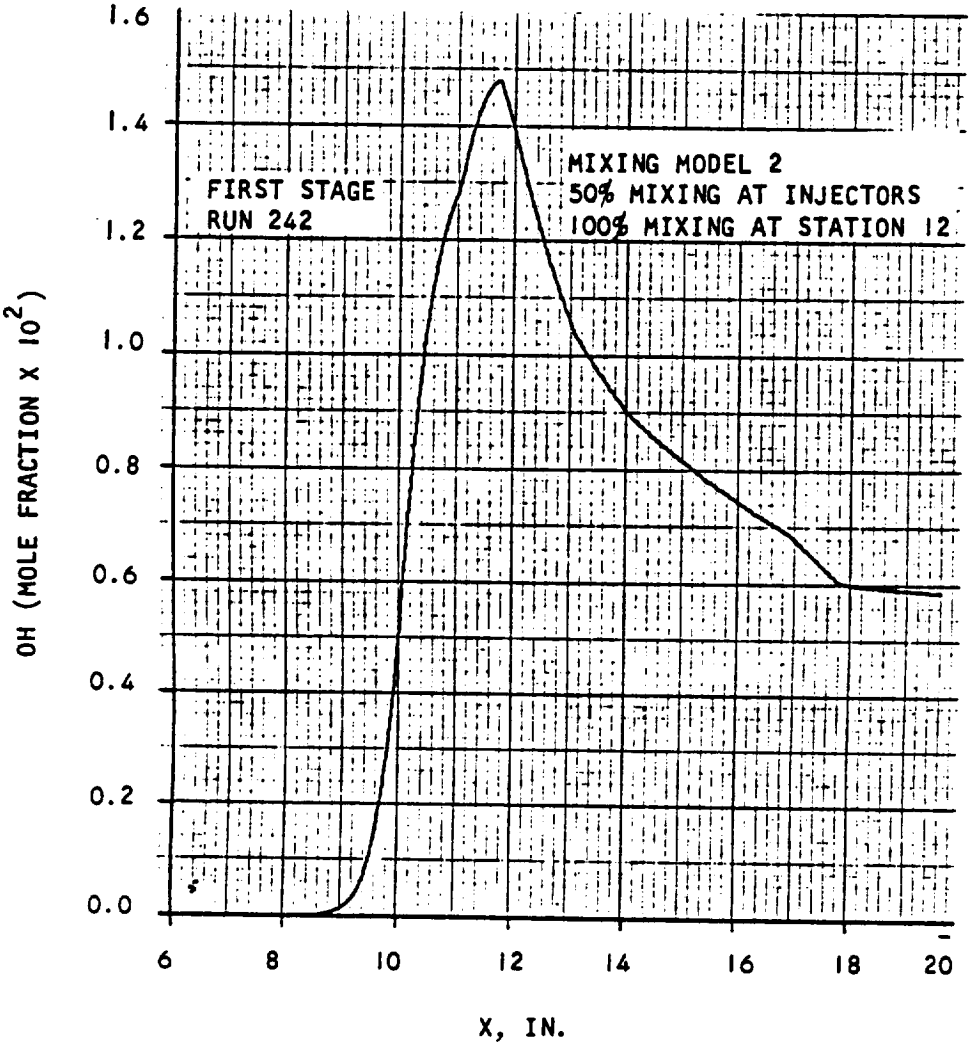

Figure B.1-5. Concentration of OH vs Axial Distance

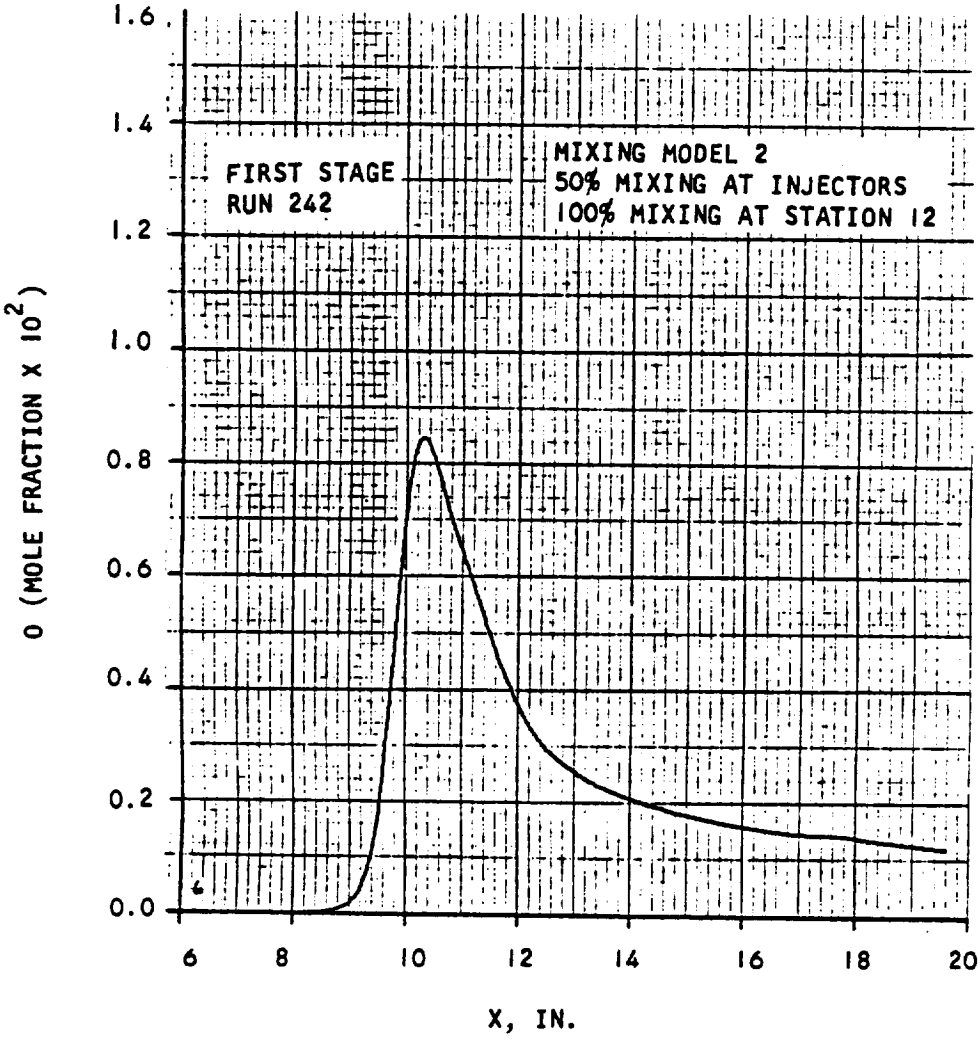

Figure B.1-6. Concentration of O vs Axial Distance

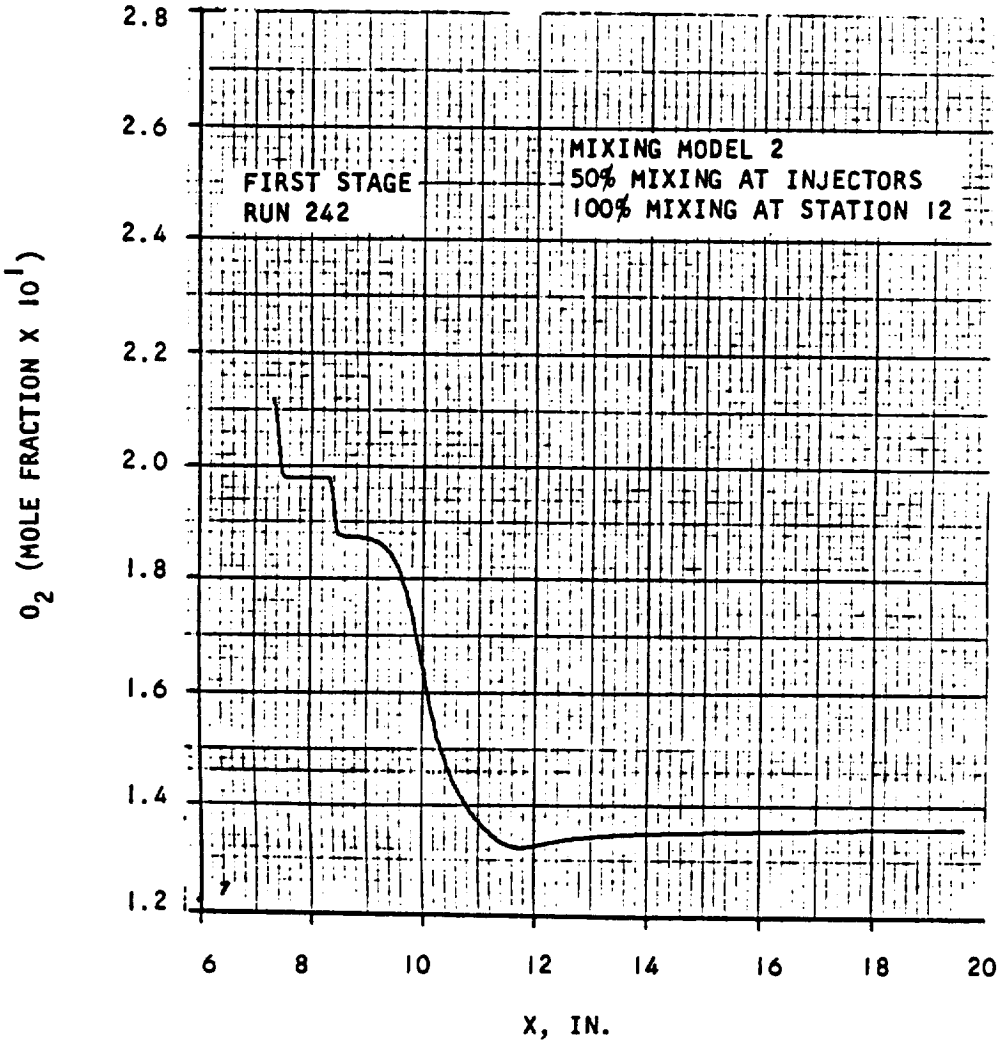

Figure B.1-7. Concentration of O_2 vs Axial Distance

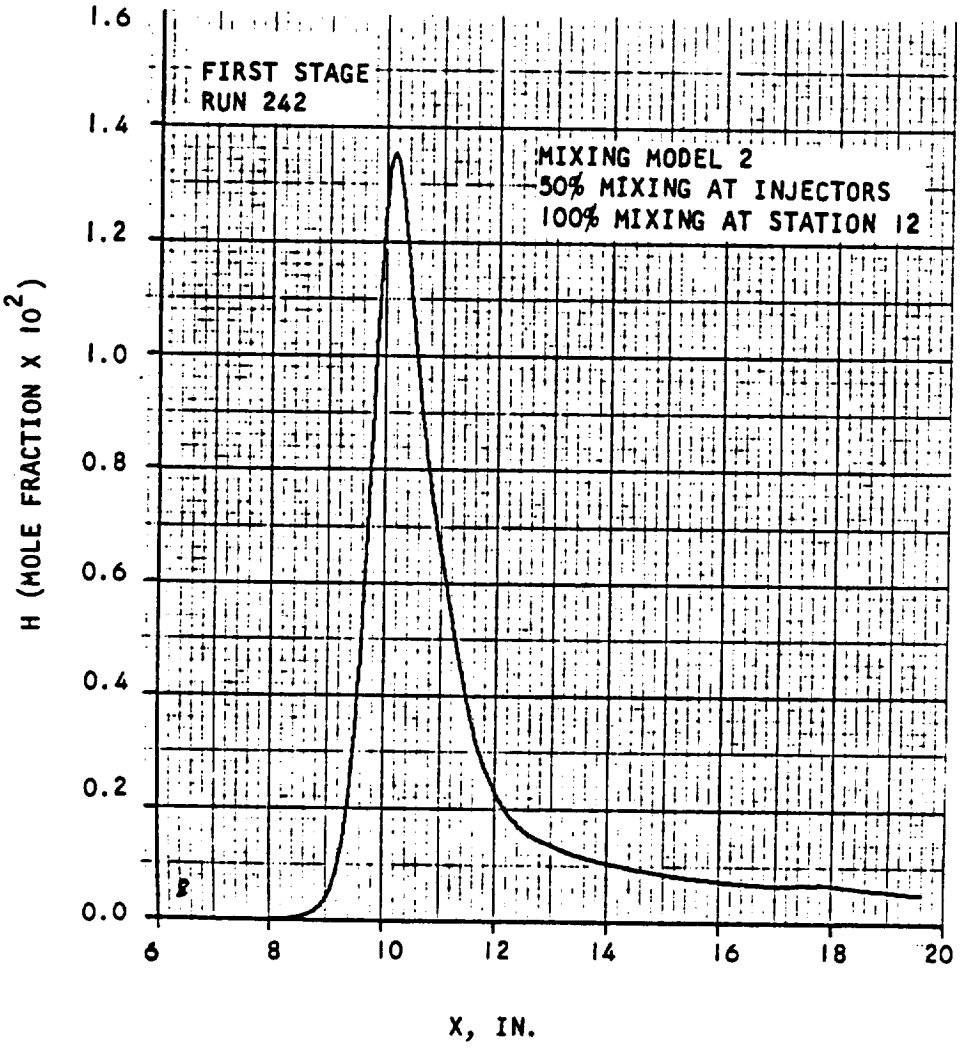

Figure B.1-8. Concentration of H vs Axial Distance

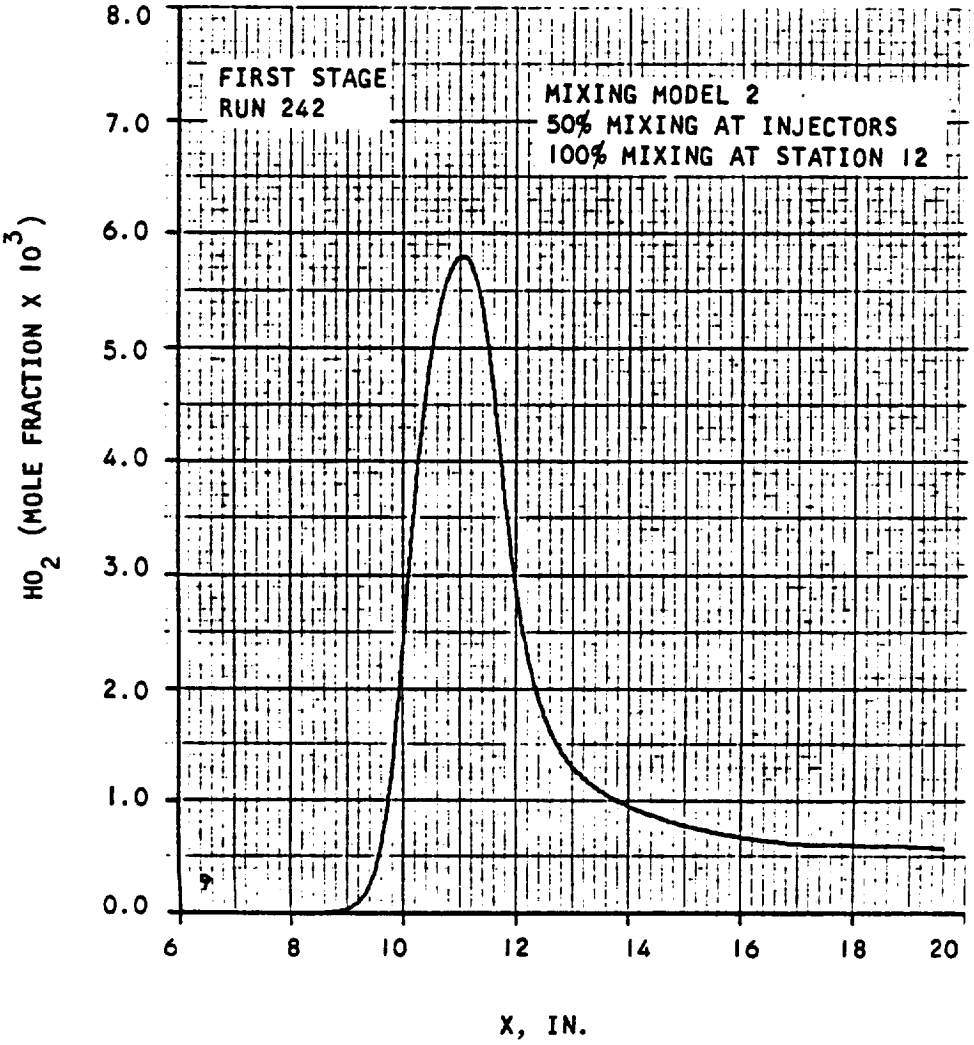

Figure B.1-9. Concentration of HO_2 vs Axial Distance

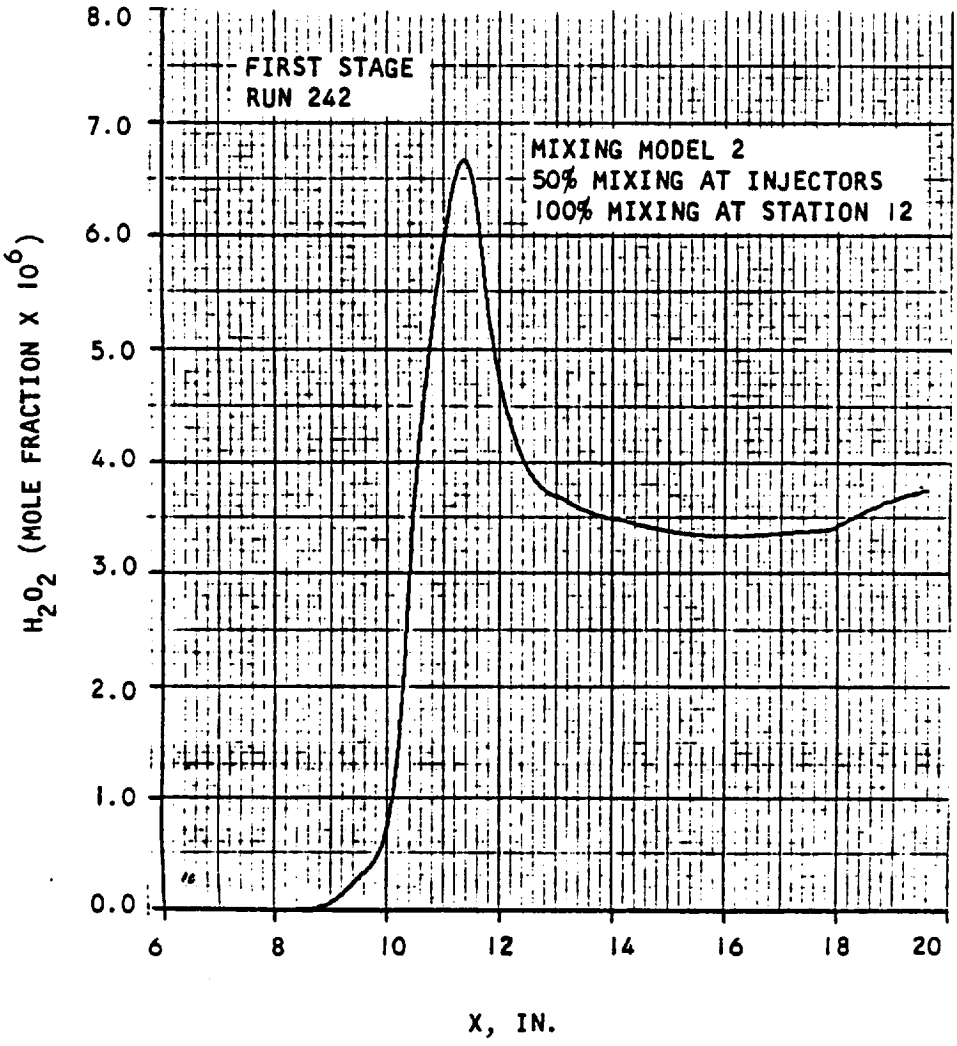

Figure B.1-10. Concentration of H_2O_2 vs Axial Distance

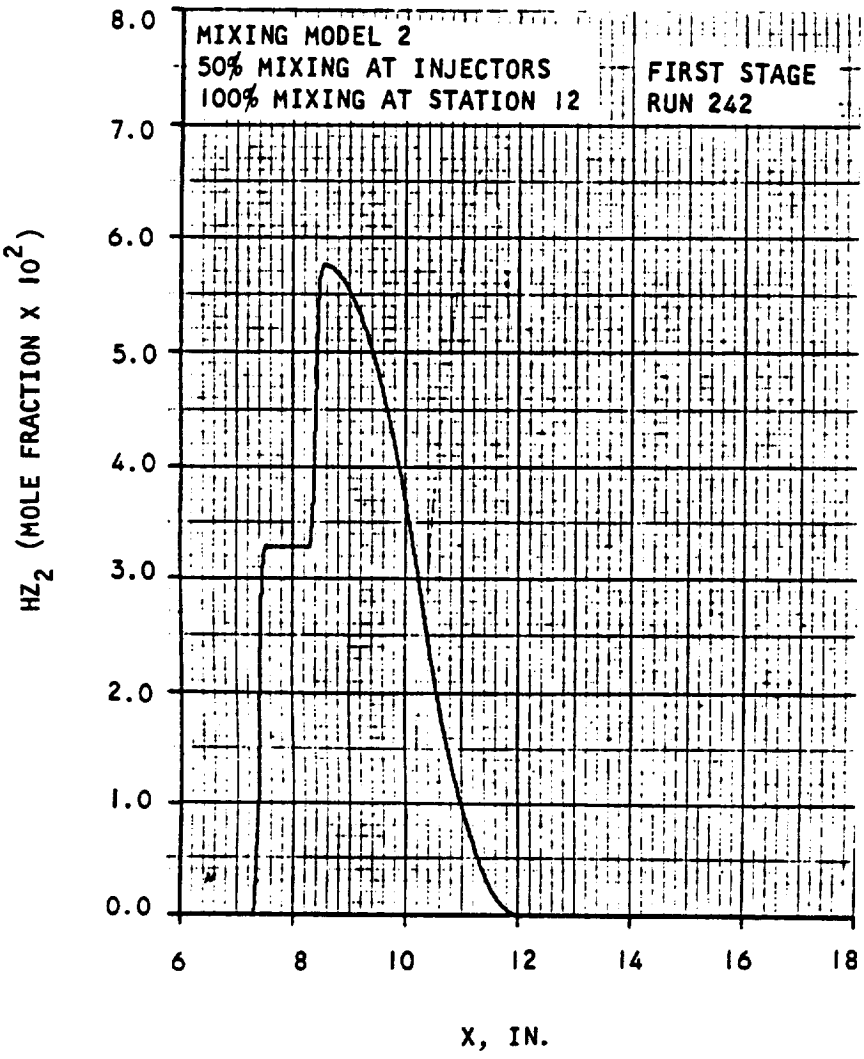

Figure B.1-11. Concentration of HZ_2 vs Axial Distance

2. Second Stage Combustor - Run 242
Mixing Model 2, 50 percent mixing at each injector, 100 percent mixing at Station 28.75.

Station	A(in.^{2})	$\dot{m}$(lb m/sec)	$\dot{m}_{H_2}$ (mixed)	η_m	η_c	$\dot{m}_{H_2} + \dot{m}_{Hz_2}$	ϕ
19.6000	4.762	1.55240	0.016400	1.0	0.9824	0.01640	0.3073
19.8262	5.443	1.57318	0.026800	0.27	0.6738	0.03718	0.6966
20.5112	5.648	1.57318	0.026800	0.27	0.8854	0.03718	0.6966
20.9012	6.508	1.59100	0.035730	0.64	0.8211	0.05500	1.0305
21.5012	6.915		0.036007	0.65	0.8831		
22.0237	7.093		0.036584	0.67	0.9043		
22.6062	7.509		0.037597	0.68	0.9129		
23.0737	7.815		0.038692	0.70	0.9118		
23.6737	7.904		0.040465	0.74	0.9098		
24.2112	8.224		0.042404	0.77	0.8999		
24.8112	9.269		0.044961	0.82	0.8846		
25.5487	9.426		0.048187	0.88	0.8657		
26.2862	9.503		0.050797	0.92	0.8586		
27.0287	10.169		0.052794	0.96	0.8537		
27.8112	9.538	↓	0.054213	0.99	0.8539	↓	↓
28.5487	10.065		0.054908	0.999	0.8607		
28.7487	10.334	1.59100	0.055000	1.0	0.8624	0.05500	1.0305
19.6912	5.043						
19.9762	5.451						
25.0062	9.725						
25.9487	9.278						
28.0062	9.448						

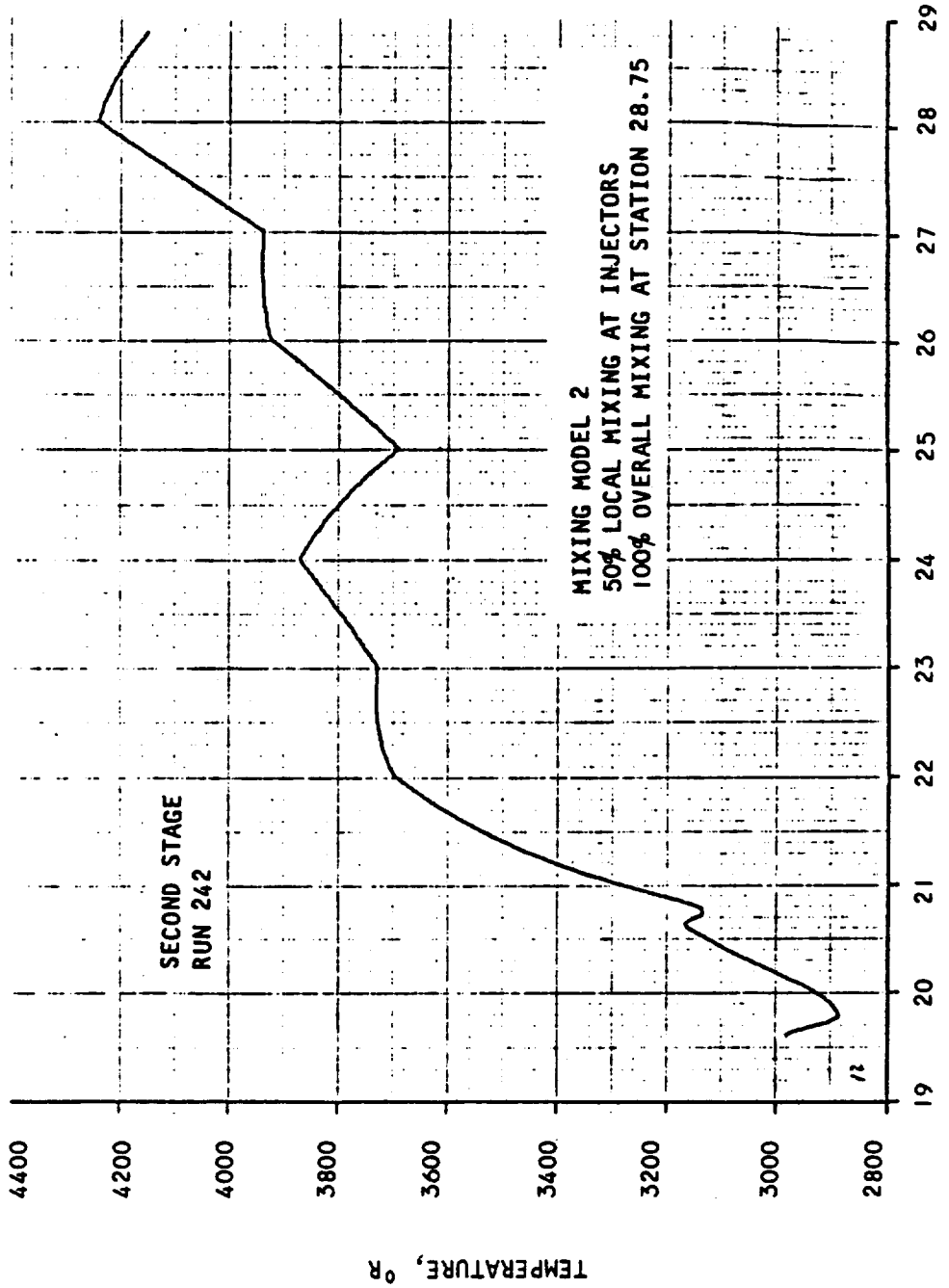

Figure B.2-1. Temperature vs Axial Distance

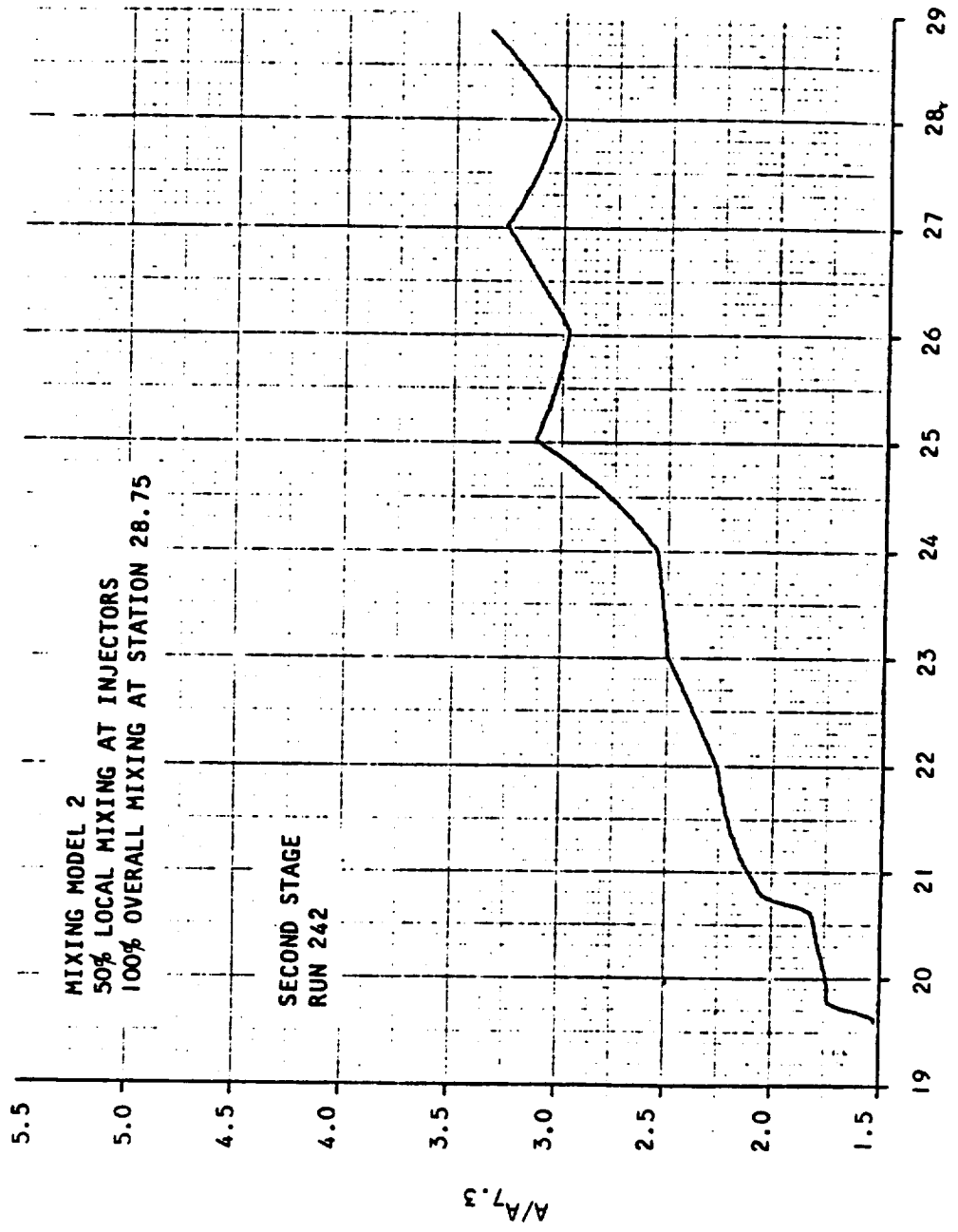

Figure B.2-2. Area Ratio vs Axial Distance

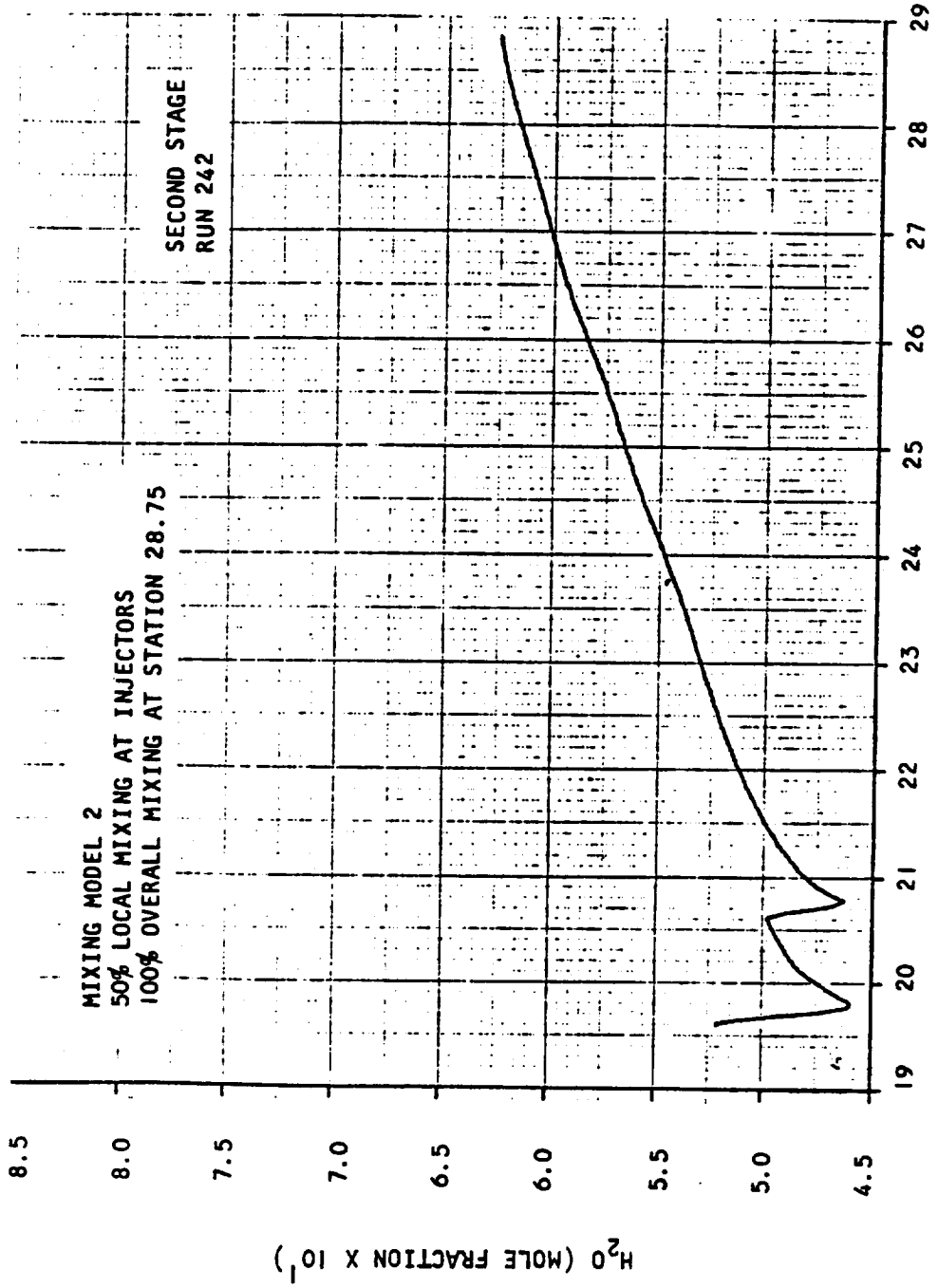

Figure B.2-3. Concentration of H_2O vs Axial Distance

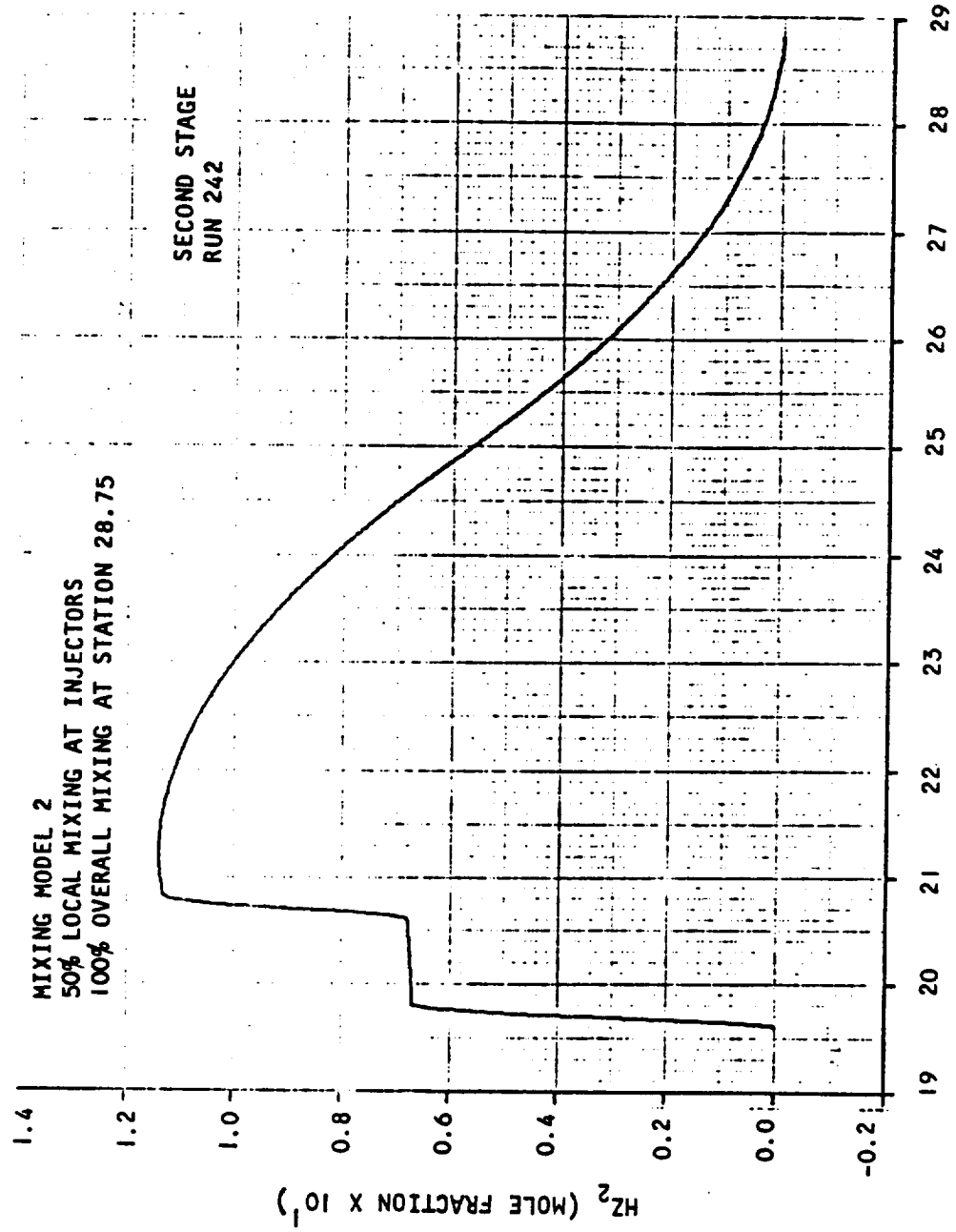

Figure B.2-11. Concentration of HZ_2 vs Axial Distance

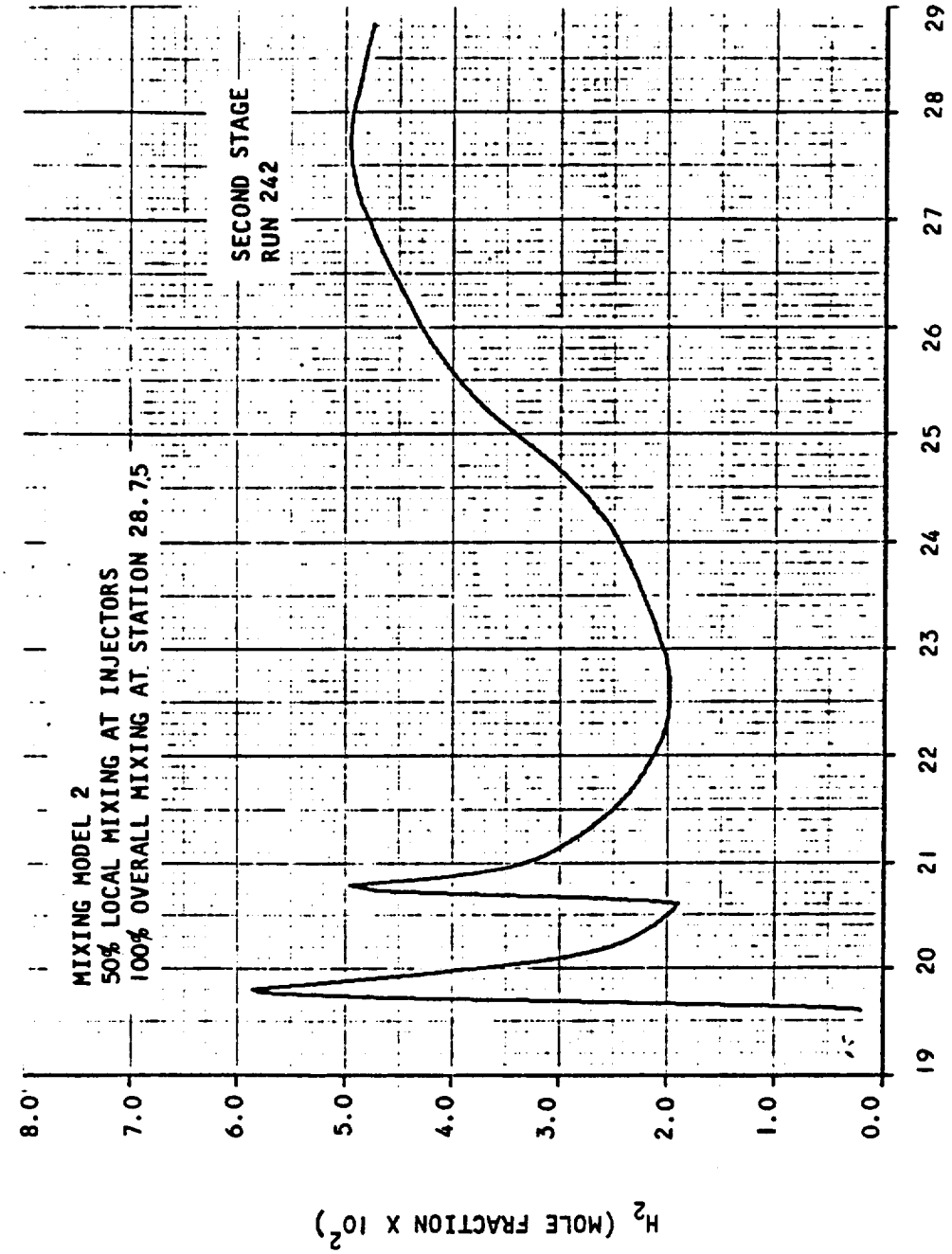

Figure B.2-4. Concentration of H_2 vs Axial Distance

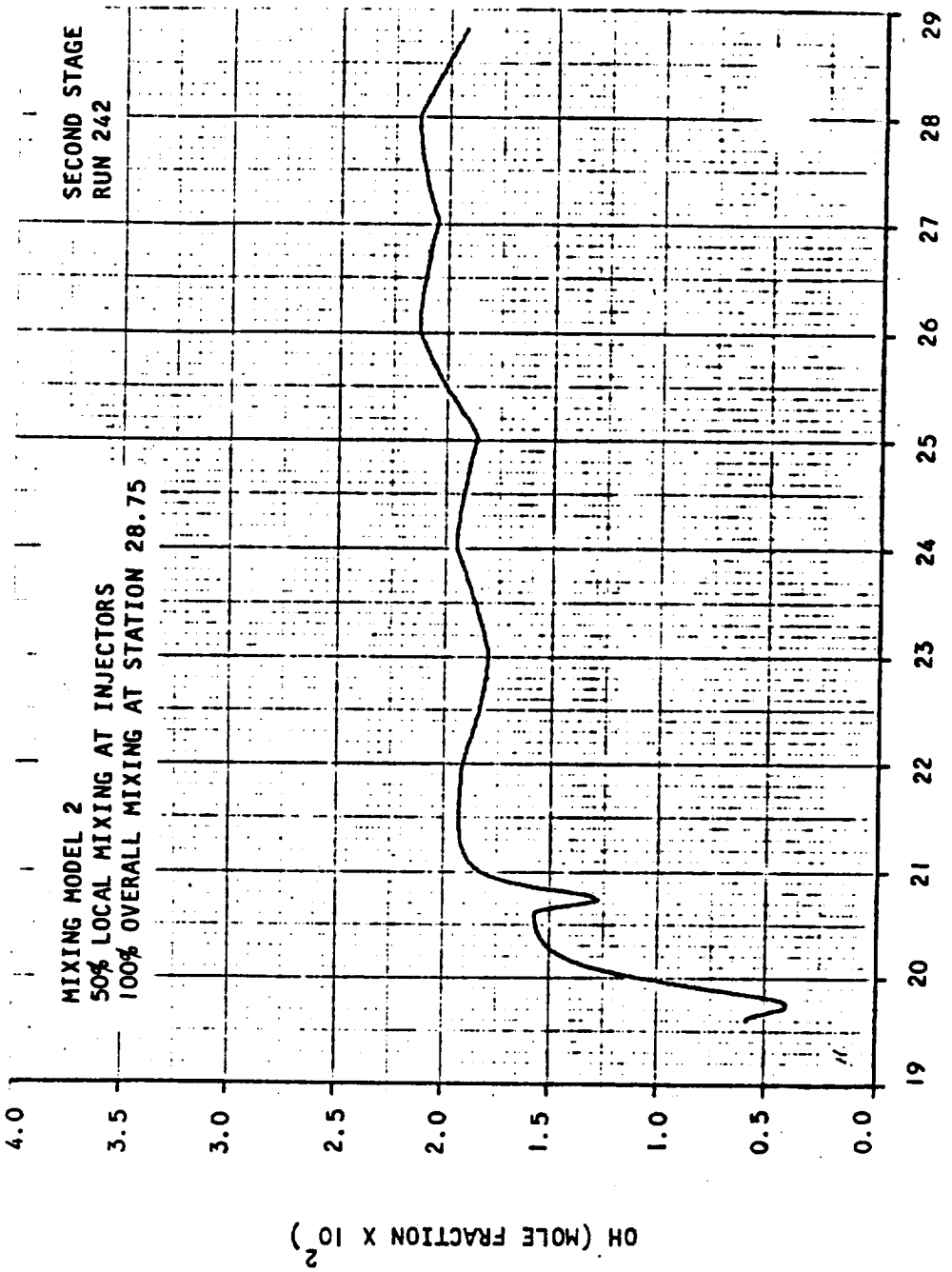

Figure B.2-5. Concentration of OH vs Axial Distance

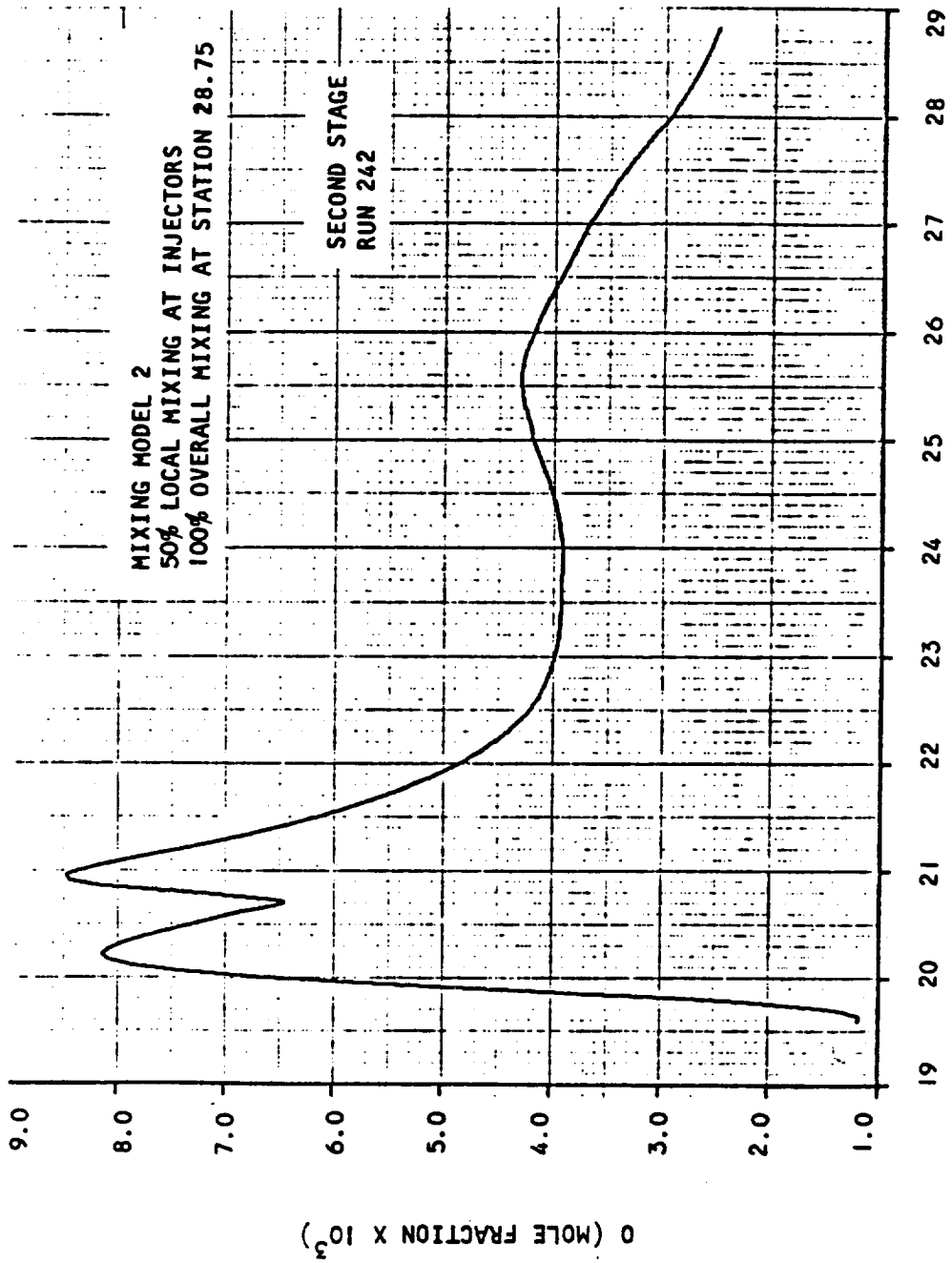

Figure B.2-6. Concentration of O vs Axial Distance

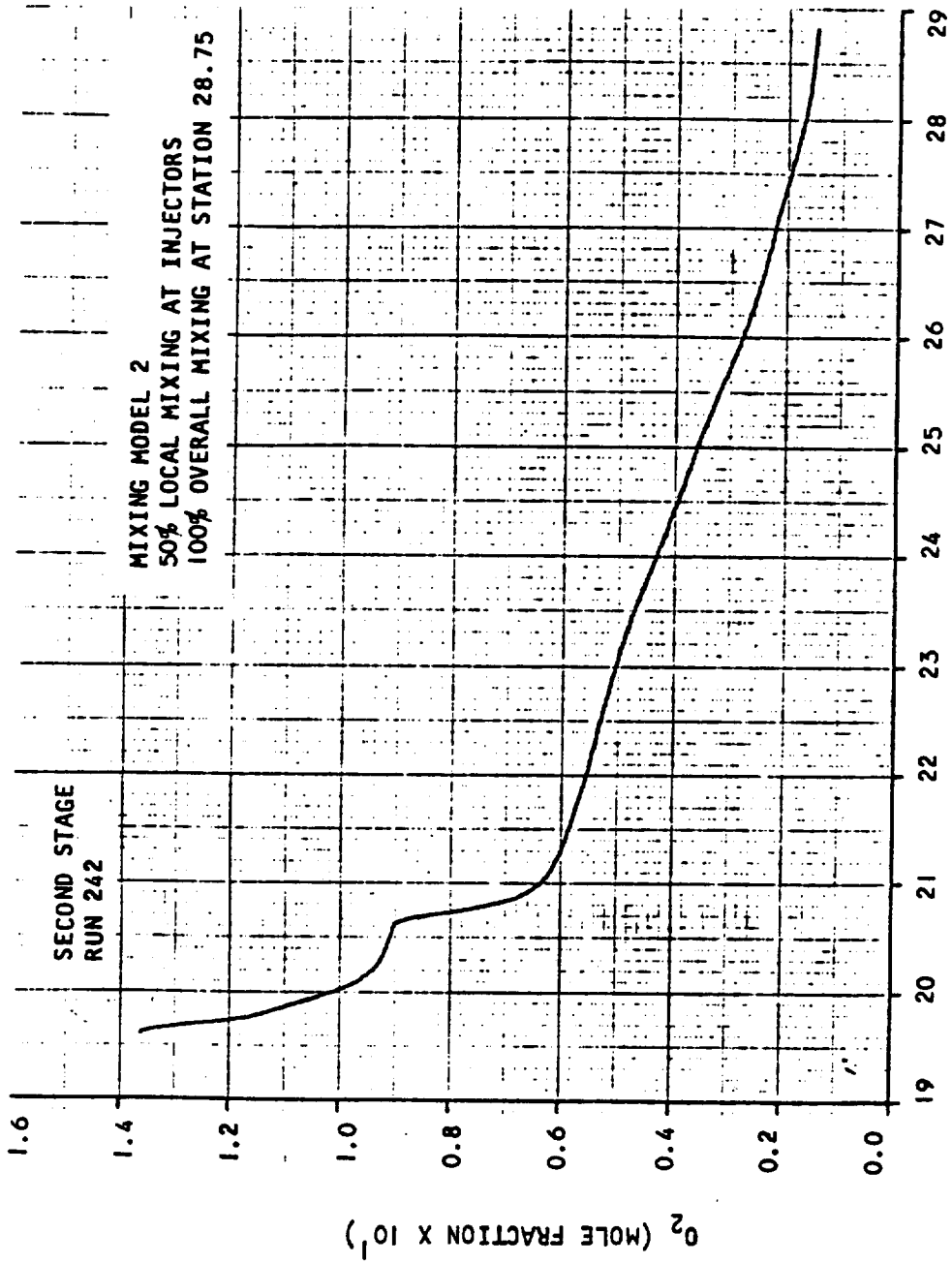

Figure B.2-7. Concentration of O_2 vs Axial Distance

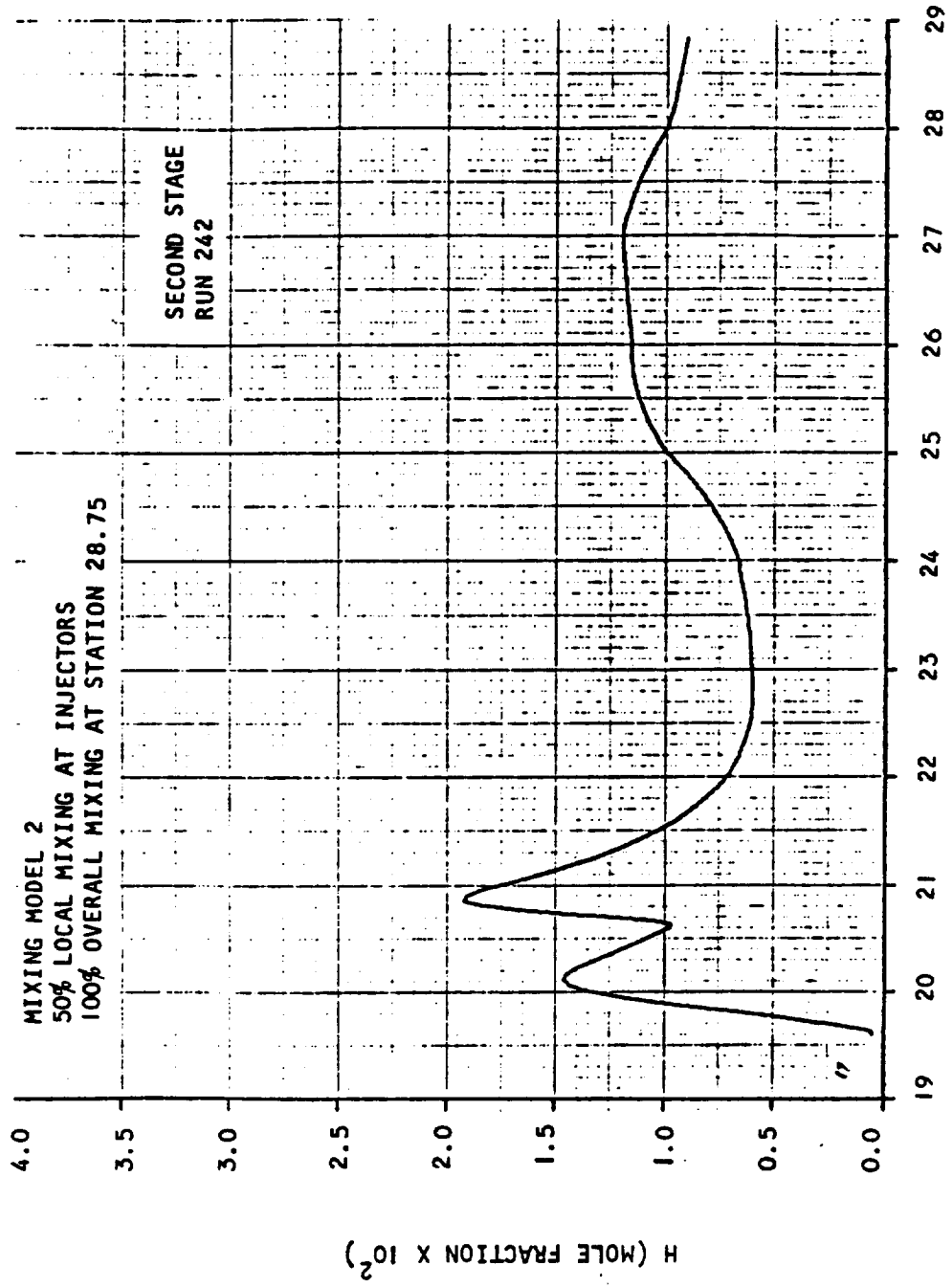

Figure B.2-8. Concentration of H vs Axial Distance

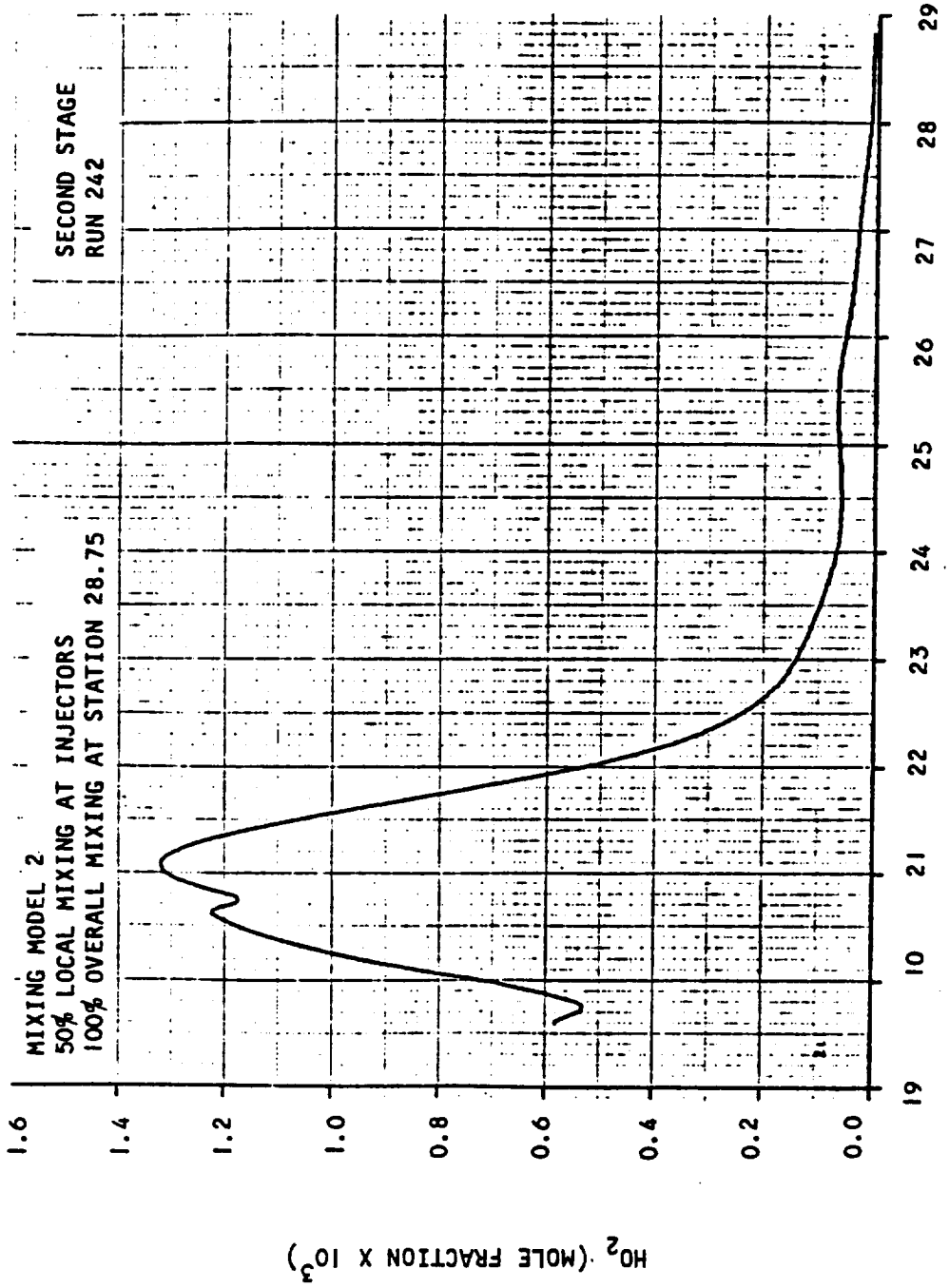

Figure B.2-9. Concentration of HO_2 vs Axial Distance

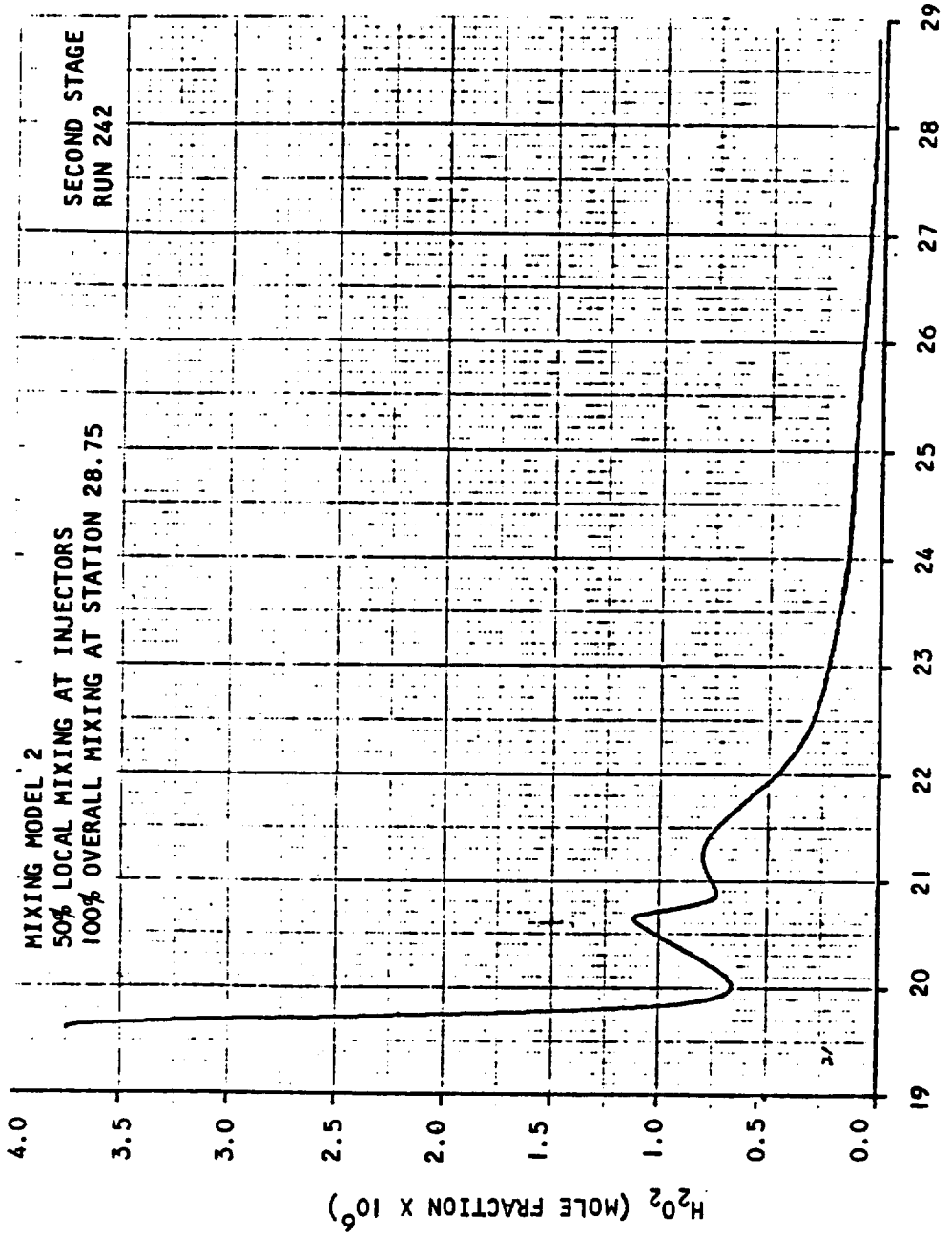

Figure B.2-10. Concentration of H_2O_2 vs Axial Distance

3. Second Stage Combustor - Run 242
Mixing Model 1, 50 percent local mixing at each injector, 60 percent mixing at Station 24.9.

Station	A(in.^{2})	$\dot{m}$(lb m/sec)	$\dot{m}_{H_2}$ (mixed)	η_m	η_c	$\dot{m}_{H_2} + \dot{m}_{Hz_2}$	ϕ
19.6000	4.762	1.5524	0.016400	1.0	0.9824	0.01640	0.3073
19.8825	5.428	1.5732	0.020382	0.55	0.8382	0.03718	0.6966
20.4825	5.390	1.5732	0.020382	0.55	0.8382	0.03718	0.6966
20.9550	6.048	1.5910	0.025140	0.46	0.8567	0.05500	1.0305
21.5150	6.218		0.027167	0.49	0.8869		
22.0600	6.399		0.028842	0.52	0.9002		
22.6600	6.852		0.030347	0.55	0.9086		
23.0812	7.137		0.031191	0.57	0.9120		
23.6462	7.223		0.032048	0.58	0.9181		
24.0237	7.290		0.032445	0.59	0.9234		
24.5912	8.072		0.032777	0.596	0.9302		
24.9912	8.861		0.032824	0.597	0.9344		
25.7287	8.426				0.9400		
26.0662	8.316				0.9431		
26.6662	8.715				0.9476		
27.0287	8.943				0.9495		
27.6112	8.357				0.9526		
28.0062	8.073				0.9554		
28.5487	8.586	↓	↓	↓	0.9587	↓	↓
28.7487	8.816				0.9594		
29.0000	9.144	1.5910	0.032824	0.597	0.9602	0.05500	1.0305

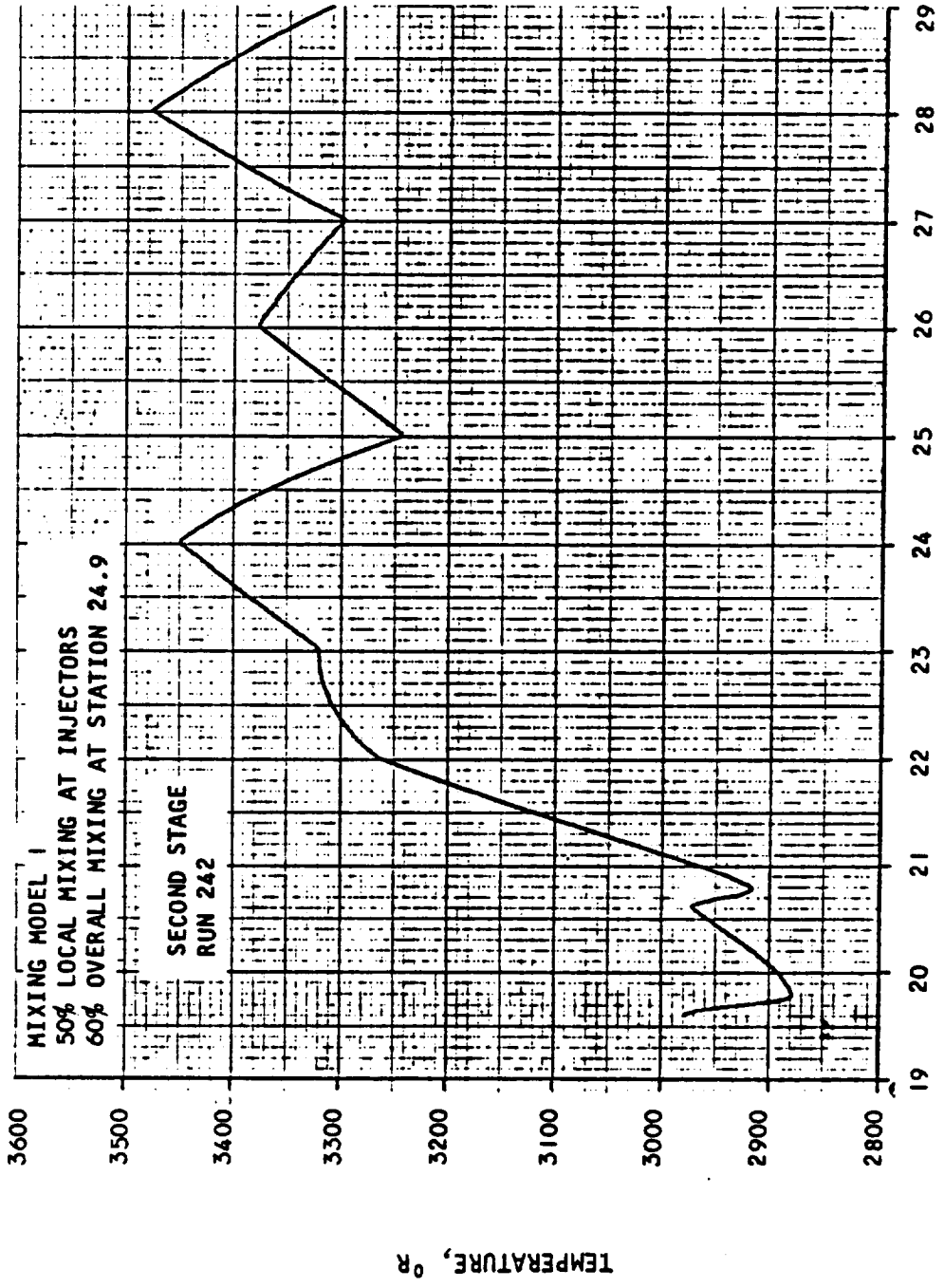

Figure B.3-1. Temperature vs Axial Distance

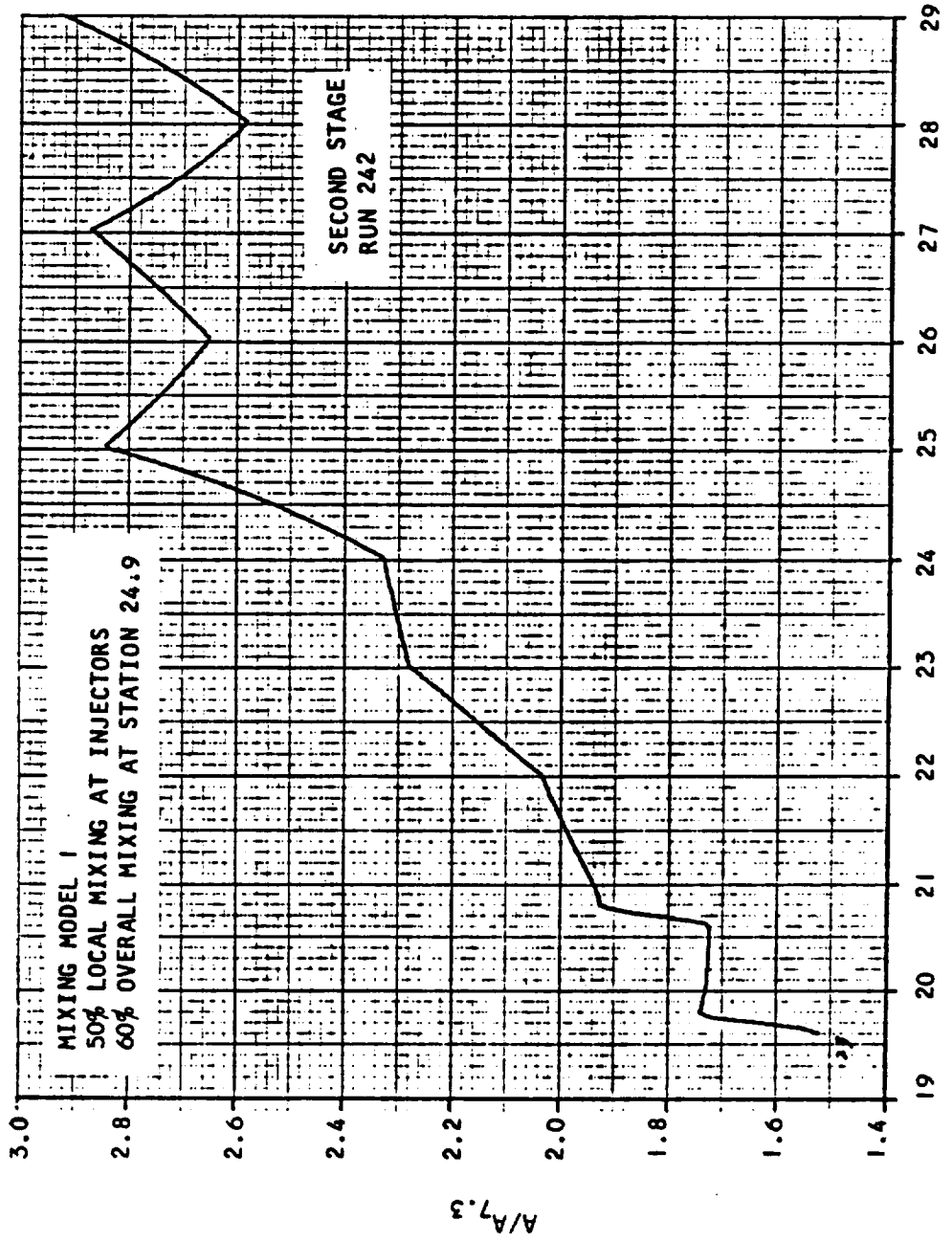

Figure B.3-2. Area Ratio vs Axial Distance

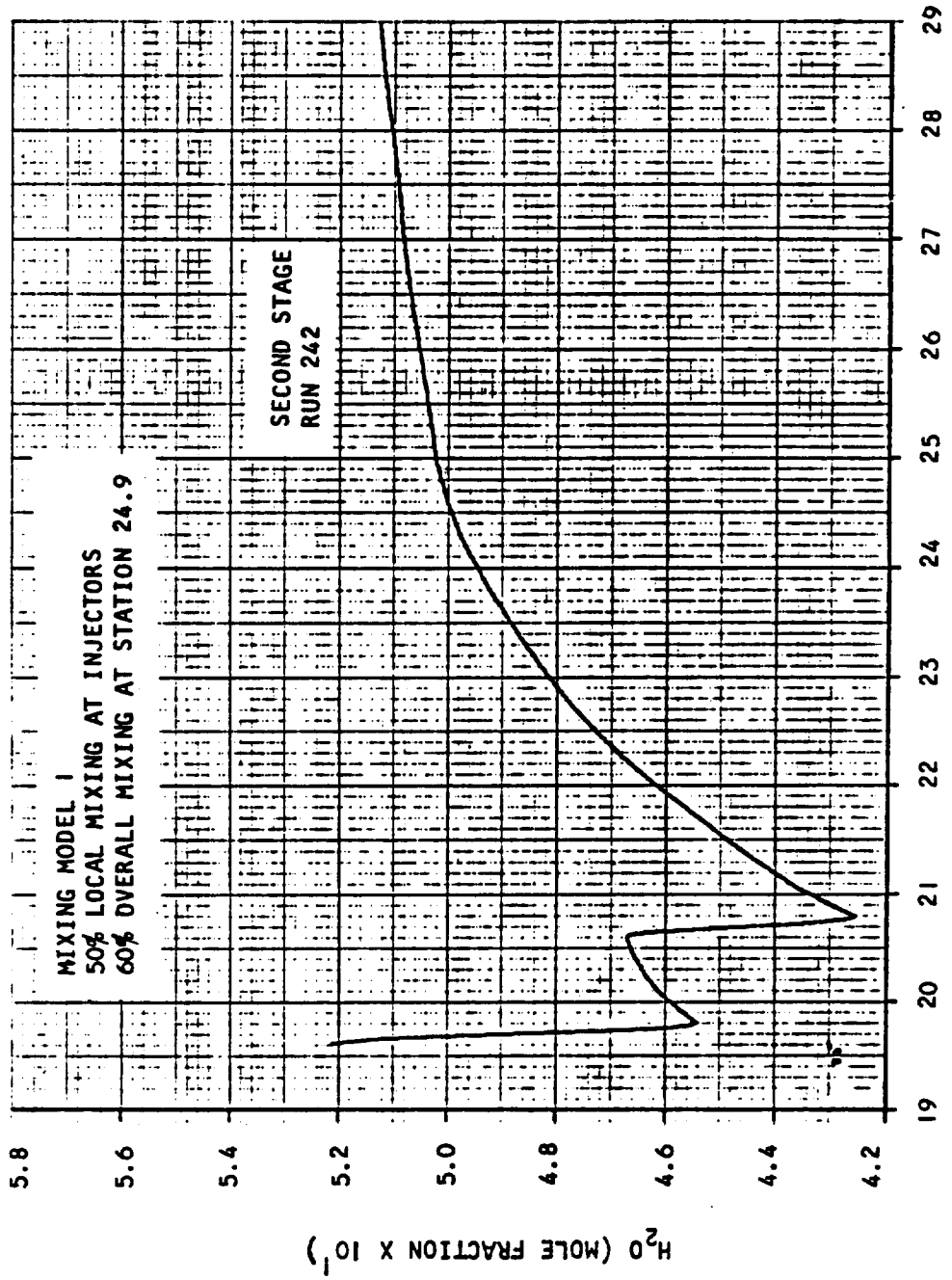

Figure B.3-3. Concentration of H_2O vs Axial Distance

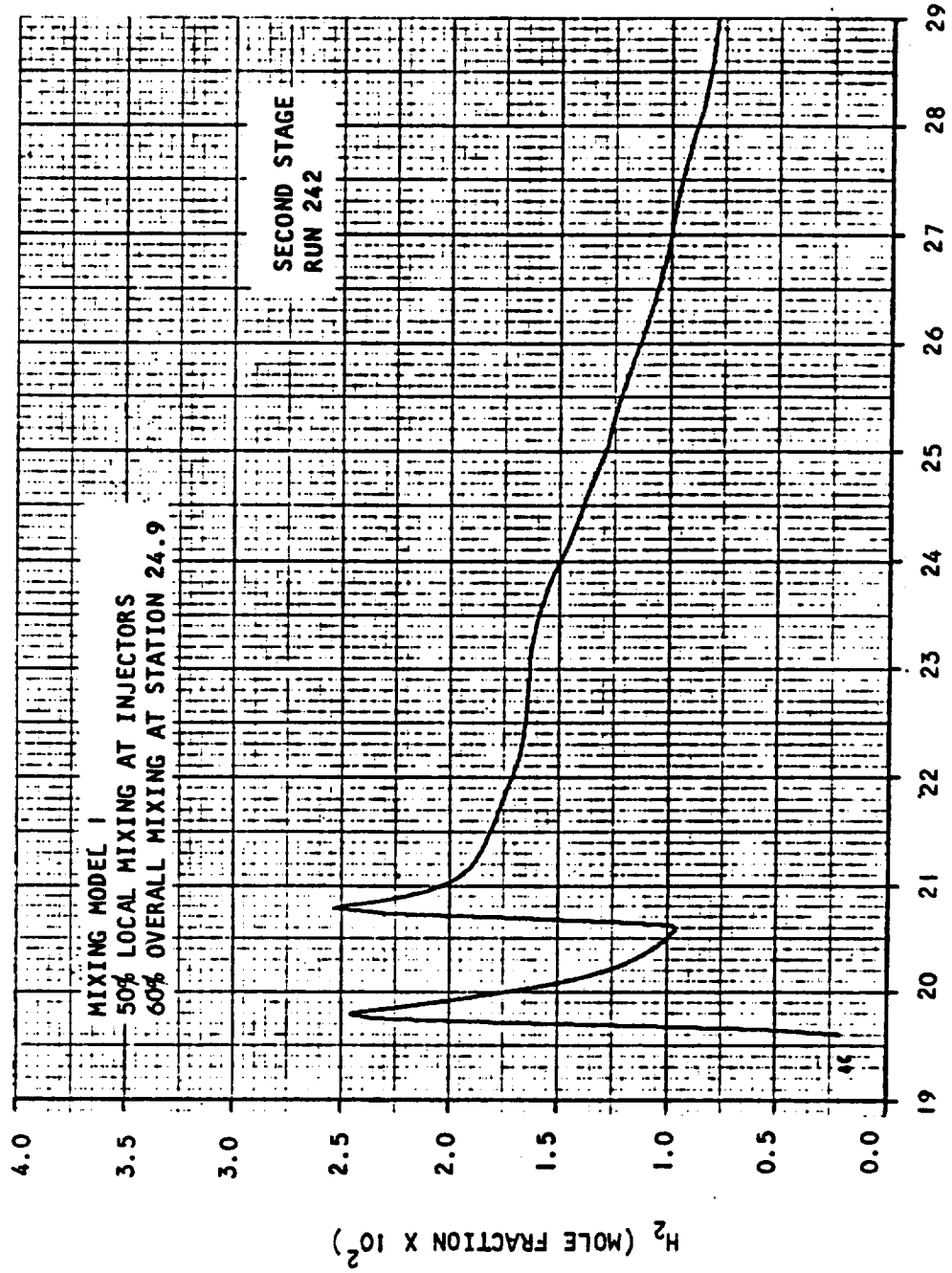

Figure B.3-4. Concentration of H_2 vs Axial Distance

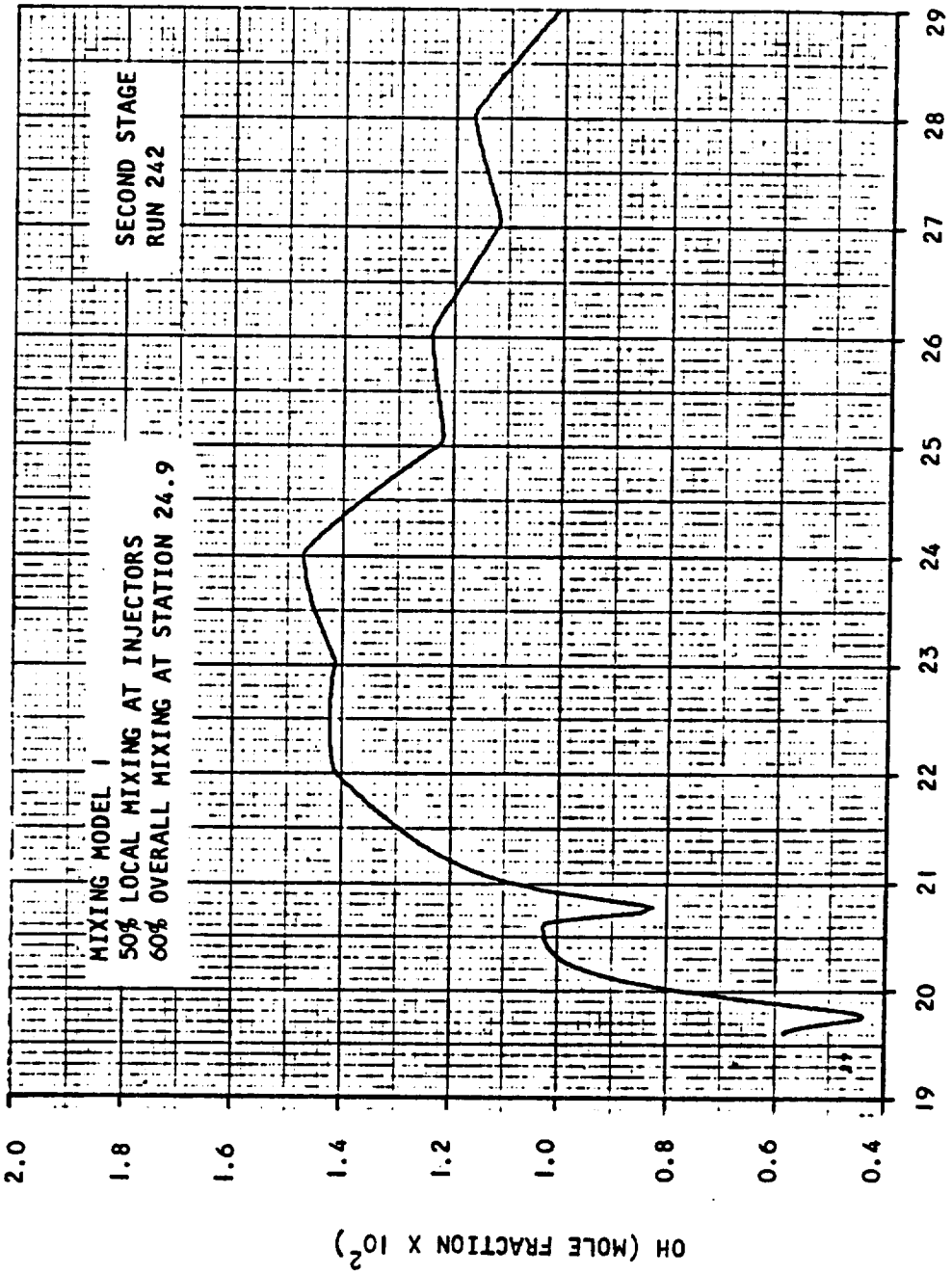

Figure B.3-5. Concentration of OH vs Axial Distance

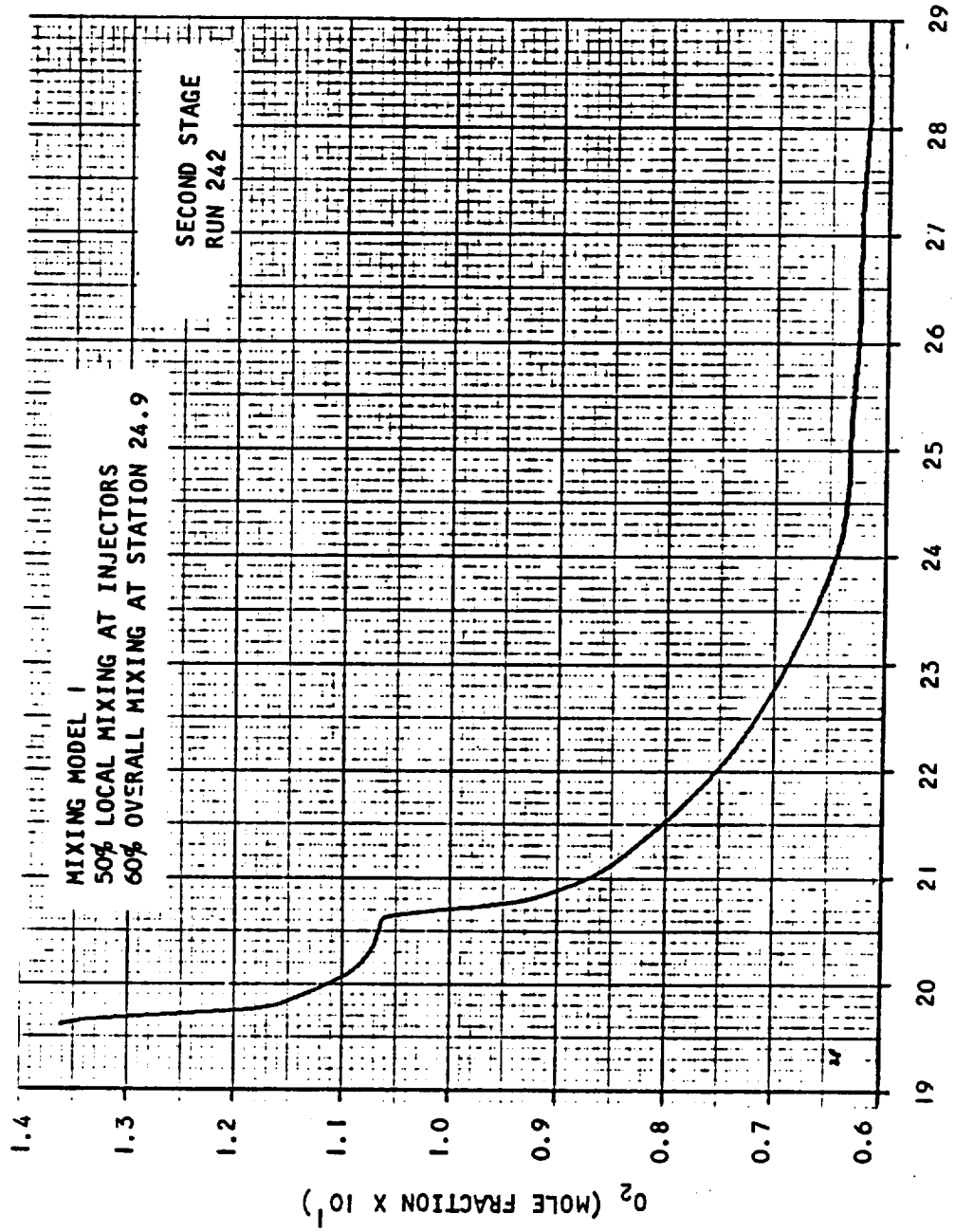

Figure B.3-6. Concentration of O_2 vs Axial Distance

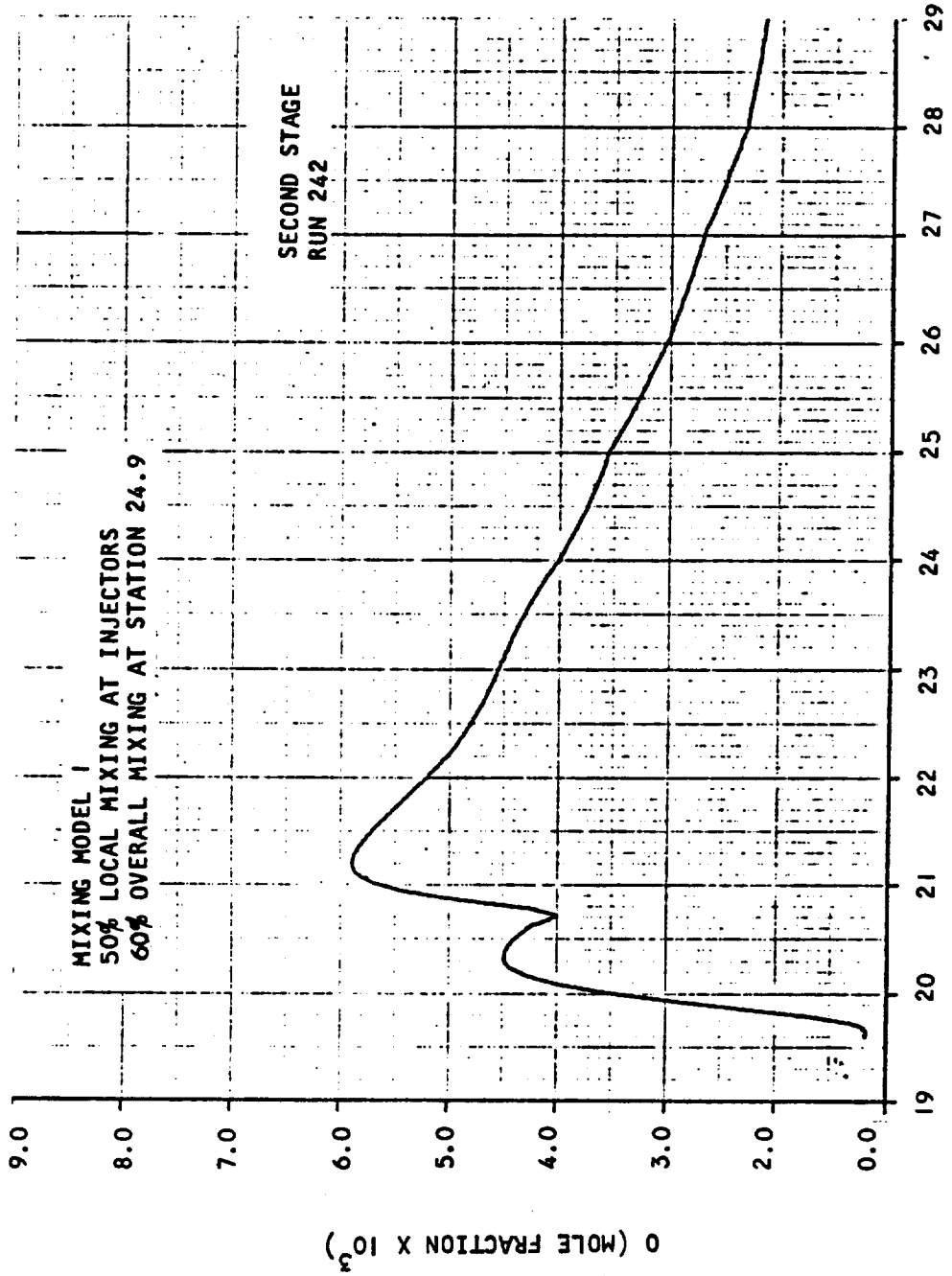

Figure B.3-7. Concentration of O vs Axial Distance

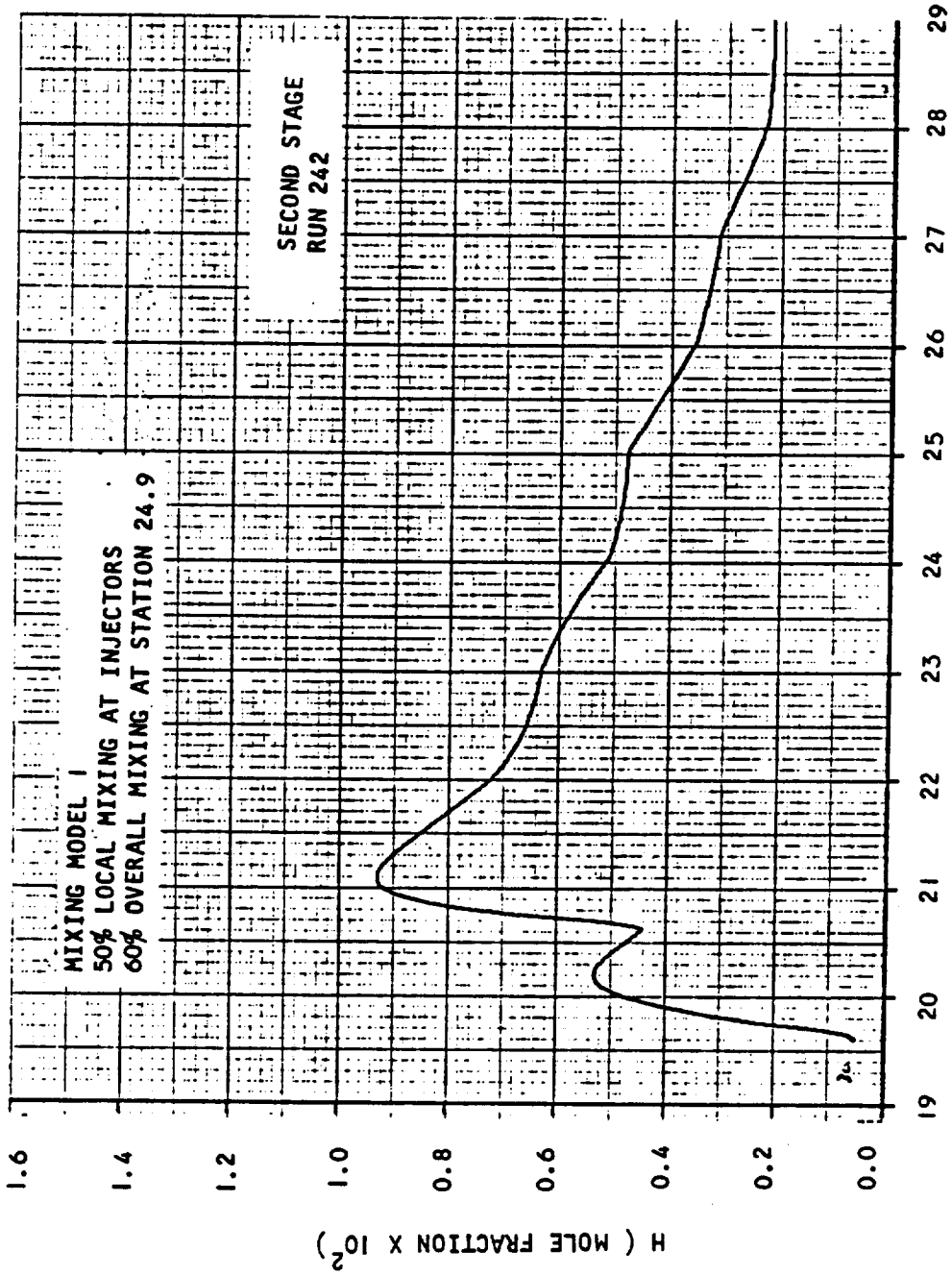

Figure B.3-8. Concentration of H vs Axial Distance

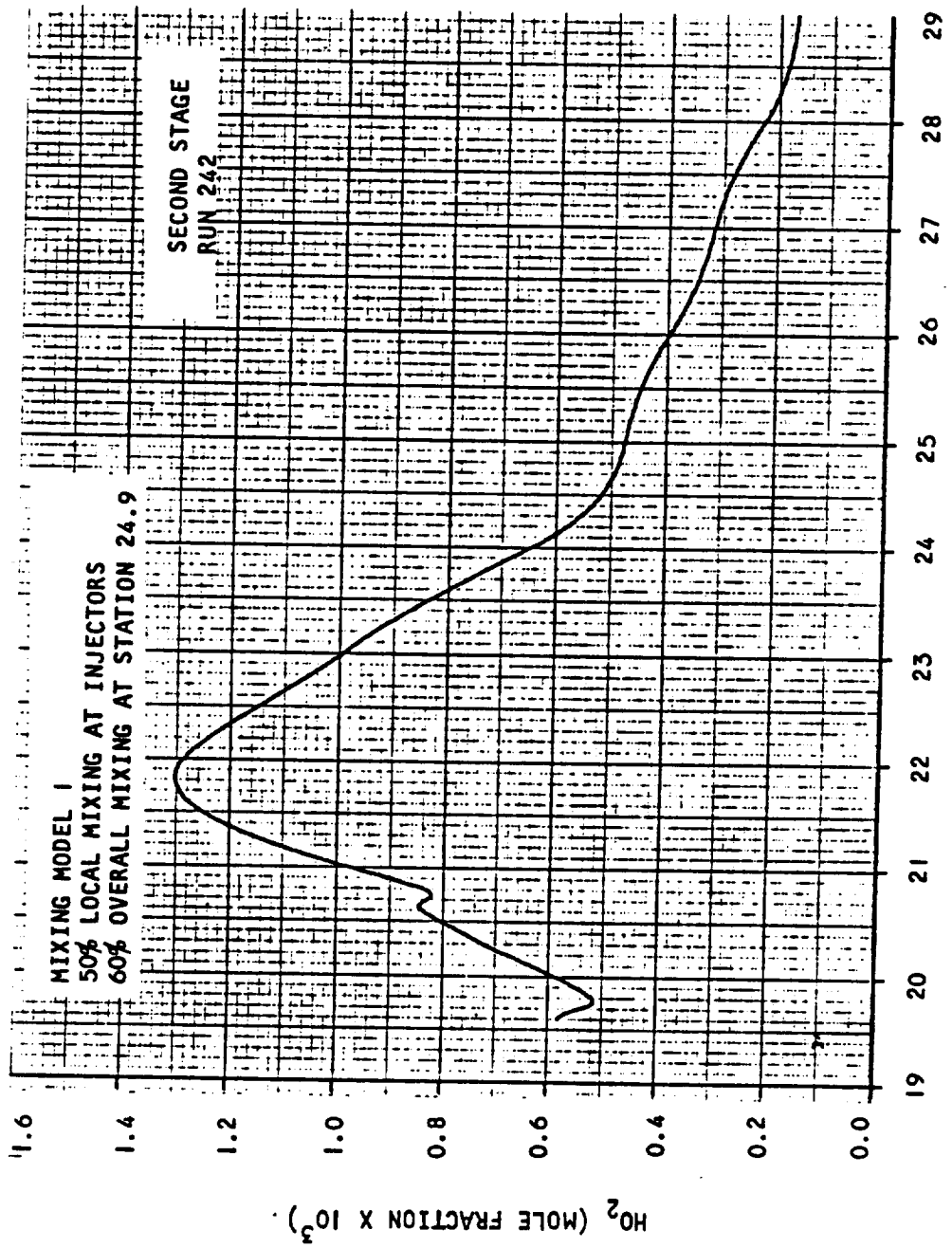

Figure B.3-9. Concentration of HO_2 vs Axial Distance

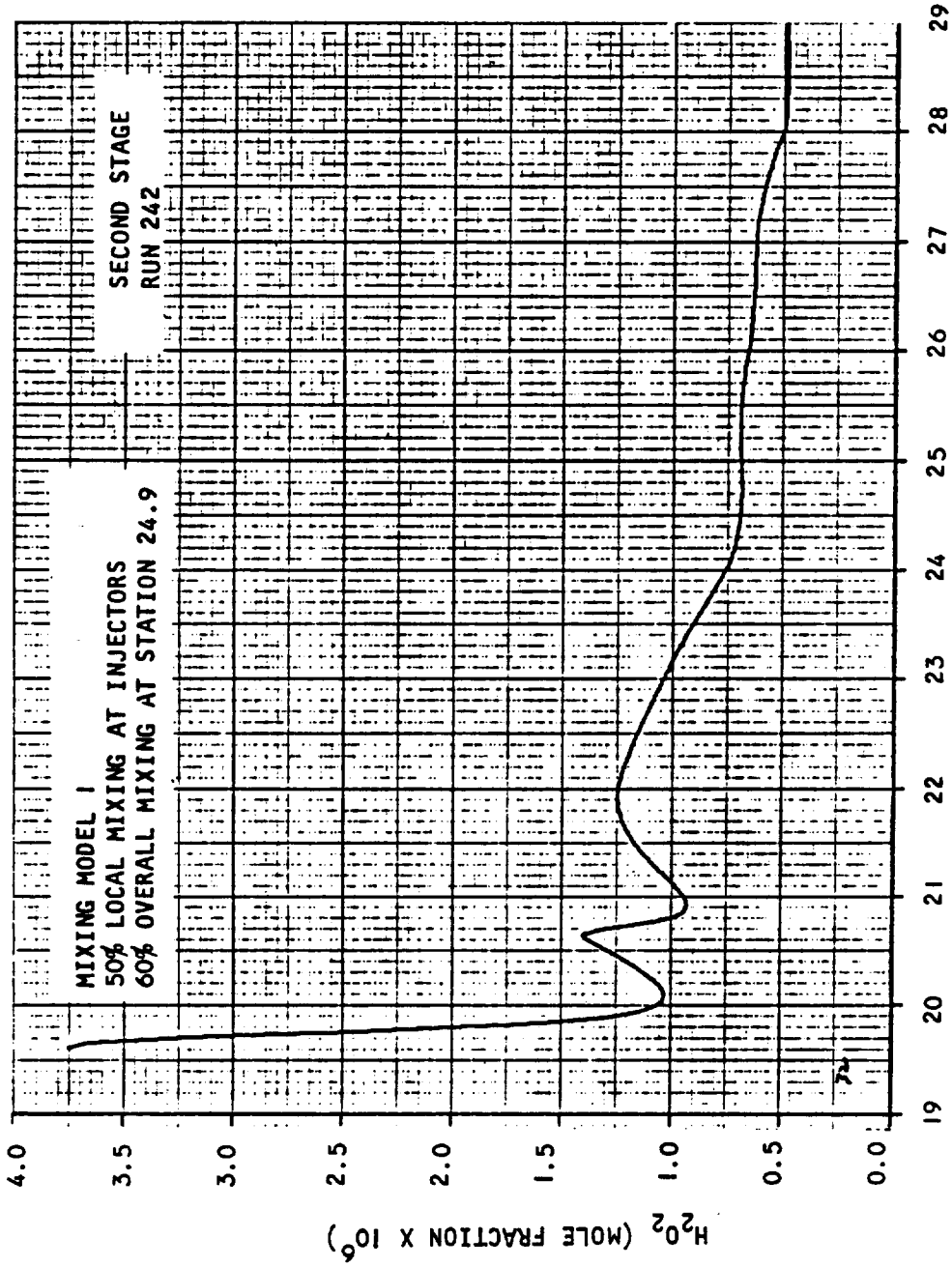

Figure B.3-10. Concentration of H_2O_2 vs Axial Distance

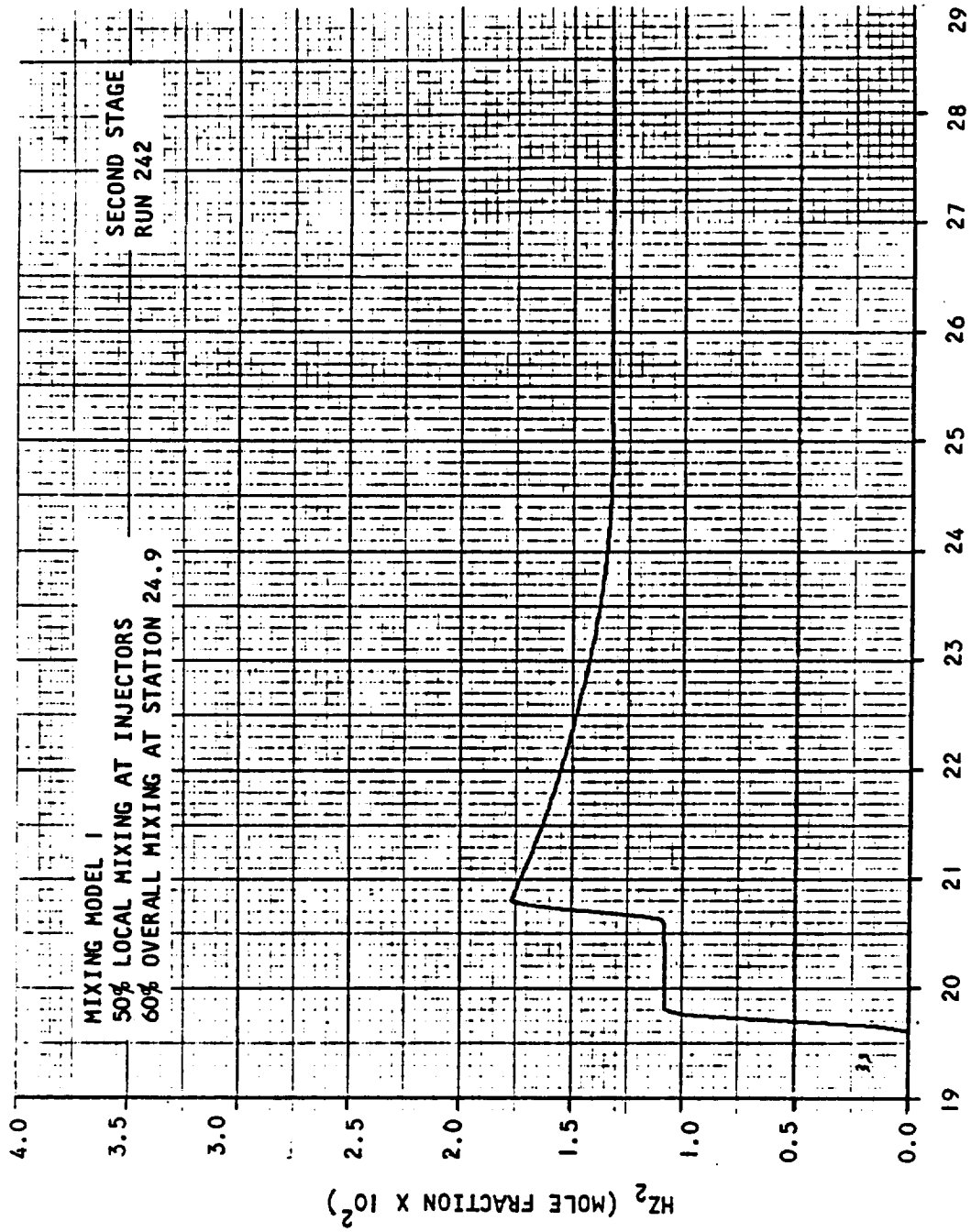

Figure B.3-11. Concentration of HZ_2 vs Axial Distance

4. Second Stage Combustor - Run 242
Mixing Model 1, 50 percent local mixing at each injector, 60 percent mixing at Station 29.

Station	A(in.^{2})	$\dot{m}$(lb m/sec)	$\dot{m}_{H_2}$ (mixed)	η_m	η_c	$\dot{m}_{H_2} + \dot{m}_{Hz_2}$	ϕ
19.6000	4.762	1.5524	0.016400	1.0	0.9824	0.01640	0.3073
20.4825	5.390	1.5732	0.020382	0.55	0.9232	0.03718	0.6966
20.9050	6.036	1.5910	0.024745	0.45	0.8547	0.05500	1.0305
21.2162	6.114	1.5910	0.025355	0.46	0.8877		
21.6162	6.206		0.026104	0.47	0.9024		
22.3537	6.507		0.027381	0.50	0.9181		
22.9287	6.900		0.028284	0.51	0.9223		
23.6312	7.020		0.029276	0.53	0.9256		
24.3762	7.519		0.030195	0.55	0.9292		
24.9762	8.588		0.030836	0.56	0.9279		
25.1137	8.587		0.030970	0.56	0.9271		
25.3137	8.457		0.031157	0.57	0.9265		
25.5137	8.339		0.031334	0.57	0.9266		
25.7137	8.231		0.031501	0.57	0.9271		
26.4512	8.394		0.032032	0.58	0.9304		
27.1962	8.599		0.032432	0.59	0.9326		
27.9962	7.964		0.032710	0.59	0.9388		
28.5337	8.474	↓	0.032807	0.596	0.9437	↓	↓
28.7337	8.709		0.032825	0.597	0.9451		
29.0000	9.060	1.5910	0.032834	0.597	0.9467	0.05500	1.0305
19.7975	5.443						
22.0162	6.282						
24.0162	7.071						
24.1762	7.257						
24.5762	7.821						
24.7762	8.172						
26.0512	8.122						
26.2512	8.255						
27.0212	8.790						

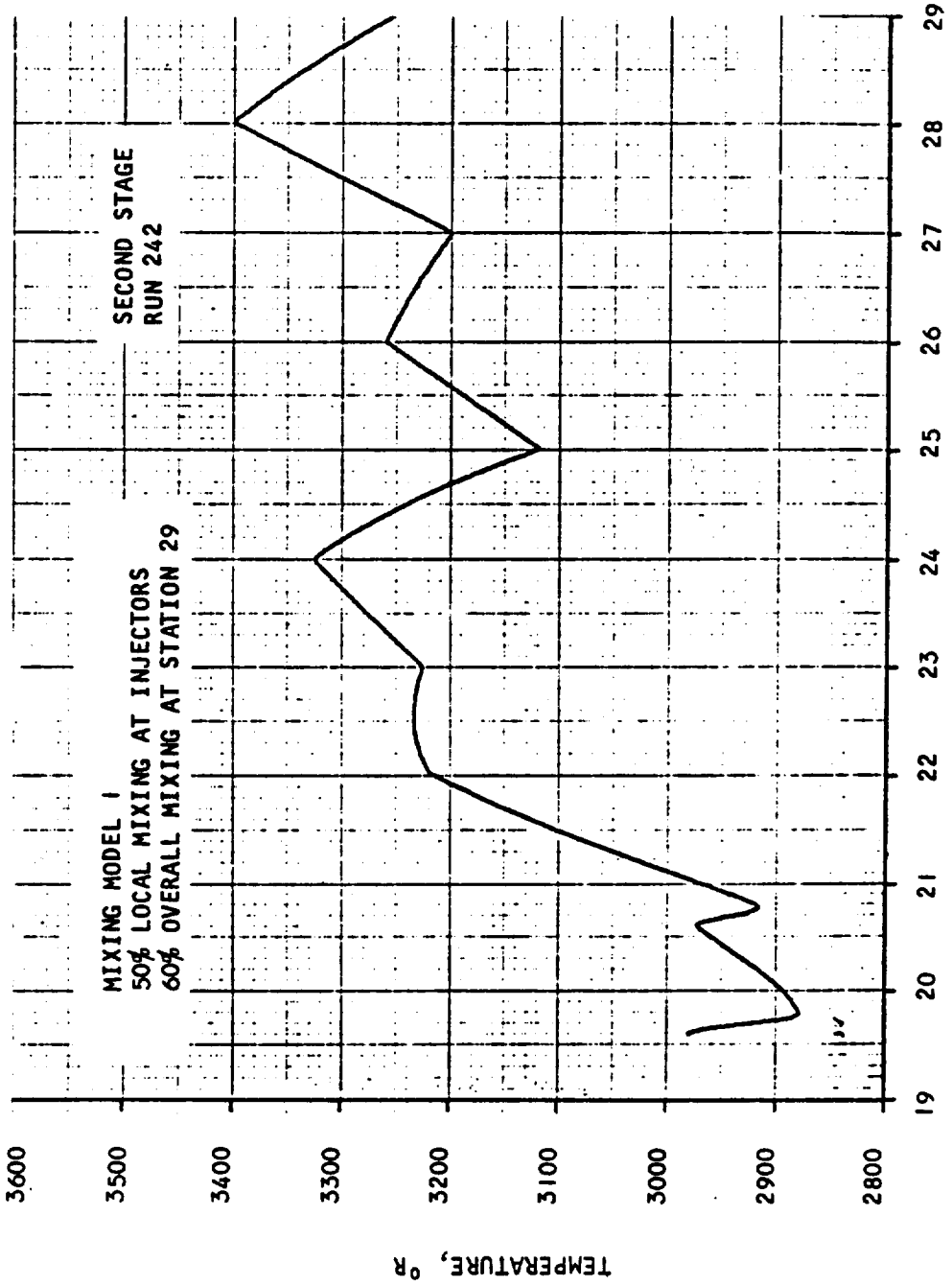

Figure B.4-1. Temperature vs Axial Distance

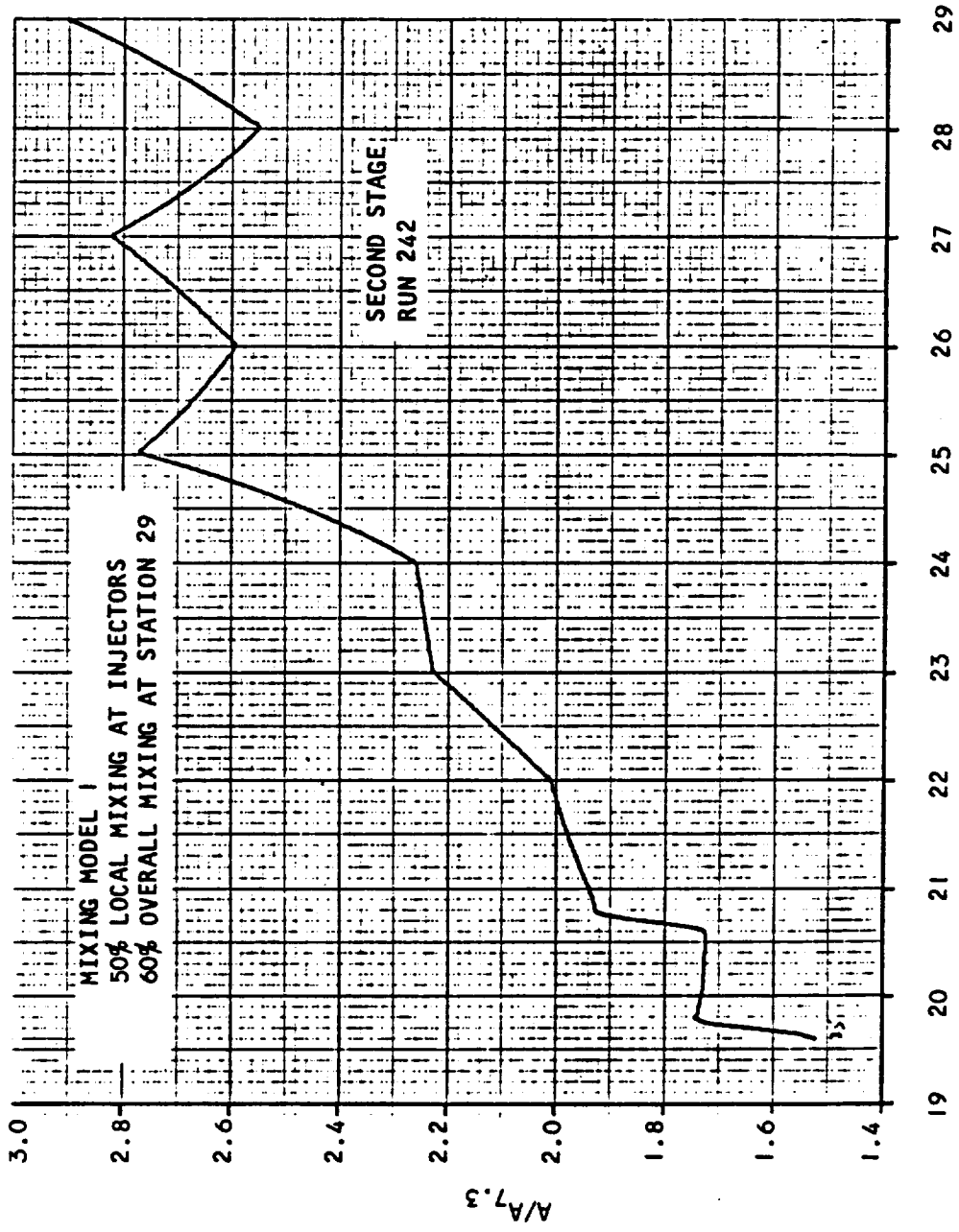

Figure B.4-2. Area Ratio vs Axial Distance

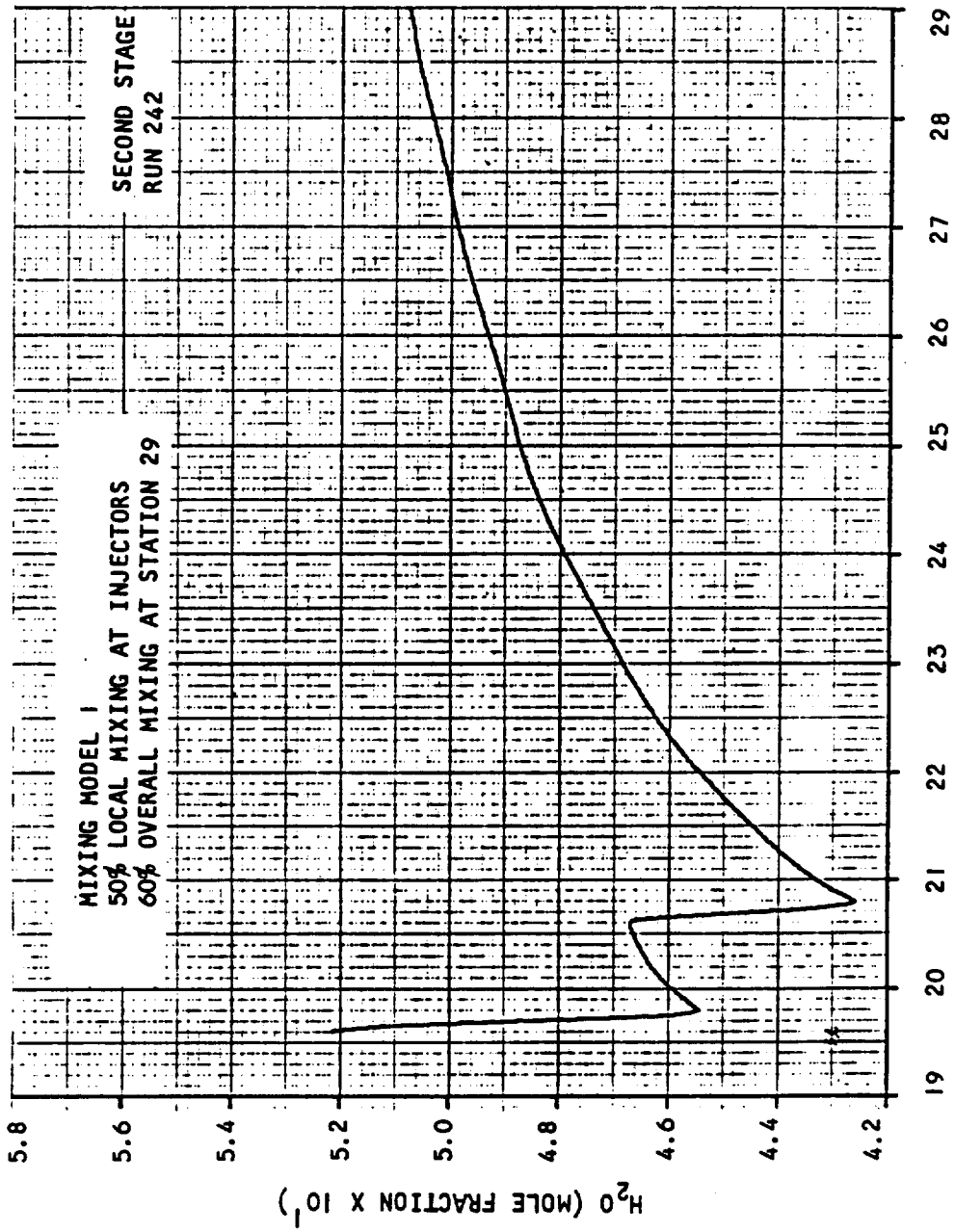

Figure B.4-3. Concentration of H_2O vs Axial Distance

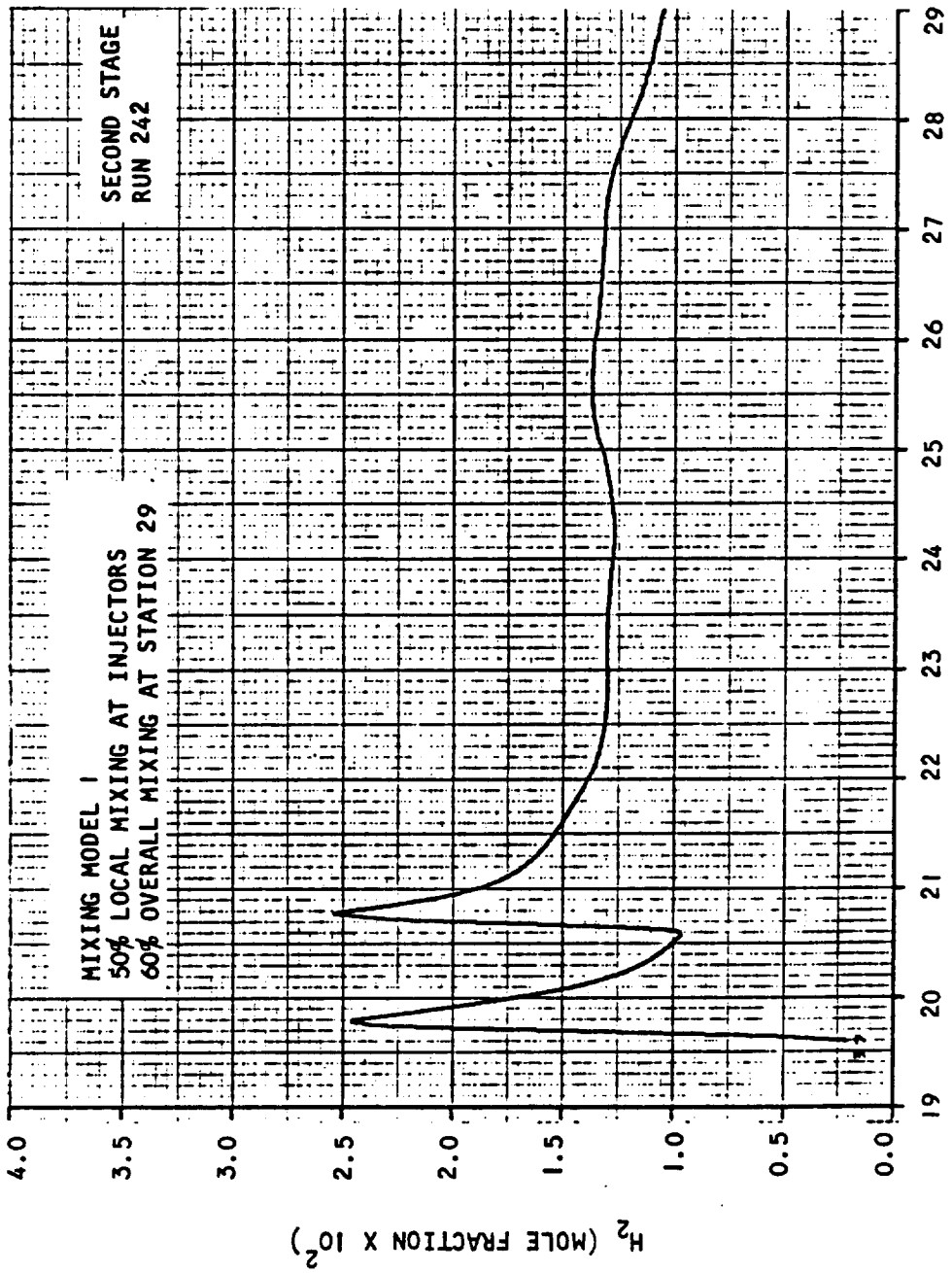

Figure B.4-4. Concentration of H_2 vs Axial Distance

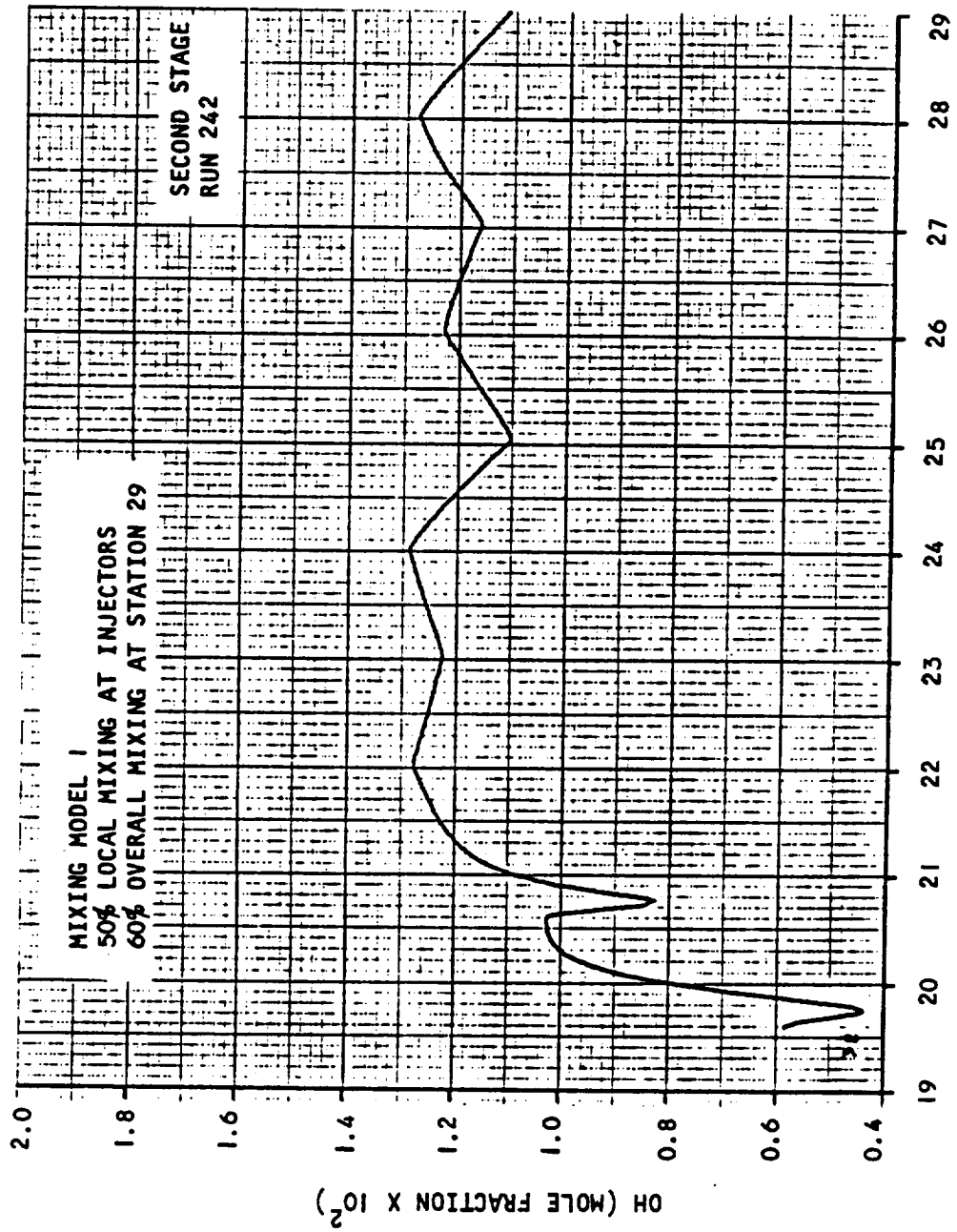

Figure B.4-5. Concentration of OH vs Axial Distance

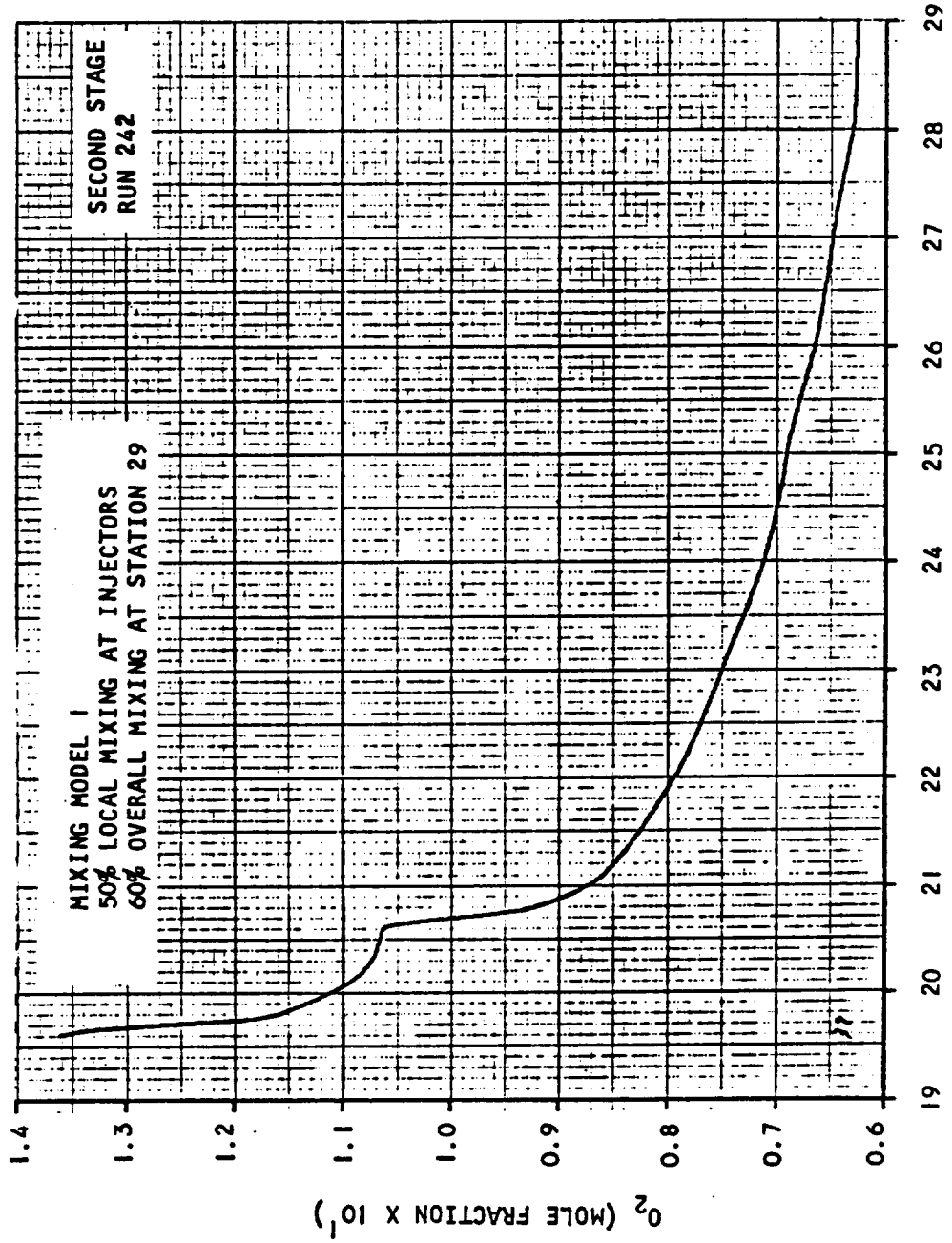

Figure B.4-6. Concentration of O_2 vs Axial Distance

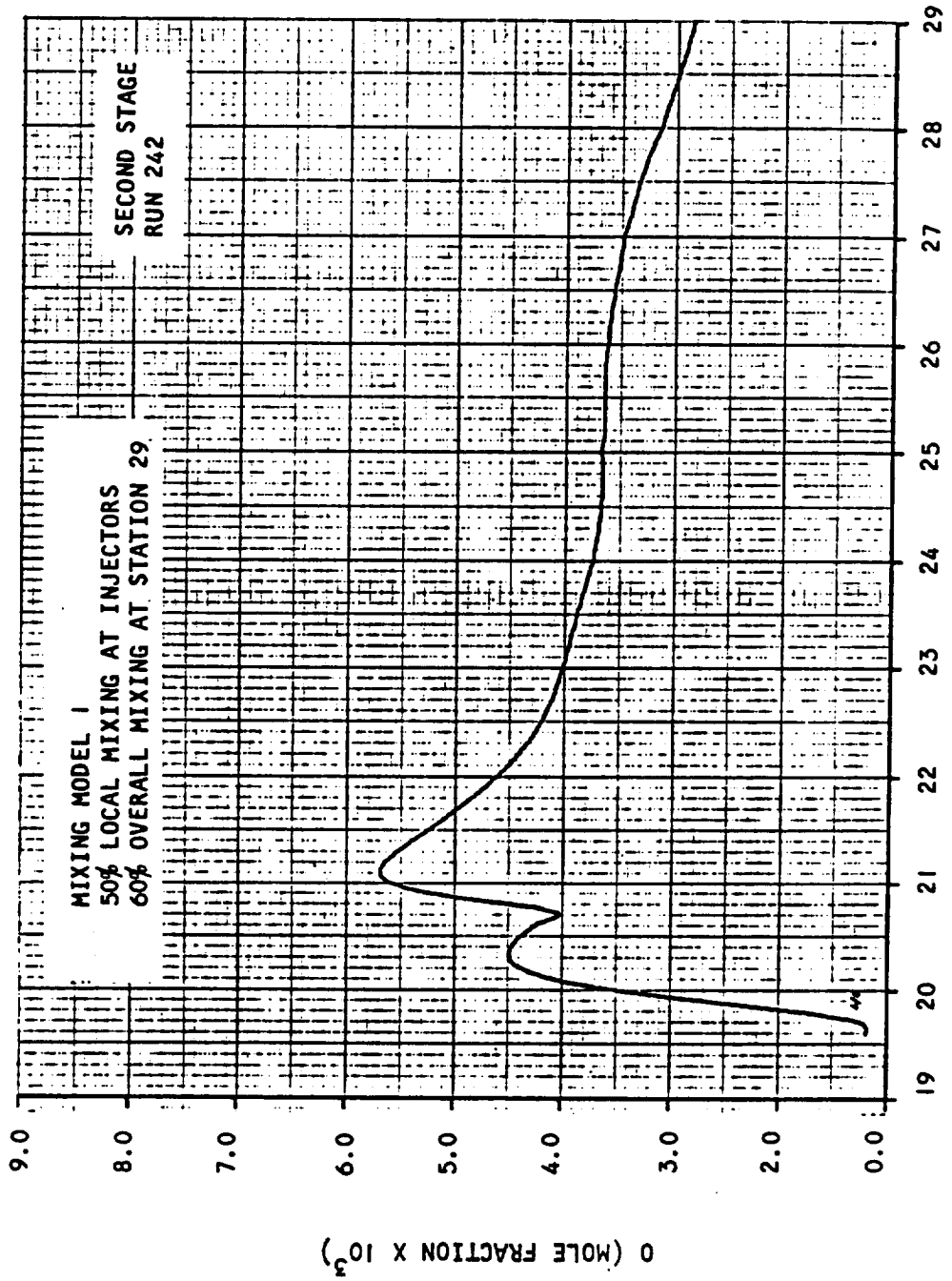

Figure B.4-7. Concentration of O vs Axial Distance

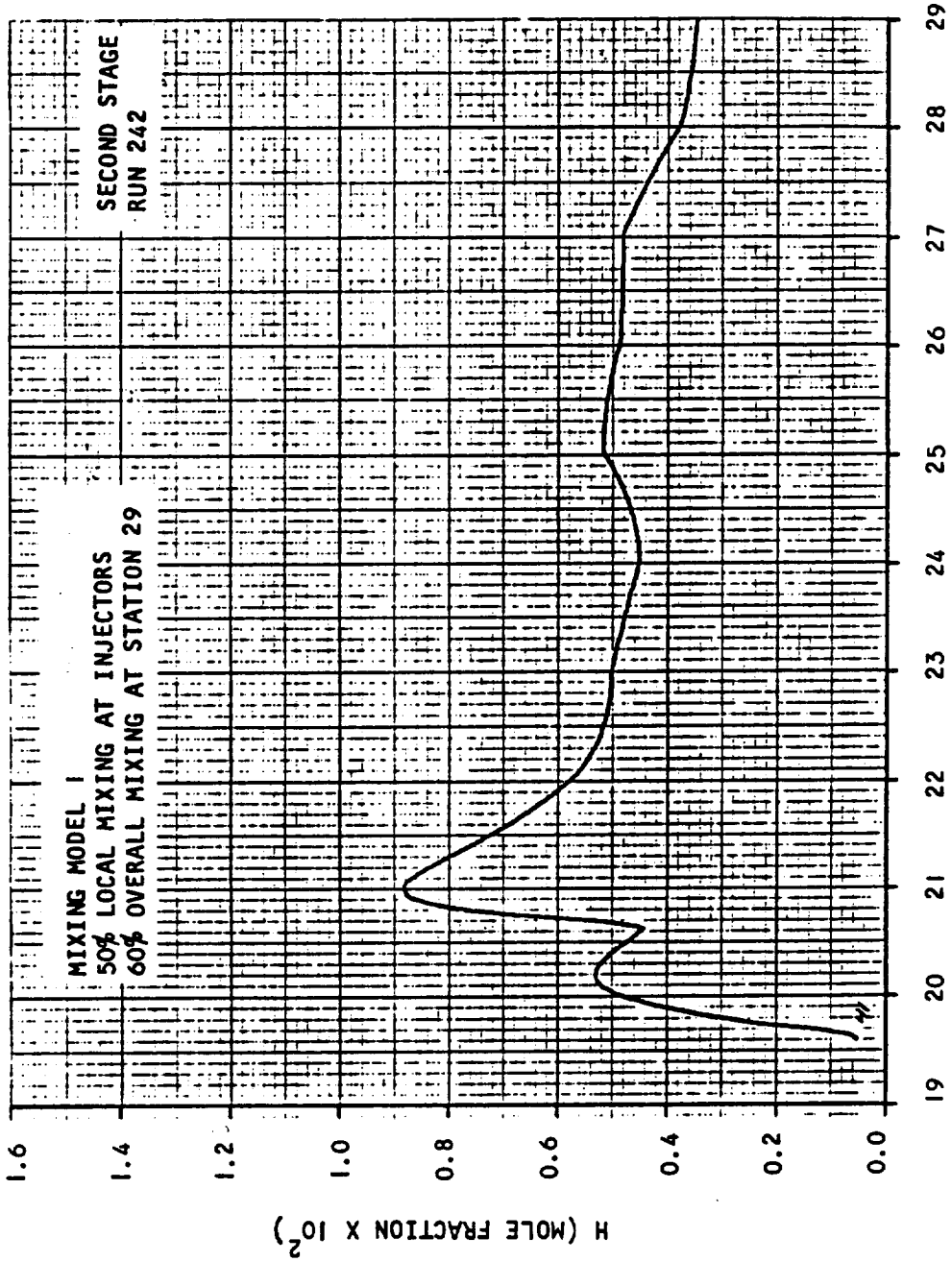

Figure B.4-8. Concentration of H vs Axial Distance

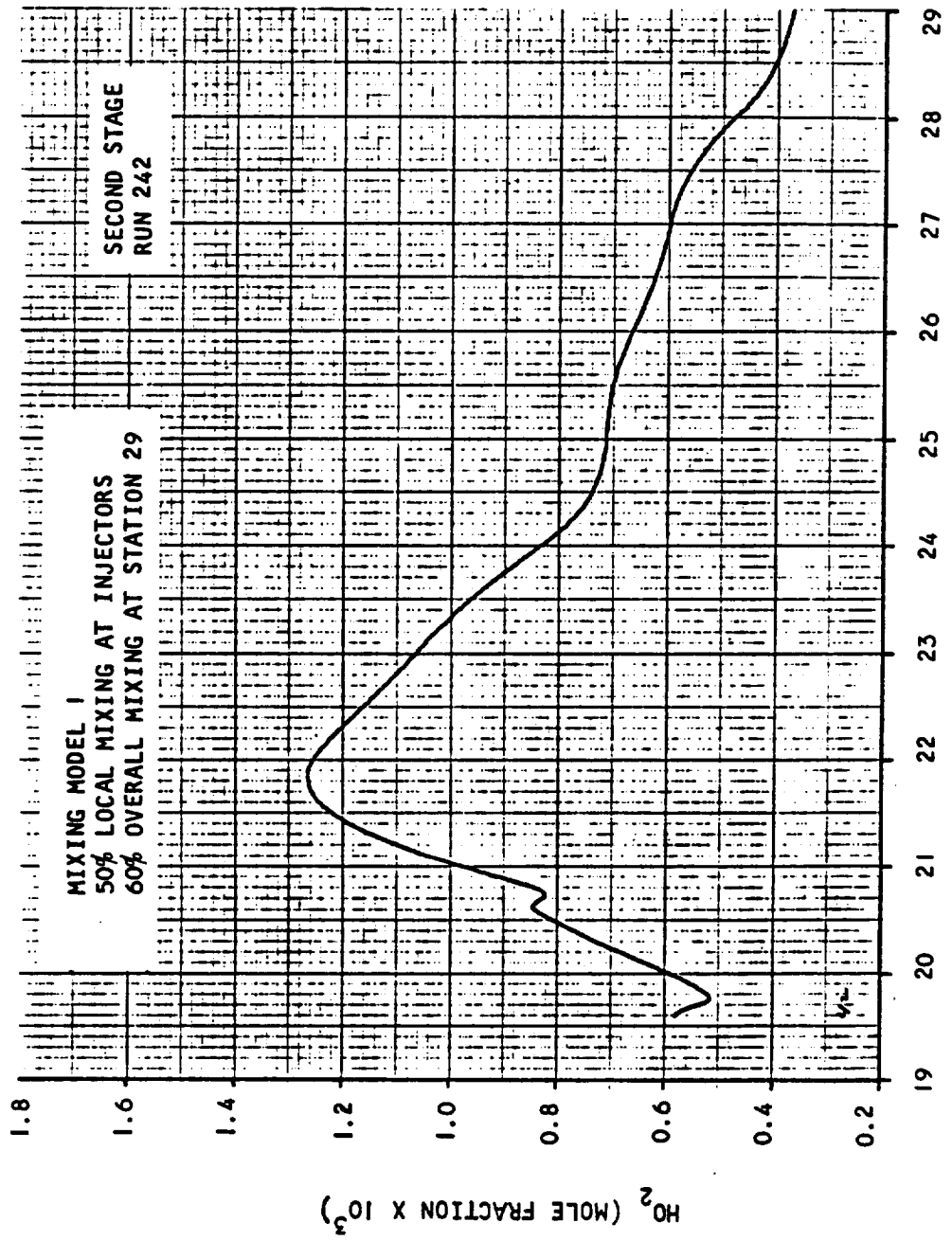

Figure B.4-9. Concentration of HO_2 vs Axial Distance

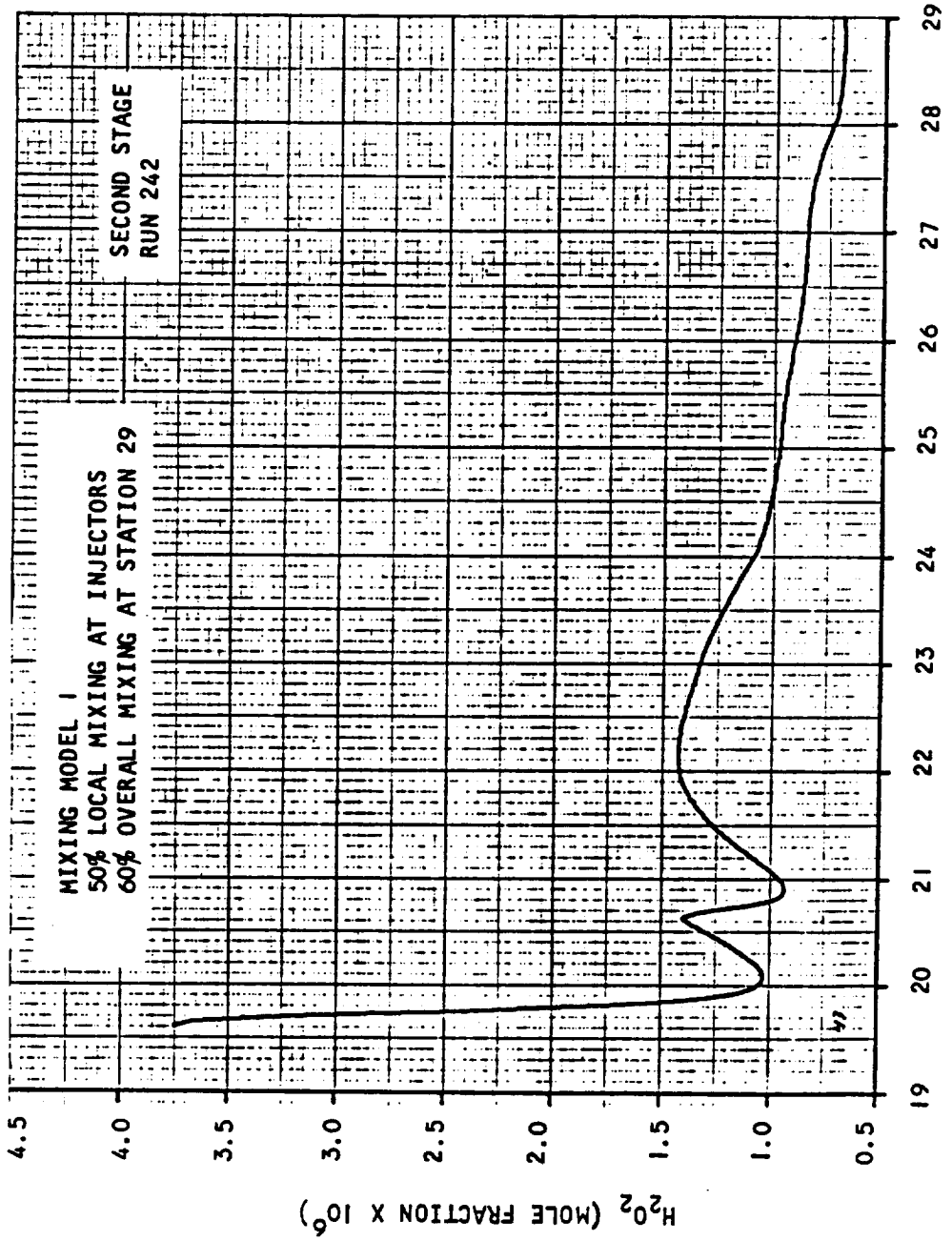

Figure B.4-10. Concentration of H_2O_2 vs Axial Distance

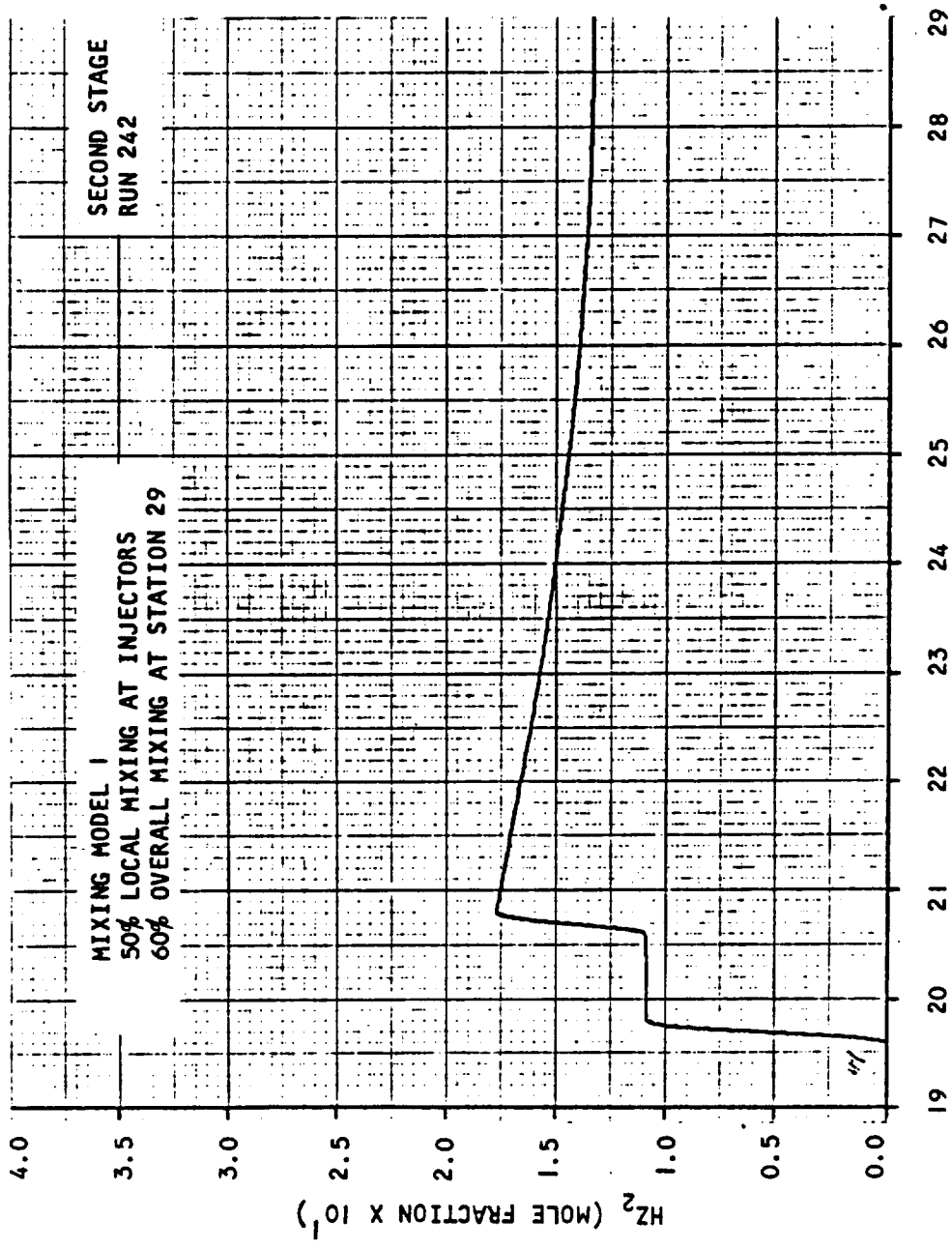

Figure B.4-11. Concentration of HZ_2 vs Axial Distance